JPL PUBLICATION 80-92

(NASA-CR-163975) EXPERIMENTAL AND ANALYTICAL EVALUATION OF ION THRUSTER/SPACECRAFT INTERACTIONS (Jet Propulsion Lab.) 233 p HC A11/MF A01 CSCL 21C G3/20

N81-17129 THRU N81-17139 Unclas 40576

Experimental and Analytical Evaluation of Ion Thruster/Spacecraft Interactions

M. R. Carruth
Editor

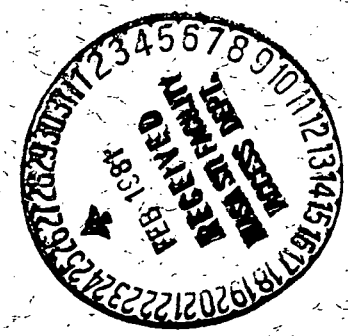

January 15, 1981

National Aeronautics and Space Administration

Jet Propulsion Laboratory
California Institute of Technology
Pasadena, California

REPRODUCED BY
U.S. DEPARTMENT OF COMMERCE
NATIONAL TECHNICAL
INFORMATION SERVICE
SPRINGFIELD, VA 22161

JPL PUBLICATION 80-92

Experimental and Analytical Evaluation of Ion Thruster/Spacecraft Interactions

M. R. Carruth
Editor

January 15, 1981

National Aeronautics and
Space Administration

Jet Propulsion Laboratory
California Institute of Technology
Pasadena, California

The research described in this publication was carried out by the Jet Propulsion Laboratory, California Institute of Technology, under NASA Contract No. NAS7-100.

Preface

The contents of this report present the results of a study conducted at the Jet Propulsion Laboratory (JPL) aimed at understanding the effects of ion thruster operation on spacecraft performance. Studies were conducted to both identify the environment produced by ion thrusters and to assess the interaction of this environment on a typical spacecraft and typical science instruments.

At the time much of this study was in progress, there was a preproject comet rendezvous mission study ongoing at JPL. That particular mission was to make use of a Solar Electric Propulsion System (SEPS) of which ion thrusters are the propulsion devices. Because of the anticipated use of SEPS for this mission, the "strawman" payload and preliminary spacecraft design were used as a baseline spacecraft for the ion thruster/spacecraft interactions study described in this report. Some discussion of the mission is given in the AIAA paper 79-2107, "Interactions Between a Spacecraft and an Ion Thruster Produced Environment", which was presented at the 14th International Electric Propulsion Conference in 1979. A comet rendezvous mission is not now anticipated for the near future, but the evaluation of ion thruster effects on spacecraft, which are presented in the above named paper, is still felt to be valid.

This report is intended to bring the results of the interactions study together into one document. However, throughout the time that this study has been conducted, information has been made available through conference papers and publications. These papers have been included in this report. New material, not previously reported, is also included as well as introductions to each section which are designed to tie the various parts of the report together. Papers which are included in this report and have previously been presented are listed below.

"Charge-Exchange Plasma Environment for an Ion Drive Spacecraft", JPL Publication 79-90, October 1979.

"Propagation of Charge-Exchange Plasma Produced by an Ion Thruster", AIAA Paper No. 80-1388, presented at the AIAA 13th Fluid and Plasma Dynamics Conference, July 1980.

"Radiated and Conducted EMI from a 30-cm Ion Thruster", AIAA Paper No. 79-1328, presented at the AIAA/SAE/ASME 15th Joint Propulsion Conference, June 1979.

"Interactions Between a Spacecraft and an Ion Thruster Produced Environment", AIAA Paper No. 79-2107, presented at the Princeton/AIAA/DGLR 14th International Electric Propulsion Conference, October 1979.

"Ion Thruster Plume Effects on Spacecraft Surfaces", AIAA Paper No. 80-1228, presented at the AIAA/SAE/ASME 15th Joint Propulsion Conference, July 1980.

TABLE OF CONTENTS

ABSTRACT

This report presents the results of a study to evaluate the interactions between ion thrusters and a spacecraft, including its science instrument payload. Because of the unique environment produced by ion thrusters and expected long electric propulsion mission duration, it is necessary to understand how an ion propulsion system will interact with typical spacecraft. It is for this reason that this study was performed. There were two goals of the work; one was to understand and characterize the environment produced by ion thrusters, and the other was to evaluate the impact of this environment on spacecraft and science instrument operation. Data and models pertaining to the ion thruster environment are given in this report as well as evaluations of interactive effects. No detrimental interactions which would seem to obviously threaten spacecraft or mission success were identified. Possible preventive measures for the detrimental effects which were identified are given in this report. Areas where additional work is required for an adequate understanding of ion thruster/spacecraft interactions, especially for specific spacecraft and mission designs, are specified.

INTRODUCTION

Ion thrusters have been under development for about twenty years and are presently nearing the end of this development state and will be ready for application as a primary propulsion device. A plasma is produced in the ion thruster's discharge chamber and the ions are electrically accelerated downstream to produce thrust. Electrons are also added downstream to maintain spacecraft neutrality. Ion thrusters can be used for both interplanetary missions as well as Earth orbital applications. Ion thrusters are very efficient devices and can operate with a very high specific impulse so that with the high exit velocity of the ions from the thruster, a small amount of fuel is consumed to produce the same momentum transfer as compared to typical chemical propulsion. In chemical rocket engines the energy that may be transferred to the kinetic energy of a spacecraft is limited to that energy which is locked up in chemical bonds and released as thermal energy in the combustion chamber. Therefore, there is a limited amount of energy which may be obtained from a given amount of propellant. This is not the case for an ion propelled spacecraft since the energy is continually supplied by a solar array or nuclear reactor. There are missions which require a very large total energy change of the spacecraft which can only be obtained by the use of ion thrusters or a similar electric propulsion device.

Ion thrusters are low thrust devices; fractions of a pound. Therefore, in order for ion thrusters to impart the large energy change to a spacecraft required for electric propulsion missions, the ion thrusters must operate for a long period of time. Where typical chemical rockets operate at most for tens of minutes, ion thrusters must operate for

years. This long operating time dictates that special consideration be given to ion thruster-spacecraft interactions since very minute, short-term effects may become significant after such a long exposure time. Ion thrusters are very different from chemical engines since they: 1) produce a plasma beam (energetic ion beam and added electrons for neutralization), and a low energy charge-exchange plasma which can surround the spacecraft, 2) have permanent and varying magnetic fields associated with their operation, and 3) operate at a high electrical power level so that radio frequency (rf) and conducted electrical noise is generated. The interaction between ion thrusters and ion propelled spacecraft and their science instruments must be determined because of the unique environment produced by ion thrusters and the duration of spacecraft exposure to this environment.

It is obvious that any determination of the interaction between an ion thruster produced environment and a spacecraft and its subsystems is only as good as the definition of the environment. Some portions of the environment, such as the permanent magnetic fields and the primary beam are well understood and characterized. However, some of the ion thruster generated plasmas and fields are not well understood. In fact, various models of the upstream density of the charge-exchange plasma predict densities which vary by orders of magnitude. Therefore, a major part of this program was to better characterize the ion thruster produced environment around a spacecraft and then assess its interaction with spacecraft and science instruments. The 30-cm Hughes/NASA LeRC mercury ion thruster has been developed for primary propulsion purposes and was therefore the ion thruster assumed in this study.

This report is structured such that under major categories, as listed in the table of contents, there are papers authored by the people who performed the work described in those individual papers. Some introduction to each of these papers and their relationship to other papers and the total interactions study effort will be addressed in the introduction of each major section of this report.

There are some things which were not pursued in detail in this report because they were either considered lower priority items or they were too complex to sufficiently address in this study. They will be outlined here, with some assessment of their importance and our present understanding.

The permanent and varying magnetic fields associated with the mercury ion thruster will be of concern to science instruments such as magnetometers, plasma wave, and charged particle-detecting instruments. A study of such fields, their effects on science instruments and means of cancelling the fields was made and is reported in AIAA Paper #75-373, "Magnetic Compatibility of Solar Electric Propulsion Module with Spacecraft and Science", by R.M. Cowgill, et al. There are means of reducing fields at science instruments such as alternating the polarity of adjacent ion thruster's permanent magnets or actively bucking out the field at the instrument location. It was felt that additional studies, necessarily involving different spacecraft geometries and science instruments, would be very involved to consider details beyond those considered in the report named above. Certainly, for specific science instruments and spacecraft configurations a detailed evaluation of the various fields' effects will necessarily be performed. It is felt that this

can better be accomplished under the cognizance of the Solar Electric Propulsion System (SEPS) designers and/or the flight project for which the instrument is considered.

An interesting possibility regarding spacecraft potential will be addressed here. As is discussed in the papers, "Solar Array/Spacecraft Biasing" and "Ion Thruster Plume Effects on Spacecraft Surfaces", it may be advantageous, for several reasons, to allow biasing of the spacecraft by using the ion-thruster system. The primary reasons for this would be to prevent charge-exchange mercury ion bombardment of spacecraft surfaces at energies of 10-20 eV (the potential between the spacecraft ground and plasma potential) and to prevent perturbation of low energy particle science data. However, there may be another reason. The spacecraft ground potential can be brought to the potential of the charge-exchange plasma at the point where the spacecraft structure makes contact with the charge-exchange plasma. This will be near the thrusters where the density is the greatest. The whole of the spacecraft will be at this potential. However, upstream of the ion thrusters the charge-exchange plasma potential will be becoming more negative for less dense regions. Therefore, at the forward end of the spacecraft, where the science instruments exist, the spacecraft potential will be slightly positive with respect to the local plasma. This will repel mercury charge-exchange ions and possibly prevent their arrival at spacecraft surfaces. As will be pointed out in the paper, "Interactions Between a Spacecraft and an Ion Thruster Produced Environment", there is a concern that on extremely cold surfaces, such as science instrument passive radiators or sun shaded portions of the spacecraft, mercury may tend to condense. There are means of preventing this which will, however, cost

spacecraft mass, power and complexity. If the spacecraft is actively biased, the problem will automatically be taken care of for positions either far enough upstream or obstructed so as to lower the charge-exchange plasma density. A real determination of the degree to which portions of the spacecraft will be positive of the surrounding plasma requires more of a study than was performed in the work described in this report.

The ion optics screen and accelerator grids are made from molybdenum. Some of the charge-exchange ions that are created near the downstream side of the accelerator grids are attracted back to the grid by its negative potential of a few hundred volts. The impact of these ions sputter molybdenum from the grids. The charge-exchange cross-section for $Hg^{+} + Mo^{\circ} \rightarrow Hg^{\circ} + Mo^{+}$ is about a factor of six less than $Hg^{+} + Hg^{\circ} \rightarrow Hg^{\circ} + Hg^{+}$. The sputtered molybdenum also has a much higher directed neutral velocity than the mercury atoms. All this works in favor of making small the probability of charge exchange and the flow of molybdenum ions upstream. However, with mission times of years, and a sticking coefficient of about unity, a small molybdenum deposition may develop on surfaces upstream of the spacecraft. Depositions of a few Angstoms can produce significant changes in the thermo-optical properties of materials. Therefore, an effort was undertaken to measure molybdenum ion backflow in the charge-exchange plasma. Because of the very low fluence which could be expected to accumulate in a reasonable laboratory test period, sensitive means of identifying and measuring molybdenum, accumulated on one square inch coupons of carbon, were required. A combination of scanning electron microscope X-ray analysis and neutron activation was chosen.

The coupons were placed in shallow, open boxes in locations upstream of the thruster and pointing across the chamber to positions just downstream of the thruster optics. Baffles were used so that molybdenum atoms sputtered from the end of the chamber or molybdenum ions, formed by charge exchange and originating from the end of the chamber, would not be likely to get onto the sample. Also, the chamber wall was baffled to reduce bouncing of molybdenum atoms from the wall onto the carbon sample. In the event some neutral molybdenum was able to get into the sample box, precautions were taken. The sample boxes were placed in groups of three. One box was electrically floating, one box was biased about ten volts negative and one was biased about ten volts positive. Since the experiment was designed to observe molybdenum ions, the positively biased sample would be expected to have the least molybdenum since the ions would be repelled. In all cases the positively and negatively biased samples contained larger quantities of molybdenum than the floating sample. This is a surprising result. It may be possible that negative ions of molybdenum trioxide are being formed within the test chamber (personal communication, Y.S. Kuo, JPL) and producing the results we see. It appears that measurement of any molybdenum constituency in the charge-exchange plasma upstream of the thruster is virtually impossible to measure reliabily in a ground facility. Any such measurements can only be made in a space test.

A model of the molybdenum ion portion of the charge-exchange plasma is included in the paper, "Charge-Exchange Plasma Environment for an Ion Drive Spacecraft". It does not account for the high directed velocity of the sputtered molybdenum atom. Therefore, the model predictions

are felt to be very conservative in that the model predictions for upstream positions should be high.

There is one last note to make in this introductory section of this report. Because ion thruster development has been ongoing for so many years there is a host of technical papers regarding the environment produced by an ion thruster and its interactions with a spacecraft. For the reader who wishes to refer to these papers it is suggested that the paper, "A Review of Electron Bombardment Thruster Systems/Spacecraft Field and Particle Interfaces", by David C. Byers, NASA TM-78850 (also Journal of Spacecraft and Rockets, Vol. 16, No. 5, 1979) be consulted.

Spacecraft Grounding

PRECEDING PAGE BLANK NOT FILMED

INTRODUCTION

The paper entitled, "Solar Array/Spacecraft Biasing", is the only one in this section on spacecraft grounding. It discusses the fact that biasing techniques may be applied to control spacecraft potential. Normally when a spacecraft is operated with ion thrusters, the spacecraft will be 10-20 volts negative of the surrounding plasma. This will affect scientific measurements and will allow ions from the charge-exchange plasma to bombard the spacecraft surfaces with a few tens of volts of energy. Based on the small amount of data in the paper, "Ion Thruster Plume Effects on Spacecraft Surfaces", this condition may not be tolerable. A proper bias system can bring the spacecraft to or near the potential of the surrounding plasma. A concern was also voiced in the paper on spacecraft biasing regarding an ion thruster neutralizer failure. It was feared that in single operation or with a cluster of thrusters, the failure of an ion thruster neutralizer will allow the spacecraft to very quickly charge to dangerously large negative potentials. It has been shown by W.R. Kerslake and S. Domitz in NASA TM-79271, "Neutralization Tests On The SERT II Spacecraft", that electrons from a thruster neutralizer adjacent to the thruster with a failed neutralizer can supply the necessary neutralization current. The above specified reference and the spacecraft grounding paper in this report should be consulted regarding spacecraft charging and neutralization with operating thrusters.

SOLAR ARRAY/SPACECRAFT BIASING

D. J. Fitzgerald
Jet Propulsion Laboratory
California Institute of Technology
Pasadena, California

Introduction

The ion engine provides thrust by accelerating positive ions through a potential which is maintained between the ion source and the surrounding space plasma. At some distance from the spacecraft the undisturbed space plasma contains approximately equal positive and negative charged particles. This macroscopically neutral plasma will be chosen as the reference (zero) potential in the following discussion.

An object emersed in space has capacitance with respect to space plasma reference and is generally maintained at some potential by various natural charging mechanisms. The capacitance is a function of the size and shape of the object as well as the Debye length or screening distance of the ambient plasma. Natural charging mechanisms such as plasma diffusion and photoelectron emission are competitive processes which charge the spacecraft several volts negative or positive respectively, depending on which mechanism predominates. However, the operation of an ion thruster introduces additional charging mechanisms which, in general, dominate the potential of the spacecraft.

Ion Thruster Operation

The relationship between the ion thruster, the spacecraft, and space plasma reference is shown in the circuit diagram in Figure 1. The thruster is assumed to be electrically isolated from the spacecraft in this case. It is apparent from this figure that an electron current (neutralizer) must be provided to match the ion beam current of the thruster, otherwise it will not be possible to maintain the potential difference between the ion source and the surrounding plasma. The relative magnitudes of the capacitance and currents are shown schematically in the figure. Note that even a so-called isolated thruster has a tremendous influence on the spacecraft potential by means of plasma diffusion and capacitive coupling.

The Hughes 30-cm thruster utilizes a hollow cathode neutralizer to provide the required electron emission. A small discharge is maintained between the hollow cathode and an electrode called the "keeper". The electrons from the cathode are accelerated through a region called the "cathode fall" and form a plasma. The neutralizer plasma potential is generally within a few volts of space plasma reference and the cathode (or neutralizer common) is approximately 15 volts negative. During normal operation the ion beam plasma adjacent to the thruster is on the order of 20 volts positive with respect to space plasma reference. The potential difference between the beam plasma and neutralizer plasma provides the necessary coupling voltage for extracting the electron emission current. The proper coupling voltage is maintained automatically when the thruster/neutralizer pair is isolated and the neutralizer is operating normally. The consequence of neutralizer failure will be described later.

Figure 2 shows a more detailed diagram of an operating thruster including the inevitable leakage current through the high voltage insulators to the spacecraft. A resistor has been added between the neutralizer common and the spacecraft to provide a return path for this leakage thus preventing excessive spacecraft charging. A value of 10 Kilohm is considered low enough for leakage return yet sufficiently large to provide a high degree of isolation between the thruster and spacecraft; i.e., to assure good neutralizer to beam coupling with each thruster/neutralizer pair.

Neutralizer Failure

It is also shown in Figure 2 that the mercury feed system is at spacecraft ground which makes it necessary to provide isolators for the transfer to mercury vapor between the vaporizers (3) and the ion source. The cathode and main vaporizer isolators are currently designed to operate reliably at 1100 volts (3000 seconds specific impulse). The neutralizer isolator is rated at 250 volts and is therefore quite adequate for normal neutralizer operation; however, it must be protected against the higher voltages that may be present during a neutralizer failure.

Figure 3 shows a zener diode network for "n" thrusters which is designed to provide protection for the neutralizer isolator for a few seconds until corrective action (high voltage turnoff) can be taken. The operating sequence is described as follows. When a neutralizer begins to fail, the neutralizer common voltage goes negative until the zener diode voltage is exceeded. The failing neutralizer's zener will then conduct which in turn will positively bias the zener diodes of the other thrusters. The next effect is that the neutralizers of the remaining operating thrusters provide the necessary emission current for the failing neutralizer. An additional zener diode is placed between the zener common and spacecraft bus to provide the ultimate protection, in the event that the emission from the other neturalizers is inadequate. As a rule it is assumed that at least two thrusters will be operating at any given moment in order to balance the swirl torques which may be produced by the ion thrusters. Thus, under most circumstances, there will be at least one back-up neutralizer to provide the extra emission current.

The zener protective circuitry has not been tested, but the values given in Figure 3 are probably reasonable. A test is also required to determine the capability of the neutralizer to perform a back-up role, and to evaluate the effect of neutralizer failure on the adjacent thrusters and spacecraft alike. The back-up mode should be limited to a few seconds otherwise the operating neutralizers may be damaged. In addition, a neutralizer failure sensor and high voltage shut-off logic must be incorporated into the power conditioner.

Spacecraft Bias

With the proposed grounding scheme, the spacecraft will normally be maintained at the neutralizer common potential (-15 volts) with respect to the ambient space plasma. This negative potential repels most of the electrons from the thruster induced sources of plasma as well as the ambient plasma but attracts ions to the spacecraft surface. Measure-

ments in a ground facility have shown that the electron flux to the spacecraft may increase substantially if the spacecraft is biased to zero potential. Most of the electrons are drawn directly from the neutralizer and charge-exchange plasma to neighboring structure. Dielectric coatings and/or electrically floating structure may be necessary in the vicinity of the thruster, if spacecraft bias is a requirement. The final thruster mounting assembly must be tested in a floating configuration to evaluate the additional neutralizer emission requirements.

The use of spacecraft biasing has been proposed by some scientists to minimize the interaction between the spacecraft and the ambient plasma. Low energy charge particle and plasma wave measurements are particularily vulnerable to the electric fields which are normally present around a spacecraft. The ion thruster has been successfully used in space as a charge particle release device in a feasiblity test of spacecraft biasing.

Besides being able to supply a zero potential spacecraft for science acquisition, there are other reasons for which a spacecraft bias should be considered. Because the spacecraft will be some 10-20 volts negative of the beam plasma, ions will impact the spacecraft surface with this energy. This energy could be sufficient to produce some chemical interactions and possibly even physical sputtering. Such interactions could produce undesireable changes in the thermo-optical properties of spacecraft and science instrument surfaces. By biasing the spacecraft the proper potential, such interactions can be greatly reduced or eliminated.

A system designed to bias some element of the spacecraft requires a method of removing excess charged particles from the vehicle. A choice exists between using a dedicated charge release system or an ion thruster/neutralizer pair. The latter bias method will be the only one considered here, because it has a direct impact on the thruster grounding scheme. The following is a general description of a bias system utilizing multiple thrusters.

Figure 4 indicates a method of biasing the solar array with multiple thrusters. The same technique can be applied to biasing the spacecraft itself or any special surface, such as a shield. A separate variable conductance supply is used for each thruster to compensate for differences between neutralizer characteristics. This allows direct control over the distribution of bias emission current between the neutralizers and prevents the possibility of one neutralizer drawing a larger current than is consistent with the lifetime of the device. The diode between the neutralizer common and the variable conductance is used to protect the bias supply in the event of neutralizer failure. Figure 5 shows the path of an electron which has been absorbed on a biased surface in terms of the changes in potential.

The diagram in Figure 6 shows how the variable conductance supplies are used to balance the emission current for two neutralizers with slightly different emission characteristics. The variable conductance power supply is adjusted for each neutralizer by the computer to distribute the emission current evenly between neutralizers. Once they have been adjusted, the bias may be changed over a fairly wide dynamic range without changing this balance. However, periodic (daily) adjustments may have to be made to compensate for relative changes in the neutralizer characteristics.

In Figure 6 there are two curves which represent the relative neutralizer common potential as a function of emission current for two different thruster/neutralizer pairs. The square symbol of these curves indicates the emission current required to match the beam current of the respective thrusters. The variable conductance power supplies are represented by load lines which originate at a common point on the axis which is the bias common potential. The intersection of the load line and the neutralizer common characteristic curve is the operating point of the neutralizer which is shown with a solid circle. The difference between the operating point and the beam current, gives the amount of emission current provided to the bias system from the respective thruster. In the case shown in Fig. 6, the load lines for the two thrusters have been adjusted to give approximately the same total emission current in spite of the differences in the beam current from each thruster. The dashed lines on the figure show what happens when the bias is increased without changing the variable conductance. In this case, the operating point is indicated by open symbols.

The bias system must be provided with a sensor to establish the surrounding plasma potential reference. This sensor would be part of the control of the bias power supply. Details of the sensor are beyond this report.

The grounding network and bias circuitry have not been tested as a total system. However, many parts of this system have been tested in ground facilities and proven in space. This lack of information leaves the question of using a bias system still open.

Solar array biasing represents a drastic change from the conventional resistance isolation method currently used to prevent signal source failures. Therefore, prior to incorporation into a solar array system, this biasing concept will need further investigation and testing.

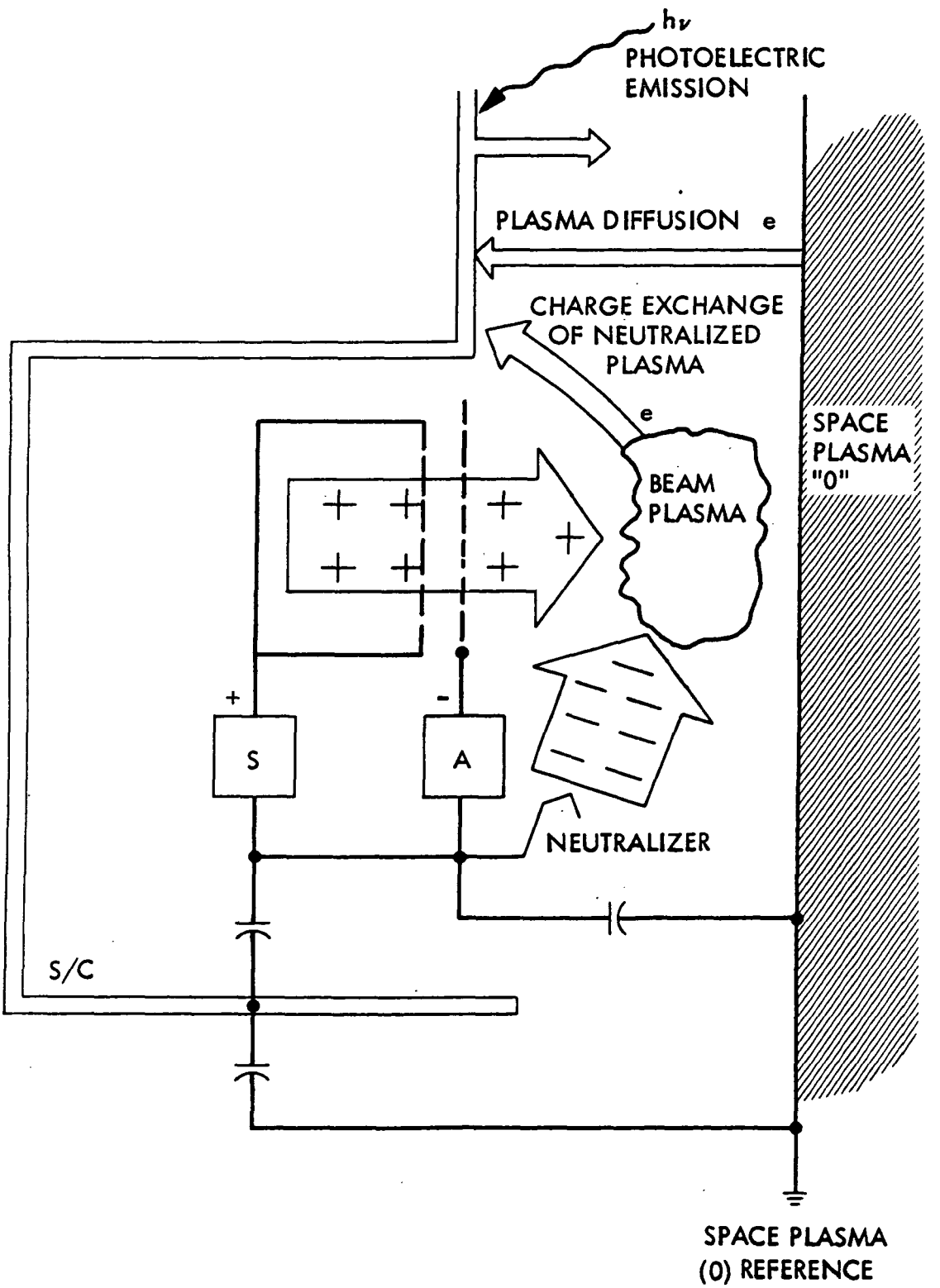

Figure 1. Relationship Between the Ion Thruster, the Spacecraft and Space Plasma

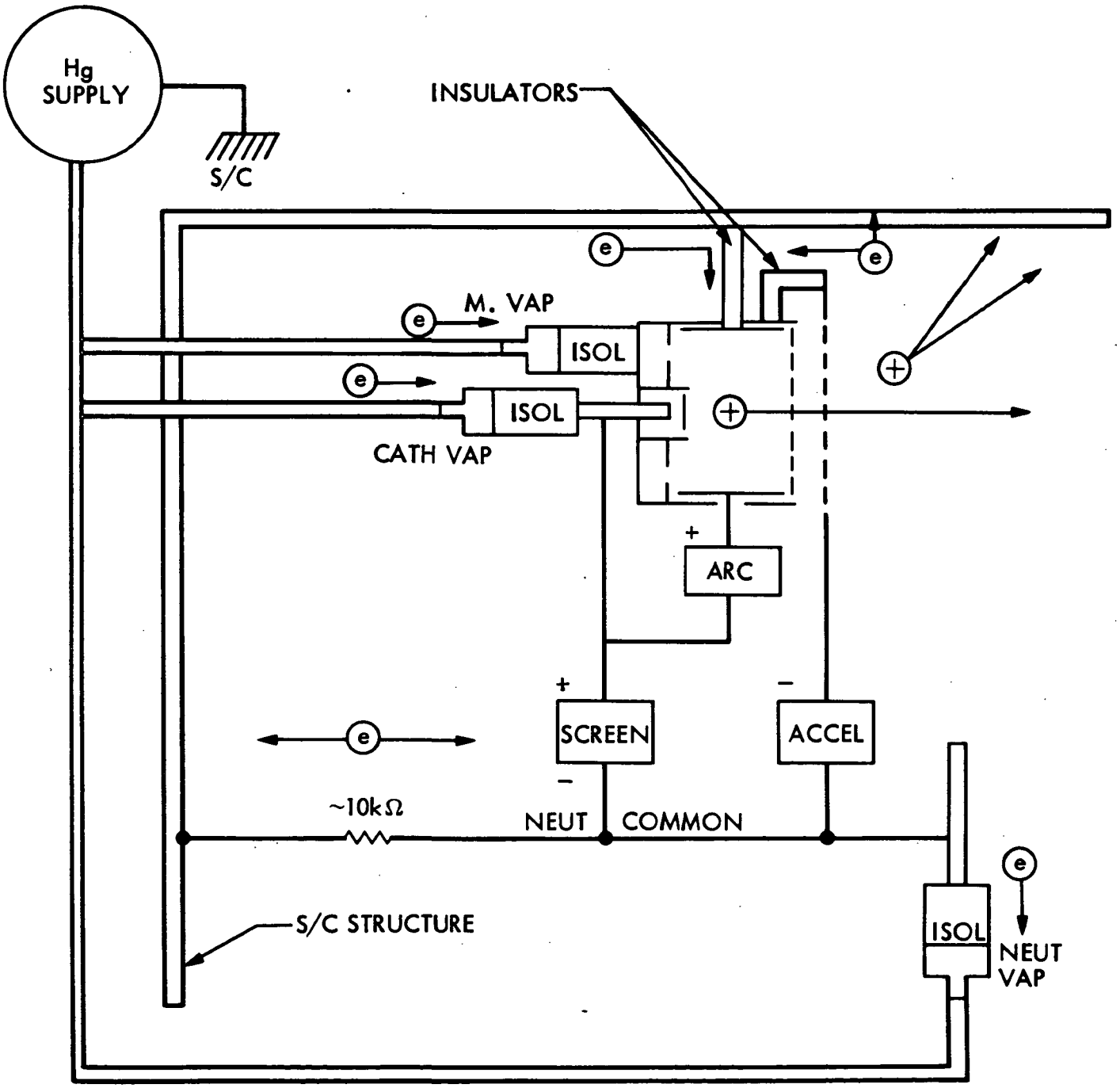

Figure 2. Diagram of Operating Ion Thruster

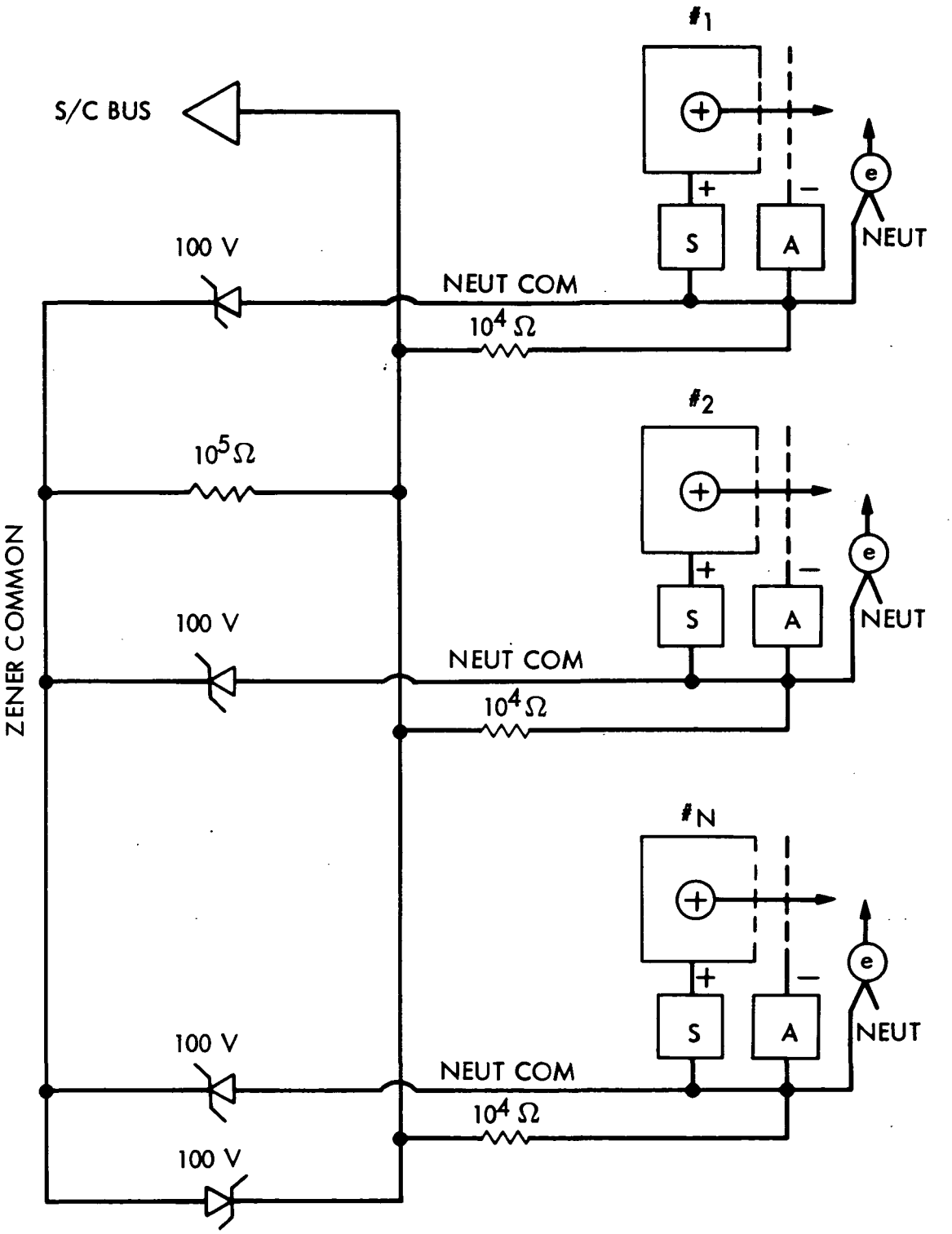

Figure 3. Zener Diode Network for Neutralizer Sharing to Prevent Spacecraft Charging

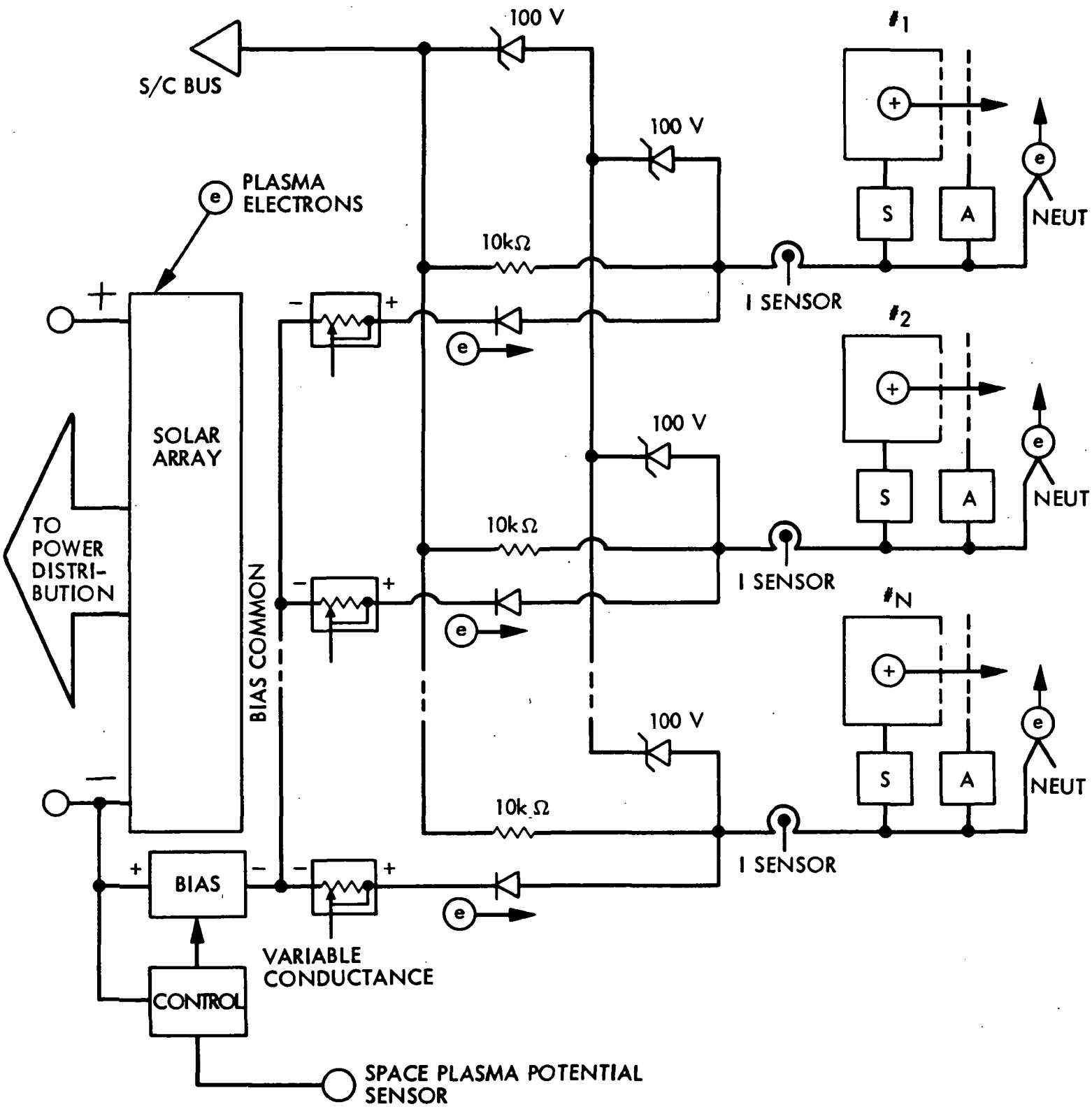

Figure 4. Network for Biasing of Solar Array

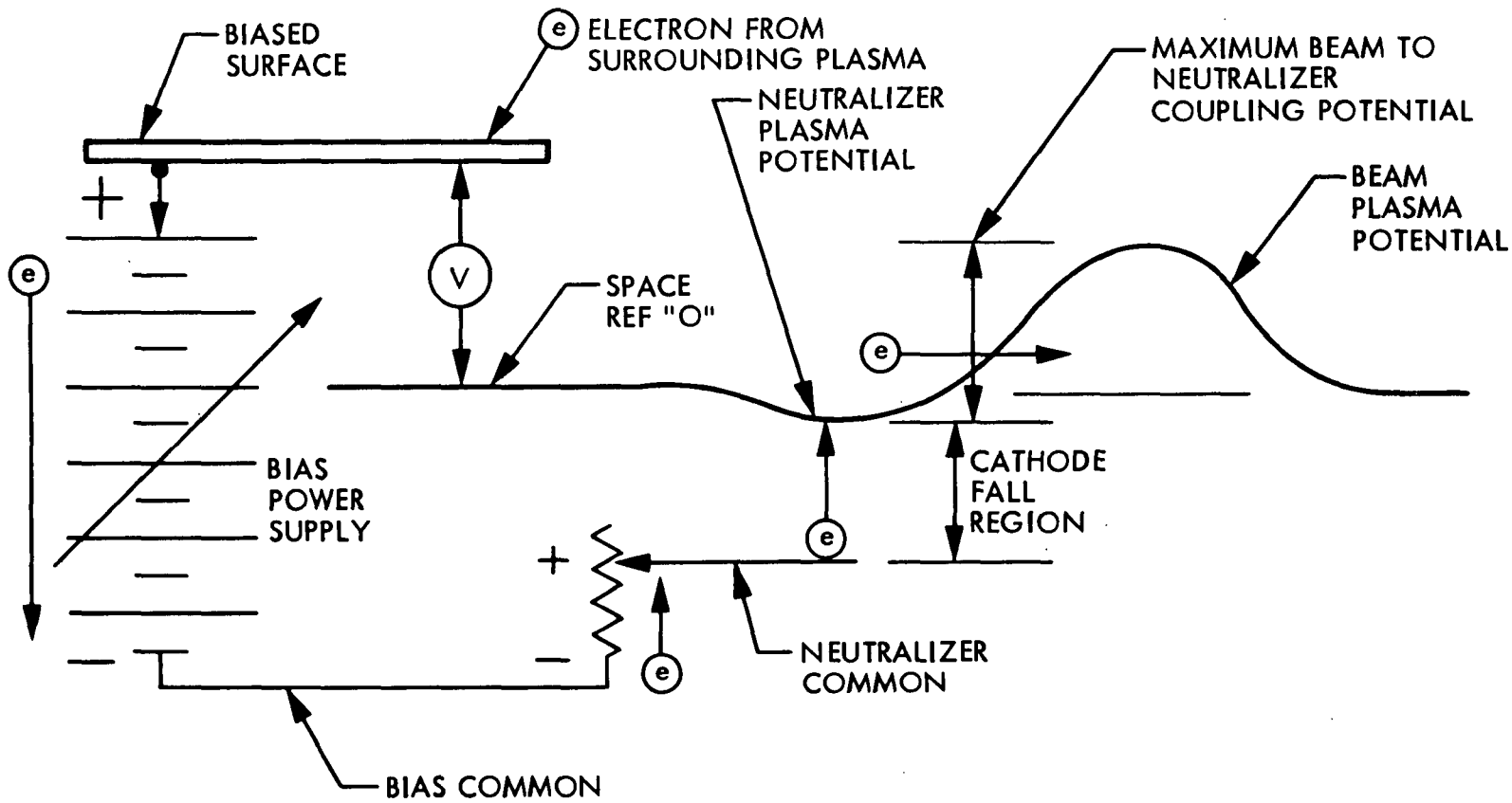

Figure 5. Relative Potentials Associated with Ion Beam Neutralization

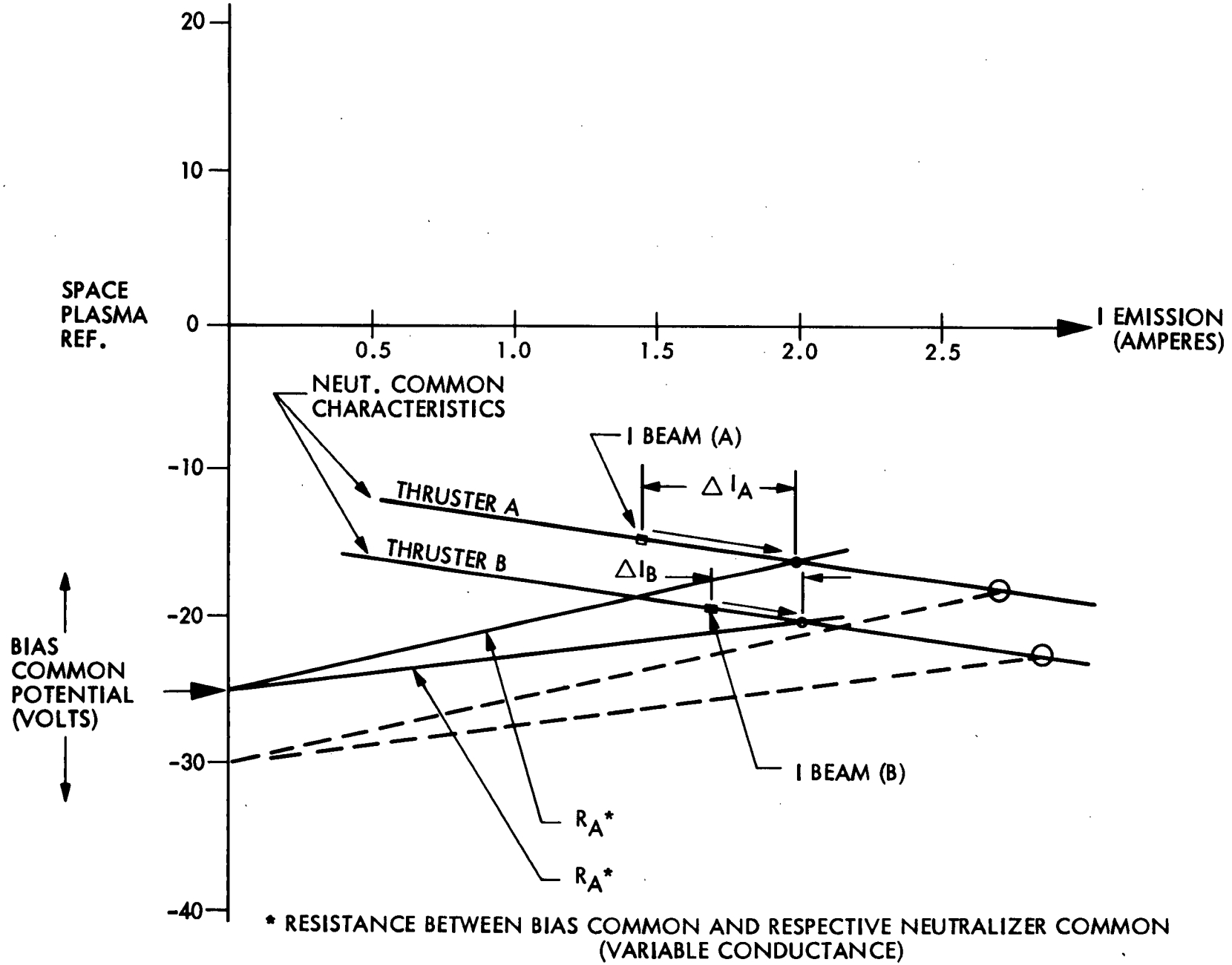

Figure 6. Use of Variable Conductance Supplies to Balance Emission Current from Two Thrusters

Charge-Exchange Plasma

INTRODUCTION

The reader will probably notice that a large portion of this report lies within the section on the charge-exchange plasma generated by ion thrusters. Of the plasma species generated by an ion thruster, the charge-exchange plasma is the most difficult to make experimental measurements of, yet poses the most concern to a spacecraft. The high energy primary ion beam is very energetic and highly directed. It is relatively easy to design a spacecraft so that the beam is not able to intercept portions of it. Even the very divergent parts of the primary beam can be made to miss most portions of the spacecraft, except for nearby spacecraft structure or the outer portions of the solar array when the thrusters are gimballed. The same is true for all the line-of-sight particles generated by the thrusters; such as the primary beam, neutral atoms leaking through the ion optics, and molybdenum atoms sputtered from the accelerator grid of the ion optics. The charge-exchange plasma is produced by charge-exchange collisions between the energetic beam ions and the neutral mercury which leaks through the optics system. The result of the charge-exchange collision is an energetic neutral atom and a thermal ion. There are internal fields in the beam plasma which accelerate the charge-exchange ions radially. When they leave the beam, with neutralizing electrons, they diffuse by an ambipolar diffusion process since the electrons are so much more mobile than the mercury ions. This allows the plasma to move upstream.

It has been experimentally determined that within both the primary beam and the surrounding charge-exchange plasma, the "barometric equation" holds. This is a form of the Boltzmann distribution law and is

given by:

$$n_e = n_{e,ref} \, EXP(-eV/kT_e) \qquad (1)$$

where n_e is the electron density at the location with plasma potential, V, and electron temperature, T_e. The symbols k and e are the Boltzmann constant and unit of charge, respectively. The reference point in the plasma, where the electron density is $n_{e,\,ref}$, has plasma potential defined as zero volts. Regions of density lower than $n_{e,\,ref}$ tend to be negative.

As stated earlier, there are various models which predict the flow of the charge-exchange plasma upstream. They are referenced in the second paper in this section. The plasma densities they predict for positions upstream of an ion thruster varies by orders of magnitude. The reason for this has largely been because of the difficulty in obtaining experimental data because of the interference of facility produced charge-exchange plasma. The ions in this plasma are created by charge-exchange reactions between beam ions and mercury atoms which have already encountered the facility structure. There has been sufficient disagreement between various experimental determinations of the facility produced plasma, that values of true ion thruster charge-exchange plasma density upstream of the thruster have not been agreed on. This has also lead to the development of analytical models which do not make a comparison with experimental data and give density predictions that vary by orders of magnitude. This is why better definition of the charge-exchange flow became a primary concern. Its flow upstream had to be known with a greater degree of confidence in order to evaluate charge-exchange plasma/spacecraft interactions.

The first paper in this section, "Charge-Exchange Plasma Environment for an Ion Drive Spacecraft", presents a model of the charge-exchange plasma production and experimentally obtained data. The fact that experimental data is involved, places some uncertainties in its predictions for the reasons outlined in the previous paragraph. However, a comparison between the model in this paper and the data given in, "Beam Efflux Measurements", by Komatsu and Sellen (referenced in the second paper in this section) show that they are roughly consistent within a factor of two or three for the region within which data was collected, about 20 cm upstream. Besides presenting a model of the charge-exchange plasma, some of its interactions with spacecraft and ambient plasma are discussed.

Typically, in the past, experimental data on the charge-exchange plasma has been obtained with standard Langmuir probe techniques or Retarding Potential Analyzer-Faraday cups. Not only did the facility plasma interfere with measurements but the flow pattern of the charge-exchange ions, which do possess a directed flow of from fractions to a few eV, could not be determined by these methods. A new experimental technique was applied to the experimental study of the charge-exchange plasma flow. The technique and experimental results are described in this section's second paper, "Propagation of Charge-Exchange Plasma Produced by an Ion Thruster". The flow direction is accurately determined; independent of the facility produced plasmas.

Since the "barometric equation" has been experimentally determined to hold, at least near the thruster, it can be used to model the flow of the charge-exchange plasma. The third paper, "Computer Code for Charge-

Exchange Plasma Production", uses the barometric equation and the calculated charge-exchange plasma production rate and distribution to model the flow and density of this plasma's flow upstream of an ion thruster. No experimental data is used in the model development as in the first paper in this section. This model gives us a basis from which to work. Such considerations as spacecraft geometry, multi-thruster operation, initial thermal velocity of charge-exchange ions, or possible changes in the electron temperature as the plasma expands, have not yet been addressed in this computer code.

In order to better understand the production and distribution of the facility produced plasma, an analytical model of the facility plasma's production and distribution was derived. The initial purpose was to explain anomalies in data presented in the paper, "Ion Plume/S-Band Carrier Interactions Study". This attempt was not successful because of problems produced by the antennas and RF absorber material that was placed in the chamber (this is discussed more in the section on electromagnetic interference.) However, a model of the facility produced plasma density was produced for the case in which the liquid nitrogen cooled chamber walls were bare. Comparison with experimental data is reasonable, approximately within a factor of two. This work is presented in the paper, "Facility Produced Charge-Exchange Ions".

JPL PUBLICATION 79-90

Charge-Exchange Plasma Environment for an Ion Drive Spacecraft

Harold R. Kaufman
Colorado State University
M. Ralph Carruth, Jr.
Jet Propulsion Laboratory

October 1, 1979

National Aeronautics and
Space Administration

Jet Propulsion Laboratory
California Institute of Technology
Pasadena, California

The research described in this publication was carried out by the Jet Propulsion Laboratory, California Institute of Technology, under NASA Contract No. NAS7-100.

ABSTRACT

It is necessary to have an understanding of the charge-exchange plasma environment around a spacecraft that uses mercury ion thrusters for propulsion so that the interactions between this environment and the spacecraft can be determined. A model is reviewed which describes the propagation of the mercury charge-exchange plasma and extended to describe the flow of the molybdenum component of the charge-exchange plasma. The uncertainties in the models for various conditions are discussed throughout this report. Such topics as current drain to the solar array, charge-exchange plasma material deposition, and the effects of space plasma on the charge-exchange plasma propagation are addressed.

CONTENTS

CONTENTS (cont)

Figure

Note: The Table of Contents shown here indicates the original pagination of the document and has not been changed to reflect the pagination of the present report.

A. INTRODUCTION

Ion thrusters will be used in the near future as a primary propulsion device for interplanetary spacecraft and for attitude control and orbit transfer of spacecraft near earth. Because of the plasma environment produced by the thruster it is important to understand how this propulsion device will affect various spacecraft subsystems. An interplanetary spacecraft will likely be most affected by the ion thruster environment because of the use of multiple thrusters and thrusting periods of years.

This paper will describe the charge-exchange plasma environment produced by the thrust subsystem and how this environment will interact with the spacecraft. The effect that the space plasma will have on the charge-exchange plasma will also be addressed.

In order to describe the thruster produced environment, the various ion species emitted by a thruster are described. To distinguish the various ion species emitted by an ion thruster the notation of group I, group II, group III, and group IV ions was introduced.[1] The group I ions are those of the primary beam which travel downstream within a cone that has a small divergence. They are accelerated by the total potential difference between the bombardment discharge and the neutralized thrust beam. Group II ions are energetic ions that leave a thruster at angles up to nearly 90 degrees to the beam axis.[1] They are formed by charge-exchange between the screen and accelerator grids of the thruster optics. The group III ions are charge-exchange ions that are formed just downstream of the accelerator grid. These ions are drawn back into the acceleration grid by its negative potential. This produces a sputtered efflux from the accelerator optics that is somewhat more peaked (in the downstream direction) than a cosine distribution.[2-5] The neutrals which leave the thruster do so in approximately a cosine distribution.[6] All of the preceding effluxes are essentially limited to line-of-sight trajectories from the ion optics of the thruster.

Two other efflux categories, the group IV ions, are not limited to line-of-sight trajectories, and therefore can pose special spacecraft contamination problems. These effluxes are the low-energy mercury and molybdenum charge-exchange ions that are generated downstream of a thruster.[6,7] Because these effluxes are low energy ions, the trajectories can depart substantially from straight lines due to only moderate electric fields. The natural tendency is

for less dense regions of the charge-exchange plasma to be negative relative to the dense regions, so that ion trajectories are bent from the more dense to the less dense regions. As a result, the entire volume around a spacecraft becomes filled with charge-exchange plasma, with the density of this plasma depending on the ease of access from the region of generation downstream of a thruster. The charge-exchange plasma is macroscopically neutral so that everywhere electron density equals ion density.

The propagation of a charge-exchange plasma from a thruster has been the subject of study[8-10] due to the possible interactions with spacecraft. Further study of this propagation is expected. This report is intended as a summary of the present understanding of this propagation, interaction effects thereof, and possible verification experiments. The limitations of this present understanding will also be given, where possible. The calculations presented in this report will be limited to mercury propellant and molybdenum grid material, although the process with other materials would be expected to differ mostly due to different cross sections and yield coefficients. All equations presented herein are in SI (mks) units unless otherwise stated.

B. MERCURY CHARGE-EXCHANGE MODEL

The Hg charge-exchange model presented here is essentially the same as one presented in a previous publication.[10] The assumed point of origin for the Hg charge-exchange plasma is indicated in Fig. 1. For a single thruster, this point is one thruster radius, r_t, downstream of the ion optics and on the thruster centerline, as indicated in Fig. 1(a). This point was selected because it gave the best correlation of experimental data from several tests.

For a circular array of thrusters, the effective point of origin would be expected to be one radius of the thruster array, r_t' (see Fig. 1(b)), downstream of the center of the array. For a noncircular array, the effective origin would be expected to be downstream of the center of the array, between half the maximum array dimension and half the minimum array dimension. A noncircular array would also be expected to cause some departures from axial symmetry in the distribution of Hg charge-exchange plasma. But, because Hg charge-exchange measurements have not been made with thruster arrays, the exact extent of these departures from axial symmetry is not known.

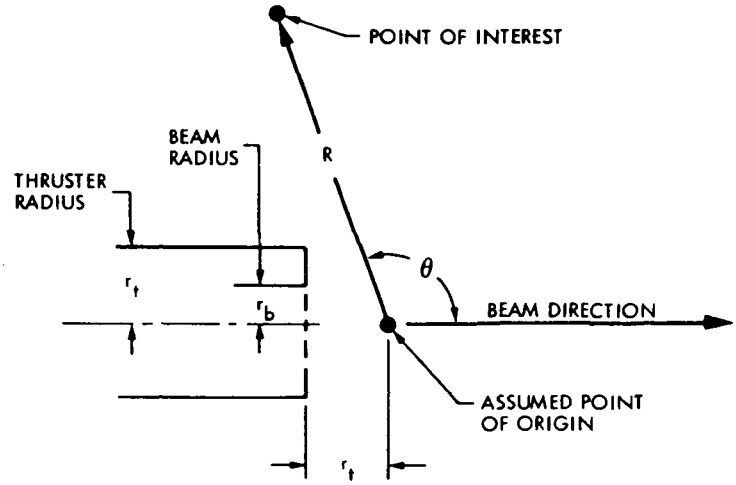

(a) SINGLE THRUSTER

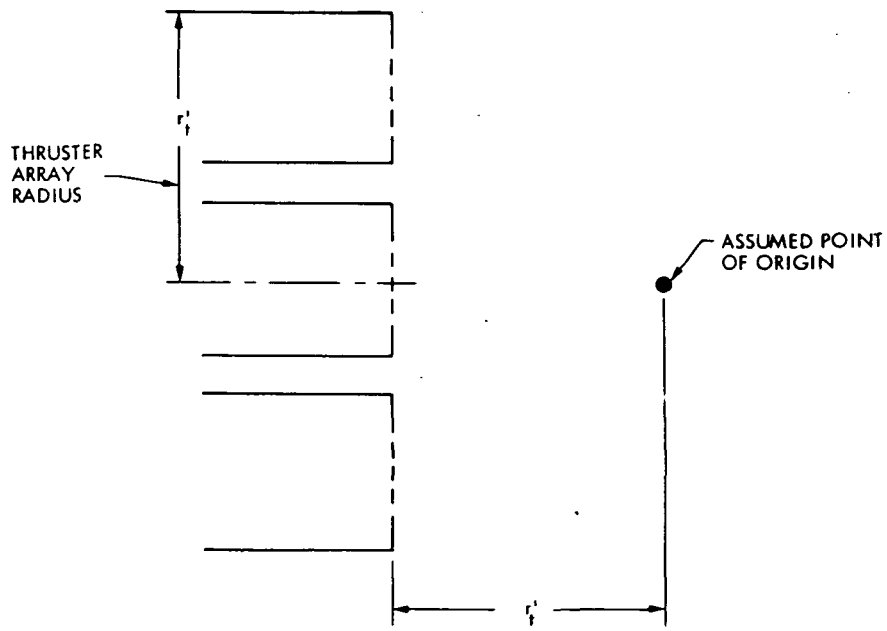

(b) THRUSTER ARRAY

Figure 1. Parameters for Calculation of Charge-Exchange Plasma Generated by Thruster.

To calculate the electron density and saturation electron current density, select parameter values from Tables I and II for the angle θ (see Fig. 1) of interest and substitute in the equations below:

$$n_e = [J_b^2(1 - \eta_u)/r_b R^2 \eta_u][\text{Table I Param.}],\ m^{-3} \quad (1)$$

$$j_e = [J_b^2(1 - \eta_u)/r_b R^2 \eta_u][\text{Table II Param.}],\ Am^{-2} \quad (2)$$

Table I. Electron Density Parameter as a Function of Angle from a Beam Direction

θ, Deg.	Parameter	θ, Deg.	Parameter
90	2.5×10^{12}	140	3.2×10^{11}
100	1.8×10^{12}	150	1.9×10^{11}
110	1.2×10^{12}	160	1.1×10^{11}
120	8.2×10^{11}	170	6.7×10^{10}
130	5.1×10^{11}	180	3.8×10^{10}

Table II. Electron Current Density Parameter as a Function of Angle From Beam Direction

θ, Deg.	Parameter	θ, Deg.	Parameter
90	0.12	140	0.017
100	0.091	150	0.011
110	0.064	160	0.0059
120	0.044	170	0.0034
130	0.028	180	0.0022

The beam current, J_b, is in amperes (A). It is the total current such that if a beam is produced by six thrusters each operating at 2A, J_b will be 12A. The propellant utilization, η_u, is a dimensionless quantity which can be expected to

be ~0.9. The beam radius, r_b, and the radius R are defined by Fig. 1. Both are measured in meters.

Tables I and II represent the mean values of experimental data. The upstream hemisphere (90-180 deg. from beam direction) is the region of most interest. In this hemisphere the data ranged upwards and downwards from the values used for Tables I and II by about a factor of two.

For electron density, the electron temperature is also a consideration. The production rate of charge-exchange ions is independent of electron temperature, but the velocity of departure for these ions varies as the square-root of electron temperature. To the first approximation, then, ion (and electron) density will vary inversely as the square-root of electron temperature. From available data, the electron temperature in the charge-exchange plasma around the thruster is about half of the electron temperature in the ion beam. The data used for Tables I and II had electron temperatures in the charge-exchange plasma of 2.5 and 3.5 eV. These values are believed representative of 5-15 cm Hg ion thrusters. The electron temperature within a 30-cm Hg thruster beam was found to be 0.35 eV.[11] Including the factor of two lower electron temperature in the charge-exchange plasma, a 30-cm thruster would be expected to have about a factor of four higher electron density than given by Eq. (1) with the parameter values listed in Table I.

The scaling of electron density inversely as the square-root of electron temperature, as described above, is actually of limited accuracy. Another consideration is the directed neutral velocity before charge exchange. Because the neutral temperature varies only slightly between different sizes of thrusters, this initial velocity is much more significant where electron temperatures are small. We do not know the magnitude of this effect, but we do know its direction. The initial downstream neutral velocity of charge-exchange ions will bias their distribution towards the downstream direction, thus reducing their density in the upstream hemisphere. Because of the smaller plasma electron energy in large thrusters, this effect will be most noticeable in such thrusters. The additional effect of neutral velocity, beyond the density varying inversely as the square-root of electron temperature, should make the actual electron density lower than the calculated values for 30-cm thrusters in the upstream hemisphere. At present, the magnitude of the reduction is not known.

Electron temperature is not as important for the saturation electron current density. Except for the bias due to initial neutral velocity, the effects of electron temperature cancel for electron current density.

The ion arrival rate is closely related to the saturation electron current. The ion velocity can be closely approximated by the Bohm, or ion acoustic, velocity based on electron temperature in the ion beam.[8,9] The electron velocity is, of course, a Maxwellian distribution corresponding to the temperature in the charge-exchange plasma. For a surface normal to the local ion velocity, the ratio of ion current to electron saturation current is

$$j_i/j_e = 2\sqrt{\pi m_e/m_i} = 5.9 \times 10^{-3}. \tag{3}$$

It should be kept in mind that the ion velocity is substantially directed, while that of the electrons is isotropic. With this limitation in mind, Eq. (3) can be used to obtain ion current densities from Eq. (2). For convenience the following extension to Eq. (3) gives the time (t) in seconds for a monolayer to form. This is assuming that the surface is cold enough to condense all the mercury arriving there. Also, the theory does not allow for geometrical considerations such as shielding. Shielding may act to reduce the arrival rate but the charge-exchange plasma will be able to flow around obstructions.

$$t = 3.3 \times 10^{2}/j_e \tag{3a}$$

1. Sample Calculation for Spacecraft

A sample calculation, using the charge-exchange plasma model described, is performed to illustrate the variation in plasma and current densities around a typical spacecraft. The spacecraft has an assumed configuration which utilizes eight 30-cm thrusters[12] arranged in two parallel rows of four each. Each row of four has center-to-center spacings of 76 cm, while the center-to-center spacing between the two rows of four is 51 cm. The two solar array panels extend radially outwards from the axis of the spacecraft, with the inside end of the panels starting 254 cm from the spacecraft centerline and 432 cm upstream of the thruster exhaust plane.

The calculation procedure used is that described above. Seven of the eight thrusters are assumed to be operating at a beam current of 2A each with a propellant utilization of 0.9. The other thruster is not operating. Although the nominal diameter is 30 cm for these thrusters, the actual beam diameter is closer to 28 cm.

The charge-exchange plasma is assumed to have an electron temperature equal to half the measured ion-beam electron temperature (from single thruster tests) of 0.35 eV. This lower electron temperature, compared to the data used for Tables I and II, should result in an electron density increase of about $20^{\frac{1}{2}}$. As mentioned above, there is no similar correction for the current density parameter. Another assumption concerns the point of origin for the charge-exchange plasma.

For the non-circular thruster array of this spacecraft, the total array area is equivalent to a circle with a radius of 0.885 m. The effective origin of the charge-exchange plasma is assumed to be 0.885 m downstream of the center of the thruster array. Some nonsymmetry of the charge-exchange plasma about the thrust axis is expected to result from the nonsymmetrical distribution of thrusters, but the charge-exchange plasma will tend to redistribute itself so as to reduce this effect. The maximum increase in electron density or electron current is therefore estimated at less than a factor of two for a distance of one meter or more from the thruster array. (This factor increases the overall uncertainty to about a factor of four.)

The plasma properties at the centerline of the solar array were calculated as a function of distance from the inboard end of the solar array and plotted in Fig. 2. The combined effects of radial distance, R, and angle, θ, give maximum electron density and current density near, but not at, the inboard end of each solar array. For the assumed dimensions of 3.8 m x 44.3 m for each array, the integrated total of the current density shown in Fig. 3 is 1.7 A for both arrays. This current includes no increase in effective array size due to sheath thickness. The electron density ranges from about 1 to 12 x 10^{11} m^{-3}, which, at 0.175 eV, corresponds to a range from 3 mm to 1 cm in Debye distance. For a solar array that is 400 V positive of the surrounding plasma, for example, the total sheath thickness would range from about 20 to 60 cm. The effect of sheath thickness can clearly be significant, but will not change the qualitative effects shown in Fig. 3.

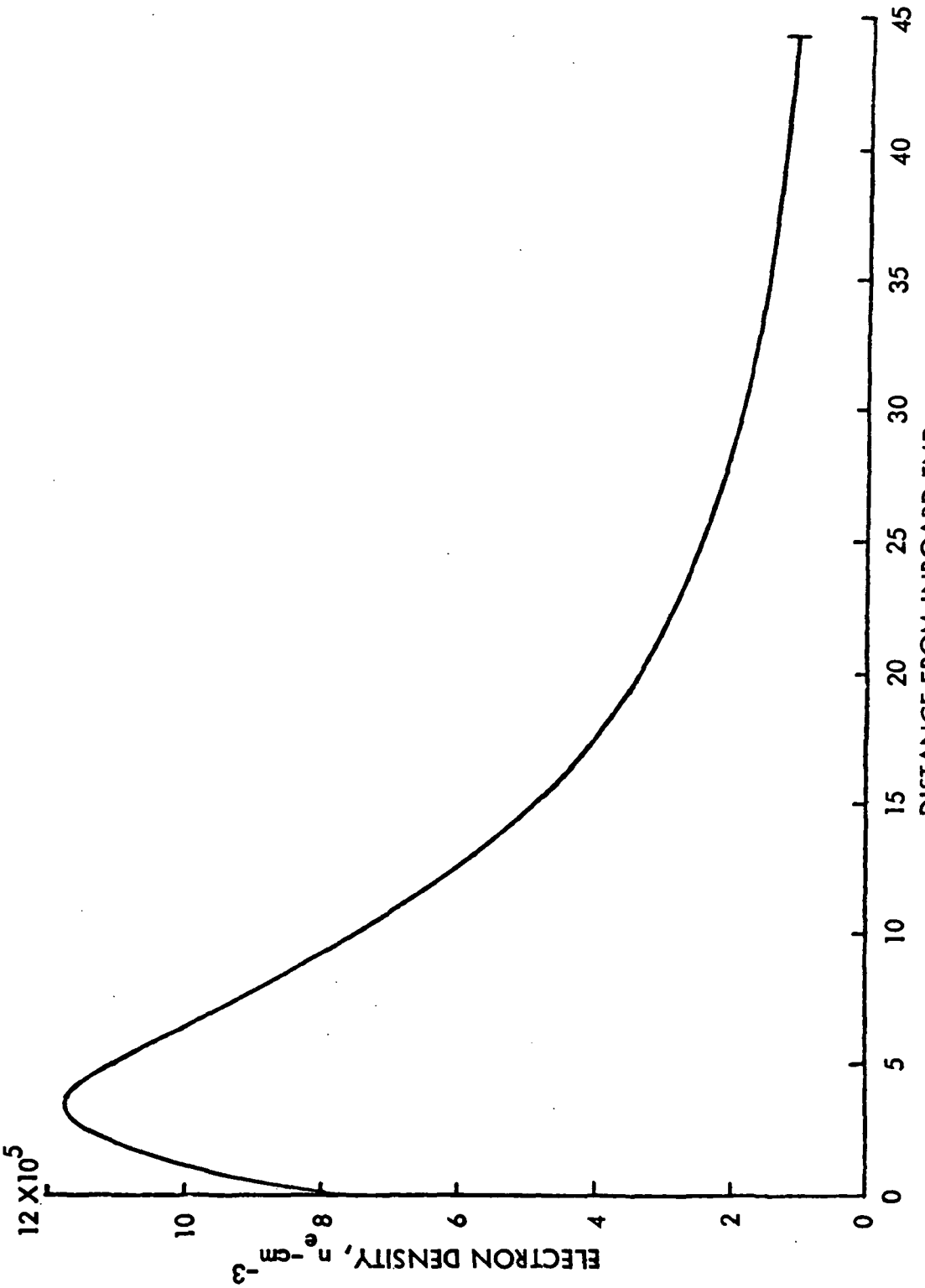

Figure 2. Electron Density Along Centerline of Solar Array

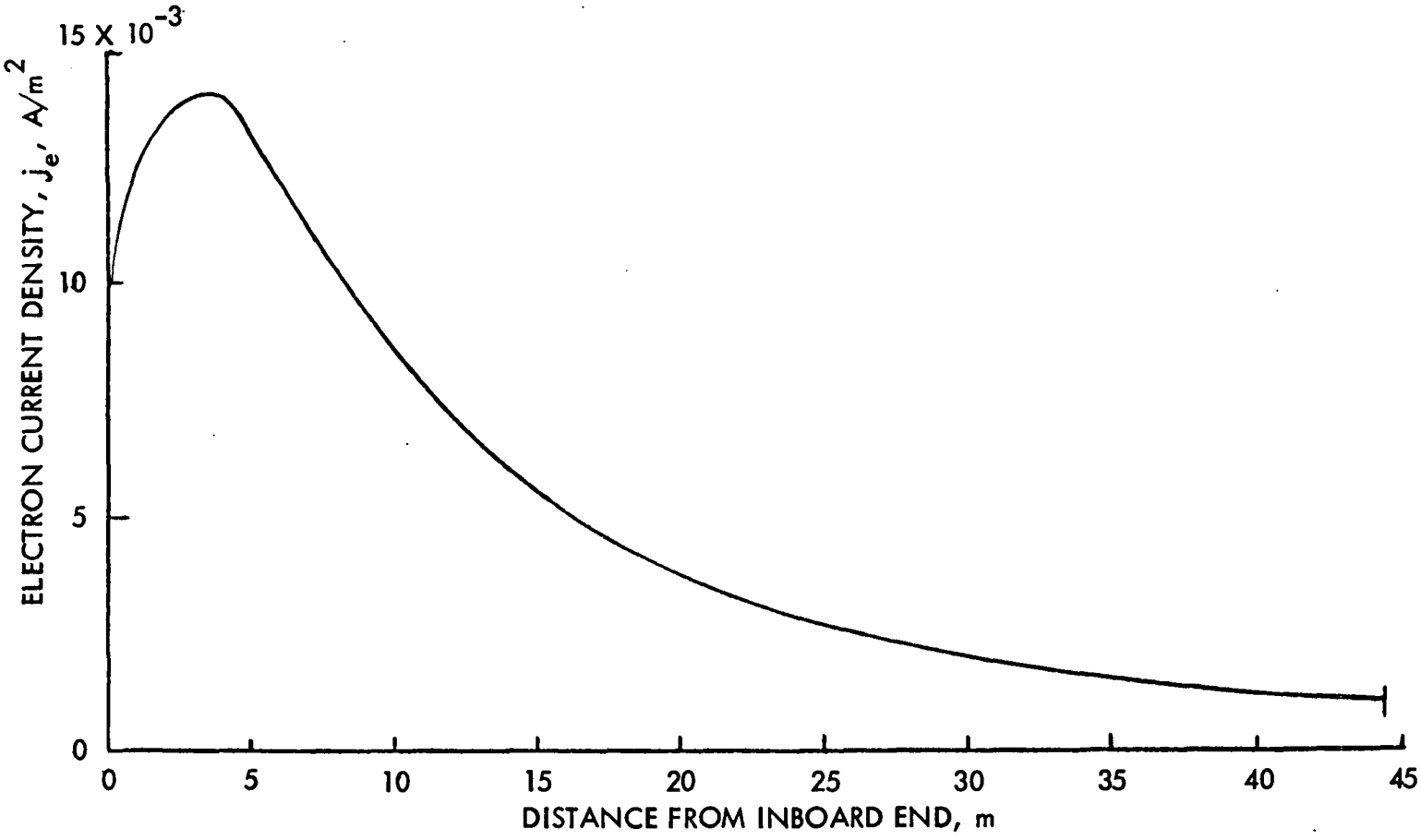

Figure 3. Saturation Electron Current Density Along Centerline of Solar Array

The locations on the spacecraft correspond to wide ranges of both radial distance, R, and angle from beam direction, θ. Two dimensional plots of electron density and saturation electron current density are shown in Figs. 4 and 5. Both plan and side views of the assumed spacecraft are shown in each of these figures. The assumed point of origin for the charge-exchange plasma is indicated in Figs. 4 and 5 and is, as was mentioned previously, 0.885 m downstream of the center of the thruster-array exhaust plane. As shown in Fig. 4, the expected electron density can range from about 10^5 to 10^7 cm^{-3}. In Fig. 5, the saturation electron current density is shown to range from 1 to 100 mA/m^2. From Fig. 5 and Eq. (3) the corresponding arrival rate of Hg ions would range from 6 to 600 $\mu A/m^2$. Figure 6 shows the arrival rate of Hg in terms of monolayer formation. One monolayer of mercury is $\sim$2.9Å.

As mentioned, seven operating thrusters were assumed for the calculations whose results are shown in Figs. 2 through 6. For fewer thrusters or less than rated operating conditions, both the electron densities and the electron and ion current densities would have to be reduced. For fewer operating thrusters, these parameters should be reduced in proportion to the number of thrusters. For less than rated conditions, the plasma parameters would be proportional to $J_b^2(1 - \eta_u)/\eta_u$. For the usual throttled operation near the discharge-performance "knee", $J_b^2(1 - \eta_u)/\eta_u$ will be nearly proportional to J_b.

The orientation of a surface relative to the propagation of the charge-exchange plasma will influence the density and arrival rates observed at the surface. Some reduction of these parameters would be expected for more protected surface orientations and surfaces that are locally shielded by parts of the spacecraft. Because of the proven capability of a charge-exchange plasma to flow around corners, the amount of this reduction cannot be estimated at the present time.

A variety of devices has been suggested and tried for diverting or collecting the charge-exchange plasma. Shields near the thruster can displace or divert the charge exchange plasma, but do not appear to significantly reduce the number of charge-exchange ions that escape to the surrounding volume,[9] presumably because electric fields do not extend far into the plasma. Positive surfaces will repel charge-exchange ions, but the large electron currents also collected will usually make this approach impractical. Insulated surfaces will draw equal numbers of electrons and ions, which means that all of the arriving ions will be collected

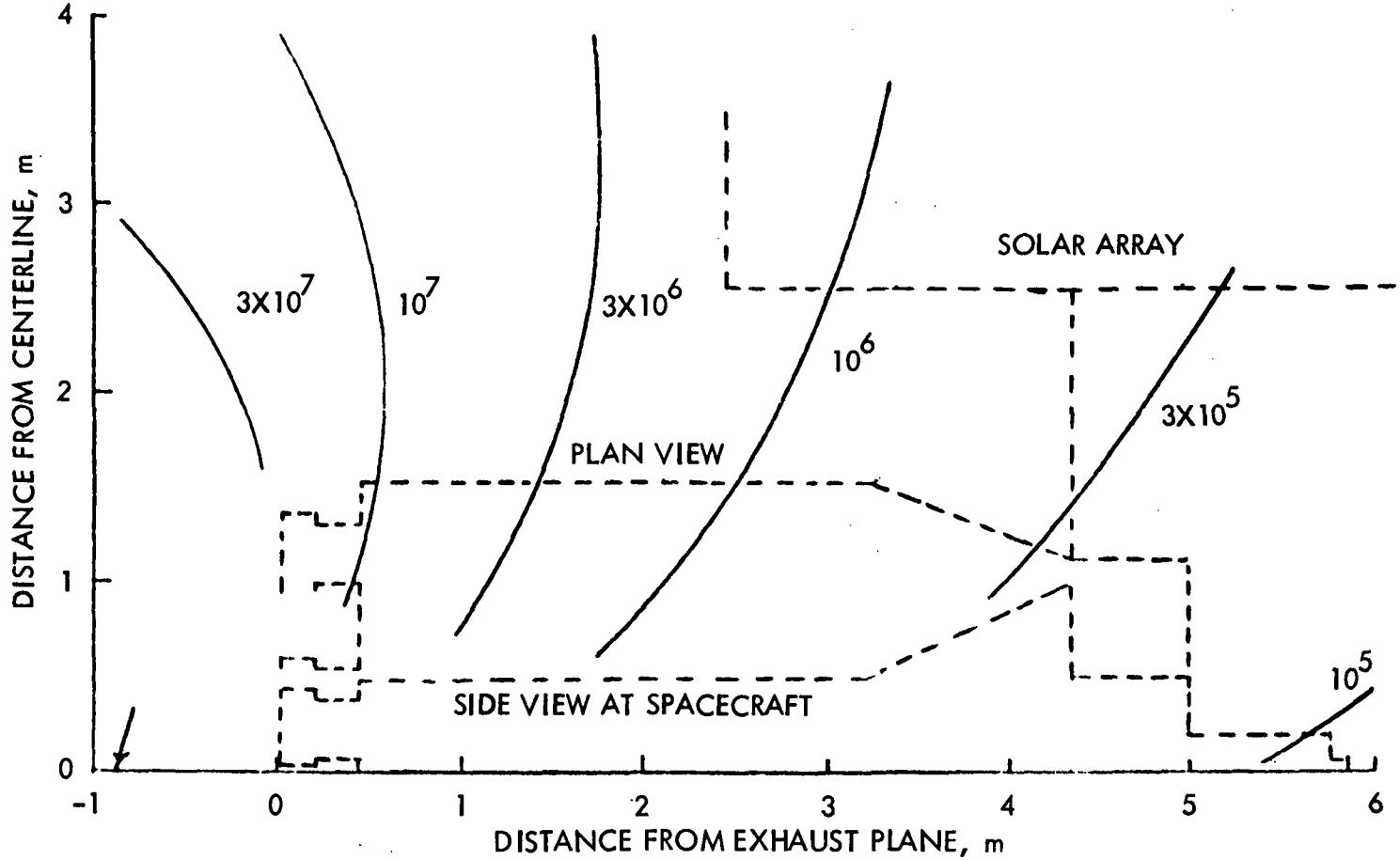

Figure 4. Electron Density, n_e, cm^{-3}, for Assumed Spacecraft Configuration

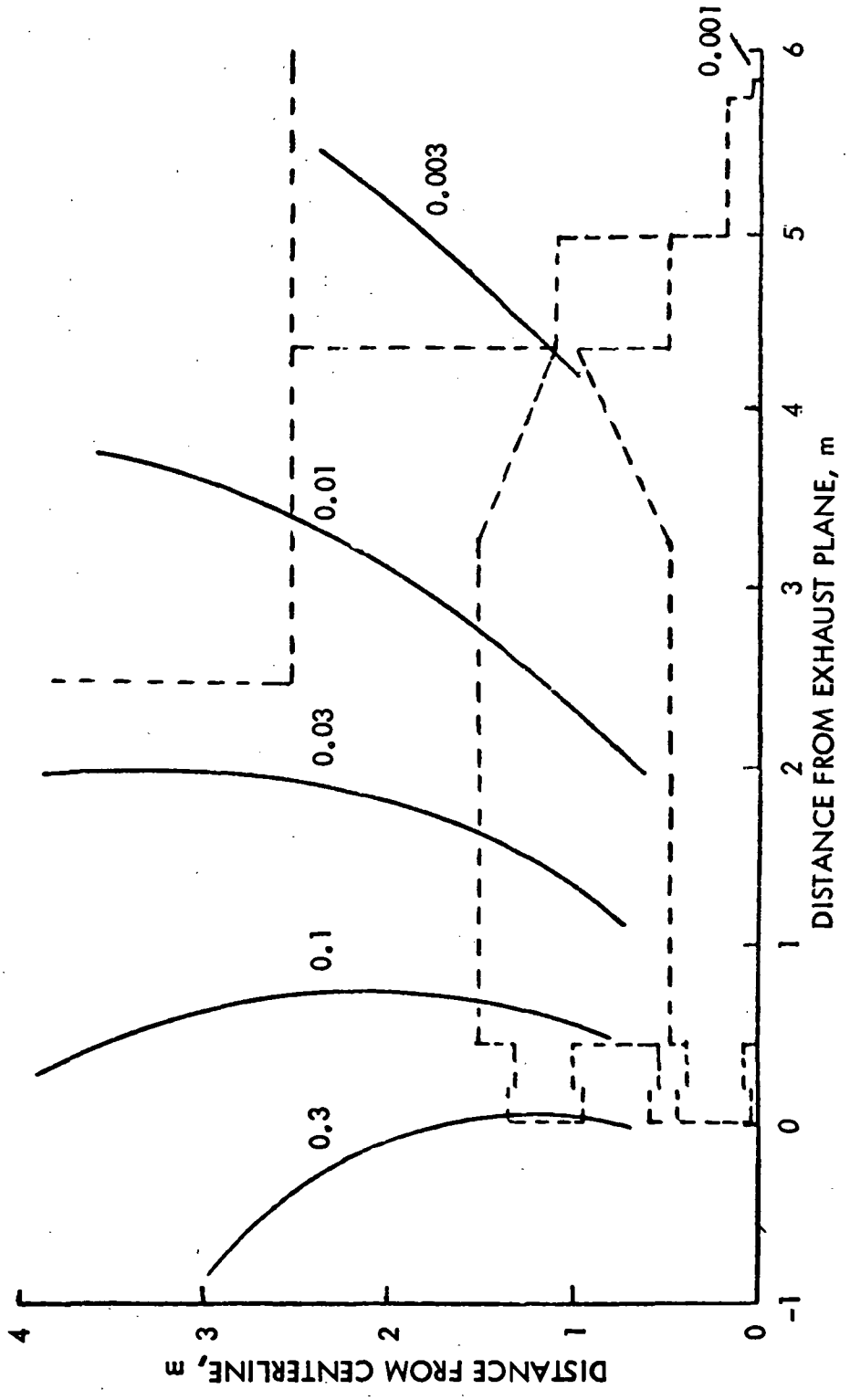

Figure 5. Saturation Electron Current Density, A/m^2, for Assumed Spacecraft Configuration

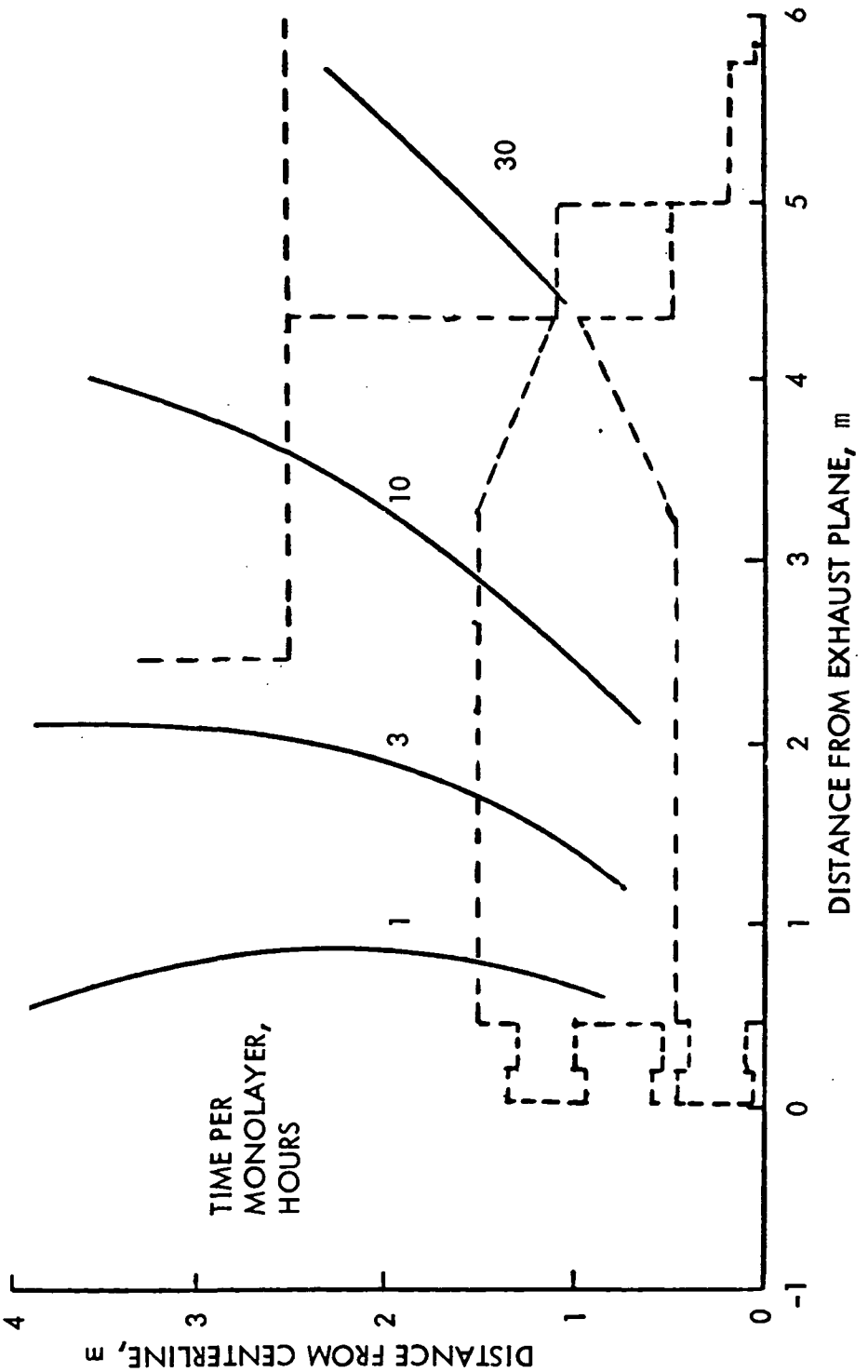

Figure 6. Arrival Rate of Hg^+, Expressed as Time for Monolayer (Sticking Depends on Surface Conditions)

and most of the electrons will be reflected. Negative surfaces will reflect electrons and collect only ions, but this effect appears to be of little value in significantly reducing the upstream flow of the charge-exchange plasma.

2. Discussion of Sample Calculation

The amount of electron current collected by a positive and exposed solar-cell array is one of the significant results of the calculation presented above. A high voltage array would be more seriously affected by a fixed level of electron current collection, so the results are also voltage dependent. For a 400 V array, for example, the 1.7 A electron current would correspond to a maximum loss of ~680 watts. If there is a significant variation in voltage along the length of the array, this loss can be reduced by placing the high voltage end of the array at the outboard end, where the electron current density is smallest. This approximation assumes there are exposed conducting paths for the electrons to be drawn from the charge-exchange plasma.

The arrival rate of electrons is a maximum of 14 mA/m^2 on the solar array (see Fig. 3). By Eq. (3a), this arrival rate corresponds to a monolayer buildup of mercury at that position in about 6 hours. A 1000 Å layer with near zero transmittance will be deposited in about 83 days. Significant effects are likely to occur with layers less than 1000 Å. From experience with mercury vapor, we know that no accumulation occurs when the surface involved is above the evaporation temperature for that rate. There are still two reasons to be concerned though. If the surface should fall below this temperature, an accumulation will occur that will require a considerable excess of temperature to evaporate again. This could very likely be the case for the exterior of the sun-shaded sides of thermal blankets, passive radiators, and other spacecraft surfaces. Once the mercury is accumulated, it may be difficult to evaporate away. This is because mercury evaporation can be orders of magnitude below equilibrium values when the surface is less than very clean and the temperature is below roughly 100°C.

A less clear aspect of possible Hg accumulation is that the arriving Hg is ionized and is probably arriving with several eV of energy. Because 1 eV corresponds to 11,600°K, we should not be too hasty in assuming that no damage will occur.

3. Limitations of Model Accuracy

Most of the limitations associated with the Hg charge-exchange model and calculation have been mentioned earlier. They will be summarized here for completeness.

The model was obtained from tests of rather simple configurations, hence is not suited to estimating the effects of nonsymmetrical thruster arrays and complicated spacecraft shapes. Even the effects of surface orientation are not fully understood.

The electron temperature in the charge-exchange plasma is an important, but only partially evaluated parameter. We know that smaller thrusters tend to have higher temperatures in this plasma, but we do not know if arrays of thrusters will depart from the values obtained with single thrusters. We also know that initial neutral velocity will be more important at small electron temperatures, resulting in a bias of charge-exchange ion trajectories in the downstream direction. The magnitude of this bias, though, has not been evaluated.

Finally, there is an electron temperature effect that has not been mentioned. The space environment includes a plasma. The electrons of this space plasma will interact with the electrons of the charge-exchange plasma, possibly resulting in a different electron temperature than obtained in ground tests. This effect will be discussed in the section, Electron Temperature in Space.

The uncertainties that now exist in the model are summarized in Fig. 7.

C. MOLYBDENUM CHARGE-EXCHANGE MODEL

As mentioned in the introduction, a small fraction of the Mo atoms that are sputtered from the accelerator grid charge exchange with beam Hg ions downstream of the thruster. These Mo charge-exchange ions share the ability of Hg charge-exchange ions to flow around obstacles. As will be shown, the rate of production of Mo ions is very low compared to that of Hg ions. It is therefore difficult to make an experimental evaluation of Mo ions. At this time, only a simple theoretical analysis can be presented, based on the Hg charge-exchange model presented previously.

Thrusters		Simulated Spacecraft	Test Location	T_c,CV	Uncertainty Factor		
No.	Size				T_e	η_e	j_e
1	5-15 cm		Ground	2.5-3.5	2X	2X	2X
1	30 cm		Ground	0.1-0.2	2X	∿4X	∿2X
7	30 cm	Simple	Ground	0.1-0.2	∿2X	∿8X	∿4X
7	30 cm	Simple	Space	0.1-20*	∿4X	∿10X	∿6X
7	30 cm	Complex	Space	0.1-20*	Larger than above		

*Dependent on charge-exchange and space plasmas' densities and temperatures

Figure 7. Estimates of Uncertainties

The approach used is to compare the production rates of Hg and Mo charge-exchange ions. The Mo ions are assumed to be distributed in the same manner as the Hg ions, but lower by a factor corresponding to the lower production rate. This approach ignores the much higher initial velocities of the Mo neutrals. These higher velocities will result in a bias of trajectories in the downstream direction. The arrival rates of Mo ions in the upstream hemisphere should, due to this effect, be less than calculated.

The production rate of Hg charge-exchange ions is

$$\dot{N}_{ce} = \frac{2J_b^2(1 - \eta_u)\sigma}{\pi r_b \eta_u q^2 \bar{v}_o} , \tag{4}$$

where q is the electronic charge, $\bar{v}_o$ is the average neutral velocity before charge exchange, σ is the charge-exchange cross section, and the other parameters are the same as defined earlier. A similar production rate for Mo charge exchange ions is

$$\dot{N}_{ce,Mo} = \frac{2F_a J_b^2 Y \sigma}{\pi r_b q^2 \bar{v}_o} , \tag{5}$$

where, in addition to previously defined variables, F_a is the ratio of accelerator impingement current to beam current, and Y is the sputter yield in atoms/ion.

The ratio of Mo to Hg charge-exchange rates is obtained by dividing Eq. (5) by Eq. (4). With the use of Hg and Mo subscripts where appropriate, this ratio is

$$\frac{\dot{N}_{ce,Mo}}{\dot{N}_{ce,Hg}} = \frac{F_a Y \eta_u \sigma_{Mo} \bar{v}_{o,Hg}}{(1 - \eta_u)\, \sigma_{Hg} \bar{v}_{o,Mo}} . \tag{6}$$

For the 30-cm thruster, the value of F_a is about 0.0025,[12] the value of Y for 1000 eV Hg ions is approximately 1.0,[13] $\sigma_{Mo}(Hg^+ + Mo \rightarrow Hg + Mo^+)$ is about 1×10^{-19} m^2,[14] $\sigma_{Hg}(Hg^+ + Hg \rightarrow Hg + Hg^+)$ is about 6×10^{-19} m^2,[15-17] $\bar{v}_{o,Mo}$ is

about 7×10^3 m/sec,[18] $v_{o,Hg}$ is about 230 m/sec (500°K), and η_u is again 0.9. With these substitutions, Eq. (6) becomes

$$\dot{N}_{ce,Mo}/\dot{N}_{ce,Hg} = 1.2 \times 10^{-4} \tag{7}$$

The uncertainty in this calculation is due to the uncertainty of distribution and yield of sputtered Mo for an operating thruster, the uncertainty of mean neutral velocity (the datum used here was for Kr^+ on Mo), the uncertainty in bombarding ion energy, and the additional bias on Mo ion trajectories due to the initial high neutral energies. All of these additional uncertainties beyond those of charge-exchange Hg are estimated to raise the factor of uncertainty from four for Hg ions to ten for Mo ions.

Equations (3) and (7), together with the electronic charge, can be used to translate the electron current density of Fig. (5) to Mo ion arrival rate per unit area. The ratio is

$$\dot{N}_{Mo}/A = 4.4 \times 10^{12}\ j_e,\ N_{Mo} \cdot m^{-2} - sec^{-1} \tag{8}$$

This ratio was used to obtain Fig. 8.

A monolayer (2.5 Å) of Mo atoms is about $1.6 \times 10^{19}/m^2$ (as compared to about $1.2 \times 10^{19}/m^2$ (2.9 Å) for Hg). For the region of the solar array with the maximum of 14 mA/m^2 of electron current, then, a monolayer would be expected to take 72,000 hours. Even with a factor of 10 increase in rate due to the estimated inaccuracy of the calculations, it would take over a year for a monolayer to form.

In situ measurements of transmittance have been made using films of the sputtered efflux from thrusters (mostly Mo).[5] These films were primarily from deposition of neutrals, rather than the charge-exchange Mo ions considered in this section. These results, however, should give an indication of the deposition effects to be expected. The total transmittance was not linear with time. It ranged from about 0.75 at 30 Å thickness, to about 0.50 at 100 Å, to about 0 at 1000 Å. It appears, though, that assuming a linear variation is conservative below 30 Å thickness. A monolayer of Mo should give about a 2.5 percent reduction in transmittance.

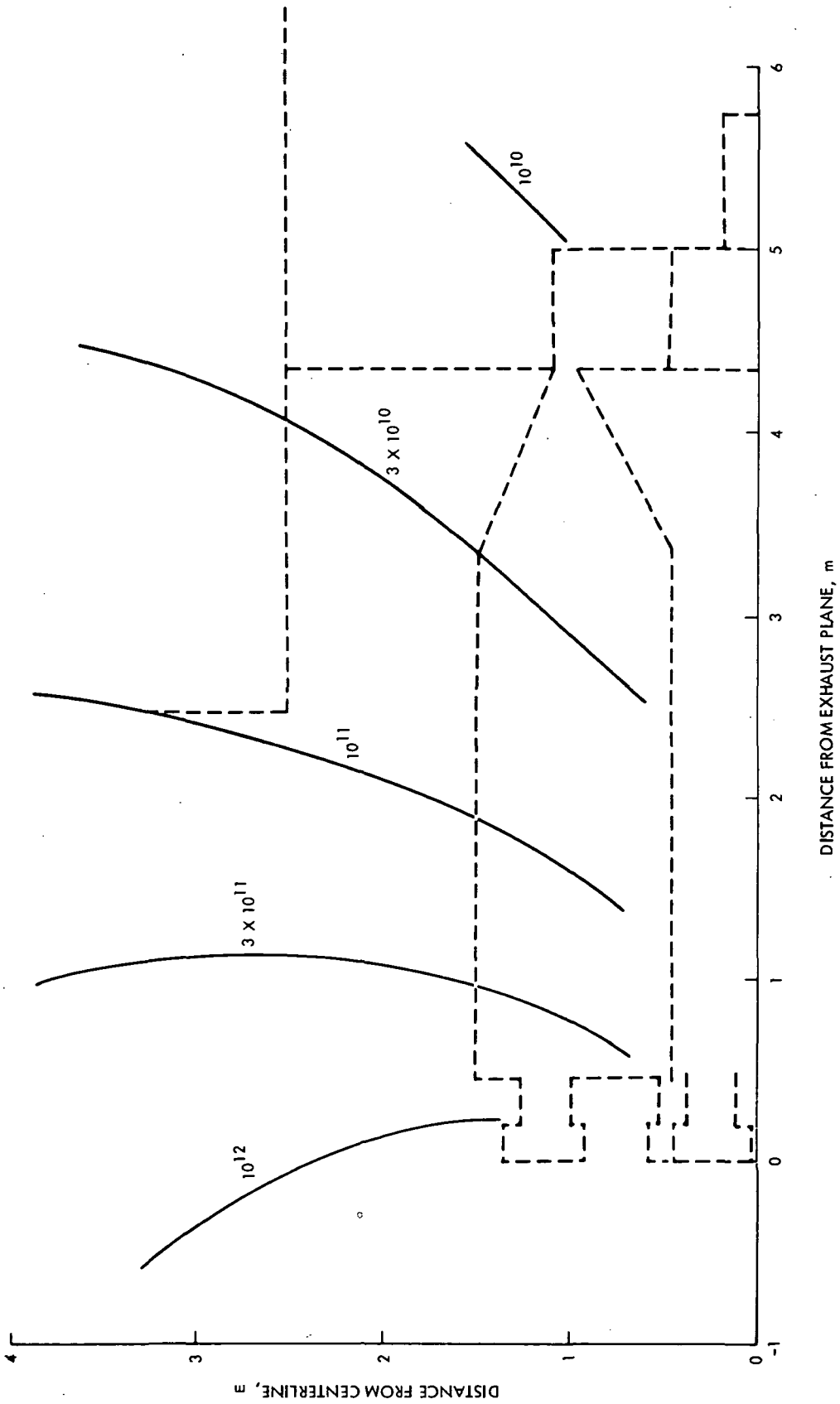

Figure 8. M_o^+ Arrival Rate, No/m^2-sec

For the worst case (ten times the predicted rate) at the worst location on the solar array, over 1 year of operation with 7 thrusters would be required to give a 2.5 percent loss in transmittance. Because other locations should be less affected, it appears that Mo deposition on the solar array will not be a significant problem for the configuration studied. A much closer location to the thruster, though, could cause problems.

The major consideration for Mo deposition (in the upstream hemisphere) appears to be sensitive instruments, optical or otherwise, that will be adversely affected by 10 to 100 percent of a monolayer. A monolayer on solar cell surfaces with a normal emissivity (ε) of 0.85 will produce $\varepsilon \sim 0.7$.[19] Molybdenum deposition could have an effect on thermal surfaces such as passive radiators used to cool instrument components.

D. CHARGE-EXCHANGE MEASUREMENTS IN GROUND TESTS

1. Mercury

The Hg ions make up the bulk of the charge-exchange plasma. Measurements of this plasma density (with Langmuir probes) will therefore give a close indication of the density of Hg ions. As described in the experimental studies,[8-10] the ions should be collected by negative boundaries, so reflection will not be a limitation on measurements. In fact, plasmas generally assume a potential more positive than surrounding surfaces, so that the proper negative wall bias is automatically attained. The only exception is for regions of very low density so that the total electron currents to boundaries associated with such regions is still quite small. Under these conditions the local plasma potential will be governed by wall potential. A moderate additional wall bias (relative to the beam target) will avoid problems in the very low density regions.

Some additional calculations or measurements are desirable to make sure that most of the charge-exchange ions are generated immediately downstream of the thruster(s), rather than from the background neutral density all along the beam(s). To meet this latter requirement simply requires a low enough facility background pressure.

The measurement of Hg charge-exchange effects is thus readily accomplished in ground tests.

2. Molybdenum

The measurement of Mo charge exchange ions poses much more difficult problems. One major problem is the background level of sputtered Mo atoms. To show the magnitude of this problem, it is necessary to go through a simple analysis.

The loss rate of sputtered Mo atoms from the accelerator grid is

$$\dot{N}_o' = F_a J_b Y/q \tag{9}$$

where all the parameters are defined the same as previously. This rate is probably an upper limit for Mo atoms in the downstream direction in that not all accelerator grid impingement is on the downstream side.

Assuming a frozen Hg target in the ground facility to minimize contamination with other sputtered material, the arrival rate of Mo atoms at this target is due to an approximately cosine distribution from the accelerator grid. Sputter pits will develop (midway between each group of three adjacent holes) on the downstream side of the accelerator grid. As this occurs, the distribution will depart from a cosine, but the departure will primarily be restricted to large angles from the beam direction. The rate of Mo arriving at the target should be nearly unchanged by these pits. The cosine distribution corresponds to a uniform arrival rate at the sphere shown in Fig. 9. The effective diameter of the beam at the target is d_t, with a corresponding area of A_t. This diameter is best determined experimentally, using the diameter over which the frozen Hg experiences net sputtering. Outside of this diameter the sputtered Mo will tend to be trapped within the condensing Hg vapor. From geometrical considerations, (Fig. 9), the fraction of sputtered Mo atoms that will be resputtered from the target is approximately the solid angle $A_t/(\ell_t/2)^2$ divided by the total sphere solid angle of 4π. The resputtered fraction is thus

$$F_{rs} = A_t/\pi\ell_t^2. \tag{10}$$

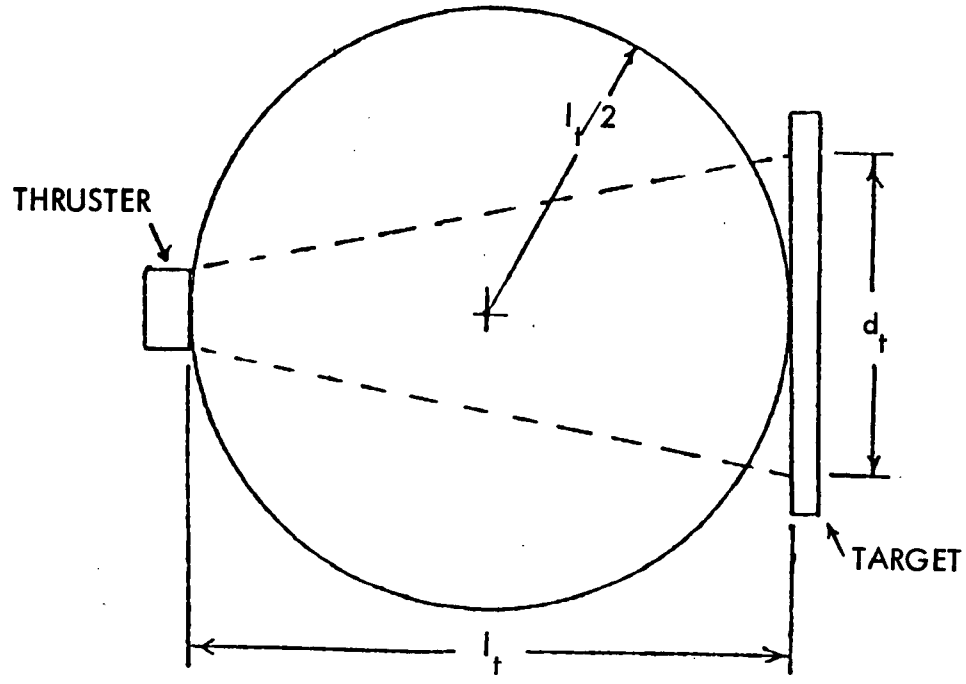

Figure 9. Thruster and Frozen Mercury Target in Ground Facility

A similar fraction can be determined for the fraction of resputtered Mo atoms that arrive at a sample coupon. Assuming that this coupon is in the plane of the accelerator system and at a radius R from the thruster, with $R<<\ell_t$,

$$F_c = A_c/\pi\ell_t^2 \quad . \tag{11}$$

Multiplying Eqs. (9) through (11) to obtain the arrival rate of neutral atoms at the coupon area A_c,

$$\dot{N}_{o,c} = F_a J_b Y A_c A_t/\pi^2 q \ell_t^4 \quad . \tag{12}$$

This rate can be compared to the arrival rate of charge-exchange Mo ions at the same location, using the preceding Mo model. From Eqs. (2), (3), and (6), together with the Table II parameter for 90 deg.,

$$\dot{N}_{ce,c} = 7.1 \times 10^{-4} A_c F_a J_n^2 Y \sigma_{Mo} \bar{v}_{o,Hg}/q r_b R^2 \sigma_{Hg} \bar{v}_{o,Mo} \quad . \tag{13}$$

The neutral Mo to charge-exchange Mo arrival rate ratio is Eq. (12) divided by Eq. (13),

$$\dot{N}_{o,c}/\dot{N}_{ce,c} = 140\ A_t r_b R^2 \sigma_{Hg} \bar{v}_{o,Mo}/\ell_t^4 J_b \sigma_{Mo} \bar{v}_{o,Hg} \quad . \tag{14}$$

Assume a 30-cm thruster, so that J_b is 2A and r_b is 0.14 m. For the other values we will assume 3.5 m for ℓ_t, 3.6 m^2 for A_t (±15 deg.), 0.5 m for R, and previously used values for q, σ_{Hg}, σ_{Mo}, $\bar{v}_{o,Hg}$, and $\bar{v}_{o,Mo}$. With these substitutions, Eq. (14) becomes

$$\dot{N}_{o,c}/N_{ce,c} = 21. \tag{15}$$

The Mo neutrals come from the target from the general downstream direction, while the Mo charge-exchange ions are generally moving radially outwards, so some separation can be made by using the proper angle and shielding for the coupon area, A_c. With a "noise" level 21 times the "signal" level, though, it may be still difficult to separate out the Mo charge-exchange rate by deposition. Also, although resputtered Mo atoms will have a "sticking" coefficient near unity, it will still be less than unity. A small percentage of Mo atoms reflected from the walls of the vacuum facility will add a nearly isotropic component that will be hard to shield.

Detection of Mo ions is a possible alternative, but this will require momentum analysis to discriminate from the nearly 10^4 times higher background of Hg charge-exchange ions (Eq. (7)). Also the rate of Mo ions is small in absolute terms. For the location used above for comparison of neutral and charged Mo, the current of Mo ions through a 1 cm^2 aperture (which is large for most momentum analysis) is only 10^{-10} A.

In summary, then, experimental detection of Mo charge-exchange ions is difficult in a ground test.

E. ELECTRON TEMPERATURE IN SPACE

The charge-exchange plasma in a ground facility fills, with varying degrees of density, the entire facility volume. The electrons in this plasma have long mean free paths, so that with sufficient energy they can pass through any part of the available volume. The electrons in both the beam and the charge-exchange plasma travel much faster than the ions. Current neutrality will therefore require, on the average, a number of electrons to be reflected at the boundaries for each one that escapes.

In space, the charge-exchange plasma must eventually blend into the ambient space plasma, rather than be terminated abruptly at facility walls. A preliminary model of the interactions of ion drive propulsion with this space plasma is presented in this section.

1. Space Plasma

Two regions in space are considered for this interaction with the ambient plasma. One is a low earth orbit, where an ion drive vehicle might be expected to start an orbit raising operation. The other is interplanetary space at the radius of earth's orbit from the sun. These two regions are by no means a complete inventory of ion drive environment. They are, however, sufficient to show the major problems involved.

The low earth orbit ($\sim$150 nautical miles) has low energy electrons (0.1 - 0.2 eV) at a high density ($\sim 10^6$ cm^{-3}).[20] For interplanetary space, the electron energy is much higher (10 - 20 eV) and the density much lower (5 - 20 cm^{-3}).[21,22]

2. Distance of Interaction

The solar wind in interplanetary space travels radially outward from the sun and the magnetic field lines are frozen into this plasma.[21] The magnetic Reynolds number can be used to assess the interaction of this magnetic field with the charge-exchange plasma. The magnetic Reynolds number is given by,[23]

$$R_m = \mu \sigma v \ell ,$$

where σ is plasma conductivity, and v and ℓ are the typical velocity and length, respectively, of the situation in question. Taking the permeability, $\mu = \mu_o$, and for reasonable values of σ, v, and ℓ for the magnetic field moving into the charge-exchange plasma, $R_m >> 1$. For this case penetration of the magnetic field is very slow and the full pressure gradient, $B^2/2\mu_o$, can develop.[23] Assuming a simple interface, the relation

$$n_i m_i v^2 = \frac{B^2}{2\mu_o} \tag{16}$$

will give an estimate of where the magnetic field gradient exists. In the frame of stationary B, the charge-exchange plasma velocity, v, will roughly be that of the solar wind. Solving Eq. (16) for n_i, ion density, and using Eq. (1), R is found to be equal $\sim 10^2$ km, where m_i is the charge-exchange ion's mass. Because the magnetic field strength is $\sim 2 \times 10^{-5}$ gauss at 1 AU, the Larmor radius is $\sim 10^3$ km. The magnetic field will decrease as the radial distance from the sun increases and the Larmor radius likewise will increase. This is a very simple

picture for a complex problem. However, it points out that for most situations the space plasma will exist around the spacecraft and not be affected by the solar wind's magnetic field.

A rough measure of the transition distance between the charge-exchange plasma and the space plasma is where their densities are equal. The procedure for calculating the Hg charge-exchange plasma has been described and has been used for calculating the equal-density radius at 90 and 180 deg. to the beam direction. This equal-density radius may also be of interest for the ion beam. For the latter calculation, the ion beam current was assumed confined to a ±15 deg. exhaust cone. The results of these calculations are shown in Table III.

The distance 180 deg. to beam direction for Low Orbit is readily available in a ground facility. The distance 90 deg. to beam direction for low orbit is available only at the very largest facilities. All other distances exceed the dimensions of the largest ground facilities. It therefore does not appear possible to simulate this interaction in a ground facility.

3. Electron Interactions

As indicated above, the electrons are much more mobile than ions, so that in a ground vacuum facility there will be many electron collisions with the facility boundaries for each electron that escapes. In space, there are two alternatives. A potential well can be formed by the plasma near the spacecraft, so that electrons are reflected at the boundaries of this well, similar to the reflection at the boundaries of a ground facility. Or the electrons in the charge-exchange plasma can escape, and be replaced by ambient space electrons.

Table III. Equal Density Radii

Direction Relative to Ion Beam	Low Orbit (10^6 cm^{-3})	Interplanetary (10 cm^{-3})
0 deg.	120. m	40 km
90 deg.	16. m	5 km
180 deg.	2. m	0.5 km

To show the magnitude of the problem, the electron escape rates were calculated for the case where no reflection occurred. For the ion beam, the electron escape rate was 46 A. For the entire charge-exchange plasma it was 24 A. With a total electron escape rate of 70 A, and only a 14 A ion escape rate in the beam, 56 A of electrons would need to be either reflected or collected from space to maintain spacecraft and plasma neutrality. The rate of electron exchange with space can clearly be quite large. Whether or not this exchange takes place will depend on collision processes for the electrons.

For interplanetary space, the interaction volume is quite large (Table III). To simplify the calculations, we will assume a sphere with a radius of 5 km for the charge-exchange plasma volume. Integrating the total number of charge-exchange electron/ion pairs in this volume gives about 1.1×10^{19}. At 3000 sec., the ion beam adds another 1.5×10^{19} electron/ion pairs in this volume. This gives a total of about 2.6×10^{19} electron/ion pairs within 5 km of the spacecraft. In comparison, the total number of Hg neutrals within this sphere is 2.1×10^{20}. In the 10 - 20 eV electron energy range, the excitation/ionization cross section of Hg is several times 10^{-20} m^2, while the Coulomb collision cross section of electrons is of the order of 10^{-18} m^2. Clearly, then, Coulomb collisions of space electrons with electrons near the spacecraft will be the dominant mechanism for capture of these high velocity, but less dense, space electrons. (Coulomb collisions with ions or elastic collisions with neutrals are not significant because of the small energy transferred.)

At 15 eV, the space electrons have an average velocity of 2.6×10^6 m/sec. For a 10^7 m^{-3} density, the space electrons should have a collision frequency of

$$\nu = n\bar{v}\sigma = 10^7 \times 2.6 \times 10^6 \times 10^{-18} = 2.6 \times 10^{-5} \qquad (17)$$

with each low energy electron in the 5 km radius sphere. For the entire 2.6×10^{19} electrons, this would give a capture rate of

$$\dot{N}_{capt} = 2.6 \times 10^{19} \times 2.6 \times 10^{-5} = 6.8 \times 10^{14} \ . \qquad (18)$$

Multiplying this rate by the electronic charge, q, gives a capture current of about 100 μA.

Comparing this electron capture rate with the possible net loss of 56 A clearly shows that capture of ambient space electrons will not be a significant process in interplanetary space. It seems reasonable to conclude, then, that the two electron populations will coexist in space with negligible interaction, similar to the two-group theory of electrons in a thruster discharge chamber. The low energy electrons must therefore be reflected to maintain charge neutrality with ions. The reflection would be expected near the surface where spacecraft plasma density equals ambient space plasma density.

At low orbit ambient conditions, the situation is considerably different. The ambient electron temperature is roughly the same as that of the charge-exchange plasma. There should therefore be no significant distinction between an escaping charge-exchange electron and a captured ambient space electron. The plasma surrounding the spacecraft should thus blend smoothly with the ambient plasma.

There is another case that is worth considering. A smaller thruster, such as might be used for spacecraft attitude control, stationkeeping, or drag makeup, would be expected to have a higher electron temperature. With a higher than ambient temperature, the space electrons would be captured while the higher energy electrons from the spacecraft would escape. One would therefore expect the electron temperature near a spacecraft to be governed by the ambient space value when that value is less than the value obtained in a ground test.

As had been mentioned earlier, the ion (and therefore electron) density is related to the Bohm, or ion acoustic velocity. We should address quantitatively the question of the effect the ambient plasma may have on this velocity. Two plasmas of different density and electron temperature will be occupying the same space. What electron temperature will govern the ion velocity? The Bohm velocity,

$$v_B = \sqrt{KT_e/m_i}\ , \tag{19}$$

can be thought of as the velocity an ion will have after being accelerated through a potential, V_o. Therefore,

$$v_B = \sqrt{\frac{2q\,|V_o|}{m_i}} \tag{20}$$

For the case of a plasma with two Maxwellian electron velocity distributions having different electron temperatures and densities, the following relation can be obtained:[24]

$$V_o = \frac{k}{2q} \frac{\left\{ n_1 \exp\left(\frac{qV_o}{kT_1}\right) + n_2 \exp\left(\frac{qV_o}{kT_2}\right) \right\} T_1 T_2}{n_1 T_2 \exp\left(\frac{qV_o}{kT_j}\right) + n_2 T_1 \exp\left(\frac{qV_o}{kT_2}\right)} \tag{21}$$

For typical densities and temperatures of the primary beam plasma and the interplanetary space plasma, the beam plasma is by far the dominating factor in establishing the Bohm velocity.

For typical values of the solar wind at 1 AU and the charge-exchange plasma from a single thruster, the dynamic pressure, $m_i n_i v_i^2$, of the solar wind and charge-exchange plasma are roughly equivalent a few tens of meters from the spacecraft. This distance will increase as the spacecraft's distance from the sun increases, and as the number of thrusters operating increases. Because one pressure does not overwhelm the other, each individual case of position relative to the sun, number of operating thrusters, and solar wind activity will have to be calculated to determine this boundary. However, since the mean free path for the situations discussed is in the multiple kilometers range, the flow of the charge-exchange plasma around the spacecraft should not be affected by the solar wind ions.

4. Discussion

The proposed interactions with the space plasma appear reasonable. Ground verification, however, ranges from difficult to effectively impossible. Plasma calculations have frequently been found invalid in the past. The reason for

the lack of validity has often been collective interactions, which can be very difficult to predict. No collective interactions were considered in this analysis.

F. CONCLUDING REMARKS

The Hg charge-exchange model described appears adequate for preliminary estimates of solar array and spacecraft interactions. The electron densities predicted by this model are subject to electron temperature uncertainties due to the variation that might be expected with thruster size, the clustering of thrusters and the interaction with the space plasma. There are other effects that introduce uncertainty in both electron density and saturation electron current density. They are the relative electron and neutral temperatures (which result in more or less trajectory bias for the charge exchange ions in the downstream direction) and the departure from axial symmetry for the thruster array. All of these effects are estimated to introduce a factor of several uncertainty in the calculations. In addition, the model is not capable of predicting detailed spacecraft shape and surface orientation effects on charge-exchange ion trajectories.

The Hg charge-exchange model, though, is adequate for predicting the rough magnitude of the electron collection problem at the solar array. It can also be used to estimate the plasma environments for spacecraft science instruments. The arrival rate of Hg ions and possible condensation problems can also be evaluated.

The possibility of surface reactions due to colliding Hg charge-exchange ions remains an unknown. Experience with Hg vapor indicates no problem should be expected. Experience with several eV Hg ions, though, is much more limited. The rate of Hg ion arrival is high enough for much of the spacecraft that coverage could become a serious problem if ions cause reactions on some surfaces that inhibit subsequent vaporization.

The Mo charge-exchange model has a larger uncertainty than the Hg model. It appears, however, that there will be no major problems with Mo deposition. The amount of deposition could still be a problem for certain sensitive instruments and thermal surfaces near the thrusters. Reducing the uncertainty in Mo deposition appears difficult with ground tests.

To summarize, there appear to be no major obstacles to the use of ion drive. There are areas where spacecraft/ion drive interactions exist, but can be controlled through the use of proper design approaches. There are also areas where uncertainties exist that could cause later problems with sensitive instruments or surfaces. Resolution of these uncertainties is recommended early in the ion drive program to avoid the possible greater expense and schedule impact of delayed resolution.

G. REFERENCES

1. J. F. Staggs, W. P. Gula, and W. R. Kerslake, "Distribution of Neutral Atoms and Charge-Exchange Ions Downstream of an Ion Thruster", J. Space. Rock., Vol. 5, pp. 159-164, Feb. 1968.

2. T. W. Reynolds and E. A. Richley, "Contamination of Spacecraft Surface Downstream of a Kaufman Thruster", NASA Tech. Note TN D-7038, Jan. 1971.

3. T. W. Reynolds, "Procedure for Estimating Effects of Ion Beam Interaction with Spacecraft", NASA Tech. Memo. TM X-68043, Apr. 1972.

4. J. V. Staskus and R. J. Burns, "Deposition of Ion Thruster Effluents on SERI II Spacecraft Surfaces", AIAA Paper No. 70-1128, Aug. 1970.

5. A. J. Weigand and M. J. Mirtich, "Measurement of Sputtered Efflux from 5-, 8-, and 30-cm Diameter Mercury Ion Thrusters", AIAA Paper No. 75-358, Mar. 1975.

6. W. R. Kerslake, "Charge-Exchange Effects on the Accelerator Impingement of an Electron-Bombardment Ion Rocket", NASA Tech. Note TN D-1657, May 1963.

7. J. V. Dugan, Jr., "Upper-Limit Charge Exchange Cross Sections for Mercury$^+$ on Molybdenum and Cesium$^+$ on Aluminum", NASA Tech. Memo. TM X-2427, Mar. 1972.

8. H. R. Kaufman, "Charge-Exchange Plasma Generated by an Ion Thruster", NASA Contr. Rep. CR-134844, June 1975.

9. H. R. Kaufman, "Interaction of a Solar Array with an Ion Thruster Due to the Charge-Exchange Plasma", NASA Contr. Rep. CR-135099, Oct. 1976.

10. H. R. Kaufman, "Charge-Exchange Plasma Generated by an Ion Thruster", NASA Contr. Rep. CR-135318, Dec. 1977.

11. G. K. Komatsu, R. K. Cole, D. K. Hoffmaster, and J. M. Sellen, Jr., AIAA Paper No. 75-428.

12. C. Collett, et al., "Fabrication and Verification Testing of ETM 30 cm Diameter Ion Thrusters", NASA Contr. Rep. CR-135193, Apr. 1977.

13. K. Meyer and A. Guntherschulze, "Kathodenzerstaubung in Quecksilberdampf bei sehr geringen Drucken", Z. Physik, Vol. 71, pp. 277-290 (1931).

14. D. A. Vroom and J. A. Rutherford, "Cross Sections for Charge Transfer between Mercury Ions and other Metals", NASA Contr. Rep. CR-135205, June 1977.

15. R. M. Kushnir, B. M. Palyukh, and L. A. Sena, "Investigation of Resonance Charge Exchange in Monatomic Gases and Metal Vapors", Bull. Acad. Sci. USSR - Phys. Ser., Vol. 23, pp. 995-999, Aug. 1959.

16. I.P. Iovitsu and N. Ionescu-Pallas, "Resonant Charge-Exchange and the Kinetics of Ions", Soviet Physics Tech. Physics, Vol. 4, pp. 781-791, 1960.

17. D. Zuccaro, "Measurement of the Charge Exchange Cross Section of Mercury", NASA Contr. Rep. CR-72398, Apr. 1968.

18. G. K. Wehner and G. S. Anderson, "The Nature of Physical Sputtering", Chap. 3 in Handbook of Thin Film Technology (L. I. Maissel and R. Glang, eds.), McGraw-Hill Book Company, New York, 1970.

19. D. F. Hall, "Electrostatic Propulsion Beam Divergence Effects on Spacecraft Surfaces", Vol. II, Jan. 1973.

20. U. Samir, "Spacecraft/Spaceplasma Interaction", Spaceflight, Vol. 10, No. 8, August, 1968.

21. E. N. Parker, Interplanetary Dynamical Processes, Wiley and Sons, New York, 1963.

22. T. N. Divine, "Interplanetary Charged Particle Environments", JPL-TM-33-637, August, 1973.

23. H. K. Messerle, "Other Plasma Phenomena and Possible Applications", Discharge and Plasma Physics, (S.C. Haydon, ed.), The University of New England, 1964.

24. K. Uehara, et al., "Ion Saturation Current of a Plasma Having Two Electron Temperatures", Japanese Journal of Applied Physics, Vol. 14, No. 11, pp. 1761-1764, Nov. 1975.

PROPAGATION OF CHARGE-EXCHANGE PLASMA PRODUCED BY AN ION THRUSTER*

M.R. Carruth, Jr.**
Jet Propulsion Laboratory
California Institute of Technology
Pasadena, California

M.E. Brady†
Boeing, Aerospace Co.
Pasadena, California

Abstract

A charge-exchange plasma is produced downstream of ion thrusters by collisions between energetic ions and neutrals escaping through the ion optics. The charge-exchange ions flow radially from the thruster beam due to electric fields produced by its density gradient. The propagation of the charge-exchange plasma after it leaves the thruster beam is the subject of this paper. Under the proper conditions there is an "end-effect" of a long, cylindrical Langmuir probe which allows a signficant increase in collected ion current when the probe is aligned with a flowing plasma. This effect is used to determine the charge-exchange plasma flow direction at various locations relative to the ion thruster. A portion of the charge-exchange plasma flows upstream of the ion thruster and can represent a contamination source to electrically propelled spacecraft. The ion current collected by the probe as a function of its angle with respect to the plasma flow allows determination of the plasma density and plasma flow velocity at the probe's location upstream of the ion thruster optics. The density values obtained from the ion current agree to within a factor of two of density values obtained by typical voltage-current Langmuir probe characteristics.

Introduction

The electron bombardment ion thruster has been under development for a number of years and is presently a candidate propulsion device for several space missions. Two significant differences between the ion thruster propulsion system and chemical propulsion systems are that the ion thrusters will be required to operate continuously for up to 15000 hours on some planetary missions and they produce a plasma environment that is capable of surrounding the spacecraft. It is necessary to understand the potential interactions between the thruster produced environment and the spacecraft so that undesirable interactions can be prevented or minimized by proper spacecraft and mission design.

A cut-away view of an ion thruster is shown in Fig. 1. The ion thrusters presently developed for space application utilize mercury as the propellant. Approximately 90% of the mercury flow into the thruster discharge chamber is ionized and is accelerated through the ion optics to produce thrust. The remaining 10% leaves through the optics as neutral mercury. Charge-exchange interactions between these neutrals and the energetic ions downstream of the thruster optics form ions with only

Nomenclature

Θ	angle of probe with respect to plasma flow
$\Theta_{1/2}$	angular width at half-maximum of ion current versus probe angle curve
τ	Dimensionless probe length
λ_D	Debye length, $(KT_e \varepsilon_o / N_e e^2)^{1/2}$
N_e	Plasma electron density
K	Boltzmann constant
T_e	Electron temperature
T_i	Ion temperature
M_i	Ion mass
U	Plasma flow velocity
R_p	Cylindrical probe radius
L	Cylindrical probe length
e	Electronic charge
V_p	Probe potential relative to plasma potential
a	Plasma sheath thickness
ψ	Dimensionless potential, $(-eV_p/K T_e)$
I	Ion current collected by "infinite" cylindrical probe
$\bar{I}$	Ion current collected due to "end-effect"
δ	Slowly varying function of ψ, λ_D, R_p

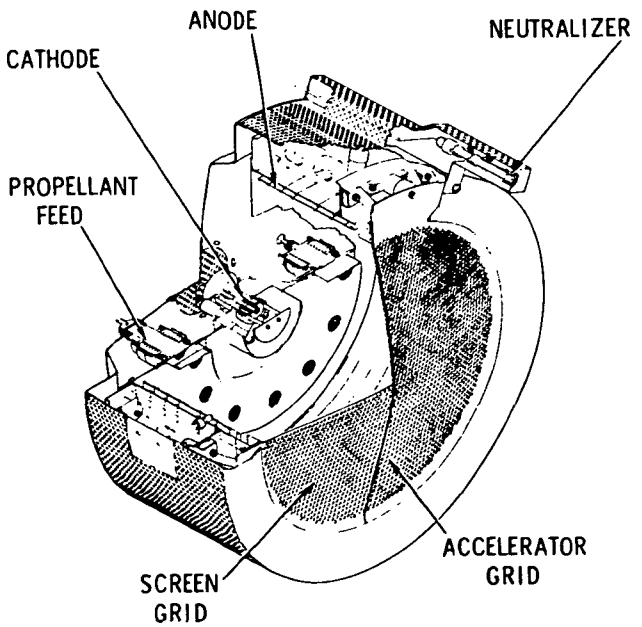

Figure 1. Cut-away View of Ion Thruster

*The research described in this paper was carried out at the Jet Propulsion Laboratory, California Institute of Technology, under NASA Contract NAS7-100.
**Engineer, Electric Propulsion and Advanced Concepts Group
†Systems Analyst

thermal energy. These ions leave the beam radially with a directed energy of a few tenths to a few eV due to the internal electric fields in the primary beam. These ions, with neutralizing electrons, constitute a charge-exchange plasma that can flow upstream around the spacecraft. The presence of this plasma around a high voltage solar array can produce a power loss in the array,[5] and deposition of plasma particles can affect thermo-optical properties of spacecraft surfaces.

By knowing the ion thruster beam density distribution, the distribution of neutrals leaving the thruster, and the resonant charge-exchange cross section of mercury, the charge-exchange ion production rate can be calculated.[6] The production of charge-exchange ions falls off very quickly with increasing distance from the thruster. The electric fields produced by the density gradient across the beam cause the charge-exchange ions to leave the beam in a radial fashion. The propagation of the charge-exchange plasma after it leaves the influence of the primary beam has been an area of uncertainty. There are various analytical models which predict the flow of the charge-exchange plasma from an ion thruster.[3,4,6-9] The densities of the charge-exchange plasma predicted by these models at points upstream of an ion thruster vary by orders of magnitude.

It is very difficult to experimentally verify such models due to the low directed energy of the ions and various effects produced by the test facility. To date, all experimental plume characterization investigations have been performed with Langmuir probes and retarding potential analyzer - Faraday cups.[2,4,7] Such techniques are useful for determining the plasma density, temperature and directed energy but are insensitive to measuring the direction of flow of this low energy plasma and can not reliably distinguish ions which are produced by charge-exchange with those neutrals which have previously encountered the facility wall. These latter ions will not be present in space.

Under the proper conditions a cylindrical Langmuir probe can be used to accurately determine the direction of flow of a plasma at the probe's location; this is referred to in the literature as an "end-effect" phenomena.[10,12] These necessary conditions are: (1) that the Debye length is greater than the probe diameter,(2) that the flow velocity is greater than the ion thermal velocity, and(3) that the probe is biased to collect an ion current. These conditions are met in the charge-exchange plasma and this "end-effect" can be used to accurately determine the flow direction of that plasma at the probe location.

Langmuir Probe "End-Effect"

The "end-effect" discussed in this paper was first reported by Bettinger and Chen (ref. 10) to explain anomolous increases in ion current observed when a cylindrical Langmuir probe on the Explorer 17 satellite was aligned with the satellite's direction of motion. The explanation for the increase in ion current is illustrated in Fig. 2. When the ion flow direction is at a large angle, Θ, with respect to the probe axis, the impact parameter for collection is very small. When the probe is aligned with the plasma flow, a significant ion current can flow through the front of the sheath. The ions experience the electric field along the probe and have a much greater likelihood of being collected. By obtaining the current as a function of the probe angle with respect to the plasma flow, a current peak can be obtained whose amplitude and half-width are dependent on various plasma parameters and the ion flow velocity. The "end-effect" can, therefore, be used for diagnostic purposes. An obvious application is the determination of the plasma flow direction at the probe's location.

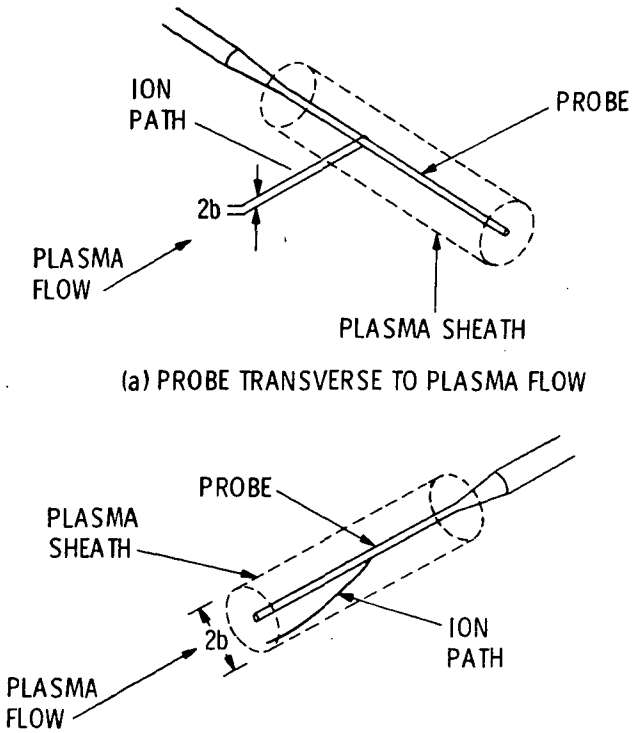

Figure 2. Illustration of Cylindrical Langmuir Probe End Effect

Hester and Sonin's (ref. 11) discussion of the "end-effect" pointed out that the Bettinger and Chen theory required a minimum length probe. The criteria for the probe to be of sufficient length for the Bettinger and Chen theory is

$$\tau \equiv \frac{L}{\lambda_D} \frac{(K T_e/M_i)^{1/2}}{U} > 3 \quad . \qquad (1)$$

Hester and Sonin presented a theory, based on numerical calculations, for the condition of the probe being smaller than this minimum length. Sanmartin (ref. 12) later presented a more complete, closed formula theory for the case of $\tau<3$. For $\tau>3$ the theory of Bettinger and Chen still applies. For the plasma and probe conditions in the experiments described in this paper, τ is greater than 3. Therefore, any quantitative data other than flow direction at the probe's location requires the use of the Bettinger and Chen theory. Hester and Sonin made comments on the original theory of Bettinger and Chen, and gave a brief summary of the theory for $\tau>3$ in an appendix to their paper.

Mott-Smith and Langmuir showed that for $KT_i << -eV_p$ and $KT_i << 1/2\ M_i\ U^2$, the ion current

collected by an "infinite" cylindrical probe, i.e., a cylindrical probe which has a length much greater than its diameter, is given by,[13]

$$I = 2 N_e e U R_p L \left(\sin^2 \Theta - \frac{2 e V_p}{M_i U^2}\right)^{1/2} . \quad (2)$$

The current decreases to a minimum at $\Theta = 0$. However, the "end-effect" can produce a large increase in ion current at $\Theta = 0$ over that predicted by Eq. (2). At $\Theta = 0$ the ratio of the end-effect current to that predicated by Eq. (2) is given by Hester and Sonin for $\tau > 3$,

$$\frac{\bar{I}}{I} = 1 + \frac{\pi^{3/2} a^2 U}{2^{3/2} R_p \psi^{1/2} L (K T_e / M_i)^{1/2}} \quad (3)$$

The half-width, $\Theta_{1/2}$, of the peak produced by plotting the probe current as a function of angle between the cylindrical probe and the plasma flow is given by,

$$\Theta_{1/2} = \sin^{-1} \frac{\sqrt{2} R_p (-eV_p)^{1/2}}{0.4 a U M_i^{1/2}} . \quad (4)$$

The half-width is the full width at half-maximum of the peak in excess of that predicted by Eq. (2). The sheath size, a, has to be obtained from a source outside the theory of Bettinger and Chen or Hester and Sonin. The sheath size is given in the theory of Sanmartin as,

$$a = (2 \psi \bar{\delta})^{1/2} \lambda_D . \quad (5)$$

The function $\bar{\delta}$ is given in graphical form by Sanmartin. It is a slowly varying function and an average value is taken so that the sheath size, a, primarily varies as a function of ψ and λ_D.

Charge-Exchange Plasma Experiment

Experimental Arrangement

A diagram of the experimental arrangement is given in Fig. 3. A vacuum chamber, 7 feet in diameter and 15 feet long, was used in this experimental study. The wall of the chamber is lined with a liquid nitrogen cooled wall for cryopumping. A mercury ion thruster is mounted at one end of the chamber such that the thruster beam strikes a frozen mercury target at the other end of the chamber. The mercury target can be rotated so that the beam may strike the frozen mercury target or the end of the chamber. The use of the frozen mercury target prevents sputtering of the steel walls of the vacuum chamber.

The ion thruster employed in this study is a 900-series, Hughes 30-cm mercury ion thruster with SHAG (small hole accelerator grid) optics. The ion beam output of the thruster is therefore equivalent to that from a J-series 30-cm ion thruster. The ion thruster was operated and throttled as recommended for a J-series thruster by NASA-LeRC.[14]

The cylindrical probe used in this experiment is made of 5 mil diameter tungsten wire with a length to diameter ratio of 450. The probe is mounted on a rail which is placed in the chamber so that the rail is parallel to the thrust beam axis. The probe can be moved linearly along the rail by means of a motor drive, and can be rotated about its midpoint from -90° to +90°, where 0° is defined as that position where the probe is perpendicular to the thruster beam axis. When the probe is at the -90° position it is parallel to the thrust beam axis and is pointed at the thruster end of the chamber. When it is at the +90° position it is pointed at the target end of the chamber. The ion thruster beam axis lies in the plane swept out by the probe rotation. Therefore, the probe always points at the thrust beam axis. The probe can be moved to various locations along the rail. At each location the probe can be rotated and the ion current versus probe angle obtained.

Results

As indicated by Eq. (2) through Eq. (5), the shape of the ion current versus probe angle curve is dependent on the plasma density and plasma flow velocity. These curves can therefore be used to determine these quantities at various locations in the chamber. The plasma flow direction at the probe's location can be determined from the angular position of the probe where the peak ion current is obtained.

Figure 4 illustrates a typical ion current versus probe angle curve. The increase in ion cur-

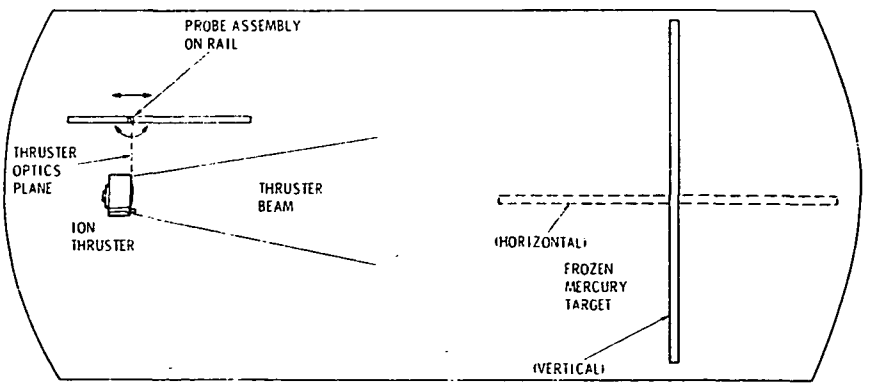

Figure 3. Experimental Arrangement. Probe may move upstream or downstream of the thrust plane and can rotate away from the target or toward it.

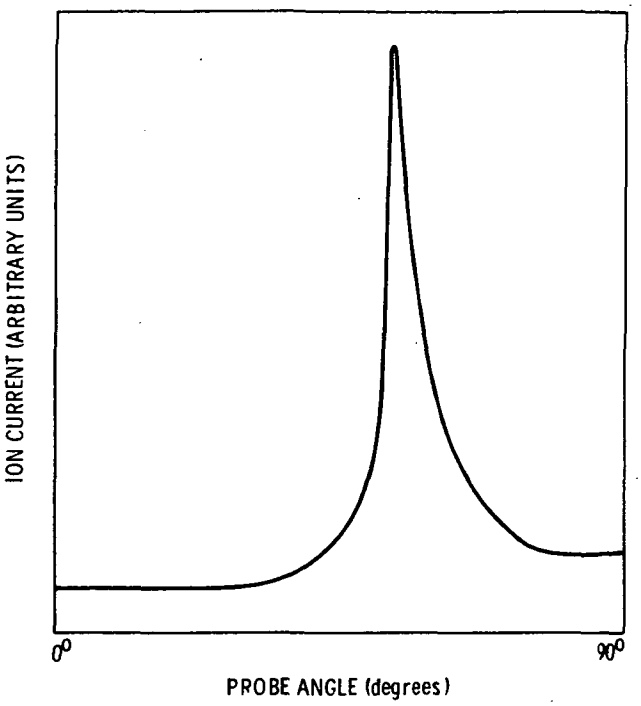

Figure 4. Typical Ion Current vs Probe Angle Curve Upstream of Thruster Optics.

rent due to the "end-effect" is very angle dependent and prominent. Figure 4 is an example of the curves obtained upstream of the plane of the thruster optics. Figure 5 is a typical example of the probe traces obtained downstream of the thruster.

Facility produced effects have long been recognized as making reliable measurements of the charge-exchange plasma difficult.[1,2,4,5] One of the major difficulties is substracting the facility produced plasma from measured signals to determine true, charge-exchange plasma values. The beam strikes the target at the end of the chamber and neutral atoms are sputtered from the target. These atoms flow upstream and may be charge-exchange ionized in the beam. This produces low energy ions which are difficult to distinguish from true charge-exchange ions; i.e., those ions which are produced by charge-exchange between beam ions and neutrals escaping from the ion thruster's discharge chamber.

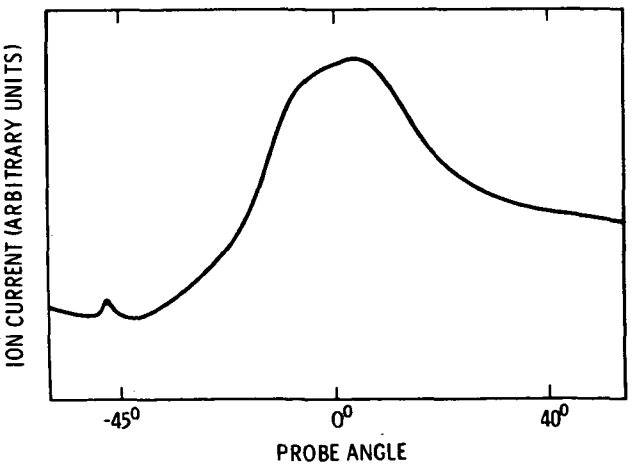

Figure 5. Typical Ion Current vs Probe Angle Curve Downstream of Thruster Optics.

The "end-effect" will produce increased ion current when the probe is aligned with a flowing plasma. If there are a number of flowing plasmas crossing at the probe's location, an ion current peak will be produced by each one as the probe is aligned with them. If the plasma ions have a distribution of directed motions, albeit in the same general direction, the "end-effect" peak will be broad. With these points in mind a number of things can be said about the curves in Figs. 4 and 5.

The narrowness of the peak in Fig. 4 indicates a well directed plasma flow at locations upstream of the ion thruster. The ion current peak is not symmetric and the ion current on either side of the peak is seen to be greater when the probe is pointed toward the frozen mercury target than when it is pointed away from the target. This increase in ion current is due to neutrals from the target flowing upstream, charge exchanging with beam ions and continuing their motion upstream. The mercury target which is intercepting the thruster beam can be rotated so that the beam is not sputtering mercury from the target but is allowed to strike the end of the chamber. This significantly decreases the facility produced ion production since the number of neutrals coming from the end of the chamber is lowered.

The ion current base is defined as the ion current measured on either side of the ion current peak. For a probe angle, θ, less than the angle where the peak occurs, the base current is described by Eq. (2). At the furthest positions upstream of the thruster the ion current base may be lowered a factor of two by rotating the mercury target so that the beam strikes the end of the chamber. When the probe is positioned near the thruster optics plane, the change in base current caused by rotating the mercury target is evident but much less significant. In all cases, the base values change but the angular positions at which the current peak occurs is altered only slightly. This indicates that the facility produced ions have a distribution of velocity vectors such that no well defined ion current peak is produced due to the "end-effect". Because the facility produced ions flow generally from the target, the base current increases when the probe is pointed toward the target. The base current here is greater than on the other side of the peak because as the probe is aligned with the facility ions the "end-effect" produces an increase in measured current. If the prominent current peaks are produced chiefly from the facility ions moving upstream from the target, then the plasma flow direction should, at all locations relative to the thruster, appear to come from the target. This is not the case. Therefore, the peak represents ions that are produced in the beam near the thruster and flow radially from the beam. After leaving the influence of the primary beam they then expand and flow upstream.

Figure 5 illustrates the curve obtained at a location downstream of the plane of the thruster optics and at some radial distance away from the thruster axis. The position of the major peak indicates that the charge-exchange plasma flows radially from the thruster beam. This is in agreement with other studies.[4,7] The width of the peak indicates that the flow direction is not as well defined as at locations upstream of the thruster. One can conclude from the ion current levels obtained as the probe is pointed toward the target, that the facility effect current is increasing as

the probe location is moved downstream of the thruster. It is of interest to note in Fig. 5 that for positions downstream of the thruster, a second, small, well defined, peak appears when the probe is pointed toward the edge of the thruster optics. It is known that the outer beamlets of the thruster optics produce the most divergent ions in the thruster beam.[15] This peak is produced by those ions.

Data was obtained with the probe at various locations along the rail and with the rail at two different radial distances from the thrust beam axis. The data was also obtained at different beam currents. The flow directions upstream of the thruster do not change as a function of beam current, which was varied from 1 to 1.8 amps, and altered only a few degrees in the downstream positions. Table I gives the probe angle at which the current peak occurs (average for all beam currents) for various axial and radial positions relative to the thruster. For the axial positions given, the negative (-) numbers are upstream of the plane of the thruster optics. The radial position is the distance from the thrust beam axis to the probe location. The probe angle has been previously defined.

Table I. Plasma Flow Direction At Probe Locations

	Probe Angle (degrees)			
	Radial Position = 48 cm		Radial Position = 66 cm	
Axial Positions (cm)	Charge-Exchange Plasma	Divergent Primary Beam	Charge-Exchange Plasma	Divergent Primary Beam
-51	70			
-46	67			
-37	63		50	
-32	59		45	
-24	54		40	
-19	47		35	
-14	39		29	
-6	29		22	
0	19		14	
6	10		9	
11	4		4	
19	-2		1	
25	-5		2	
38	-2	-60		
51	4	-57	1	-45
63	5	-63	4	-52
76	4	-66	8	-56

The plasma flow can more easily be seen in Fig. 6 which illustrates the plasma propagation for a 1.8 amp beam current. One can observe that the flow seems to originate just downstream of the thruster. Near the thruster the plasma flow is primarily radial. The plasma flow can be seen to be bending both upstream and downstream as it propagates outward. Internal electric fields in the plasma due to variations in plasma density act on the ions. This produces the added component of velocity parallel to the thruster axis.[1-5] About half a meter downstream, the maximum ion current (the peak becomes very broad here) indicates that the major flow is turning back upstream. The facility produced ions are probably becoming more dominant and causing this effect. The flow directions upstream and immediately downstream of the ion

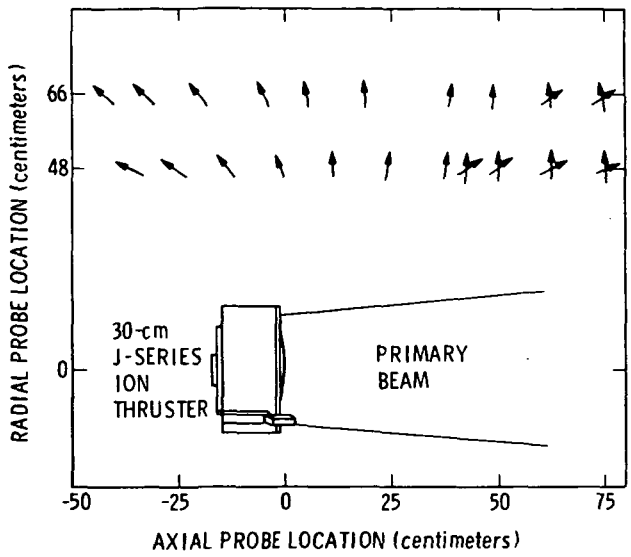

Figure 6. Plasma Flow Direction at Locations Relative to Ion Thruster.

thruster are due to the flow of charge-exchange ions created near the thruster optics and not facility ions produced due to atoms flowing from the target.

It is of interest to look at the density distribution upstream of an ion thruster. As previously mentioned, the major flow direction appears to be independent of the facility produced plasma. However, the base ion current is dependent on the facility produced ions. With this in mind, the plasma density and flow velocity are determined using Eq. (2) and Eq. (4). Both equations are dependent on the plasma density, N_e, and the flow velocity, U. Equation (4) is a result of the "end-effect" theory while Eq. (2) gives the ion current collected by an infinite probe in a flowing plasma. The position, $\Theta = 90°$, is chosen to evaluate the data curves using Eq. (2) since the "end-effect" prevents using $\Theta = 0$. The half-width of the peak on each curve is used to evaluate Eq. (4). Only those peaks upstream of the thruster are evaluated because the broadening of the current peak at downstream positions introduces additional error into Eq. (4). To reduce facility effects the curves obtained with the target horizontal are used. The probe was biased -5 volts relative to ground. By typical Langmuir probe methods, the plasma potential in all cases was found to average one to two volts above ground. Therefore, V_p is taken as -6.5 volts in the calculations. The results for a 1.8 ampere beam current are given in Table II.

Independent density measurements were made at some locations. At each location the cylindrical probe was pointed into the plasma flow and a typical voltage-current Langmuir probe characteristic obtained. Each characteristic was analyzed, using the method outlined by Chen,[16] to obtain the plasma density. The values obtained with this method and those shown in Table II agree within a factor of two, although the density values in Table II are higher than those obtained with probe voltage-current characteristics. No additional attempts have been made to assess the degree the facility produced plasma contributes to the density. Therefore, the density values in Table II are higher than the den-

Table II. Plasma Density and Directed Energy of Plasma Ions

Axial Position (cm)	Radial Position = 48 cm Density (M^{-3})	Radial Position = 48 cm Energy (eV)	Radial Position = 66 cm Density (M^{-3})	Radial Position = 66 cm Energy (eV)
-51	3.8×10^{12}	1.9		
-44	4.6×10^{12}	1.76	3.9×10^{12}	1.23
-38	6.9×10^{12}	0.85	4.8×10^{12}	2.04
-32	8.5×10^{12}	1.05	5.6×10^{12}	1.57
-25	1.2×10^{13}	1.15	8.3×10^{12}	2.07
-19	1.7×10^{13}	2.34	1.3×10^{13}	2.72
-13	2.8×10^{13}	2.68	1.7×10^{13}	2.75
-6	4.2×10^{13}	3.30	2.4×10^{13}	1.93

sity due to true ion thruster charge-exchange plasma. Based on previous studies, the error in density introduced by existence of facility ions is small near the thruster plane but can increase an uncertain amount for positions upstream of the thruster optics.[2-4] Therefore, the values given in Table II are considered accurate to within a factor of two near the thruster, but may be less accurate for positions farther upstream.

Concluding Remarks

A cylindrical, Langmuir probe "end-effect" has been used to determine the direction of flow of the charge-exchange plasma produced by a 30-cm J-series ion thruster. The flow direction is independent of the facility produced ions. The flow direction is also independent of the beam current at which the ion thruster is operated. The angular position of the ion current peak is reproducible to within a couple of degrees at each probe location.

Two well defined peaks occur in the ion current versus probe angle curves at positions downstream of the thruster optics plane. The most prominent peak is produced by the charge-exchange plasma and the additional, smaller peak is caused by ions coming from the edge of the thruster optics. These ions represent the very divergent part of the primary beam. This indicates that the "end-effect" might be useful in studies involving such divergent beam ions.

Ion current measurements were also used to determine the density and flow velocity at various locations upstream of the thruster. Due to the lack of a unique flow direction at positions downstream of the thruster, as required by Eq. (2), no density calculations were performed at these positions. Independent measurements of density obtained from typical voltage-current probe characteristics agreed with the densities obtained from the ion current measurements upstream to within a factor of two. No attempt was made to make correction for the facility produced ions. As already stated, these ions do not affect charge-exchange plasma flow direction but do affect local density. The density values given in this paper are probably high for true charge-exchange ions due to the presence of facility ions. The error introduced is expected to be small near the thruster but can increase an uncertain amount for positions farther upstream. To obtain the density upstream due to genuine charge-exchange ions the facility effects have to be accounted for. In the past this has been done but the accuracy of such corrections are uncertain.[1-5]

References

1. H.R. Kaufman, "Charge-Exchange Plasma Generated By An Ion Thruster," NASA CR-134844, 1975.
2. H.R. Kaufman, "Charge-Exchange Plasma Generated By An Ion Thruster," NASA CR-135318, 1977.
3. H.R. Kaufman and M.R. Carruth, Jr., "Charge-Exchange Plasma Environment for an Ion Drive Spacecraft," JPL Publication 79-90, 1979.
4. G.K. Komatsu and J.M. Sellen, Jr., "Beam Efflux Measurements," NASA CR-135038, 1976.
5. H.R. Kaufman, "Interaction of a Solar Array with an Ion Thruster Due to the Charge-Exchange Plasma," NASA CR-135099, 1976.
6. R.L. Poeschel, E.I. Hawthorne, et al, "Extended Performance Solar Electric Propulsion Thrust System Study," Vol. 4, NASA CR-135281, 1977.
7. J.W. Ward and R.P. Vahrenkamp, "Characterization of Ion and Neutral Efflux From a 30-cm Mercury Ion Thruster," AIAA Paper No. 75-357, 1975.
8. H.B. Liehmohn, et al, "Ion Thruster Plasma Dynamics Near High Voltage Surfaces on Spacecraft," AIAA Paper No. 79-2105, 1979.
9. D.E. Parks and I. Katz, "Spacecraft Generated Plasma Interaction with High-Voltage Solar Array," J. Spacecr. Rockets, Vol. 16, No. 4, pp. 258-263, 1979.
10. R.T. Bettinger and A.A. Chen, "An End Effect Associated with Cylindrical Langmuir Probes Moving at Satellite Velocities," J. Geophys. Res., Vol. 73, No. 7, pp. 2513-2528, 1968.
11. S.D. Hester and A.A. Sonin, "Ion Temperature Sensitive End Effect in Cylindrical Langmuir Probe Response at Ionosphere Satellite Conditions," Phys. Fluids, Vol. 13, No. 5, pp. 1265-1274, 1970.
12. J.R. Sanmartin, "End Effect in Langmuir Probe Response Under Ionospheric Satellite Conditions," Phys. Fluids, Vol. 15, No. 5, pp. 1134-1143, 1972.
13. H.M. Mott-Smith and I. Langmuir, "The Theory of Collectors in Gaseous Discharges," Phys. Rev., Vol. 28, pp. 727-763, 1926.
14. Staff-NASA Lewis Research Center, "30-Centimeter Ion Thruster Subsystem Design Manual," NASA TM 79191, 1979.
15. G. Aston and P.J. Wilbur, "The Screen Hole Plasma Sheath of an Ion Accelerator System," AIAA Paper No. 79-2114, 1979.
16. R.H. Huddleston and S.L. Leonard, Ed., Plasma Diagnostic Techniques, Chapter 4, Academic Press, New York, New York, 1965.

D4

COMPUTER CODE FOR CHARGE-EXCHANGE PLASMA PROPAGATION

by

Raymond S. Robinson

and

Harold R. Kaufman

October, 1980

This program was developed to satisfy requirements of JPL Contract No. 955322.

TABLE OF CONTENTS

Note: The Table of Contents shown here indicates the original pagination of the document and has not been changed to reflect the pagination of the present report.

ABSTRACT

The propagation of the charge-exchange plasma from an electrostatic ion thruster is crucial in determining the interaction of that plasma with the associated spacecraft. A model that describes this plasma and its propagation is described, together with a computer code based on this model.

The structure and calling sequence of the code, named PLASIM, is described. An explanation of the program's input and output is included, together with samples of both. The code is written in ANSI Standard Fortran.

INTRODUCTION

Ion thrusters can be used for a variety of primary and auxiliary space-propulsion applications. Because a charge-exchange plasma environment is produced by a thruster, it is important to understand the possible interactions of various spacecraft systems with this plasma. To this end, a detailed knowledge of the plasma propagation is important.

The production of charge-exchange ions by thrusters has been understood for some time.[1] Fast ions from the thruster interact with slow neutrals that are also escaping, resulting in the production of ions that initially have only a thermal velocity. The electric fields within the ion beam cause these ions to move approximately radially out of the ion beam. These charge-exchange ions leave the ion beam along with electrons supplied by the neutralizer, the combination constituting the charge-exchange plasma. The propagation of the charge exchange plasma depends on several factors, including the initial thermal energy of the ions, the distribution of ion production along the beam and surrounding plasma, and the potentials and detailed geometry of neighboring spacecraft surfaces.

In the Theory section of this report, the geometry of a simplified (idealized) spacecraft with an ion thruster is described, together with the assumptions used to model the ion beam. The distribution function used for charge-exchange ion production is also presented, along with the barometric equation that relates the variation in plasma potential to the variation in plasma density. The numerical methods and approximations used for the calculations are then discussed. A description of the main calculation routine, CALC, is included in this discussion.

In the program structure section, a flowchart is provided that diagrams the calling sequence of the modules, as well as descriptions of each of the modules. A guide to using the program is presented in the Input section of this report. A description of calculated results is presented in the Output section.

Also presented is a method of obtaining better resolution in the upstream region. A high-resolution option of the program which stimulates only this upstream region is presented. This option utilizes previously calculated trajectories as boundaries for the region to be simulated at higher resolution.

The final section of this report compares other experimental and theoretical results with those obtained by the computer code. Accuracy-limiting factors are also discussed.

An analytical solution was derived for the case of an infinitely long cylindrical beam with a uniform distribution of charge-exchange ion production along the beam. Expressions were obtained for the radial variations in ion density and velocity, permitting a direct comparison with results from the computer code. This analytical solution is described in an Appendix and used in the comparison described above.

THEORY

The interaction of an ion thruster with other components of an electrically propelled spacecraft through the space surrounding a spacecraft has been studied for some time. The transport of electrons from the ion beam to a solar-array surface was treated first by Knauer, et al.[2] as an electron space-charge-flow problem. Measured electron currents, though, were found to be much higher than calculated by Knauer. The difference was due to the presence of a charge-exchange plasma.

Charge-exchange ions are produced when fast beam ions pass near slow escaping neutrals. The fast neutrals that result usually present no problem, and escape following the directions they had as ions. The slow charge-exchange ions that are produced, though, initially have only the neutral thermal velocity. The small electric fields within the ion beam result in the charge-exchange ions leaving the beam in approximately radial directions. These charge-exchange ions, together with some escaping electrons, form the charge-exchange plasma that surrounds an electrically propelled spacecraft.

The production rate for the charge-exchange ions was first calculated by Staggs, et al.[1] The capability of the charge-exchange plasma to transport electrons to other parts of the spacecraft was experimentally evaluated by Worlock, et al.[3] Some detailed trajectories of charge-exchange ions have been examined by Komatsu, et al.[4] An experimental study of the charge-exchange plasma distribution, particularly upstream of the ion-beam direction, was conducted by Kaufman.[5-7] The latter study included a correlation of plasma properties in terms of the distance from the thruster and the angle relative to beam direction.

The physical processes involved in the charge-exchange plasma have become well understood as the result of the various studies that have been conducted. The electron population outside of the beam agrees with the "barometric" equation

$$n_e = n_{e,ref} \, Exp(-qV/kT_e) \qquad (1)$$

which was introduced by Sellen, et al.[8] and verified by Ogawa, et al.[9,10] for the population within the beam and by Kaufman[5] for the population in the charge-exchange plasma. The plasma potential V in Eq. (1) is defined as zero at the reference electron density $n_{e,ref}$. The electron temperature T_e in the charge-exchange plasma has been found to be about half the value in the ion beam.[5] The value in the ion beam varies with thruster size and ranges from about 7 eV for a 5 cm thruster to 5 eV for 15 cm and 0.35 eV for 30 cm.

The experimental validity of Eq. (1) is consistent with the low density and long mean-free paths in the charge-exchange plasma. The decreasing plasma density with increasing distance from the thruster forms a potential well for the electrons, so that many transits of this region are probable before an electron escapes. The many transits permit randomization of the electron population to a single Maxwellian distribution by Coulomb collisions.

The extent of the charge-exchange plasma is large compared to the Debye shielding distance, which means that the electron density must everywhere equal the ion density. Inasmuch as the ions only move outwards from the thruster, their motion is essentially collisionless and governed by the potential distribution from Eq. (1).

The approach used in this study has been to assume a cylindrical, axially symmetrical ion beam, with the charge-exchange ions leaving the beam with a uniform velocity in the radial direction. The current density of these charge-exchange ions at the cylindrical beam boundary is a function of the distance downstream from the thruster. The total charge-exchange current is divided equally into the total number of trajectories, with this total number specified as an input parameter. Approximately fifty percent of the charge-exchange ions are generated within one beam radius downstream of the thruster, so about half of the specified trajectories will initially start in this region.

A trajectory is represented as the path of a single ion in which acceleration is produced by electric fields in the plasma, which, in turn, are produced by gradients of the plasma density, as indicated by Eq. (1). Density gradients are used in two separate calculations. A gradient along the path serves to vary the ion velocity in that direction, while the density ratio normal to the path direction modifies the direction of the path.

In the simulation used herein, the ion path is represented with a stepwise progression away from the beam. It is assumed that, with small enough step sizes, following the ions through one pass of calculations is sufficient. (The validity of this assumption is checked in a later section by comparison with experimental and theoretical results.) From a physical viewpoint, the ions are moving at, or above, acoustic velocity, so disturbances should not propagate in the upstream direction. Also, the extent of the plasma is very large compared to the Debye shielding distance, hence the potentials at the flow boundaries should not extend into the bulk of the plasma.

Distances to neighboring paths are used to determine densities and density ratios. The coordinates are defined in the overall configuration sketch of Fig. 1. As indicated in Fig. 2, a normal to the path being incremented is extended in both directions. This normal is used to calculate the distances to neighboring paths, on the right and left of the path being incremented. In this report, right and left are defined in terms of relationships upon leaving the ion beam, with the viewing direction in the direction of charge-exchange ion motion. If the neighboring path was not intersected by a normal, as in Fig. 2(b), then the neighboring path is extended linearly from the last interval. The density is inversely proportional to both the distance between neighboring paths and the radial distance. The latter relationship is due to the axial symmetry and the use of only one trajectory for each axial location. The density on the left is thus given by

$$n_L = C/\Delta d_L x, \tag{2}$$

where C is a constant depending on operating conditions and the number of trajectories specified, Δd_L is the distance between the path being incremented and the path on the left, and x is the radius. The density on the right is defined in a similar manner, except that n_R and Δd_R are used. The two densities can then be expressed as a ratio and used with Eq. (1) to determine a potential difference normal to the path being incremented, $\Delta V_\perp$. Note that the constant C cancels when the density ratio is calculated. The force normal to the path direction is then

$$F_\perp = -q\Delta V_\perp / \Delta d_m \quad , \tag{3}$$

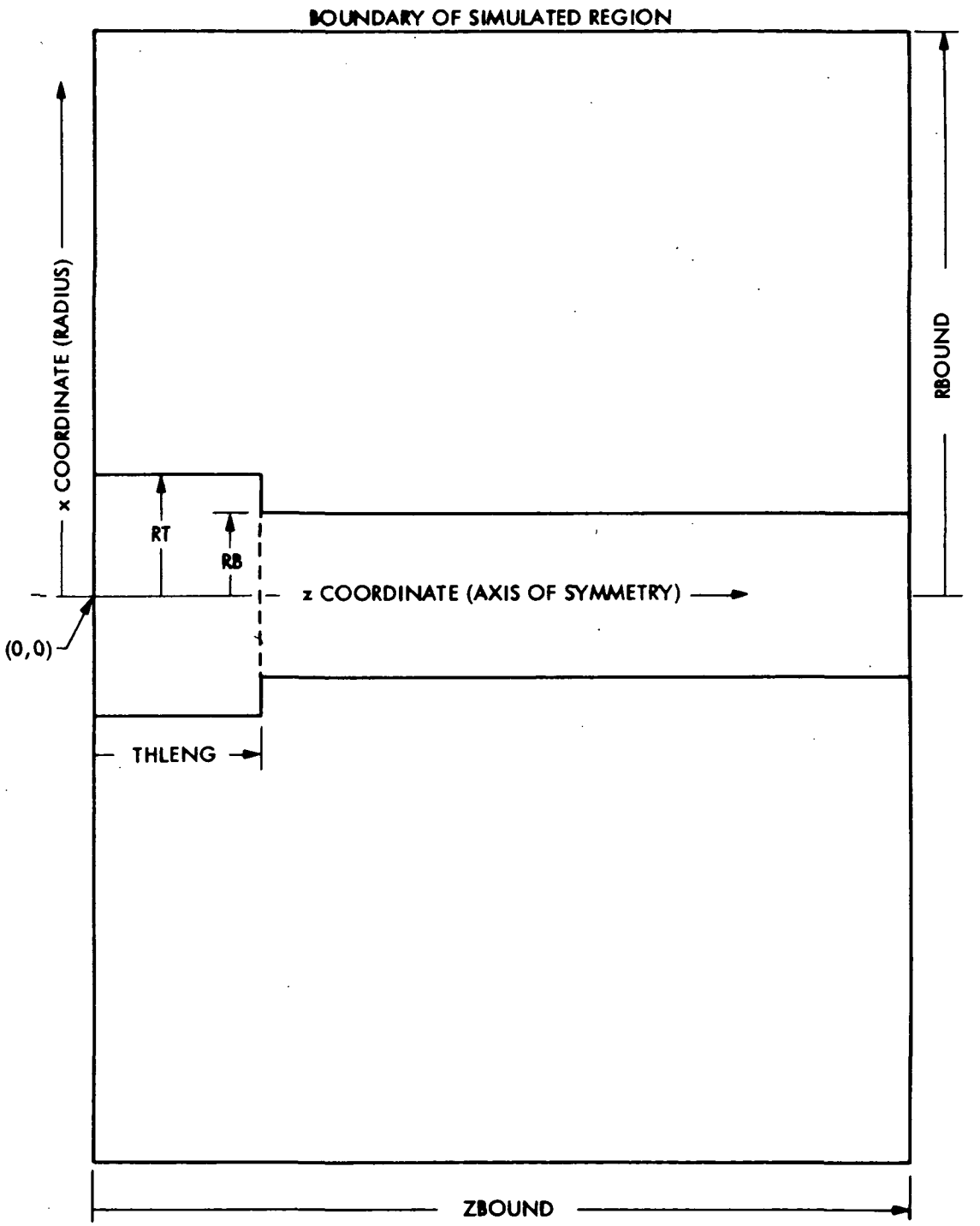

Fig. 1. Coordinate system and dimensions for simulation.

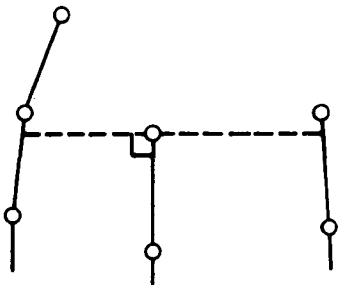

(a) PATHS INTERSECTED ON BOTH SIDES

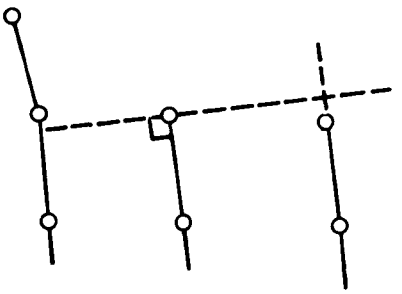

(b) APPROXIMATE VALUE USED ON RIGHT

Fig. 2. Evaluations of distances between paths.

where Δd_m is the average of Δd_L and Δd_R. This force can also be defined as

$$F_\perp = m\ \Delta v_\perp / \Delta t \quad , \tag{4}$$

with m the ion mass, $\Delta v_\perp$ the velocity component generated normal to the path direction, and Δt the size of the time interval used in the iteration. Equating these two force expressions,

$$\Delta v_\perp = -q\ \Delta V_\perp\ \Delta t / m\ \Delta d_m \quad . \tag{5}$$

This velocity change normal to the path direction is used to calculate an angular direction change. Because this velocity change is normal to the path direction, it has no effect on the magnitude of the ion velocity, only its direction.

The velocity change in the direction of ion motion is calculated using the average of the two densities (right and left). This density is compared with the same average density for the previous iteration. The ratio of average densities, with Eq. (1), yields the potential difference in the direction of motion. In a manner similar to the derivation of Eqs. (3) through (5), with Δd replaced by the distance $v\Delta t$,

$$\Delta v_{||} = -q\ \Delta V_{||} / mv \quad . \tag{6}$$

The calculation routine advances the trajectories from left to right, starting from the thruster. If an intersection is found both to

the left and right, another iteration is made. This allows paths that have less acceleration to keep in step with other paths further along, and limits the amount of extrapolation needed.

It was necessary to consider several special cases in the execution of the velocity algorithm. One was the case indicated in Fig. 2(b), mentioned briefly in the discussion of density calculation. In this case the approximation made is to take the distance between the endpoint of the path being incremented and the linear extrapolation of the missed neighboring path.

Another case involves the furthest right and left trajectories that have not been intercepted by a boundary. Without special treatment, this case would result in an undefined density on one side of the path because the normal will intercept a boundary before it intercepts another path. The boundary is treated as another path with one exception. If at any time a path would be repelled by the boundary, the direction is left unchanged. This approximates a plasma sheath which would be present at such a boundary. In general, both the distance between trajectories and the distance from a trajectory to a boundary will be much larger than the Debye distance. The accuracy of the simulation should therefore be considered questionable at any location where the distance between trajectories approaches the distance to a boundary. A better approximation in such a location would be obtained by extrapolating from deeper within the charge-exchange plasma. It would also be possible to use more trajectories, so that the space between them would be reduced.

The axial distribution of charge-exchange ion production used herein is assumed proportional to the neutral density on the axis.

This neutral density for a single thruster (no overlap of neutral effluxes from adjacent thrusters) is[5,6]

$$n(z) = n_o \left[1 - \frac{z}{(z^2 + r_b^2)^{1/2}} \right] , \qquad (7)$$

where r_b is the beam radius and n_o is a constant for a given combination of beam diameter and neutral loss rate. This function decreases rapidly with increasing z, due to the rapid divergence of neutral atom paths in free molecular flow. The beam radius, r_b, is an important parameter in this simulation, because approximately half of the total charge-exchange production occurs within about one beam radius of the thruster. This means that half of the charge-exchange trajectories will originate within the same distance.

In determining the axial locations for the origination of trajectories, the integral of Eq. (7) is used

$$\int_o^\infty n(z)dz = n_o r_b \qquad (8)$$

The region simulated is finite, so that not all of the integral can be represented. The region to be simulated was defined so that 95 percent of $n_o r_b$ is contained within this region. For N trajectories making up 0.95 $n_o r_b$, with each trajectory located at the median of the density interval that it represents, the following expression holds

$$\frac{1}{2} \sum_{i=0}^{2N} \int_{z_i}^{z_{i+1}} n(z)dz = N \int_{z_i}^{z_{i+1}} n(z)dz = 0.95\, n_o r_b/2. \qquad (9)$$

We start at the right end of the thruster (left end of the ion beam, see Fig. 1) for the first trajectory. For each successive z, we use

$$0.95r_b/2N = z_{i+1} - (z_{i+1}^2 + r_b^2)^{1/2} - z_i + (z_i^2 + r_b^2)^{1/2} \quad . \quad (10)$$

For the first trajectory, i = 0 and i + 1 = 1. The value of z_o is the right end of the thruster and the first trajectory is started at z_1. The second trajectory is started at z_3, third at z_5, and so forth.

The initial velocity upon leaving the ion beam is the Bohm value,

$$v_B = (kT_e/m)^{1/2} \quad , \quad (11)$$

where T_e is the electron temperature in the ion beam.

The plasma density is listed by the program and is generated using the following procedure. The total production rate of charge-exchange ions is assumed to be given by[6]

$$\dot{N}_{ce} = 2 J_b^2 (1-\eta_u) \sigma_{ce}/\pi r_b \eta_u q^2 \bar{v}_o \quad , \quad (12)$$

where J_b is the ion-beam current (A), η_u is the propellant utilization, σ_{ce} is the charge-exchange cross section (m^2), r_b is the beam radius (m), q is the absolute electronic charge (C), and $\bar{v}_o$ is the mean neutral thermal velocity, $(8kT_o/\pi m_o)^{1/2}$ (m/sec). With typical values for Hg neutrals and singly charged ions used,

$$\dot{N}_{ce} = 6.18 \times 10^{16} J_b^2 (1-\eta_u)/r_b \eta_u \quad (13)$$

The charge-exchange cross section varies slightly with ion energy (in an inverse manner). The value used for Eq. (13) corresponds to about 1,000 eV. A correction should therefore be used for any large departure from this energy.

The plasma density can be related to this production rate by

$$n = \dot{N}_{ce}/2\pi\Delta d_m x v_i \quad , \tag{14}$$

where Δd_m is the local mean spacing between trajectories (m), x is the radius (m), and v_i is the local ion velocity (m/sec available from code output).

PROGRAM STRUCTURE

There are two versions of the simulation, PLASIM1 and PLASIM2. The original, PLASIM1, contains the options to simulate the uniform density distribution for comparison with a theoretical solution as well as a normal run simulating a thruster. The parameter KEY is used in the selection. The second version, PLASIM2, does not contain the uniform density distribution option but instead allows better resolution in the upstream region.

To achieve the higher resolution a complete second pass of the program must be made. The parameter KEY again selects which option is in effect. This first pass (KEY=0) creates a file, called PATHS, which contains the following data:

NMAX	This is the number of trajectories written to PATHS (about NUMION/4).
NUMION	This is the total number of trajectories.
ISTAT(I)	Values for first NMAX trajectories, see p. 20.
ZION(I,N)	Values for first NMAX trajectories, see p. 20.
XION(I,N)	Values for first NMAX trajectories, see p. 20.

This file is created in addition to listing values for all the trajectories.

After determining which path is to be used as a boundary to the upstream region (path three for example), the second pass may be simulated. The path number is entered as KEY in the input deck. The value of NUMION entered will now be the number of trajectories distributed upstream of the boundary path, see Fig. 9. The value of NUMIT will

generally be much higher since the paths are packed much closer together. All other physical parameters must be exactly the same.

The simulation is made up of a main driver routine, PLASIM, several subroutines and a function, DS. The main driver flowchart is shown in Fig. 3. Immediately following the main driver is a definition of BLOCK DATA, where most of the constants are defined for the COMMON area. In particular, two constants used for the READ and WRITE statements are defined, IN and IOUT. These must correspond to the file declaration in the PROGRAM statement for INPUT and OUTPUT. The listing in this report shows the TAPE5 and TAPE6 declarations needed for a particular computer system. The file NPARAM is used by the VERSATEC plotting routine.

In most instances, writing is done by indexed calls to WRIT(i), though in the largest subroutine, CALC, a direct WRITE statement is executed.

Following BLOCK DATA is the read routine. All six data cards are read at the time READ is called by PLASIM. If the second pass is being made PATHS will also be read at this time. The subroutine INIT is called next to define all parameters necessary before calculation is initiated. The flowcharts for INIT and CALC are shown in Fig. 4. The initial trajectory locations are calculated first, either in the INIT module, for the functional density distribution, or by a call to DENSE, which determines the trajectory locations for a uniform distribution (NDSP1=0). The parameters ZBOUND, the downstream boundary of the simulated region, and VIONB, the ion Bohm velocity, are then calculated. The time step DT is calculated to advance the trajectories to a boundary within the designated number of iterations. The first values for the coordinate arrays are then calculated along with the densities at those points. Finally, INIT sets the status of each path active (ISTAT=0).

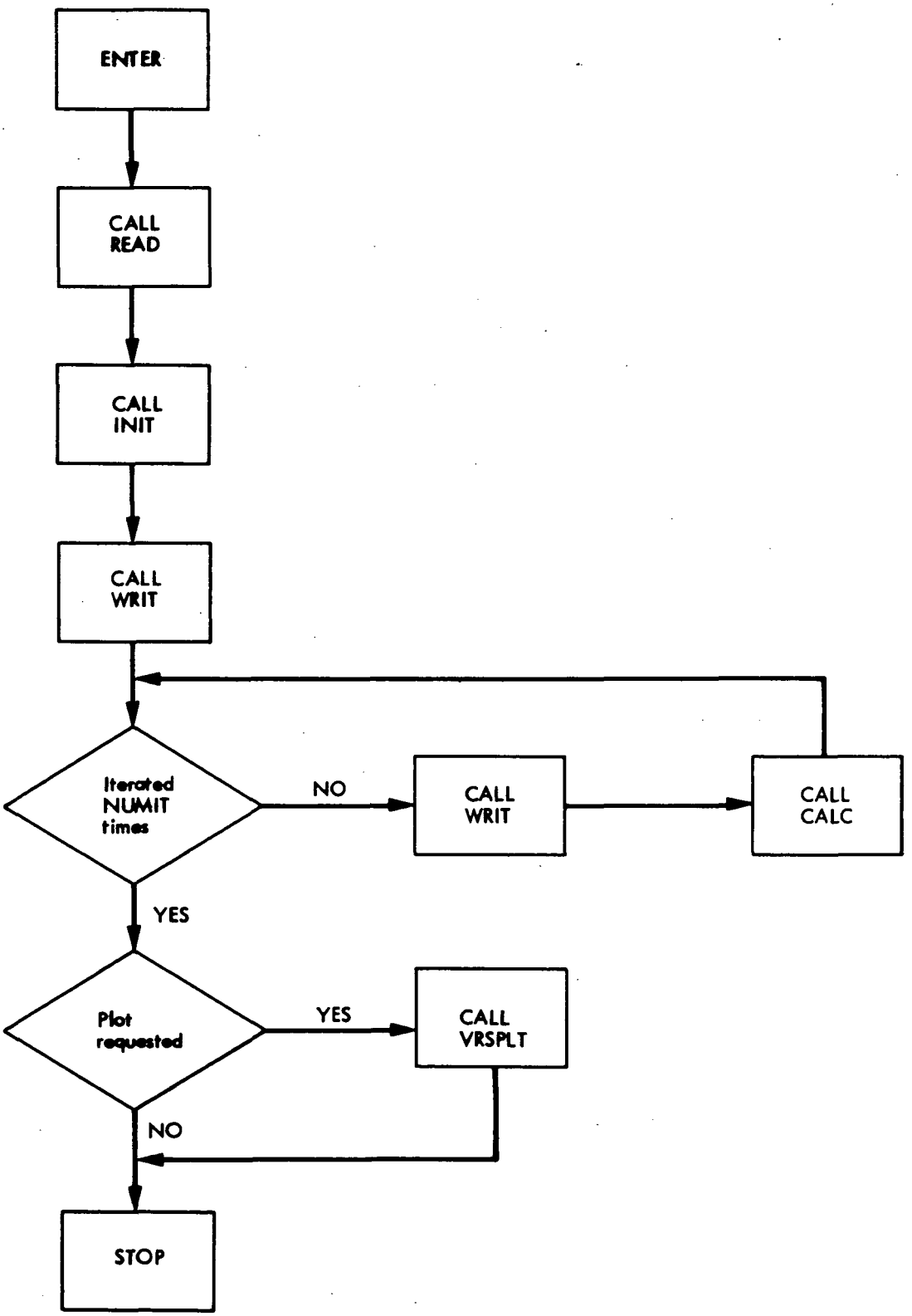

Fig. 3. Flow diagram for main driver (PLASIM).

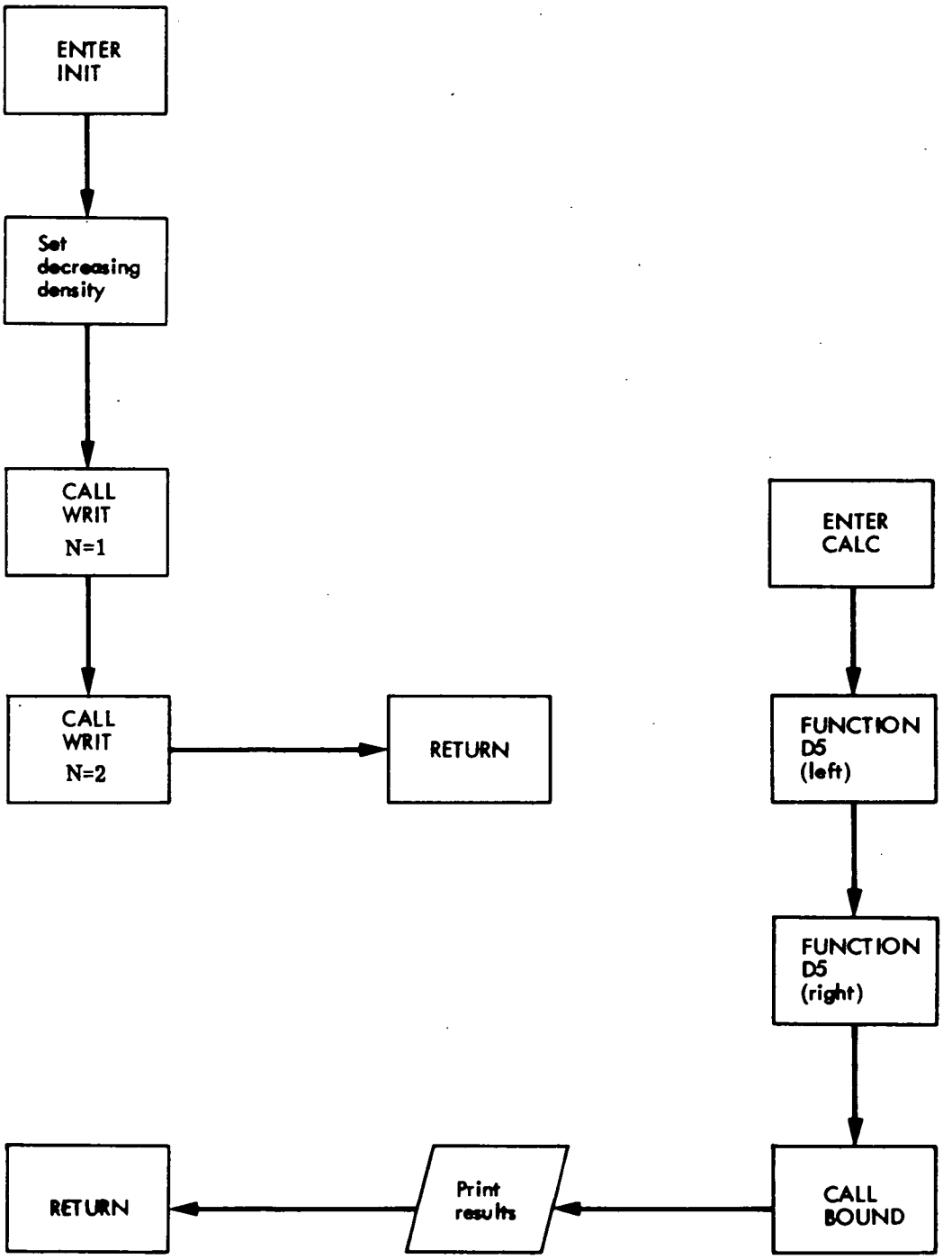

Fig. 4. Calling sequences for INIT and CALC.

Subroutine CALC is the largest and performs the analysis discussed in the theory section of this report. The distance to the left, which gives the density and potential, is calculated first, followed by similar calculations to the right. Several special cases need to be handled in both directions, some of which are: checks for inactive paths to the left or right, a check for an infinite slope of the normal intersection point, a check for the left-most or right-most active path. Once the displacements, densities, and potentials have been found, the velocity increments and coordinate increments are calculated using z and x vector components. The transverse force, with renormalization of the velocity, is calculated first, followed by the longitudinal accelerating force and its velocity increment. The arrays involved are listed with descriptions at the end of this section and the roles of variables internal to the subroutine CALC can be gathered from the comments in the program listing.

The function DS is called twice by CALC, once each in analyzing the left-most and right-most paths. The function accomplished is to determine which boundary the normal (to the current path) intersects and calculate the distance to the intersection point. Adapting the simulation to different geometries would involve changes to both DS and BOUND. The subroutine BOUND is also called by CALC after each iteration and changes the status array ISTAT to the current iteration number if the path has exceeded any of the defined boundaries.

The subroutine WRIT(KE) has a calling parameter KE which directs the module to perform one of several write sequences for information or results of the simulation. It is called from several subroutines and serves to keep most of the function of listing data or messages in

one routine. A call of WRIT(4) creates the file PATHS containing data used by a second pass of the simulation.

The final subroutine, VRSPLT, is used to display the geometry of the thruster and spacecraft, along with the ion trajectories using ZION and XION. It is designed to work with a VERSATEC plotting system, the routines called by VRSPLT being described in the appropriate literature.[11]

ARRAYS COMMON TO PLASIM

In the following notes, N refers to the current iteration being performed and I refers to the number of the trajectory.

ZION(I,N) is the z-coordinate.

XION(I,N) is the x-coordinate.

ISTAT(I) is zero for an active path. A nonzero value indicates an iteration number that a boundary was reached.

VZ(I) is the current z-component of the velocity.

VX(I) is the current x-component of the velocity.

DN(I) is the density at the current location.

NC(I) is the iteration step number for that path.

INFO, ICHAR, ITITL, AND IMAG are all used for displaying messages and data.

INPUT

The input deck consists of six cards, three of them containing comments and labels for the trajectory plot with the other three defining the input parameters for the simulation and the plotting routines.

The field length and formats of the following are defined preceeding the sample input card deck. All values have SI dimensions. If a second pass (PLASIM2) is being made (KEY>0) the file PATHS, which is created by the first pass (KEY=0), must be available to be read.

INFO - Used to place an identifying label on the particular simulation and plot; the field is eighty alphanumeric characters.

NUMION - Number of simulated ion trajectories.

NUMIT - Number of iterations to be made to reach the boundaries.

KEY - (PLASIM1) Set to one for the decreasing charge-exchange density distributing function; set to zero for the uniform distribution.

(PLASIM2) Set to zero for the first pass; set to path number to be used as boundary for second pass.

NDSP1 - Set to one to get a VERSATEC plot or zero for no plot.

NDSP2 - Set to one if intermediate results for every iteration is to be printed; two if every other iteration is to be printed, etc.

RB - The beam radius.

RBOUND - The radial distance from the beam that serves as a zero potential boundary on the simulation region.

RT - Thruster radius, or distance between paths if uniform distribution is being simulated.

THLENG - The length of thruster.

BMCUR - The beam current (amperes).

UTIL - The utilization.

TCEION - Temperature times Boltzmann's constant (SI units) of the electrons in the charge-exchange plasma.

TELBM - Temperature times Boltzmann's constant (SI units) of the electrons in the beam.

UMSION - Mass of the ions.

ITITL - Contains a label for the VERSATEC plot in the first eighty characters, a label for the z-axis in the next forty, and a label for the x-axis in the final forty characters.

The following is a typical input for PLASIM1:

```
1.   PLASMA PARAMETERS: TCEION=2.5 EV. TELBM=5.0 EV
2.           20        25         1          1          1
3.          .15       1.2        .16        .50        .63        .85
4.           4.0E-19          8.0E-19          3.0E-25
5.   PROPAGATION OF CHARGE-EXCHANGE PLASMA
6.   DISTANCE ALONG BEAM AXIS (METERS)        RADIAL DISTANCE (METERS)
```

Line 2 requires integer format (I10). Line 3 requires floating-point format (F10) and line 4 requires exponential format (E15.5). Care must be taken to enter the exponent in the right-most part of the field.

The uniform distribution simulation would be run with the following input deck:

```
1.   PLASMA PARAMETERS: TCEION=2.5 EV. TELBM=5.0 EV
2.           20        75         0          1          3
3.          .15       1.2        .16        .50        .63        .85
4.           4.0E-19          8.0E-19          3.0E-25
5.   PROPAGATION OF CHARGE-EXCHANGE PLASMA
6.   DISTANCE ALONG BEAM AXIS (METERS)        RADIAL DISTANCE (METERS)
```

The following is a typical input deck for a first pass of PLASIM2:

```
1.   PLASMA PARAMETERS: TCEION=2.5 EV. TELBM=5.0 ev
2.           20        25         0          1          1
3.          .15       1.2        .16        .50        .63        .85
4.           4.0E-19          8.0E-19          3.0E-25
5.   PROPAGATION OF CHARGE-EXCHANGE PLASMA
6.   DISTANCE ALONG BEAM AXIS (METERS)        RADIAL DISTANCE (METERS)
```

The formats are the same as for PLASIM1:

The second pass for higher upstream resolution would be run with the following input deck:

```
1.   PLASMA PARAMETERS: TCEION=2.5 EV. TELBM=5.0 EV
2.           10       175         3          1          5
3.          .15       1.2        .16       .50        .63        .85
4.           4.0E-19        8.0E-19        3.0E-25
5.   PROPAGATION OF CHARGE-EXCHANGE PLASMA
6.   DISTANCE ALONG BEAM AXIS (METERS)       RADIAL DISTANCE (METERS)
```

OUTPUT

The first two iterations in the simulation are done by the initialization module (INIT) in preparation for the general calculation algorithm. These two iterations are displayed first showing the initial step toward the axis, and the second step where each path is exactly on the beam edge. The following data are listed:

I - The trajectory number.

N - Iteration number.

ISTAT - The status of the trajectory. A value of zero means the path is active and a nonzero value indicates on which iteration a boundary was contacted.

ZION(I,N) - The z-coordinate.

XION(I,N) - The x-coordinate.

VZ(I) - The current z-component of the velocity.

VX(I) - The current x-component of the velocity.

DN(I) - The density proportion at the current location.

The initial distribution along the axis can be determined from the ZION values for these first two iterations as well as the step size that has been determined. Next is a statement describing the simulation and

a schematic of the thruster followed by input parameters and two values calculated in initialization, namely, the ion Bohm velocity (VIONB) and the z-axis boundary established (ZBOUND). These values are followed by a list of all or some of the iterations, depending on the value of NDSP2. The individual data have already been defined with the following exceptions:

ZION(I,N+1) is the result of the iteration, not the present position.

XION(I,N+1) is the result of the iteration, not the present position.

V is the magnitude of the total velocity.

ELDEN is the computed electron (ion) density at the current position.

A VERSATEC plot will then follow if specified by NDSP1.

VERIFICATION

Two studies, one theoretical and one experimental, are used for the verification of the computer code presented herein. The theoretical study was conducted as a support activity for the development of the subject computer code, and is reported in more detail in the Appendix.

THEORETICAL SOLUTION

The theoretical solution is for an infinitely long cylindrical beam with a uniform production of charge-exchange ions along the beam. Because variation was assumed in only the radial direction, an analytical solution was obtainable in a straightforward manner.

A computer solution was obtained using a uniform production of charge-exchange ions along the beam and is shown in Fig. 5. The circles indicate every tenth time interval. The radial velocity obtained with the computer solution is shown in Fig. 6, together with the analytical velocity from the Appendix. The computer simulation is seen to be within eight percent of the analytic solution over the radius range investigated.

One might suspect that the difference is due to non-negligible end effects in the computer simulation. Not only does the axial velocity component appear insignificant near the center of the simulated region, but any divergence at large radii would result in a higher radial velocity for the computer simulation, not lower.

A more likely cause of the difference shown in Fig. 6 is a second order error resulting from the linearized calculation procedure. Although a more accurate simulation is always desirable, it is not

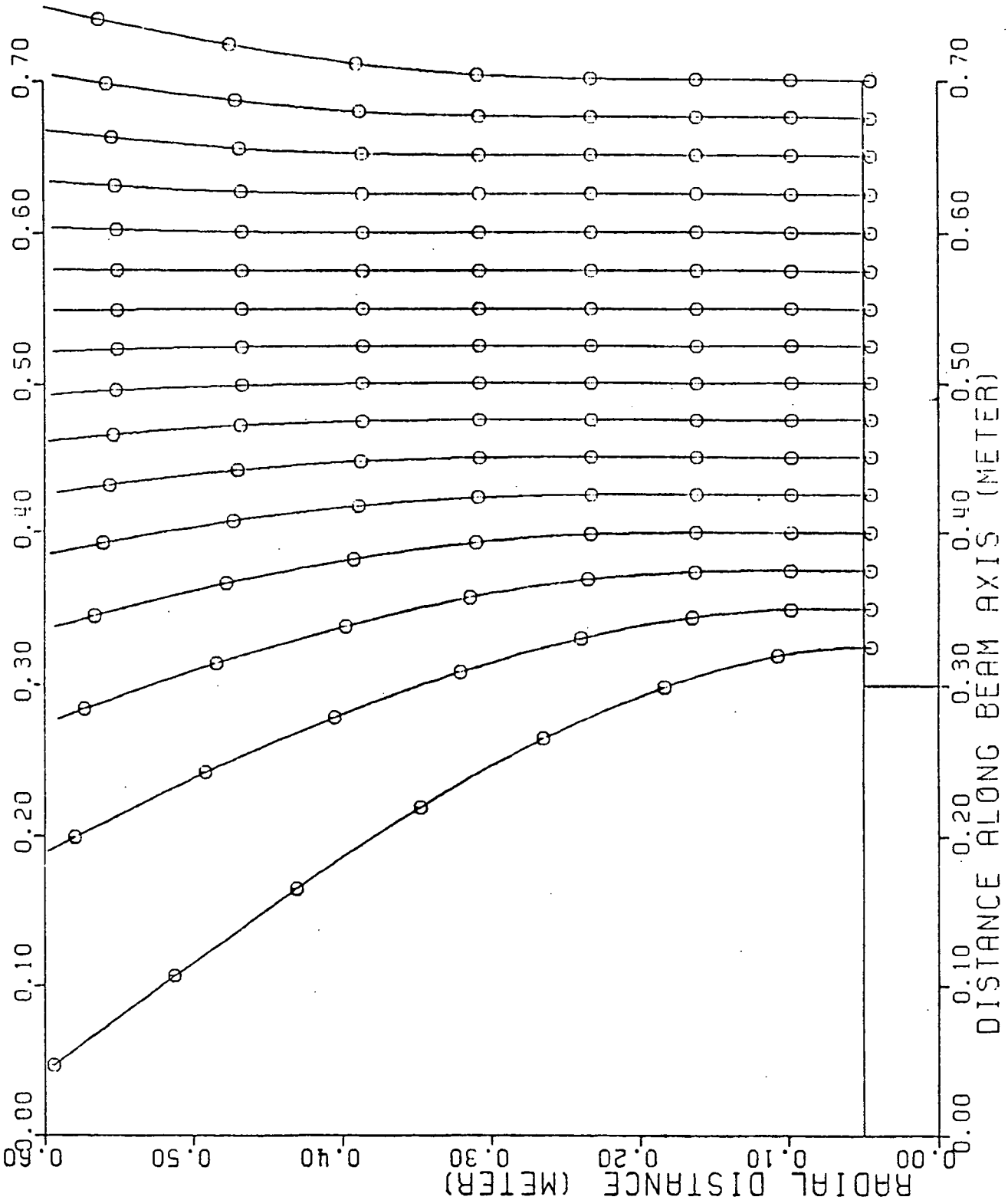

Fig. 5. Solution for uniform distribution of charge-exchange production. Electron temperature 5.0 eV in ion beam and 2.5 eV in charge-exchange plasma.

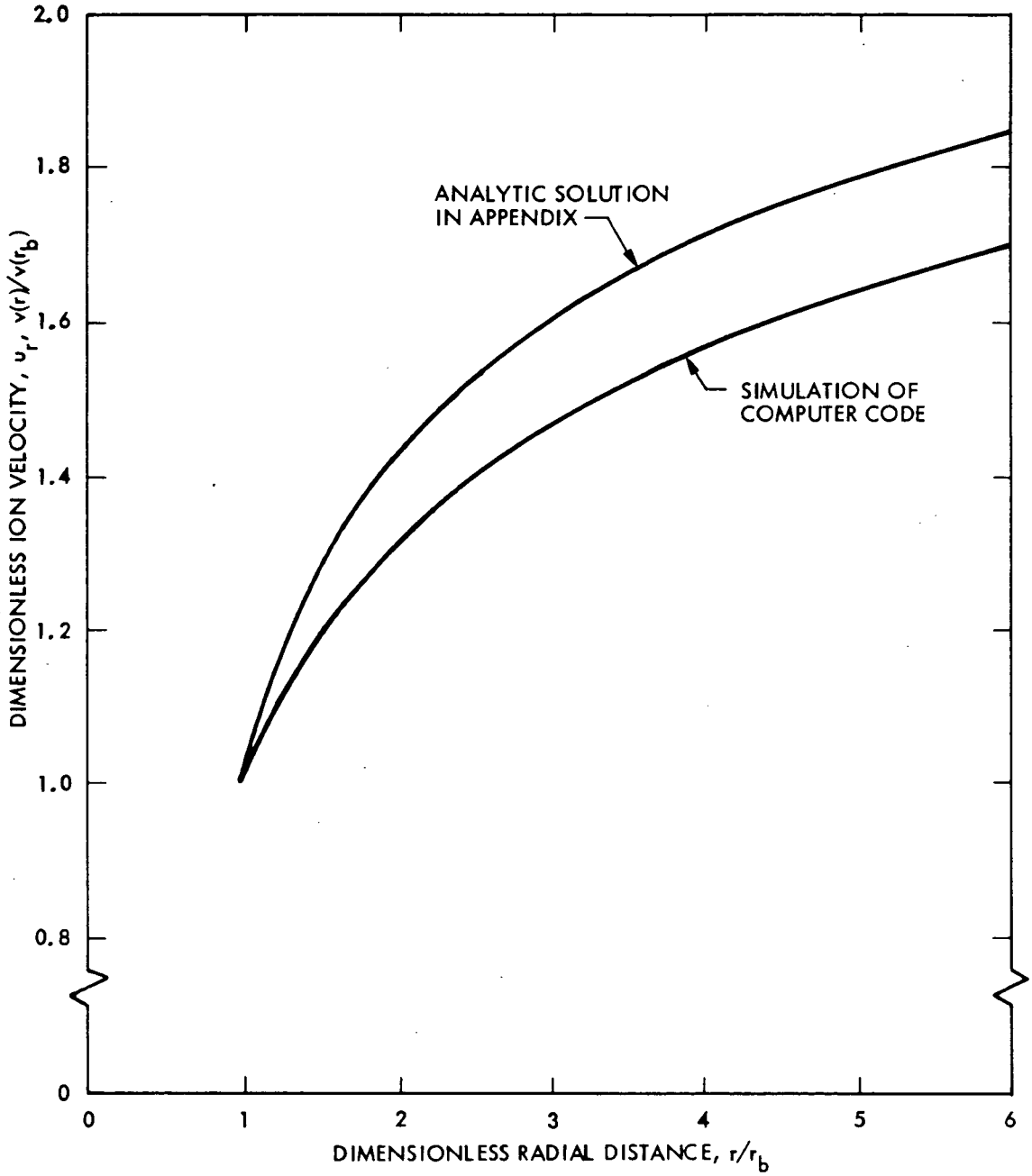

Fig. 6. Comparison of computer code with analytic solution.

clear that the complexity of nonlinear calculation procedures are justified in this case.

EXPERIMENTAL SOLUTION

An experimental survey of plasma density[6] for a 15 cm source is shown in Fig. 7. The operating conditions used for Fig. 7 were duplicated in a computer simulation and are shown in Fig. 8 and Fig. 9. Similar figures (10 and 11) are also shown for a five centimeter source.

LIMITATIONS IN USE

The major factor in the accuracy of simulation obtained is the number of ion paths used. At the low end of the practical range in this number, the crossing of paths will be observed. These crossings result from plasma properties changing so rapidly that the error in a path location will exceed the local path spacing. The procedure used for calculating the potential differences associated with each time interval depends on a "laminar" path structure. That is, no intersection of paths. The existence of any crossed paths therefore invalidates any local calculations of gradients, etc.

An indication of the number of iteration steps needed to simulate a 5, 15 and 30 centimeter source can be obtained from Figs. 12, 13 and 14. The time interval, DT, is related to the number of iterations (NUMIT) by the following formula:

$$DT = \frac{0.75 * RBOUND}{VIONB * NUMIT} . \qquad (15)$$

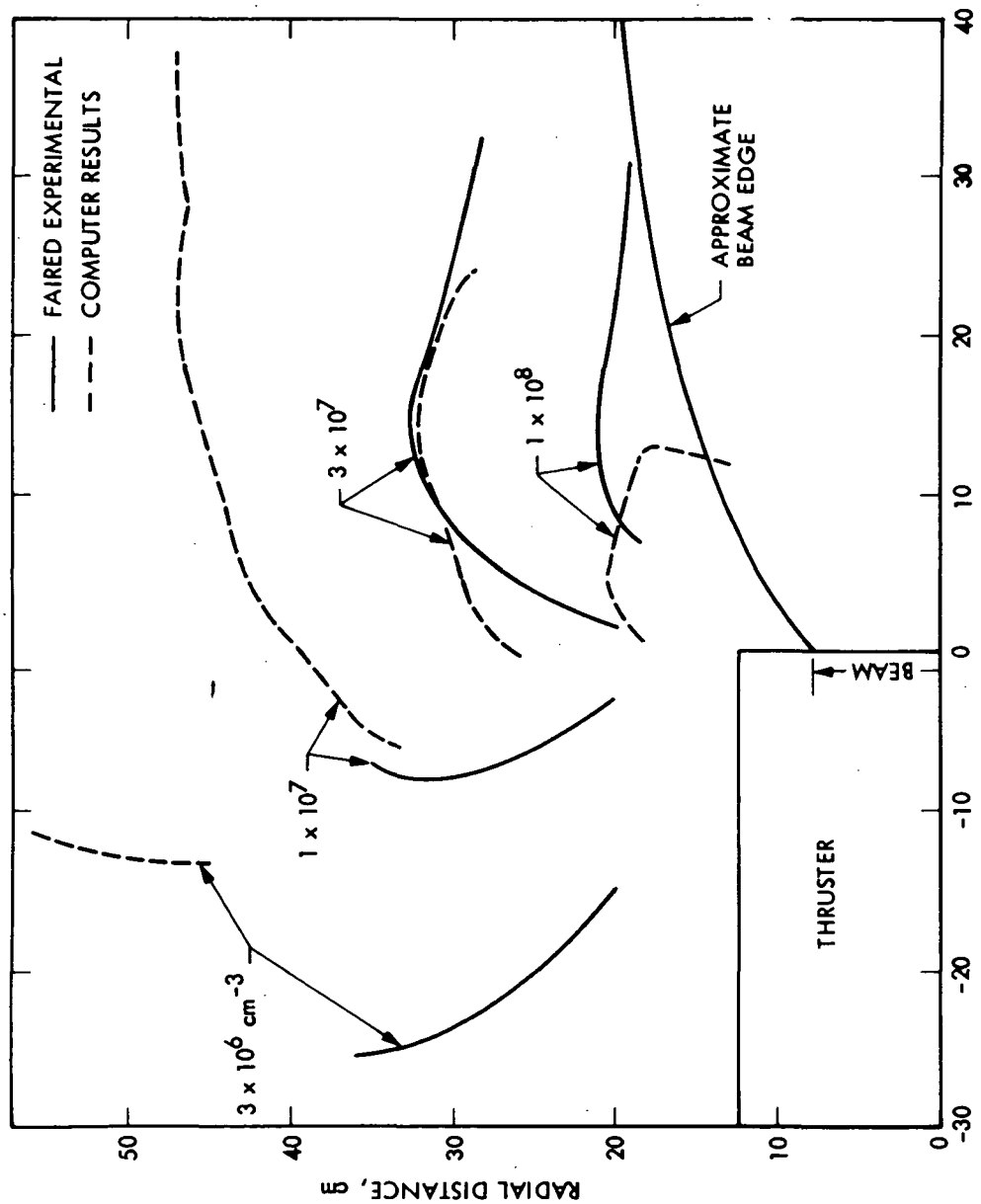

Fig. 7. Map of electron density for 15-cm thruster with a beam current of 0.63 A and a propellant utilization of 0.85. (Computer results duplicated from Figs. 8 and 9.)

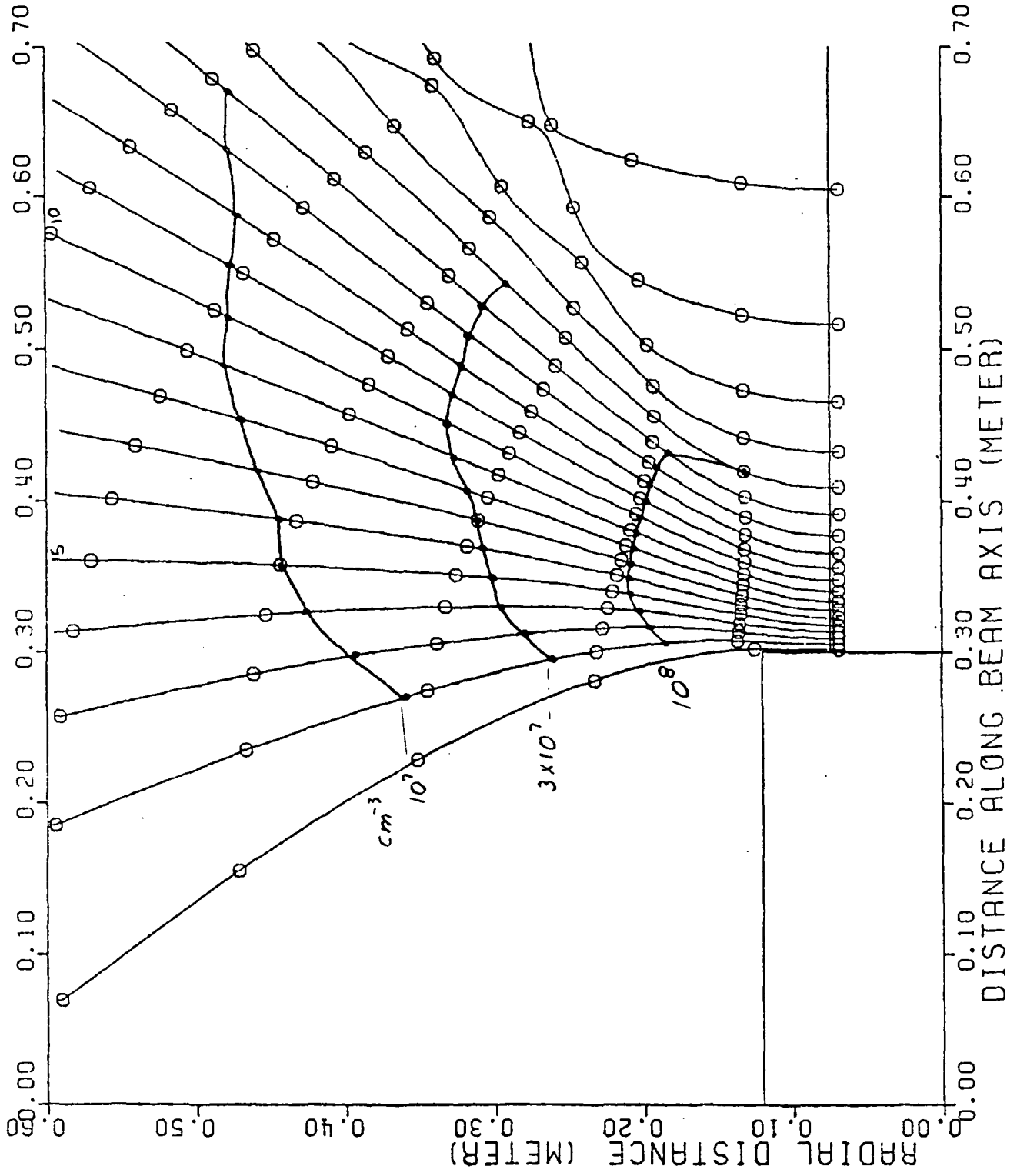

Fig. 8. Computer code solution to simulate experimental results for 15-cm thruster with a beam current of 0.63 A and a propellant utilization of 0.85.

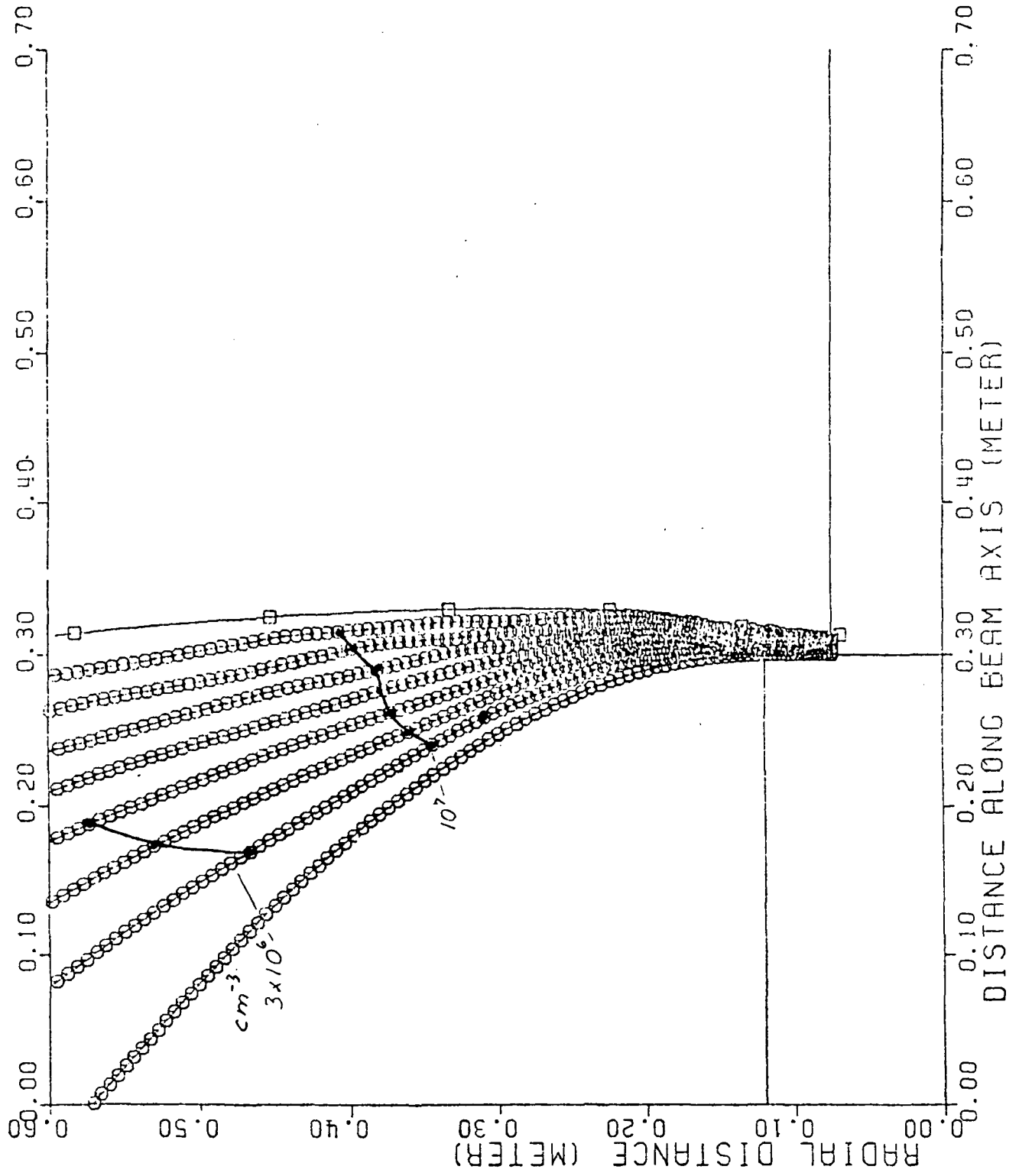

Fig. 9. Computer code solution, similar to that in Fig. 8 except higher resolution in upstream region.

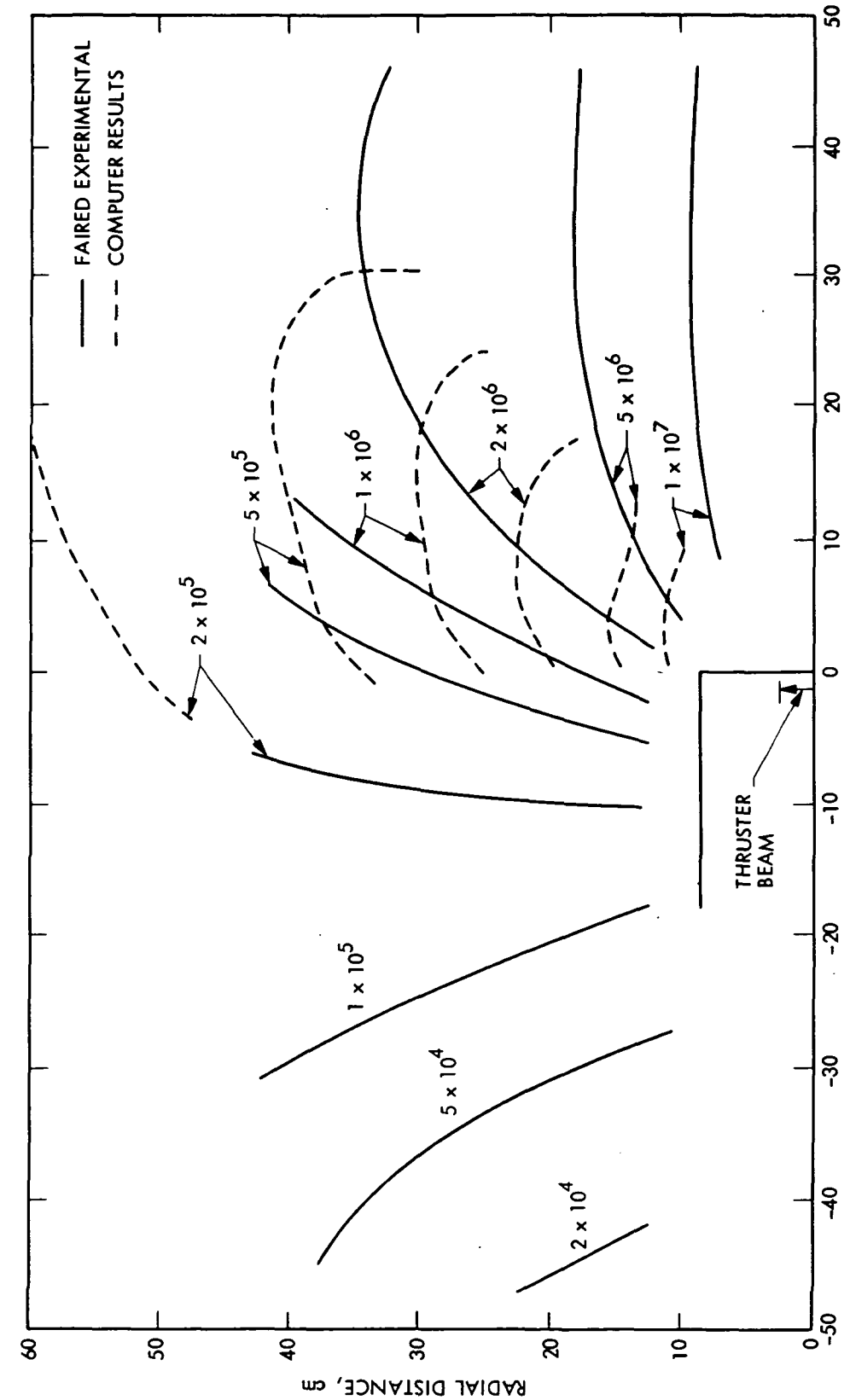

Fig. 10. Map of electron density for 5-cm thruster with a beam current of 0.050 A and a propellant utilization of 0.71. (Computer results duplicated from Fig. 11.)

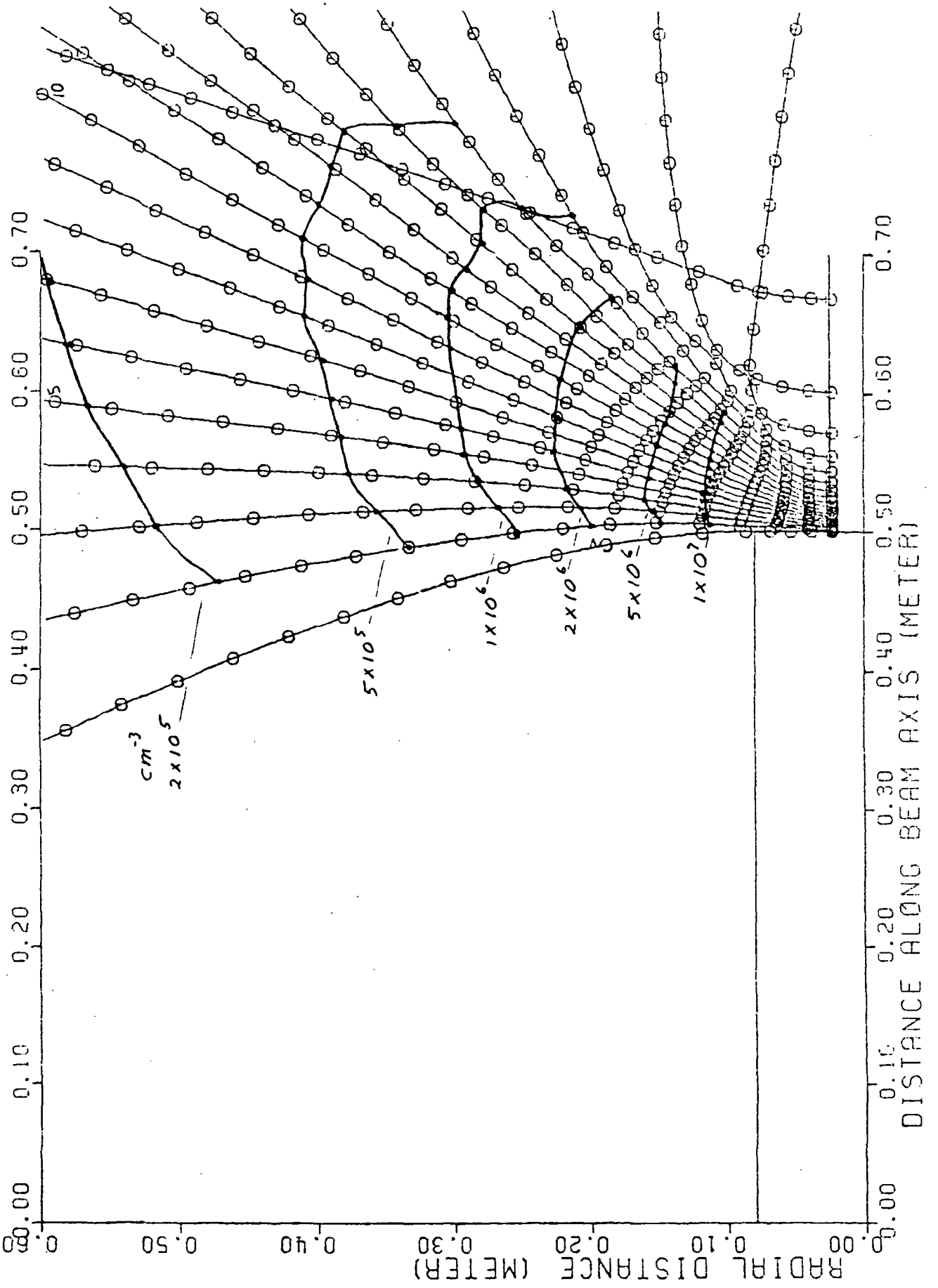

Fig. 11. Computer code solution to simulate experimental results for 5-cm thruster with a beam current of 0.050 A and a propellant utilization of 0.71.

Given the Bohm velocity, the radius of the simulated region and the number of trajectories (NUMION), a DT or a NUMIT can be approximated when the number of trajectories is selected. The approximations represented in Figs. 12, 13, and 14 are based on accumulated experience with the simulation using a wide range of parameters.

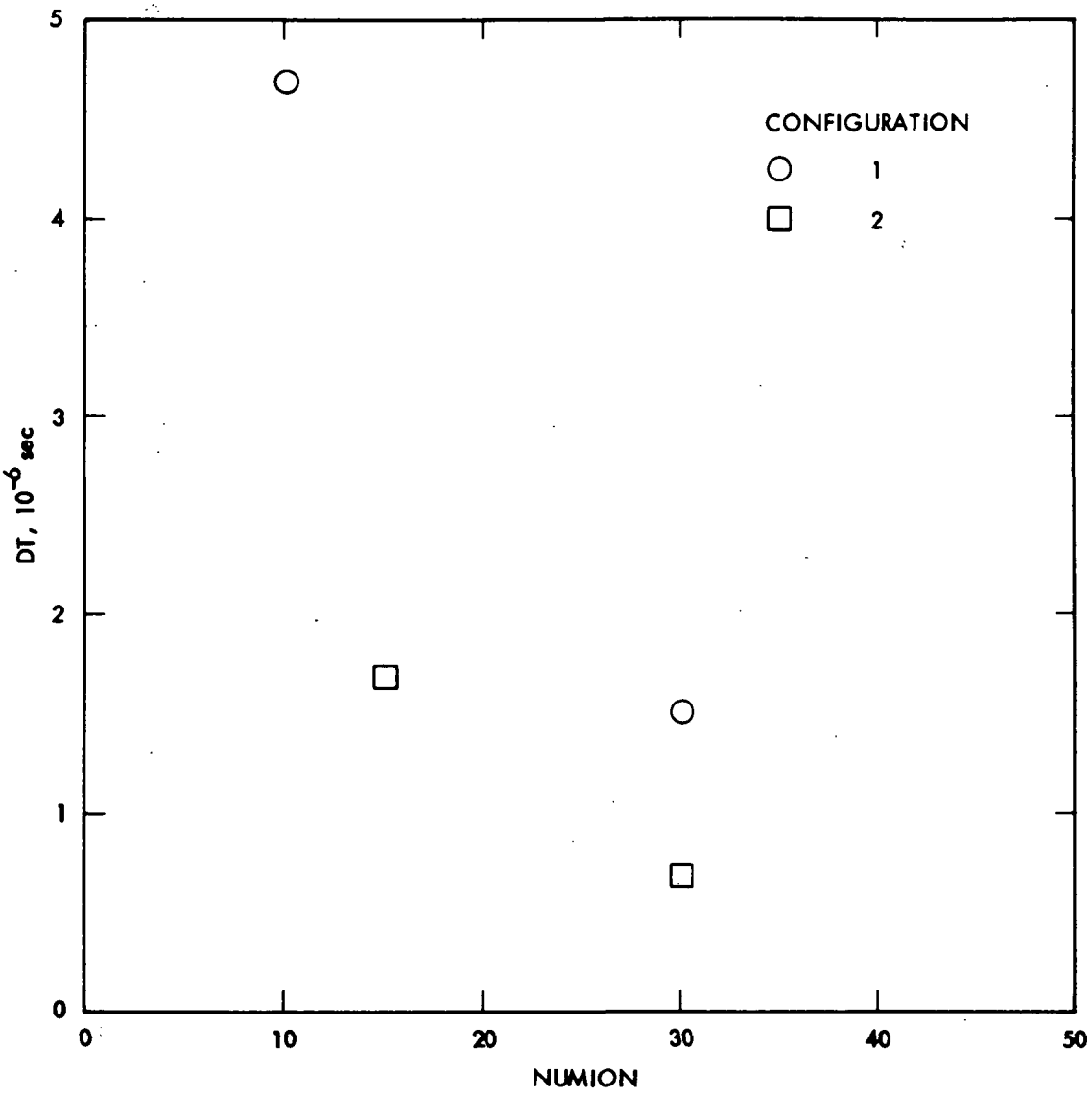

Fig. 12. Successful combinations of DT and NUMION for 5-cm thruster.

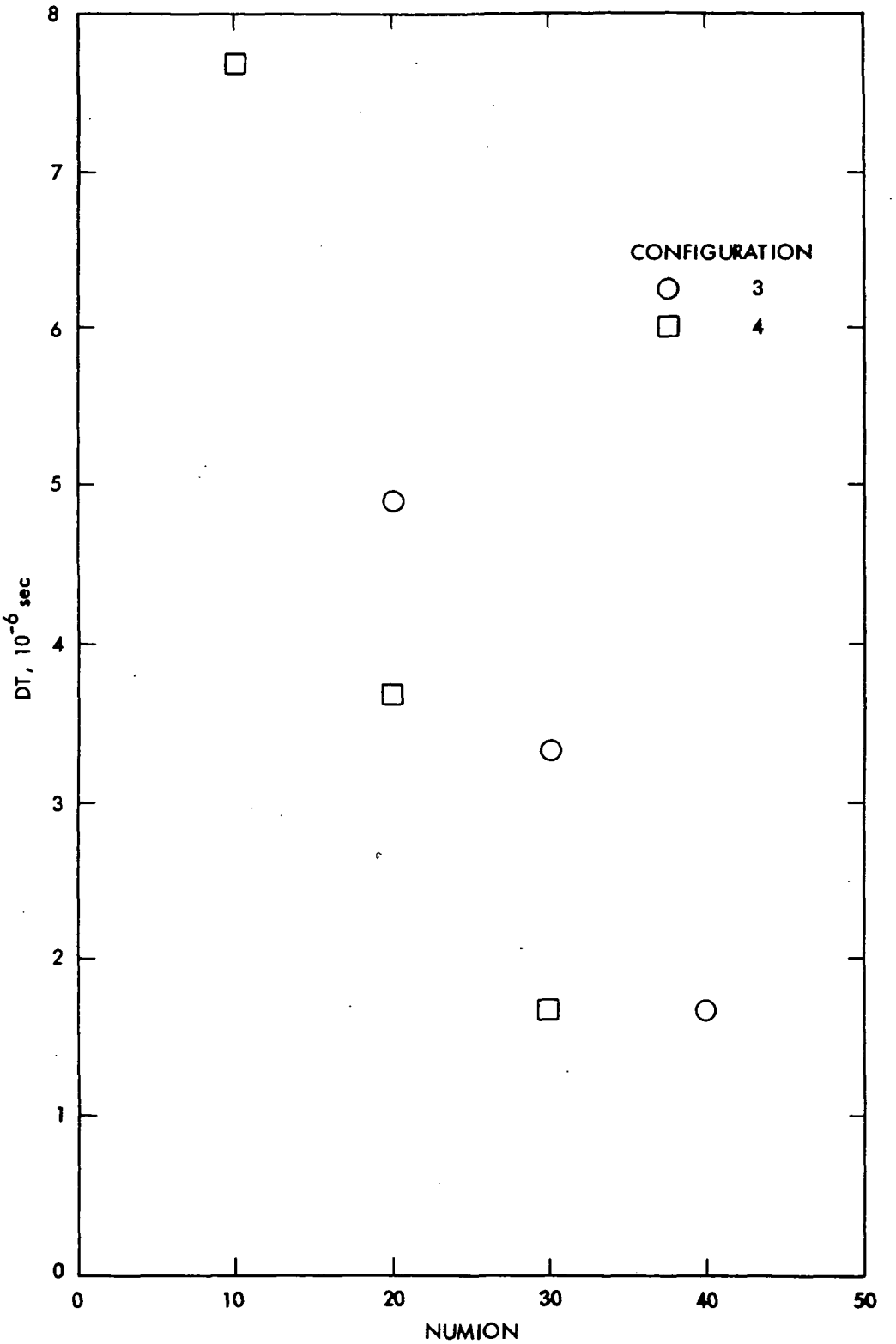

Fig. 13. Successful combinations of DT and NUMION for 15-cm thruster.

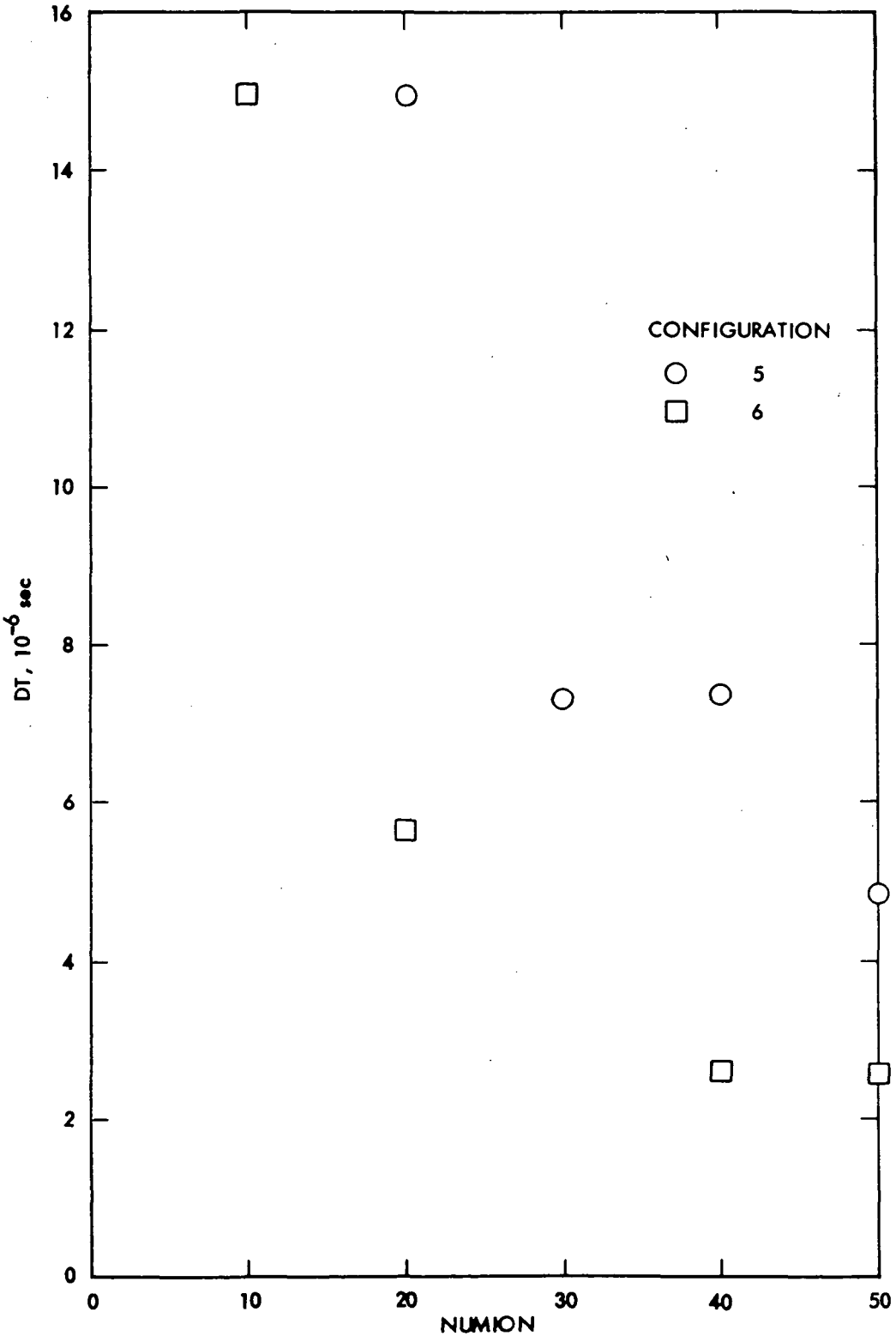

Fig. 14. Successful combinations of DT and NUMION for 30-cm thruster.

APPENDIX

A theoretical benchmark is valuable for verification of the computer code developed to model the charge-exchange plasma propagation in the vicinity of an operating ion thruster. An analytical solution was developed herein for that purpose.

A cylindrical ion beam is assumed with a length very much greater than r_b, the beam radius. The current density representing positive charge-exchange ion production in the beam is assumed uniform along the beam.

In the region exterior to the beam, three basic physical conditions are assumed to hold for the ion population and/or the plasma as a whole. The first is continuity of ion current represented by

$$\vec{\nabla} \cdot \vec{j} = 0 \tag{A1}$$

where $\vec{j}$ is the ion current density. The barometric equation is also used to relate plasma density to local potential V

$$n = n_{o,ref} \exp[e(V-Vo)/kT_e] \tag{A2}$$

where V_o is the potential at the reference density $m_{o,ref}$ and T_e is the electron temperature in the region exterior to the beam. Finally, energy conservation for singly charged ions is represented by

$$|\vec{v}| = (v_o^2 - 2e(V-Vo)/M_i)^{\frac{1}{2}} \tag{A3}$$

where $\vec{v}$ is the ion velocity and M_i is the ion mass. As a boundary condition at the beam edge, ions are assumed to have acquired the Bohm velocity

$$v_B = (kT_{e_B}/m_i)^{\frac{1}{2}} \tag{A4}$$

where T_{e_B} is the electron temperature in the beam.

The ion current density is related to the streaming velocity by

$$\vec{j} = ne\vec{v} \ . \tag{A5}$$

For the assumed symmetry, the velocity is radial and is

$$\vec{v} = v(r)\hat{r} \ . \tag{A6}$$

In cylindrical coordinates, Eq. (A1) can be written with the substitution of Eq. (A5) as

$$\frac{1}{r} n(r)v(r) + n(r) \frac{\partial v(r)}{\partial V} \frac{\partial V(r)}{\partial r} + v(r) \frac{\partial n(r)}{\partial V} \frac{\partial V(r)}{\partial r} = 0 \tag{A7}$$

which can be solved for V(r) by eliminating n(r) and v(r) using Eqs. (A2) and (A3). The solution can then be written as

$$(1 - e(V-Vo)/kT_e)^{\frac{1}{2}} \exp(-e(V-Vo)/kT_e) = r/r_b \ . \tag{A8}$$

The density and velocity can be calculated using Eq. (A8) along with Eq. (A3) or Eq. (A4).

The solution in terms of potential, density and velocity is displayed in dimensionless form in Figs. 1A, 2A, and 3A.

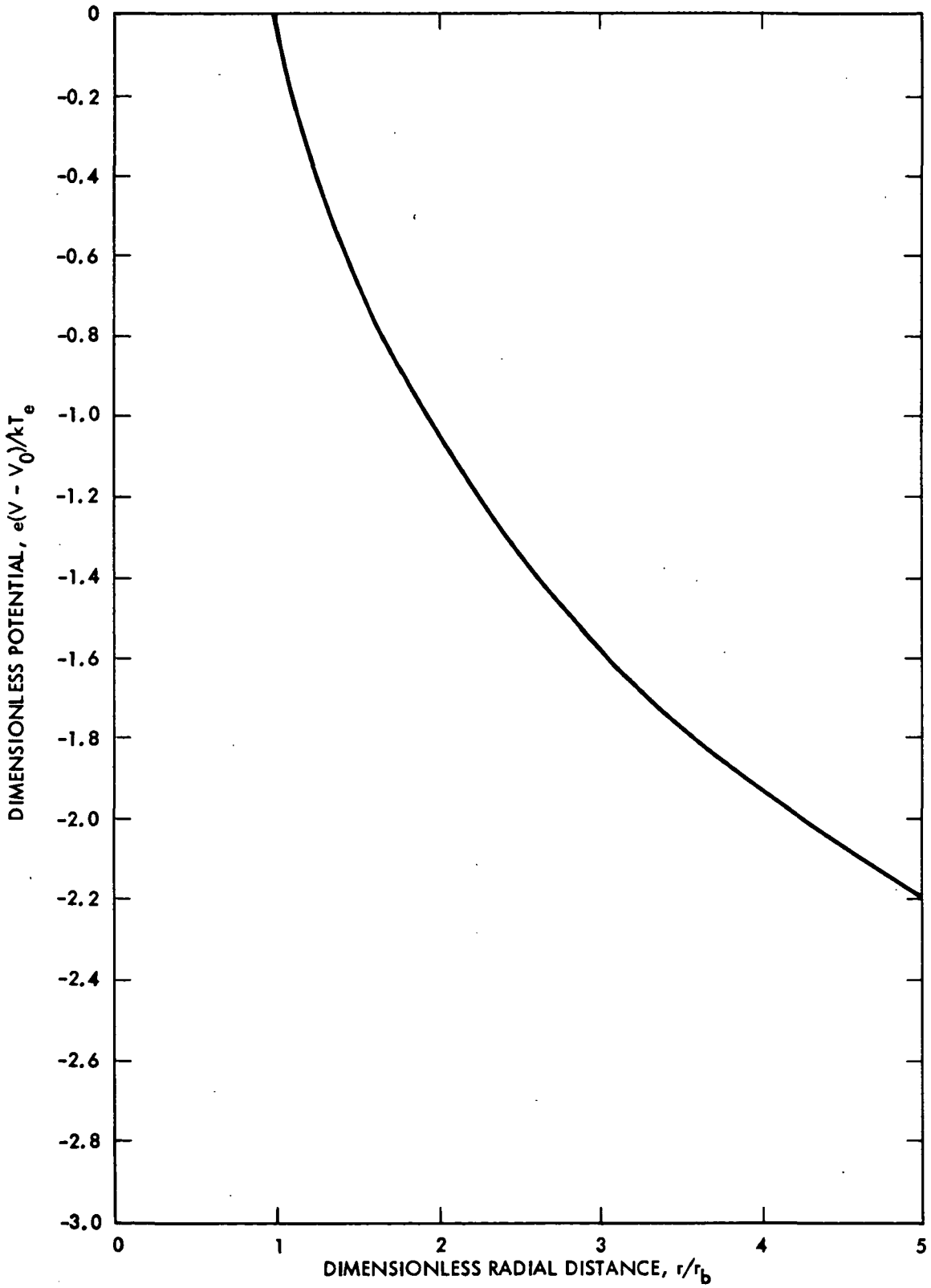

Fig. 1A. Potential as a function of radial distance.

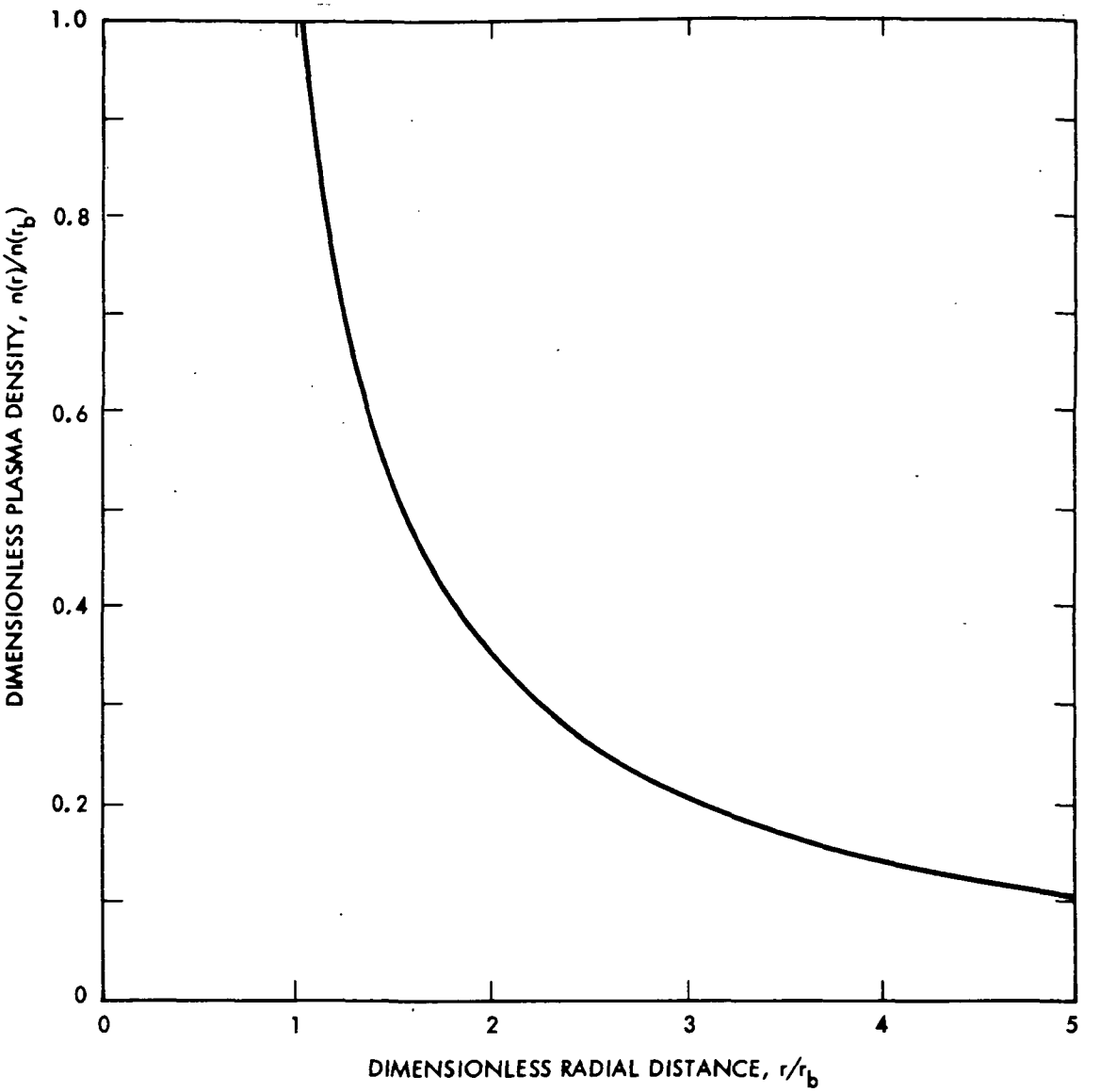

Fig. 2A. Density as a function of radial distance.

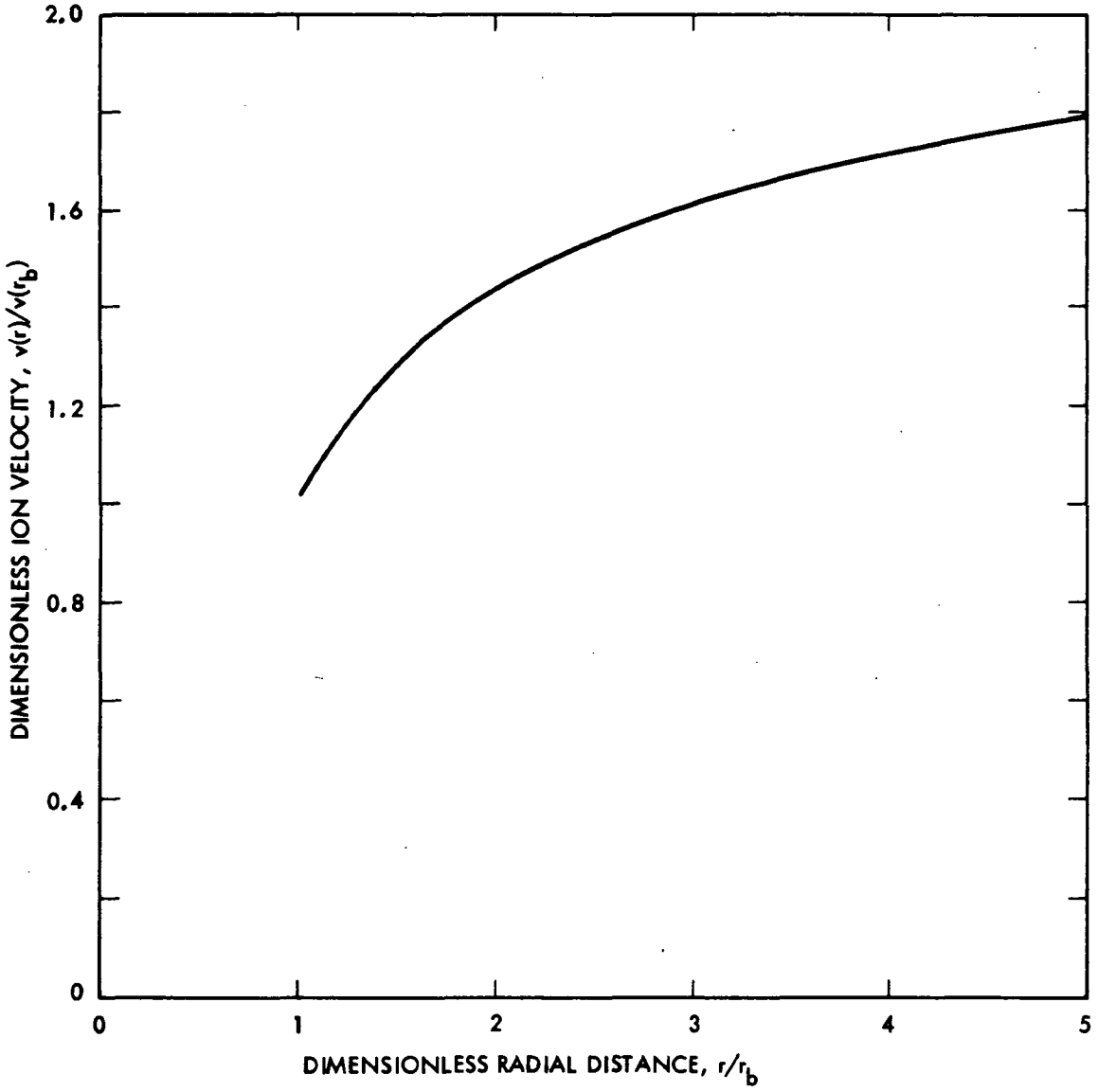

Fig. 3A. Velocity as a function of radial distance.

REFERENCES

1. J. F. Staggs, W. P. Gula, and W. R. Kerslake, J. Spacecr. Rockets, Vol. 5, pp. 159-164 (1968).

2. W. Knauer, J. R. Bayless, G. Todd, and J. W. Ward, NASA Contr. Rep. CR-72675, May 1970.

3. R. Worlock, G. Trump, J. M. Sellen, and R. F. Kemp, AIAA Paper No. 73-1101 (1973).

4. G. K. Komatsu, R. K. Cole, D. K. Hoffmaster, and J. M. Sellen, Jr., AIAA Paper No. 75-428 (1975).

5. H. R. Kaufman, NASA Contr. Rep. CR-134844, June 1975.

6. H. R. Kaufman, NASA Contr. Rep. CR-135099, Oct. 1976.

7. H. R. Kaufman, NASA Contr. Rep. CR-135318, Dec. 1977.

8. J. M. Sellen, Jr., W. Bernstein, and R. F. Kemp, Rev. Sci. Instr., Vol. 36, pp. 316-322 (1965).

9. H. S. Ogawa, R. K. Cole, and J. M. Sellen, Jr., AIAA Paper No. 69-263 (1969).

10. H. S. Ogawa, R. K. Cole, and J. M. Sellen, Jr., AIAA Paper No. 70-1142 (1970).

11. VERSATEC Graphics Programming Manual, 50028-90001, December 1976, a XEROX Co., Santa Clara, California.

PLASIM 1

```
      PROGRAM PLASIM(INPUT,OUTPUT,TAPE5=INPUT,TAPE6=OUTPUT,NPARAM)
C FOR ZION(1,N) AND XION(I,N) I=ION PATH NUMBER,N=ITERATION
C
C**** DRIVER **** A ***************************************************
C
C  BLANK COMMON FOR LARGE ARRAYS
      COMMON ZION(51,251),XION(51,251),VZ(251),VX(251),ISTAT(51)
     1,IMAG(6180),NC(100),DN(100)
      COMMON / IO / IN,IOUT,INFO(8),KEY,NDSP1,NDSP2,ICHAR(14),ITITL(28)
C  COMMON / PARAM / FOR PARAMETERS
      COMMON/PARAM/N,NUMION,NUMIT,DT ,RB,RBOUND,RT,TCEION,BMCJR,UTIL,
     1 TELBM,THLENG,UMSION,VIONB,ZBOUND,IL,IR,PI,BK,Q,DNO,DNZRB<
      CALL READ
C PERFORM INITIALIZATION
      CALL INIT
C WRITE OUT INITIAL PARAMETERS
      CALL WRIT(1)
C CALCULATE NEXT POSITION FOR EACH ION PATH
      DO 20 NN=2,NUMIT
      N=NN
      CALL WRIT(3)
      CALL CALC
 20   CONTINUE
C  GO TO PLOTTING ROUTINE
      IF(NDSP1.EQ.1) CALL VRSPLT
      STOP
      END
        BLOCK DATA
C  BLANK COMMON FOR LARGE ARRAYS
      COMMON ZION(51,251),XION(51,251),VZ(251),VX(251),ISTAT(51)
     1,IMAG(6180),NC(100),DN(100)
      COMMON / IO / IN,IOUT,INFO(8),KEY,NDSP1,NDSP2,ICHAR(14),ITITL(28)
C  COMMON / PARAM / FOR PARAMETERS
      COMMON/PARAM/N,NUMION,NUMIT,DT ,RB,RBOUND,RT,TCEION,BMCJR,UTIL,
     1 TELBM,THLENG,UMSION,VIONB,ZBOUND,IL,IR,PI,BK,Q,DNO,DNZRB<
C--DATA FOR IO  BUFFERS: TAPE 5 FOR INPUT, TAPE6 FOR OUTPUT
      DATA  IN,IOUT /5,6/
C  DATA FOR CONSTANTS
      DATA BK,Q,PI /1.3806E-23,1.602E-19,3.14159/
      END
       SUBROUTINE READ
C  READ PROVIDES INITIAL VALUES FOR PARAMETERS
C
C**** READ ROUTINE ****************************************************
C
C  BLANK COMMON FOR LARGE ARRAYS
      COMMON ZION(51,251),XION(51,251),VZ(251),VX(251),ISTAT(51)
     1,IMAG(6180),NC(100),DN(100)
      COMMON / IO / IN,IOUT,INFO(8),KEY,NDSP1,NDSP2,ICHAR(14),ITITL(28)
C  COMMON / PARAM / FOR PARAMETERS
      COMMON/PARAM/N,NUMION,NUMIT,DT ,RB,RBOUND,RT,TCEION,BMCJR,UTIL,
```

```
     1 TELBM,THLENG,UMSION,VIONB,ZBOUND,IL,IR,PI,BK,Q,DNO,DNZRBK
C-- KEY.EQ.1  REGULAR DISTRIBUTION
C--  KEY.EQ.0  BENCHMARK UNIFORM DISTRIBUTION
  11  FORMAT(14A6)
C  READ 80 COLUMNS OF INFORMATION DESCIBING RUN
      READ(IN,11) INFO
C  READ NUMBER OF IONS AND ITERATIONS, ALSO KEY FOR OUTPUT
      READ(IN,12) NUMION,NUMIT,KEY,NDSP1,NDSP2
  12  FORMAT(7I10)
C  READ BOUNDARY SPECIFICATIONS
      READ(IN,13) RB,RBOUND,RT,THLENG,BMCUR,UTIL
  13  FORMAT(7F10.5)
C  READ STEPSIZE AND ION SPECIFICATIONS
      READ(IN,14) TCEION,TELBM,UMSION
  14  FORMAT(4E15.5)
C  READ GRAPH INFORMATION
      READ(IN,15) ITITL
  15  FORMAT(8A10)
  99  CONTINUE
      RETURN
      END
      SUBROUTINE INIT
C
C**** INITIALIZE ROUTINE **** B1 ****************************************
C
C  BLANK COMMON FOR LARGE ARRAYS
      COMMON ZION(51,251),XION(51,251),VZ(251),VX(251),ISTAT(51)
     1,IMAG(6180),NC(100),DN(100)
      COMMON / IO / IN,IOUT,INFO(8),KEY,NDSP1,NDSP2,ICHAR(14),ITITL(28)
C  COMMON / PARAM / FOR PARAMETERS
      COMMON/PARAM/N,NUMION,NUMIT,DT ,RB,RBOUND,RT,TCEION,BMCJR,UTIL,
     1 TELBM,THLENG,UMSION,VIONB,ZBOUND,IL,IR,PI,BK,Q,DNO,DNZRBK
C CALCULATE DISTANCE BETWEEN ION EXIT POINTS
      IF(KEY.EQ.0) CALL DENSE(1)
      IF(KEY.EQ.0) GO TO 110
      DNZRBK=FLOAT(NUMION)/(0.95*RB)
      DH=.001
      ZIM=0.
      ZUP=ZIM+RB
      NUM=2*NUMION+1
      DO 100 IJ=1,NUM
      ZLOW=ZIM
      DO 60 J=1,100
      HS=DNZRBK*((ZUP-ZIM)-SQRT(ZUP**2+RB**2)+SQRT(ZIM**2+RB**2))
      IF(HS-0.5) 60,70,70
  60  ZUP=2.*ZUP
      CALL WRIT(5)
  70  ZI=ZUP
      DO 90 K=1,1000
      ZI=(ZUP+ZLOW)*0.5
      HS=DNZRBK*((ZI-ZIM)-SQRT(ZI**2+RB**2)+SQRT(ZIM**2+RB**2))
      IF(ABS(HS-0.5)-DH) 95,95,75
  75  IF(HS-0.5) 85,85,80
  80  ZUP=ZI
      GO TO 90
```

```
   85  ZLOW=ZI
   90  CONTINUE
   95  IK=MOD(IJ,2)
       IF(IK.EQ.0) GO TO 100
       I=(IJ+1)/2
       ZION(I,2)=ZI
       XION(I,2)=RB
  100  ZIM=ZI
       DO 105 I=1,NUM
  105  ZION(I,2)=THLENG+ZION(I,2)
C THE LAST ITERATION WILL SET BOUNDARY ON Z AXIS
  110  CONTINUE
       ZBOUND=ZION(NUMION+1,2)
C CALCULATE RADIAL ION EXIT VELOCITY FROM BEAM
       VIONB=SQRT(TELBM/UMSION)
C INITIALIZE VELOCITY ARRAYS, VZ(I) AND VX(I), NC(I)
       DO 115 I=1,NUMION
       VZ(I)=0.
       VX(I)=VIONB
       NC(I)=2
  115  CONTINUE
C CALCULATE ITERATION STEP SIZE
       DT=0.75*RBOUND/(VIONB*FLOAT(NUMIT))
C CALCULATE FIRST ITERATION (N=1) BACKWARDS USING VIONB AND DT
       DO 120 I=1,NUMION
       DELV=VIONB*ALOG(1.0+(VIONB*DT/RB))
       XION(I,1)=XION(I,2)-(VIONB+DELV)*DT
       ZION(I,1)=ZION(I,2)
  120  CONTINUE
C CALCULATE INITIAL DENSITY CONSTANTS FOR EACH PATH
       DNO=(6.175E+16)*(BMCUR**2.)*(1.-UTIL)/(UTIL*RB*PI*FLOAT(NUMION))
       DN(1)=DNO*(1.0/(ZION(2,1)-ZION(1,1))+1.0/(ZION(1,1)-THLENG))/
      1     (2.0*XION(1,1))
       DO 125 I=2,NUMION
       DN(I)=DNO*(1.0/(ZION(I+1,1)-ZION(I,1))+1.0/(ZION(I,1)-
      1     ZION(I-1,1)))/(2.0*XION(I,1))
  125  CONTINUE
C SET ALL IONS ACTIVE
       DO 130 I=1,NUMION
       ISTAT(I)=0
  130  CONTINUE
C SET LEFT-MOST AND RIGHT-MOST PATH ACTIVE INDICIES
       IL=1
       IR=NUMION
C**** RETURN TO DRIVER ************************************************
       N=1
       CALL WRIT(2)
       N=2
       CALL WRIT(2)
       RETURN
       END
        SUBROUTINE CALC
C
```

```
C**** CALCULATION ROUTINE **** 83 ************************************
C
C  BLANK COMMON FOR LARGE ARRAYS
      COMMON ZION(51,251),XION(51,251),VZ(251),VX(251),ISTAT(51)
     1,IMAG(6180),NC(100),DN(100)
      COMMON / IO / IN,IOUT,INFO(8),KEY,NDSP1,NDSP2,ICHAR(14),ITITL(28)
C  COMMON / PARAM / FOR PARAMETERS
      COMMON/PARAM/N,NUMION,NUMIT,DT ,RB,RBOUND,RT,ICEION,BMCJR,UTIL,
     1 TELBM,THLENG,UMSION,VIONB,ZBOUND,IL,IR,PI,BK,Q,DNO,DNZRBK
      DO 435 I=1,NUMION
  302 N=NC(I)
      MISSL=0
      MISSR=0
      NOACCL=0
C CHECK FOR INACTIVE IONS
       IF(ISTAT(I)) 499,305,430
C GET SLOPE OF LINE PERPENDICULAR TO TRAJECTORY
  305 DXI=XION(I,N)-XION(I,N-1)
      IF(DXI.EQ.0.) DXI=1.0E-12
  313 DZI=ZION(I,N-1)-ZION(I,N)
      DXDZP=DZI/DXI
      THETAP=ATAN2(DZI,DXI)
      XPO=XION(I,N)-DXDZP*ZION(I,N)
C CHECK ION DENSITY PROPORTION TO LEFT
C IF FIRST ACTIVE PATH HANDLE AS SPECIAL CASE
  310 IF(I-IL) 499,490,312
  312 NL=NC(I-1)
C GET SLOPE TO ENDPOINT TO PATH ON LEFT
  318  DZIL=ZION(I,N)-ZION(I-1,NL)
      IF(DZIL.EQ.0.) DZIL=1.0E-12
  320  DXIL=XION(I,N)-XION(I-1,NL)
      THETAL=ATAN2(DXIL,DZIL)
       DXDZL=DXIL/DZIL
C IF NO INTERSECTION IS FOUND, GET APPROXIMATE DISTANCE
      IF(THETAL-THETAP) 325,325,340
C FIND INTERVAL IN WHICH THE LINES INTERSECT
  325  DZIL=ZION(I,N)-ZION(I-1,NL-1)
      MISSL=1
      IF(DZIL.EQ.0.) DZIL=1.0E-12
  330  DXIL=XION(I,N)-XION(I-1,NL-1)
      THETAL=ATAN2(DXIL,DZIL)
       DXDZL=DXIL/DZIL
      IF(THETAP-THETAL) 340,340,335
C RESET NL AND GO BACK AND CHECK EARLIER INTERVAL
  335  NL=NL-1
      IF(NL-1) 499,340,325
C BEST INTERVAL FOUND ----- FIND X INTERCEPTS,THEN INTERSECTION POINT
  340 DZIL=ZION(I-1,NL)-ZION(I-1,NL-1)
      IF(DZIL.EQ.0.) DZIL=1.0E-12
      DXDZL=(XION(I-1,NL)-XION(I-1,NL-1))/DZIL
      XLO=XION(I-1,NL)-DXDZL*ZION(I-1,NL)
      ZLINTR=(XPO-XLO)/(DXDZL-DXDZP)
      XLINTR=DXDZP*ZLINTR+XPO
```

```
C CALCULATE PERPENDICULAR DISTANCE TO LEFT ION PATH
        DSPL=SQRT((ZLINTR-ZION(I,N))**2+(XLINTR-XION(I,N))**2)
C CALCULATE POTENTIAL TO THE LEFT
 343   DNL=DNO/(XION(I,N)*DSPL)
       VL=-ALOG(DNL)*TCEION
C * * * * * * * * * * * * * * * * * * * * * * * * * * * * * * * * * * *
C CHECK ION DENSITY PROPORTION TO RIGHT
C IF LAST ACTIVE PATH HANDLE AS SPECIAL CASE
 345   IF(IR-I) 499,495,350
 350    NR=NC(I+1)
C GET SLOPE TO ENDPOINT OF PATH ON RIGHT
 360    DZIR=ZION(I+1,NR)-ZION(I,N)
       IF(DZIR.EQ.0.) DZIR=1.0E-12
 365    DXIR=XION(I+1,NR)-XION(I,N)
       THETAR=ATAN2(DXIR,DZIR)
        DXDZR=DXIR/DZIR
C IF NO INTERSECTION IS FOUND, GET APPROXIMATE DISTANCE
       IF(THETAP-THETAR) 370,370,385
C FIND INTERVAL IN WHICH THE LINES INTERSECT
 370    DZIR=ZION(I+1,NR-1)-ZION(I,N)
       MISSR=1
       IF(DZIR.EQ.0.) DZIR=1.0E-12
 375   DXIR=XION(I+1,NR-1)-XION(I,N)
       THETAR=ATAN2(DXIR,DZIR)
       DXDZR=DXIR/DZIR
       IF(THETAR-THETAP) 385,385,380
C RESET NR AND GO BACK AND CHECK EARLIER INTERVAL
 380    NR=NR-1
       IF(NR-1) 499,385,370
C BEST INTERVAL FOUND ----- FIND X INTERCEPT,THEN INTERSECTION POINT
 385   DZIR=ZION(I+1,NR)-ZION(I+1,NR-1)
       IF(DZIR.EQ.0.) DZIR=1.0E-12
       DXDZR=(XION(I+1,NR)-XION(I+1,NR-1))/DZIR
       XRO=XION(I+1,NR)-DXDZR*ZION(I+1,NR)
       ZRINTR=(XRO-XPO)/(DXDZP-DXDZR)
       XRINTR=DXDZP*ZRINTR+XPO
C CALCULATE PERPENDICULAR DISTANCE TO RIGHT ION PATH
        DSPR=SQRT((ZRINTR-ZION(I,N))**2+(XRINTR-XION(I,N))**2)
C CALCULATE POTENTIAL TO THE RIGHT
 387   DNR=DNO/(XION(I,N)*DSPR)
       VR=-ALOG(DNR)*TCEION
C CALCULATE PERPENDICULAR FORCE , POSITVE RIGHT * NEGATIVE LEFT
       IF(I-IL) 499,392,394
 392   IF(VL.GT.VR) GO TO 394
       VL=VR
       NOACCL=1
 394   IF(IR-I) 499,396,398
 396   IF(VR.GT.VL) GO TO 398
       VR=VL
       NOACCL=1
 398    F=(VR-VL)*2.0/(DSPL+DSPR)
C GET Z AND X COMPONENTS OF FORCE USING PERPENDICULAR SLOPE
       SINP=SIN(THETAP)
       COSP=COS(THETAP)
```

```
      FZ=F*COSP
      FX=F*SINP
C CALCULATE VELOCITY COMPONENTS FOR THIS ITERATION
      C=DT/UMSION
      VELZ=FZ*C
      VELX=FX*C
C CALCULATE TOTAL VELOCITY COMPONENTS AND MAGNITUDE OF TOTAL VELOCITY
       VELTX=VELX+VX(I)
       VELTZ=VELZ+VZ(I)
       VELT=SQRT(VELTX**2+VELTZ**2)
C NORMALIZE VELOCITY COMPONENTS
      V=SQRT(VZ(I)**2+VX(I)**2)
      VELTZ=V*VELTZ/VELT
      VELTX=V*VELTX/VELT
C * * * * CALCULATE LONGITUDINAL ACCELERATING FORCE * * * * * * * * * *
C GET APPROXIMATE DENSITY (AVERAGE) CONSTANT
      DNA=(DNL+DNR)/2.
      ELDEN=DNO/((DSPL+DSPR)*XION(I,N)*V)
C GET POTENTIAL DIFFERENCE TO LAST ITERATION
      DV=ALOG(DNA/DN(I))*TCEION
      IF(NOACCL.EQ.1) DV=0.0
      F=-DV/SQRT((ZION(I,N)-ZION(I,N-1))**2+(XION(I,N)-XION(I,N-1))**2)
C CALCULATE VELOCITY COMPONENTS
      VELZ=-F*SINP*C
      VELX=F*COSP*C
      VZ(I)=VELTZ+VELZ
      VX(I)=VELTX+VELX
C CALCULATE NEXT POSITION OF ION
      ZION(I,N+1)=VZ(I)*DT+ZION(I,N)
      XION(I,N+1)=VX(I)*DT+XION(I,N)
      DN(I)=DNA
C  GO SEE IF NEW POINT IS OUTSIDE BOUNDARIES
      CALL BOUND(ZION(I,N+1),XION(I,N+1),I)
 430   CONTINUE
      J=MOD(NC(I),NDSP2)
      IF(J.NE.0) GO TO 432
      V=SQRT(VZ(I)**2+VX(I)**2)
      WRITE(IOUT,497) I,N,ISTAT(I),ZION(I,N+1),XION(I,N+1),VZ(I),
     2  VX(I),V,DN(I),ELDEN
 497  FORMAT(I3,2I4,12E10.3)
 432  NC(I)=NC(I)+1
      IF((MISSL*MISSR).EQ.1) GO TO 302
 435  CONTINUE
      RETURN
C * * * * * * * SPECIAL CASES * * * * * * * * * * * * * * * * * * * * *
C LEFT - MOST ACTIVE PATH --- GET DISTANCE TO LEFT BOUNDARY
 490  DSPL=DS(ZION(I,N),XION(I,N),THETAP,XPO,0)
      GO TO 343
C RIGHT - MOST ACTIVE PATH --- GET DISTANCE TO RIGHT BOUNDARY
 495  DSPR=DS(ZION(I,N),XION(I,N),THETAP,XPO,1)
       GO TO 387
C ERROR EXIT * * * * * * * * * * * * * * * * * * * * * * * * * * * *
 499  ISTAT(I)=8888
      GO TO 430
      END
```

```
      SUBROUTINE BOUND(Z,X,I)
C
C**** ROUTINE TO CHECK IF POINT (Z,X) IS OUTSIDE BOUNDARIES **********
C**** RETURN, ISTAT.GT.0 - OUTSIDE, ISTAT=0 - WITHIN BOUNDS **********
C
C  BLANK COMMON FOR LARGE ARRAYS
      COMMON ZION(51,251),XION(51,251),VZ(251),VX(251),ISTAT(51)
     1,IMAG(6180),NC(100),DN(100)
      COMMON / IO / IN,IOUT,INFO(8),KEY,NDSP1,NDSP2,ICHAR(14),ITITL(28)
C  COMMON / PARAM / FOR PARAMETERS
      COMMON/PARAM/N,NUMION,NUMIT,DT ,RB,RBOUND,RT,TCEION,BMCJR,UTIL,
     1 TELBM,THLENG,UMSION,VIONB,ZBOUND,IL,IR,PI,BK,J,DNO,DNZRB
       IF(X-RB) 770,770,700
  700  IF(RBOUND-X) 770,770,710
  710  IF(ZBOUND-Z) 770,770,720
  720  IF(Z) 770,770,730
  730  IF(THLENG.GT.Z.AND.RT.GT.X) GO TO 770
       GO TO 790
  770  ISTAT(I)=N
C IF LEFT-MOST OR RIGHT-MOST PATH, RESET INDEX
       IF(I.NE.IL) GO TO 780
       DO 773 II=1,NUMION
       LIP=I+II
       IF(ISTAT(LIP)) 775,775,773
  773  CONTINUE
  775  IL=I+II
       RETURN
  780  IF(I.NE.IR) GO TO 790
       DO 783 II=1,IR
       LIM=I-II
       IF(ISTAT(LIM)) 785,785,783
  783  CONTINUE
  785  IR=I-II
  790   RETURN
        END
       SUBROUTINE WRIT(KE)
C--WRIT PRINTS INFORMATION ABOUT THE SIMULATION
C--KE=1 : HEADING, INITIAL INFO AND DATA
C--KE=2: INTERIM STATUS OF MAIN VARIABLES
C--KE=3: FINISH OF A PASS, RESULTS, START OF NEW PASS
C--KE=4: FINISH OF LAST PASS, RESULT
C--KE=5: QUIT, ERROR SUMMARY IF FOUND BY THIS PROGRAM
C
C  BLANK COMMON FOR LARGE ARRAYS
      COMMON ZION(51,251),XION(51,251),VZ(251),VX(251),ISTAT(51)
     1,IMAG(6180),NC(100),DN(100)
      COMMON / IO / IN,IOUT,INFO(8),KEY,NDSP1,NDSP2,ICHAR(14),ITITL(28)
C  COMMON / PARAM / FOR PARAMETERS
      COMMON/PARAM/N,NUMION,NUMIT,DT ,RB,RBOUND,RT,TCEION,BMCJR,UTIL,
     1 TELBM,THLENG,UMSION,VIONB,ZBOUND,IL,IR,PI,BK,J,DNO,DNZRB
      DATA IPAG,LAB,NPAS /0,6HPLASIM,1  /
C--   FORMATS
   10 FORMAT( 43H0     THIS RUN MAY BE CHARACTERIZED BY INFO=,//7X,14A6/
   11 FORMAT(1H1,//,60X,A10,I3,//////  )
```

```
   12  FORMAT(7X,7A10,/    )
   13   FORMAT(////17X,33HP L A S M A   S I M U L A T I O N,///
      2       17X,43HA COMPUTER CODE TO DESCRIBE THE PROPAGATION,//
      3       17X,43HOF A CHARGE-EXCHANGE PLASMA IN THE VICINITY,//
      4       17X,40HOF AN ELECTRICALLY PROPELLED SPACECRAFT ,///
      5       17X,38HWRITTEN BY JOHN BARNES AND DALE WINDER,//
      6       17X,33HFOR THE JET PROPULSION LABORATORY,//
      7       21X,27H( J P L  P. O. NO. 955322 ),///
      8       17X,41HHAROLD R. KAUFMAN, PRINCIPAL INVESTIGATOR ,//
      9       27X,21HDEPARTMENT OF PHYSICS,//
      1       25X,25HCOLORADO STATE UNIVERSITY,//
      2       26X,23HFORT COLLINS, CO  80523  ,//
      3       32X,10HJULY, 1979)
   14   FORMAT(1H1,//60X,A10,I3,/////,10X,21HSCHEMATIC OF THRUSTER,///
      2       11X,3H- :,/,11X,3HA :,/,11X,3H: :,/,11X,3H: :, /,
      3       11X,3H: :,5X,6HTHLENG,/,11X,3H: :,7X,1HV,/,
      4       11X,11H: ---------,43X,6HZBOUND,/,11X,1H:,6X,4HA  :,44X,1HV
      5       /,9X,6HRBOUND,3X,4H:  :,/11X,1H:,6X,1H:,2X,45(1H=),/,
      6       11X,1H:,6X,2HRT,5X,1HA,40X,1H:,/,11X,2(1H:,6X)2HRB,39X,1H:,/
      7       4(11X,1H:,6X,1H:,6X,1H:,40X,1H:,/),13X,1H+,13(4H- . )/
      8       11X,5H(0,0),50X,1H:,/,5(66X,1H:,/),21X,45(1H=),/,
      9       2(21X,1H:,/),13X,9(1H-),/,6(13X,1H:,/),///)
   15   FORMAT(20X,28HINITIAL VALUES OF PARAMETERS,//,
      2       7X,52HRBOUND  RT   RB   THLENG  ZBOUND  NUMION NUMIT VIONB,
      3       13H  BMCUR  UTIL,/,7X,3F5.2,2F9.2,
      4       2(3X,I3),2X,F5.0,2(2X,F5.2),///,7X,6HTCEION,6X,
      5       5HTELBM,7X,6HUMSION,10X,2HDT,/7X,4(E10.2,2X)///)
   21  FORMAT(1H1,12(5H -2- ),A10,I3//10X,27HINTERIM STATUS -- ITERATION,
      2       I4,3H OF,I4,11H ITERATIONS,
      3       //,9X,55HI  N ISTAT  ZION(I,N) XION(I,N)   VZ(I)   VX(I)   D
      4N(I),/)
   22  FORMAT(5X,3I4,9E10.3)
   31  FORMAT( 27H RESULTS OF PASS--ITERATION,I4,3H OF,I4,11H ITERATIONS,
      2 /,79H I  N ISTAT  ZION(N+1) XION(N+1)  VZ(I)    VX(I)     V
      3  ON(I)       ELDEN,/)
   41  FORMAT(1H1,12(5H -4- ),A10,I3,//,17X,20HRESULTS OF LAST PASS  ,//
      2       17X,9HITERATION,I4,3H OF,I4,11H TOTAL PASS,I4,
      3       //,9X,45HI  N ISTAT  ZION(I,N) XION(I,N)  VZ(I)  VX(I),//)
   51  FORMAT(1H0,7X,6(10H....5----X),10H**ERROR***  ,/
      2       17X,9HITERATION,I4,3H OF,I4,11H TOTAL PASS,I4, /
      3       //,9X,45HI  N ISTAT  ZION(I,N) XION(I,N)  VZ(I)  VX(I),//)
C--    WHAT KIND OF CALL IS IT
       GOTO  (1,2,3,4,5), KE
C--       1         1         1
C--INITIAL STATE--HEADING AND DATA
    1  IPAG=IPAG + 1
       WRITE(IOUT,11)LAB,IPAG
       WRITE(IOUT,13)
        IPAG = IPAG + 1
       WRITE(IOUT,14)LAB,IPAG
       WRITE(IOUT,10) INFO
       WRITE(IOUT,15)RBOUND,RT,RB,THLENG,ZBOUND,NUMION,NUMIT,VIONB,
      2 BMCUR,UTIL,TCEION,TELBM,UMSION,DT
       RETURN
```

```
C--      2          2          2
C--THIS SECTION PRINTS THE INTERIM STATUS AT THE NTH ITERATION
    2   IPAG = IPAG + 1
        WRITE(IOUT,21) LAB,IPAG,N,NUMIT
        DO 28 I=1,NUMION
   28   WRITE(IOUT,22) I,N,ISTAT(I),ZION(I,N),XION(I,N),VZ(I),VX(I),
       2  DN(I)
        RETURN
C--      3          3          3
C THIS SECTION PRINTS RESULT OF A PASS AT NTH EXTRAPOLATION
    3   IPAG = IPAG + 1
        WRITE(IOUT,31) N,NUMIT
        RETURN
C--      4          4          4
C THIS SECTION PRINTS RESULT OF THE LAST PASS AT NTH ITERATION
    4   IPAG = IPAG + 1
        WRITE(IOUT,41) LAB,IPAG,N,NUMIT,NPAS
        DO 48 I=1,NUMION
  48    WRITE(IOUT,22) I,N,ISTAT(I),ZION(I,N),XION(I,N),VZ(I),VX(I)
        RETURN
C--      5          5          5
C THIS IS FOR ERROR EXIT IF DETECTED BY PLASIM
  5     WRITE(IOUT,51) N,NUMIT,NPAR
        DO 58 I=1,NUMION
  58    WRITE(IOUT,22) I,N,ISTAT(I),ZION(I,N),XION(I,N),VZ(I),VX(I)
        RETURN
        END
        FUNCTION DS(Z,X,ANG,B,LR)
C
C**** ROUTINE TO FIND DISTANCE TO POINT ON BOUNDARY
C**** LR=0 FOR LEFT,LR=1 FOR RIGHT,ANG,NE,90 DEGREES ******************
C
C   BLANK COMMON FOR LARGE ARRAYS
        COMMON ZION(51,251),XION(51,251),VZ(251),VX(251),ISTAT(51)
       1,IMAG(6180),NC(100),DN(100)
        COMMON / IO / IN,IOUT,INFO(8),KEY,NDSP1,NDSP2,ICHAR(14),ITITL(28)
C   COMMON / PARAM / FOR PARAMETERS
        COMMON/PARAM/N,NUMION,NUMIT,DT ,RB,RBOUND,RT,TCEION,BMCJR,UTIL,
       1 TELBM,THLENG,UMSION,VIONB,ZBOUND,IL,IR,PI,BK,Q,DNO,ONZRBK
C IF DISTANCE ON RIGHT IS DESIRED, SUBTRACT 3.14159 FROM PHI
        PHI=ANG
        IF(LR.EQ.1) PHI=PHI-PI
        SLOPE=TAN(PHI)
C INTERVAL BETWEEN BEAM EDGE AND THRUSTER CORNER
   12   PHIB=ATAN2((X-RT),(Z-THLENG))
        IF(Z-THLENG) 23,600,600
  600   PHIA=ATAN2((X-RB),(Z-THLENG))
        IF((PHI-PHIA)*(PHIB-PHI)) 23,610,610
  610   ZINT=THLENG
        XINT=SLOPE*THLENG+B
        GO TO 680
C INTERVAL BETWEEN THRUSTER CORNER AND SPACECRAFT
   23   PHIA=ATAN2((X-RT),Z)
```

```
      IF(PHI-PHIA) 34,620,620
 620  ZINT=(RB-B)/SLOPE
      XINT=RT
      GO TO 680
C INTERVAL ALONG SPACECRAFT SURFACE
  34  PHIB=ATAN2((X-RBOUND),Z)
      IF(PHI-PHIB) 45,630,630
 630  ZINT=0.
      XINT=B
      GO TO 680
C INTERVAL BETWEEN SPACECRAFT AND (ZBOUND,RBOUND)
  45  PHIA=ATAN2((X-RBOUND),(Z-ZBOUND))
      IF(PHI-PHIA) 56,640,640
 640  ZINT=(RBOUND-B)/SLOPE
      XINT=RBOUND
      GO TO 680
C INTERVAL BETWEEN (ZBOUND,RBOUND) TO (ZBOUND,RB)
  56  PHIB=ATAN2((X-RB),(Z-ZBOUND))
      IF(PHIB-PHI-PI) 650,650,61
 650  ZINT=ZBOUND
      XINT=SLOPE*ZBOUND+B
      GO TO 680
C INTERVAL ALONG BEAM EDGE
  61  ZINT=(RB-B)/SLOPE
      XINT=RB
C CALCULATE DISTANCE TO BOUNDARY
 680  DS=SQRT((Z-ZINT)**2+(X-XINT)**2)
      RETURN
      END
      SUBROUTINE DENSE(KASE)
C
C--DENSE DEFINES UNIFORM DISTRIBUTION FOR BENCHMARK SIMULATION
C
C  BLANK COMMON FOR LARGE ARRAYS
      COMMON ZION(51,251),XION(51,251),VZ(251),VX(251),ISTAT(51)
     1,IMAG(6180),NC(100),DN(100)
      COMMON / IO / IN,IOUT,INFO(8),KEY,NDSP1,NDSP2,ICHAR(14),ITITL(28)
C  COMMON / PARAM / FOR PARAMETERS
      COMMON/PARAM/N,NUMION,NUMIT,DT ,RB,RBOUND,RT,TCEION,BMCJR,UTIL,
     1 TELRM,THLENG,UMSION,VIONB,ZBOUND,IL,IR,PI,BK,Q,UNO,DNZRBK
      IF(KASE-1) 200,10,200
  10  DO 70 I=1,NUMION
      ZION(I,2)=THLENG+FLOAT(I)*RT
      XION(I,2)=RB
  70  CONTINUE
      ZION(NUMION+1,2)=ZION(NUMION,2)+THLENG
C RESET THRUSTER RADIUS TO BEAM RADIUS
      RT=RB
      RETURN
 200  CONTINUE
      RETURN
      END
      SUBROUTINE VRSPLT
C
```

```
C--VRSPLT USES VERSATEC PLOTTER TO PLOT ARRAYS X() AND Y()
C
C  BLANK COMMON FOR LARGE ARRAYS
      COMMON ZION(51,251),XION(51,251),VZ(251),VX(251),ISTAT(51)
     1,IMAG(6180),NC(100),ON(100)
      COMMON / IO / IN,IOUT,INFO(8),KEY,NOSP1,NOSP2,ICHAR(14),ITITL(28)
C  COMMON / PARAM / FOR PARAMETERS
      COMMON/PARAM/N,NUMION,NUMIT,DT ,RB,RBOUND,RT,TCEION,BMCJR,UTIL,
     1 TELBM,THLENG,UMSION,VIONB,ZBOUND,IL,IR,PI,BK,Q,DNO,DNZRB<
      DIMENSION SAVZ(2),SAVX(2)
      DATA ZAXLN,XAXLN,INC,LINTYP /7.0,6.0,1,+10/
C--FIRST ENTRY--SET UP THE SYSTEM, SCALE, AXES AND TITLE IF DESIRED
      CALL PLOTS(0.,0.,0.)
C--SET ORIGIN OF PLOT
      CALL PLOT (1.,1.,-3)
      CALL SETMSG(1)
      SAVZ(1)=0.
      SAVX(1)=0.
      SAVZ(2)=RBOUND/XAXLN
      SAVX(2)=SAVZ(2)
      ZMAX=ZAXLN*SAVZ(2)
      CALL AXIS(0.,0.,ITITL(9),-40,ZAXLN,0.,SAVZ(1),SAVZ(2))
      CALL AXIS(0.,XAXLN,1H ,1,ZAXLN,0.,SAVZ(1),SAVZ(2))
      CALL AXIS(0.,0.,ITITL(13),40,XAXLN,90.,SAVX(1),SAVX(2))
      CALL SYMBOL(1.,8.0,0.14,ITITL(1),0.,80)
      DO 80 J=2,NUMION
      IF(ZION(J,1).GT.ZMAX) GO TO 82
   80 CONTINUE
   82 NUMPT=J-1
      DO 150 J=1,NUMPT
      NPTS=ISTAT(J)
      IF(ISTAT(J).EQ.0) NPTS=NC(J)
      DO 100 NM=1,NPTS
      VZ(NM)=ZION(J,NM)
      VX(NM)=XION(J,NM)
  100 CONTINUE
      DO 120 I=1,2
      NPT=NPTS+I
      VZ(NPT)=SAVZ(I)
  120 VX(NPT)=SAVX(I)
      CALL LINE(VZ,VX,NPTS,INC,LINTYP,1)
  150 CONTINUE
      VX(1)=RT
      VX(2)=RT
      VZ(1)=0.
      VX(3)=0.
      VZ(2)=THLENG
      VZ(3)=THLENG
      VZ(4)=THLENG
      VX(4)=RB
      VX(5)=RB
      VZ(5)=ZMAX
      NPTS=5
      DO 200 I=1,2
```

```
      NPT=NPTS+I
      VZ(NPT)=SAVZ(I)
 200  VX(NPT)=SAVX(I)
      CALL LINE(VZ,VX,NPTS,1,0,0)
C--TERMINATE ALL PLOTTING--RELEASE OUTPUT TO VERSATEC PLOTTER
   3  CALL PLOT(0.,0., +999)
      RETURN
      END
        20        175          1          1          1
      .075        0.6        .12        .30        .63        .85
        4.0E-19          8.0E-19        3.34E-25
PROPAGATION OF CHARGE-EXCHANGE PLASMA
DISTANCE ALONG BEAM AXIS (METER)          RADIAL DISTANCE (METER)
#
```

PLASIM2

```
      PROGRAM PLASIM(INPUT,OUTPUT,TAPE5=INPUT,TAPE6=OUTPUT,NPARAM,   PLAS1
     1  PATHS,TAPE7=PATHS)
C FOR ZION(I,N) AND XION(I,N) .I=ION PATH NUMBER,N=ITERATION
C
C**** DRIVER **** A ************************************************
C
C  BLANK COMMON FOR LARGE ARRAYS
      COMMON ZION(51,251),XION(51,251),VZ(251),VX(251),ISTAT(51)
     1,IMAG(6180),NC(51),DN(51)
      COMMON / IO / IN,IOUT,INFO(8),KEY,NDSP1,NDSP2,ICHAR(14),ITITL(28)
     1  ,IPATHS
      COMMON/PARAM/N,NUMION,NUMIT,DT,RB,RBOUND,RT,TCEION,BMCUR,JTIL,
     1 TELBM,THLENG,UMSION,VIONB,ZBOUND,IL,IR,PI,BK,Q,DNO,DNZRBK,DRATIO
      CALL READ
C PERFORM INITIALIZATION
      CALL INIT
C WRITE OUT INITIAL PARAMETERS
      CALL WRIT(1)
C CALCULATE NEXT POSITION FOR EACH ION PATH
      DO 20 NN=2,NUMIT
      N=NN
      CALL WRIT(3)
      CALL CALC
 20   CONTINUE
      IF(KEY.EQ.0)  CALL WRIT(4)
C  GO TO PLOTTING ROUTINE
      IF(NDSP1.EQ.1) CALL VRSPLT
      STOP
      END
        BLOCK DATA
C  BLANK COMMON FOR LARGE ARRAYS
      COMMON ZION(51,251),XION(51,251),VZ(251),VX(251),ISTAT(51)
     1,IMAG(6180),NC(51),DN(51)
      COMMON / IO / IN,IOUT,INFO(8),KEY,NDSP1,NDSP2,ICHAR(14),ITITL(28)
     1  ,IPATHS
      COMMON/PARAM/N,NUMION,NUMIT,DT,RB,RBOUND,RT,TCEION,BMCUR,JTIL,
     1 TELBM,THLENG,UMSION,VIONB,ZBOUND,IL,IR,PI,BK,Q,DNO,DNZRBK,DRATIO
C--DATA FOR IO  BUFFERS: TAPE 5 FOR INPUT, TAPE6 FOR OUTPUT
      DATA  IN,IOUT,IPATHS /5,6,7/
C  DATA FOR CONSTANTS
      DATA BK,Q,PI /1.3806E-23,1.602E-19,3.14159/
      END
       SUBROUTINE READ
C  READ PROVIDES INITIAL VALUES FOR PARAMETERS
C
C**** READ ROUTINE ************************************************
C
C  BLANK COMMON FOR LARGE ARRAYS
      COMMON ZION(51,251),XION(51,251),VZ(251),VX(251),ISTAT(51)
     1,IMAG(6180),NC(51),DN(51)
      COMMON / IO / IN,IOUT,INFO(8),KEY,NDSP1,NDSP2,ICHAR(14),ITITL(28)
     1  ,IPATHS
```

```
      COMMON/PARAM/N,NUMION,NUMIT,DT,RB,RBOUND,RT,TCEION,BMCUR,JTIL,
     1 TELBM,THLENG,UMSION,VIONB,ZBOUND,IL,IR,PI,BK,Q,DNO,DNZRBK,DRATIO
C-- KEY.EQ.1  REGULAR DISTRIBUTION
C--  KEY.EQ.0  BENCHMARK UNIFORM DISTRIBUTION
  11  FORMAT(14A6)
C  READ 80 COLUMNS OF INFORMATION DESCIBING RUN
      READ(IN,11) INFO
C  READ NUMBER OF IONS AND ITERATIONS, ALSO KEY FOR OUTPUT
      READ(IN,12) NUMION,NUMIT,KEY,NDSP1,NDSP2
  12  FORMAT(7I10)
C  READ BOUNDARY SPECIFICATIONS
      READ(IN,13) RB,RBOUND,RT,THLENG,BMCUR,UTIL
  13  FORMAT(7F10.5)
C  READ STEPSIZE AND ION SPECIFICATIONS
      READ(IN,14) TCEION,TELBM,UMSION
  14  FORMAT(4E15.5)
C  READ GRAPH INFORMATION
      READ(IN,15) ITITL
  15  FORMAT(8A10)
C IF HIGHER UPSTREAM RESOLUTION RUN READ IN PATHS
      IF(KEY) 40,99,40
  40  READ(IPATHS) NMAX,LNUMIN
      READ(IPATHS) (ISTAT(I),I=1,NMAX)
      DO 45 I=1,NMAX
      ISAT=ISTAT(I)
  45  READ(IPATHS) (ZION(I,NN),XION(I,NN),NN=1,ISAT)
      ISAT=ISTAT(KEY)
      DO 50 NN=1,ISAT
      ZION(NUMION+1,NN)=ZION(KEY,NN)
  50  XION(NUMION+1,NN)=XION(KEY,NN)
      ISTAT(NUMION+1)=ISAT
      NC(NUMION+1)=ISAT
      DRATIO=(FLOAT(KEY)-0.5)/FLOAT(LNUMIN)
 99   CONTINUE
       RETURN
       END
      SUBROUTINE INIT
C
C**** INITIALIZE ROUTINE **** B1 ***********************************
C
C  BLANK COMMON FOR LARGE ARRAYS
      COMMON ZION(51,251),XION(51,251),VZ(251),VX(251),ISTAT(51)
     1,IMAG(6180),NC(51),DN(51)
      COMMON / IO / IN,IOUT,INFO(8),KEY,NDSP1,NDSP2,ICHAR(14),ITITL(28)
     1  ,IPATHS
      COMMON/PARAM/N,NUMION,NUMIT,DT,RB,RBOUND,RT,TCEION,BMCUR,JTIL,
     1 TELBM,THLENG,UMSION,VIONB,ZBOUND,IL,IR,PI,BK,Q,DNO,DNZRBK,DRATIO
C CALCULATE DISTANCE BETWEEN ION EXIT POINTS
      DNZRBK=FLOAT(NUMION)/(0.95*RB)
      IF(KEY.GT.0) DNZRBK=DNZRBK/DRATIO
      DH=.00001
      ZIM=0.
      ZUP=ZIM+RB
      SAVE=ZION(NUMION+1,2)
```

```
      NUM=2*NUMION+1
      DO 100 IJ=1,NUM
      ZLOW=ZIM
      DO 60 J=1,100
      HS=ONZRBK*((ZUP-ZIM)-SQRT(ZUP**2+RB**2)+SQRT(ZIM**2+RB**2))
      IF(HS-0.5) 60,70,70
   60 ZUP=2.*ZUP
   70 ZI=ZUP
      DO 90 K=1,1000
      ZI=(ZUP+ZLOW)*0.5
      HS=ONZRBK*((ZI-ZIM)-SQRT(ZI**2+RB**2)+SQRT(ZIM**2+RB**2))
      IF(ABS(HS-0.5)-OH) 95,95,75
   75 IF(HS-0.5) 85,85,80
   80 ZUP=ZI
      GO TO 90
   85 ZLOW=ZI
   90 CONTINUE
   95 IK=MOD(IJ,2)
      IF(IK.EQ.0) GO TO 100
      I=(IJ+1)/2
      ZION(I,2)=ZI
      XION(I,2)=RB
  100 ZIM=ZI
      DO 105 I=1,NUM
  105 ZION(I,2)=THLENG+ZION(I,2)
C THE LAST ITERATION WILL SET BOUNDARY ON Z AXIS
  110 CONTINUE
      ZBOUND=ZION(NUMION+1,2)
      IF(KEY.EQ.0) GO TO 113
      ZION(NUMION+1,2)=SAVE
      ISAT=ISTAT(NUMION+1)
      ZMAX=ZION(NUMION+1,2)
      DO 112 NN=3,ISAT
      IF(ZMAX-ZION(NUMION+1,NN)) 111,112,112
  111 ZMAX=ZION(NUMION+1,NN)
  112 CONTINUE
      ZBOUND=ZMAX
C CALCULATE RADIAL ION EXIT VELOCITY FROM BEAM
  113 VIONB=SQRT(TELBM/UMSION)
C INITIALIZE VELOCITY ARRAYS, VZ(I) AND VX(1), NC(1)
      DO 115 I=1,NUMION
      VZ(I)=0.
      VX(I)=VIONB
      NC(I)=2
  115 CONTINUE
C CALCULATE ITERATION STEP SIZE
      DT=0.75*RBOUND/(VIONB*FLOAT(NUMIT))
      IF(KEY.GT.0) DT=DT*0.75
C CALCULATE FIRST ITERATION (N=1) BACKWARDS USING VIONB AND DT
      DO 120 I=1,NUMION
      DELV=VIONB*ALOG(1.0+(VIONB*DT/RB))
      XION(I,1)=XION(I,2)-(VIONB+DELV)*DT
      ZION(I,1)=ZION(I,2)
  120 CONTINUE
```

```
C CALCULATE INITIAL DENSITY CONSTANTS FOR EACH PATH
      DN0=(6.175E+16)*(BMCUR**2.)*(1.-UTIL)/(UTIL*RB*PI*FLOAT(NJMION))
      IF(KEY.GT.0) DN0=DN0*DRATIO
      DN(1)=DN0*(1.0/(ZION(2,1)-ZION(1,1))+1.0/(ZION(1,1)-THLENG))/
     1     (2.0*XION(1,1))
      DO 125 I=2,NUMION
      DN(I)=DN0*(1.0/(ZION(I+1,1)-ZION(I,1))+1.0/(ZION(I,1)-
     1     ZION(I-1,1)))/(2.0*XION(I,1))
 125  CONTINUE
C SET ALL IONS ACTIVE
      DO 130 I=1,NUMION
      ISTAT(I)=0
 130  CONTINUE
C SET LEFT-MOST AND RIGHT-MOST PATH ACTIVE INDICIES * * * * * * * * * *
C ADD ONE TO IR IF SPECIAL UPSTREAM RUN (KEY.GT.0)
      IL=1
      IR=NUMION
      IF(KEY.GT.0) IR=NUMION+1
C**** RETURN TO DRIVER ***************************************************
      N=1
      CALL WRIT(2)
      N=2
      CALL WRIT(2)
      RETURN
      END
       SUBROUTINE CALC
C
C**** CALCULATION ROUTINE **** B3 ***************************************
C
C  BLANK COMMON FOR LARGE ARRAYS
      COMMON ZION(51,251),XION(51,251),VZ(251),VX(251),ISTAT(51)
     1,IMAG(6180),NC(51),DN(51)
      COMMON / IO / IN,IOUT,INFO(8),KEY,NDSP1,NDSP2,ICHAR(14),ITITL(28)
     1  ,IPATHS
      COMMON/PARAM/N,NUMION,NUMIT,DT,RB,RBOUND,RT,ICEION,BMCUR,UTIL,
     1 IELBM,THLENG,UMSION,VIONB,ZBOUND,IL,IR,PI,BK,Q,DN0,DNZRBK,DRATIO
      DO 435 I=1,NUMION
 302  N=NC(I)
      MISSL=0
      MISSR=0
      NOACCL=0
C CHECK FOR INACTIVE IONS
       IF(ISTAT(I)) 499,305,430
C GET SLOPE OF LINE PERPENDICULAR TO TRAJECTORY
 305  DXI=XION(I,N)-XION(I,N-1)
      IF(DXI.EQ.0.) DXI=1.0E-12
 313  DZI=ZION(I,N-1)-ZION(I,N)
      DXDZP=DZI/DXI
      THETAP=ATAN2(DZI,DXI)
      XP0=XION(I,N)-DXDZP*ZION(I,N)
C CHECK ION DENSITY PROPORTION TO LEFT
C IF FIRST ACTIVE PATH HANDLE AS SPECIAL CASE
 310  IF(I-IL) 499,490,312
```

```
 312  NL=NC(I-1)
C GET SLOPE TO ENDPOINT TO PATH ON LEFT
 318   DZIL=ZION(I,N)-ZION(I-1,NL)
      IF(DZIL.EQ.0.) DZIL=1.0E-12
 320   DXIL=XION(I,N)-XION(I-1,NL)
      THETAL=ATAN2(DXIL,DZIL)
       DXDZL=DXIL/DZIL
C IF NO INTERSECTION IS FOUND, GET APPROXIMATE DISTANCE
      IF(THETAL-THETAP) 325,325,340
C FIND INTERVAL IN WHICH THE LINES INTERSECT
 325   DZIL=ZION(I,N)-ZION(I-1,NL-1)
      MISSL=1
      IF(DZIL.EQ.0.) DZIL=1.0E-12
 330   DXIL=XION(I,N)-XION(I-1,NL-1)
      THETAL=ATAN2(DXIL,DZIL)
       DXDZL=DXIL/DZIL
      IF(THETAP-THETAL) 340,340,335
C RESET NL AND GO BACK AND CHECK EARLIER INTERVAL
 335   NL=NL-1
      IF(NL-1) 499,340,325
C BEST INTERVAL FOUND ----- FIND X INTERCEPTS,THEN INTERSECTION POINT
 340  DZIL=ZION(I-1,NL)-ZION(I-1,NL-1)
      IF(DZIL.EQ.0.) DZIL=1.0E-12
      DXDZL=(XION(I-1,NL)-XION(I-1,NL-1))/DZIL
      XLO=XION(I-1,NL)-DXDZL*ZION(I-1,NL)
      ZLINTR=(XPO-XLO)/(DXDZL-DXDZP)
      XLINTR=DXDZP*ZLINTR+XPO
C CALCULATE PERPENDICULAR DISTANCE TO LEFT ION PATH
       DSPL=SQRT((ZLINTR-ZION(I,N))**2+(XLINTR-XION(I,N))**2)
C CALCULATE POTENTIAL TO THE LEFT
 343  DNL=DNO/(XION(I,N)*DSPL)
      VL=-ALOG(DNL)*TCEION
C * * * * * * * * * * * * * * * * * * * * * * * * * * * * * * * * * * * * * *
C CHECK ION DENSITY PROPORTION TO RIGHT
C IF LAST ACTIVE PATH HANDLE AS SPECIAL CASE
 345  IF(IR-I) 499,495,350
 350   NR=NC(I+1)
C GET SLOPE TO ENDPOINT OF PATH ON RIGHT
 360   DZIR=ZION(I+1,NR)-ZION(I,N)
      IF(DZIR.EQ.0.) DZIR=1.0E-12
 365   DXIR=XION(I+1,NR)-XION(I,N)
      THETAR=ATAN2(DXIR,DZIR)
       DXDZR=DXIR/DZIR
C IF NO INTERSECTION IS FOUND, GET APPROXIMATE DISTANCE
      IF(THETAP-THETAR) 370,370,385
C FIND INTERVAL IN WHICH THE LINES INTERSECT
 370   DZIR=ZION(I+1,NR-1)-ZION(I,N)
      MISSR=1
      IF(DZIR.EQ.0.) DZIR=1.0E-12
 375  DXIR=XION(I+1,NR-1)-XION(I,N)
      THETAR=ATAN2(DXIR,DZIR)
      DXDZR=DXIR/DZIR
      IF(THETAR-THETAP) 385,385,380
```

```
C RESET NR AND GO BACK AND CHECK EARLIER INTERVAL
 380    NR=NR-1
        IF(NR-1) 499,385,370
C BEST INTERVAL FOUND ----- FIND X INTERCEPT,THEN INTERSECTION POINT
 385   DZIR=ZION(I+1,NR)-ZION(I+1,NR-1)
        IF(DZIR.EQ.0.) DZIR=1.0E-12
        DXDZR=(XION(I+1,NR)-XION(I+1,NR-1))/DZIR
        XRO=XION(I+1,NR)-DXDZR*ZION(I+1,NR)
        ZRINTR=(XRO-XPO)/(DXDZP-DXDZR)
        XRINTR=DXDZP*ZRINTR+XPO
C CALCULATE PERPENDICULAR DISTANCE TO RIGHT ION PATH
        DSPR=SQRT((ZRINTR-ZION(I,N))**2+(XRINTR-XION(I,N))**2)
C CALCULATE POTENTIAL TO THE RIGHT
 387   DNR=DNO/(XION(I,N)*DSPR)
        VR=-ALOG(DNR)*TCEION
C CALCULATE PERPENDICULAR FORCE , POSITVE RIGHT * NEGATIVE LEFT
        IF(I-IL) 499,392,394
 392   IF(VL.GT.VR) GO TO 394
        VL=VR
        NOACCL=1
 394   IF(IR-1) 499,396,398
 396   IF(VR.GT.VL) GO TO 398
        VR=VL
        NOACCL=1
 398    F=(VR-VL)*2.0/(DSPL+DSPR)
C GET Z AND X COMPONENTS OF FORCE USING PERPENDICULAR SLOPE
        SINP=SIN(THETAP)
        COSP=COS(THETAP)
        FZ=F*COSP
        FX=F*SINP
C CALCULATE VELOCITY COMPONENTS FOR THIS ITERATION
        C=DT/UMSION
        VELZ=FZ*C
        VELX=FX*C
C CALCULATE TOTAL VELOCITY COMPONENTS AND MAGNITUDE OF TOTAL VELOCITY
         VELTX=VELX+VX(I)
         VELTZ=VELZ+VZ(I)
         VELT=SQRT(VELTX**2+VELTZ**2)
C NORMALIZE VELOCITY COMPONENTS
        V=SQRT(VZ(I)**2+VX(I)**2)
        VELTZ=V*VELTZ/VELT
        VELTX=V*VELTX/VELT
C * * * * CALCULATE LONGITUDINAL ACCELERATING FORCE * * * * * * * * * *
C GET APPROXIMATE DENSITY (AVERAGE) CONSTANT
        DNA=(DNL+DNR)/2.
        ELDEN=DNO/((DSPL+DSPR)*XION(I,N)*V)
C GET POTENTIAL DIFFERENCE TO LAST ITERATION
        DV=ALOG(DNA/DN(I))*TCEION
        IF(NOACCL.EQ.1) DV=0.0
        F=-DV/SQRT((ZION(I,N)-ZION(I,N-1))**2+(XION(I,N)-XION(I,N-1))**2)
C CALCULATE VELOCITY COMPONENTS
        VELZ=-F*SINP*C
        VELX=F*COSP*C
        VZ(I)=VELTZ+VELZ
```

```
      VX(I)=VELTX+VELX
C CALCULATE NEXT POSITION OF ION
      ZION(I,N+1)=VZ(I)*DT+ZION(I,N)
      XION(I,N+1)=VX(I)*DT+XION(I,N)
      DN(I)=DNA
C  GO SEE IF NEW POINT IS OUTSIDE BOUNDARIES
      CALL BOUND(ZION(I,N+1),XION(I,N+1),I)
 430   CONTINUE
      J=MOD(NC(I),NDSP2)
      IF(J.NE.0) GO TO 432
      V=SQRT(VZ(I)**2+VX(I)**2)
      WRITE(IOUT,497) I,N,ISTAT(I),ZION(I,N+1),XION(I,N+1),VZ(I),
     2  VX(I),V,DN(I),ELDEN
 497  FORMAT(I3,2I4,12E10.3)
 432  NC(I)=NC(I)+1
      IF((MISSL*MISSR).EQ.1) GO TO 302
 435  CONTINUE
      RETURN
C * * * * * * * SPECIAL CASES * * * * * * * * * * * * * * * * * * * * * *
C LEFT - MOST ACTIVE PATH --- GET DISTANCE TO BOUNDARY
 490  DSPL=DS(ZION(I,N),XION(I,N),THETAP,XP0,0)
      GO TO 343
C RIGHT - MOST ACTIVE PATH --- GET DISTANCE TO BOUNDARY
 495  DSPR=DS(ZION(I,N),XION(I,N),THETAP,XP0,1)
       GO TO 387
C ERROR EXIT * * * * * * * * * * * * * * * * * * * * * * * * * * * * * *
 499  ISTAT(I)=8888
      GO TO 430
      END
      SUBROUTINE BOUND(Z,X,I)
C
C**** ROUTINE TO CHECK IF POINT (Z,X) IS OUTSIDE BOUNDARIES **********
C**** RETURN, ISTAT.GT.0 - OUTSIDE, ISTAT=0 - WITHIN BOUNDS **********
C
C  BLANK COMMON FOR LARGE ARRAYS
      COMMON ZION(51,251),XION(51,251),VZ(251),VX(251),ISTAT(51)
     1,IMAG(6180),NC(51),DN(51)
      COMMON / IO / IN,IOUT,INFO(8),KEY,NDSP1,NDSP2,ICHAR(14),ITITL(28)
     1  ,IPATHS
      COMMON/PARAM/N,NUMION,NUMIT,DT,RB,RBOUND,RT,TCEION,BMCUR,JTIL,
     1 TELBM,THLENG,UMSION,VIONB,ZBOUND,IL,IR,PI,BK,Q,DNO,DNZRBK,DRATIO
       IF(X-RB) 770,770,700
 700   IF(RBOUND-X) 770,770,710
 710   IF(ZBOUND-Z) 770,770,720
 720  IF(Z) 770,770,730
 730  IF(THLENG.GT.Z.AND.RT.GT.X) GO TO 770
      GO TO 790
 770  ISTAT(I)=N
C IF LEFT-MOST OR RIGHT-MOST PATH, RESET INDEX
      IF(I.NE.IL) GO TO 780
      DO 773 II=1,NUMION
      LIP=I+II
      IF(ISTAT(LIP)) 775,775,773
 773  CONTINUE
```

```
 775  IL=I+II
      RETURN
 780  IF(I.NE.IR) GO TO 790
      DO 783 II=1,IR
      LIM=I-II
      IF(ISTAT(LIM)) 785,785,783
 783  CONTINUE
 785  IR=I-II
 790   RETURN
       END
      SUBROUTINE WRIT(KE)
C--WRIT PRINTS INFORMATION ABOUT THE SIMULATION
C--KE=1 : HEADING, INITIAL INFO AND DATA
C--KE=2: INTERIM STATUS OF MAIN VARIABLES
C--KE=3: FINISH OF A PASS, RESULTS, START OF NEW PASS
C--KE=4: CREATE FILE OF PATH COORDINATES
C--KE=5: UNUSED
C
C  BLANK COMMON FOR LARGE ARRAYS
      COMMON ZION(51,251),XION(51,251),VZ(251),VX(251),ISTAT(51)
     1,IMAG(6180),NC(51),DN(51)
      COMMON / IO / IN,IOUT,INFO(8),KEY,NDSP1,NDSP2,ICHAR(14),IIITL(28)
     1  ,IPATHS
      COMMON/PARAM/N,NUMION,NUMIT,DT,RB,RBOUND,RT,ICEION,BMCUR,UTIL,
     1 TELBM,THLENG,UMSION,VIONB,ZBOUND,IL,IR,PI,BK,Q,ONO,DNZRBK,DRATIO
      DATA IPAG,LAB,NPAS /0,6HPLASIM,1  /
C--   FORMATS
  10  FORMAT( 43H0    THIS RUN MAY BE CHARACTERIZED BY INFO*,///7X,14A6/)
  11  FORMAT(1H1,//,60X,A10,I3,//////  )
  12  FORMAT(7X,7A10,/   )
 13   FORMAT(////17X,33HP L A S M A   S I M U L A T I O N,///
     2       17X,43HA COMPUTER CODE TO DESCRIBE THE PROPAGATION,//
     3       17X,43HOF A CHARGE-EXCHANGE PLASMA IN THE VICINITY,//
     4       17X,40HOF AN ELECTRICALLY PROPELLED SPACECRAFT ,///
     5       17X,38HWRITTEN BY JOHN BARNES AND DALE WINDER,//
     6       17X,33HFOR THE JET PROPULSION LABORATORY,//
     7       21X,27H( J P L  P. O. NO. 955322 ),///
     8       17X,41HHAROLD R. KAUFMAN, PRINCIPAL INVESTIGATOR ,//
     9       27X,21HDEPARTMENT OF PHYSICS,//
     1       25X,25HCOLORADO STATE UNIVERSITY,//
     2       26X,23HFORT COLLINS, CO  80523  ,//
     3       32X,10HJULY, 1979)
 14   FORMAT(1H1,//60X,A10,I3,/////,10X,21HSCHEMATIC OF THRUSTER,///
     2       11X,3H- :,/,11X,3HA :,/,11X,3H: :,/,11X,3H: :, /,
     3       11X,3H: :,5X,6HTHLENG,/,11X,3H: :,7X,1HV,/,
     4       11X,11H: ----------,43X,6HZBOUND,/,11X,1H:,6X,4HA  :,44X,1HV
     5       /,9X,6HRBOUND,3X,4H:  :,/11X,1H:,6X,1H:,2X,45(1H=),/,
     6       11X,1H:,6X,2HRT,5X,1HA,40X,1H:,/,11X,2(1H:,6X)2HRB,39X,1H:,/
     7       4(11X,1H:,6X,1H:,6X,1H:,40X,1H:,/),13X,1H+,13(4H- . ),/
     8       11X,5H(0,0),50X,1H:,/,5(66X,1H:,/),21X,45(1H=),/,
     9       2(21X,1H:,/),13X,9(1H-),/,6(13X,1H:,/),///)
 15   FORMAT(20X,28HINITIAL VALUES OF PARAMETERS,//,
     2       7X,52HRBOUND  RT   RB   THLENG  ZBOUND  NUMION NUMIT VIONB,
     3       20H  BMCUR  UTIL    KEY,/,7X,3F5.2,2F9.2,
```

```
     4       2(2X,I4),2X,F5.0,2(2X,F5.2),3X,I4,///,7X,6HTCEION,6X,
     5       5HTELBM,7X,6HUMSION,10X,2HDT,/7X,4(E10.2,2X)///)
  21  FORMAT(1H1,12(5H -2- ),A10,I3//10X,27HINTERIM STATUS -- ITERATION,
     2       I4,3H OF,I4,11H ITERATIONS,
     3       //,9X,55HI  N ISTAT  ZION(I,N) XION(I,N)   VZ(I)    VX(I)    D
     4N(I),/)
  22  FORMAT(5X,3I4,9E10.3)
  31  FORMAT( 27H RESULTS OF PASS--ITERATION,I4,3H OF,I4,11H ITERATIONS,
     2 /,79H I  N ISTAT  ZION(N+1) XION(N+1)  VZ(I)    VX(I)      V
     3  DN(I)       ELDEN,/)
C--    WHAT KIND OF CALL IS IT
       GOTO  (1,2,3,4,5), KE
C--       1          1          1
C--INITIAL STATE--HEADING AND DATA
    1  IPAG=IPAG + 1
       WRITE(IOUT,11)LAB,IPAG
       WRITE(IOUT,13)
        IPAG = IPAG + 1
       WRITE(IOUT,14)LAB,IPAG
       WRITE(IOUT,10) INFO
       WRITE(IOUT,15)RBOUND,RT,RB,THLENG,ZBOUND,NUMION,NUMIT,VIONB,
     2 BMCUR,UTIL,KEY,TCEION,TELBM,UMSION,DT
       RETURN
C--       2          2          2
C--THIS SECTION PRINTS THE INTERIM STATUS AT THE NTH ITERATION
    2  IPAG = IPAG + 1
       WRITE(IOUT,21) LAB,IPAG,N,NUMIT
       DO 28 I=1,NUMION
  28   WRITE(IOUT,22) I,N,ISTAT(I),ZION(I,N),XION(I,N),VZ(I),VX(I),
     2  DN(I)
       RETURN
C--       3          3          3
C THIS SECTION PRINTS RESULT OF A PASS AT NTH EXTRAPOLATION
    3  IPAG = IPAG + 1
       WRITE(IOUT,31) N,NUMIT
       RETURN
C--       4          4          4
C THIS SECTION CREATES FILE OF PATH COORDINATES
    4  NMAX=IFIX(FLOAT(NUMION)/4.)
       WRITE(IPATHS) NMAX,NUMION
       WRITE(IPATHS) (ISTAT(I),I=1,NMAX)
       DO 44 I=1,NMAX
       ISAT=ISTAT(I)
  44   WRITE(IPATHS) (ZION(I,NN),XION(I,NN),NN=1,ISAT)
       RETURN
C--       5          5          5
C THIS IS UNUSED ******************************
 5     CONTINUE
       RETURN
       END
       FUNCTION DS(Z,X,ANG,B,LR)
C
C**** ROUTINE TO FIND DISTANCE TO POINT ON BOUNDARY
C**** LR=0 FOR LEFT,LR=1 FOR RIGHT,ANG.NE.90 DEGREES ******************
```

```
C
C   BLANK COMMON FOR LARGE ARRAYS
      COMMON ZION(51,251),XION(51,251),VZ(251),VX(251),ISTAT(51)
     1,IMAG(6180),NC(51),DN(51)
      COMMON / IO / IN,IOUT,INFO(8),KEY,NDSP1,NDSP2,ICHAR(14),ITITL(28)
     1   ,IPATHS
      COMMON/PARAM/N,NUMION,NUMIT,DT,RB,RBOUND,RT,TCEION,BMCUR,JTIL,
     1 TELBM,THLENG,UMSION,VIONB,ZBOUND,IL,IR,PI,BK,Q,DNO,DNZRBK,DRATIO
C IF DISTANCE ON RIGHT IS DESIRED, SUBTRACT 3.14159 FROM PHI
      PHI=ANG
      IF(LR.EQ.1) PHI=PHI-PI
      SLOPE=TAN(PHI)
C INTERVAL BETWEEN BEAM EDGE AND THRUSTER CORNER
   12 PHIB=ATAN2((X-RT),(Z-THLENG))
      IF(Z-THLENG) 23,600,600
  600 PHIA=ATAN2((X-RB),(Z-THLENG))
      IF((PHI-PHIA)*(PHIB-PHI)) 23,610,610
  610 ZINT=THLENG
      XINT=SLOPE*THLENG+B
      GO TO 680
C INTERVAL BETWEEN THRUSTER CORNER AND SPACECRAFT
   23 PHIA=ATAN2((X-RT),Z)
      IF(PHI-PHIA) 34,620,620
  620 ZINT=(RB-B)/SLOPE
      XINT=RT
      GO TO 680
C INTERVAL ALONG SPACECRAFT SURFACE
   34 PHIB=ATAN2((X-RBOUND),Z)
      IF(PHI-PHIB) 45,630,630
  630 ZINT=0.
      XINT=B
      GO TO 680
C INTERVAL BETWEEN SPACECRAFT AND (ZBOUND,RBOUND)
   45 PHIA=ATAN2((X-RBOUND),(Z-ZBOUND))
      IF(PHI-PHIA) 56,640,640
  640 ZINT=(RBOUND-B)/SLOPE
      XINT=RBOUND
      GO TO 680
C INTERVAL BETWEEN (ZBOUND,RBOUND) TO (ZBOUND,RB)
   56 PHIB=ATAN2((X-RB),(Z-ZBOUND))
      IF(PHIB-PHI-PI) 650,650,61
  650 ZINT=ZBOUND
      XINT=SLOPE*ZBOUND+B
      GO TO 680
C INTERVAL ALONG BEAM EDGE
   61 ZINT=(RB-B)/SLOPE
      XINT=RB
C CALCULATE DISTANCE TO BOUNDARY
  680 DS=SQRT((Z-ZINT)**2+(X-XINT)**2)
      RETURN
      END
      SUBROUTINE VRSPLT
C
C--VRSPLT USES VERSATEC PLOTTER TO PLOT ARRAYS X() AND Y()
```

```
C
C  BLANK COMMON FOR LARGE ARRAYS
      COMMON ZION(51,251),XION(51,251),VZ(251),VX(251),ISTAT(51)
     1,IMAG(6180),NC(51),DN(51)
      COMMON / IO / IN,IOUT,INFO(8),KEY,NDSP1,NDSP2,ICHAR(14),ITITL(28)
     1  ,IPATHS
      COMMON/PARAM/N,NUMION,NUMIT,DT,RB,RBOUND,RT,TCEION,BMCUR,JTIL,
     1 IELBM,THLENG,UMSION,VIONB,ZBOUND,IL,IR,PI,BK,Q,DNO,DNZRBK,DRATIO
      DIMENSION SAVZ(2),SAVX(2)
      DATA ZAXLN,XAXLN,INC,LINTYP,ISYM /7.0,6.0,1,+10,1/
C--FIRST ENTRY--SET UP THE SYSTEM, SCALE, AXES AND TITLE IF DESIRED
      CALL PLOTS(0.,0.,0.)
C--SET ORIGIN OF PLOT
      CALL PLOT (1.,1.,-3)
      CALL SETMSG(1)
      SAVZ(1)=0.
      SAVX(1)=0.
      SAVZ(2)=RBOUND/XAXLN
      SAVX(2)=SAVZ(2)
      ZMAX=ZAXLN*SAVZ(2)
      CALL AXIS(0.,0.,ITITL(9),-40,ZAXLN,0.,SAVZ(1),SAVZ(2))
      CALL AXIS(0.,XAXLN,1H ,1,ZAXLN,0.,SAVZ(1),SAVZ(2))
      CALL AXIS(0.,0.,ITITL(13),40,XAXLN,90.,SAVX(1),SAVX(2))
      CALL SYMBOL(1.,8.0,0.14,ITITL(1),0.,80)
      DO 80 J=2,NUMION
      IF(ZION(J,1).GT.ZMAX) GO TO 82
   80 CONTINUE
   82 NUMPT=J-1
      IF(KEY.GT.0) NUMPT=NUMION+1
      DO 150 J=1,NUMPT
      NPTS=ISTAT(J)
      IF(ISTAT(J).EQ.0) NPTS=NC(J)
      DO 100 NM=1,NPTS
      VZ(NM)=ZION(J,NM)
      VX(NM)=XION(J,NM)
  100 CONTINUE
      DO 120 I=1,2
      NPT=NPTS+I
      VZ(NPT)=SAVZ(I)
  120 VX(NPT)=SAVX(I)
      IF(J.EQ.NUMION+1) ISYM=0
      CALL LINE(VZ,VX,NPTS,INC,LINTYP,ISYM)
  150 CONTINUE
      VX(1)=RT
      VX(2)=RT
      VZ(1)=0.
      VX(3)=0.
      VZ(2)=THLENG
      VZ(3)=THLENG
      VZ(4)=THLENG
      VX(4)=RB
      VX(5)=RB
      VZ(5)=ZMAX
      NPTS=5
```

```
      DO 200 I=1,2
      NPT=NPTS+I
      VZ(NPT)=SAVZ(I)
  200 VX(NPT)=SAVX(I)
      CALL LINE(VZ,VX,NPTS,1,0,0)
C--TERMINATE ALL PLOTTING--RELEASE OUTPUT TO VERSATEC PLOTTER
    3 CALL PLOT(0.,0., +999)
      RETURN
      END
#
```

FACILITY PRODUCED CHARGE-EXCHANGE IONS

M. R. Carruth, Jr.
Jet Propulsion Laboratory
California Institute of Technology
Pasadena, California

Introduction

Facility produced ions have always plagued plume measurements made in vacuum chambers. These "facility" produced ions are created by charge-exchange collisions between neutral atoms and energetic thruster beam ions. The result of the electron transfer is an energetic neutral atom and an ion of only thermal energy. There are true charge-exchange ions produced by collisions with neutrals escaping from the ion thruster and being charge-exchange ionized before the neutral intercepts the tank wall. The "facility" produced charge-exchange ions will not exist in space and therefore, represent a source of error where measurements involving ion thruster plasmas and their density are involved. Therefore, an effort was made to determine the quantity of facility produced ions in the JPL Electric Propulsion Laboratory's test chamber with a 30-cm mercury ion thruster.

The Test Chamber

The test chamber at JPL, in which mercury ion thruster tests are conducted, is a 15 foot long chamber which is 7 foot in diameter. It is illustrated in Figure 1. A 30-cm ion thruster is placed at one end of the chamber. There is clearance between the thruster and chamber so that measurements can be made around the thruster and chamber effects on plasma density or potential are minimal. The cylindrical wall of the chamber has a liquid nitrogen (LN_2) cooled shroud to condense mercury

which arrives at the wall and therefore, to aid in producing and retaining the vacuum and prevent reemission of mercury which arrives at the wall, particularly low energy neutrals. At the end of the chamber opposite the thruster is a target which intercepts the beam. The target may be placed in a horizontal position such that much of the beam strikes the rear wall, which isn't cryopumped, or the target may be filled with mercury, which is frozen by LN_2 and placed in a vertical position to intercept all of the beam. This allows the mercury target to be sputtered which prevents sputtering of the chamber's non-volatile materials but significantly increases the neutral mercury in the chamber and therefore, facility produced ions. This paper addresses this condition.

Model of Facility Ions

Because the LN_2 cooled shroud will collect the mercury arriving at the tank wall, the largest contributor of facility mercury neutrals in the chamber is the beam bouncing off the end of the chamber when the target is horizontal or the mercury sputtered from the target when it is vertical such that it intercepts the primary ion beam. As expected, experimental evidence shows that a much higher neutral density exists when the frozen mercury target intercepts the beam, indicating that the frozen mercury has a high sputter yield. The mercury atoms are sputtered from the target by the energetic beam ions and flow upstream. The mercury atoms charge-exchange with the beam to produce "facility" ions. The total number of ions doesn't change in such a reaction since the electron is just being transferred between the interacting pair.

However, because the charge-exchange ions are slower and because of conservation of charge, the effective density increases.

Each point on the mercury target sputters as defined by the incoming beam density at each point on the surface. The beam ion's energy will be the same across the target. The sputtered atoms from each point on the target is assumed to be sputtered into a cosine distribution. In order to determine the "facility" plasma density at some point upstream, we will look at the contribution from across the entire target. This will be accomplished by determining the neutral flow toward the point in question from each portion of the target. The probability of charge-exchange reactions to occur between a point on the target and the point where the plasma density is to be determined will be assessed. This will allow determination of the portion of the ion density at a specified point coming from a single point on the target. By summing up the contribution from each point on the target the total facility plasma density at a specified point can be determined.

Figure 2 illustrates that because of the primary ion beam's distribution, the sputtered atoms, sputtered into a cosine distribution from each point, have a sputtered intensity distribution across the target which is related to the primary beam distribution. We assume the beam distribution as reported in Reference 1. This reference reports the beam distribution of the 30-cm mercury ion thruster as a Gaussian. Figure 3 illustrates the geometry used to perform the "facility" plasma density evaluation which has been described above. From Ref. 1 the primary beam current density, at any z position downstream, is assumed

to have a Gaussian profile with a radial, r, dependence described by

$$J(r) = J_o \, e^{-(\frac{r}{r_o})^2} \tag{1}$$

The total beam current, I*, is given by

$$I^* = \int_0^\infty 2\pi r \, J(r,z) \, dr = \pi r_o^2 \, J_o \tag{2}$$

or

$$J_o = \frac{I^*}{\pi \, r_o^2} \tag{3}$$

Therefore, J_o is the current density on axis (r=0) and r_o is a characteristic half-width of the Gaussian profile. As the primary beam moves downstream of the thruster, r_o will vary. Therefore, we assume a divergence of the beam, as described in Ref. 1, such that

$$r_o(z) \equiv r_b = \sqrt{1/3} \, (r_o + z \sin\gamma) \tag{4}$$

where r_o is the Gaussian half-width of the beam at the thruster face and γ is the divergence angle of the primary beam.

From Figure 3, we can see that,

$$R^2 = \bar{R}^2 + (z_t - z_r)^2 \tag{5}$$

$$\bar{R} = (r'^2 + \rho^2 - 2\, r'\rho \cos\theta)^{\frac{1}{2}} \tag{6}$$

$$\tan\phi = (z_t - z_r')(r'^2 + \rho^2 - 2\, r'\rho \cos\theta)^{-\frac{1}{2}} \tag{7}$$

$$\cos = \frac{(r'^2 + \rho^2 - 2\, r'\rho \cos\theta)^{\frac{1}{2}}}{(r'^2 + \rho^2 - 2\, r'\rho \cos\theta + (z_t - z_r')^{\frac{1}{2}}} \tag{8}$$

$$\sin \phi = (z_t - z_r')(r'^2 + \rho^2 - 2\, r' \rho \cos\theta + (z_r - z_r')^2)^{-\frac{1}{2}} \quad (9)$$

where the different variables, θ, ϕ, ρ, r', z_t, z_r, z_r', R and $\bar{R}$ are defined in Fig. 3.

From Eq.'s 1, 3 and 4, we see that the primary beam ion flux at some location, defined by (r,z), is given by,

$$n_b \; v_b = \frac{J_o(z)\; e^{-(r/r_b)^2}}{e} \quad (10)$$

where n_b is beam density at (r,z), v_b is beam ion velocity, and e is the unit of charge, 1.6×10^{-19} coulombs. At the target each beam ion sputters back a number of atoms, their flux given by

$$n_s(\rho)\; v_s = \frac{Y_s\; J_o(z_t) e^{-(\rho/r_t)^2}}{e} \quad (11)$$

Where n_s is the density of sputtered atoms, v_s is the sputtered atom velocity, Y_s is the sputter yield of target atoms at a given beam ion velocity, and r_t is r_b at the target.

From equations 3 and 11,

$$n_s(\rho)\; v_s = \frac{Y_s\; I^*\; e^{-(\rho/r_t)^2}}{\pi\; r_o^2\; e} \quad (12)$$

The total flux, F, from a unit area dA_t is given by,

$$F = \int_{\Omega} k \cos\beta \; d\Omega \quad = 1 \quad (13)$$

and $$F = \int_0^{\pi/2} 2\cdot\pi k \cos\beta \;\; \sin\beta \;\; d\beta \quad = 1 \quad (14)$$

Performing the integration of Eq. 14 yields the constant $k = \pi^{-1}$. From this and Eq. 12, the differential flux is given by,

$$dF_t = k\, K\, e^{-(\rho/r_t)^2} \cos\beta \; d\Omega \; dA_t \tag{15}$$

where $$K = \frac{Y_s\, I^*}{\pi r_t^2\, e} \tag{16}$$

Since the solid angle, $d\Omega$, equals $\frac{dA}{R^2}$, and the unit area, dA_t, equals $\rho\, d\rho \; d\theta$, Eq. 15 may be written,

$$\frac{dF_t}{dA} = \frac{K'\, e^{-(\rho/r_t)^2} \cos\beta \; \rho d\rho d\theta}{R^2} \tag{17}$$

where $K' = kK$ and $\frac{dF_t}{dA}$ represents that portion of the sputtered flux from some elemental area dA_t on the target into some elemental area dA at the point $P(r', z, \theta)$ defined in Fig. 3. The flux of ions, F_i, at the same point is given by,

$$dF_i = n_i\, v_i\, dA \tag{18}$$

where n_i is ion density and $v_i = v_s$. To determine what dF_i is through dA at some point P, we must consider the production of charge-exchange ions. The sputter velocity is assumed to be large enough that we can assume the resultant charge-exchange ion will keep the direction and velocity of the neutral atoms from which it was created. Therefore, we must look at the distribution of neutrals from some dA_t directed toward dA and consider the probability of charge-exchange along the path to dA.

The total ion flux through dA will then be the integral of contributions from dA_t's all over the target surface.

For charge-exchange, the ions produced along a path length $d\xi$

$$\frac{d(dF_t)}{d\xi} = -\alpha(dF_t) = -\frac{dF_i}{d\xi} \tag{19}$$

where $\alpha = \sigma n_b$ and σ is the charge-exchange cross section. Therefore,

$$dF_i = (1- e^{-P_R}) \, dF_t \tag{20}$$

where

$$P_R = \int_0^R \alpha \, d\xi \tag{21}$$

From Eq. 18 and 20 we can write

$$(1-e^{-P_R}) \, dF_t = n_i \, v_i \, dA \tag{22}$$

so that, by Eq. 17,

$$n_i(r',z,) = \frac{K'}{v_i} \int_0^{2\pi} \int_{\sigma}^{\rho t} \frac{(1-e^{-P_R})}{R^2} \cos\beta \, e^{-(\rho/r_t)^2} \rho \, d\rho \, d\theta \tag{23}$$

Substituting α for σn_b into Eq. 21 we see that P_R is given by,

$$P_R = \frac{\sigma \, J_o \, (r)}{e \, v_b} \int_o^R e^{-(r/r_b)^2} d\xi \tag{24}$$

or

$$P_R = P_o \int_0^R e^{-(r/r_b)^2} \frac{d\xi}{r_b^2} \tag{25}$$

where

$$P_o = \frac{\sigma \, I^*}{\pi \, e \, v_b} \tag{26}$$

In order to evaluate the integral in Eq. 25, we must write r and r_b in terms of ξ. The quantity r is best found using Fig. 3 and transforming to cartesian coordinates. Therefore,

$$X(\xi) = \rho \cos\theta + (r' - \rho\cos\theta)\ \xi/R \qquad (27a)$$

$$Y(\xi) = \rho \sin\theta\,(1 - \xi/R) \qquad (27b)$$

$$Z(\xi) = z_t + (z_r' - z_t)\ \xi/R \qquad (27c)$$

From Eq. 4 and 27,

$$r_b = \sqrt{1/3}\,(r_o + (z_t + (z_r' - z_t)\ \xi/R)\sin\gamma) \qquad (28)$$

and

$$r^2 = \rho^2 + 2\rho\,(r'\cos\theta - \rho)\ \xi/R + (r'^2 + \rho^2 - 2r'\rho\cos\theta)(\xi/R)^2 \qquad (29)$$

Equations 28 and 29 give the proper dependance so that the integral in Eq. 25 can be evaluated and P_R determined. With the proper substitutions for $\cos\beta$ and R, Eq. 23 becomes,

$$n_i(r',z) = \frac{K'\,(z_t - z_r')}{v_i} \int_0^{2\pi} \int_0^{\rho_t} \frac{(1 - e^{-P_R}) e^{-(\rho/r_t)^2} \rho\, d\rho\, d\theta}{(r'^2 + (z_t - z_r')^2 + \rho^2 - 2r'\rho\cos\theta)^{3/2}} \qquad (30)$$

Evaluation of Facility Plasma Density

Model Predictions

Because of the complexity of the integrals involved in Eq.'s 30 and 25, Eq. 30 had to be solved numerically by computer. In addition, the sputter yield, Ys (which is part of K'), and the sputtered ion sputtered ion velocity, v_i, had to be determined and input into Eq. 30.

No data was available in the literature regarding the sputter yield of mercury. Therefore, a theoretical approach was utilized. The theory described very completely in reference 2 was used. Also, there are a number of comparisons made between the predictions of the theory and experimentally acquired values. The agreement is quite good, lending confidence in the theory. For the condition of mercury ions bombarding the frozen mercury target with an energy of approximately a kilovolt, the sputter yield is found to be about 30. Having this value also allows us to determine the velocity of the sputtered atoms, and therefore the charge-exchange ions. For any species and proper energy range, the "sputtering efficiency" is 2.4% for self-sputtering, such as mercury ions sputtering a mercury surface.[3] Therefore, for a sputter yield of 30 at a KeV, the velocity of sputtered atoms is, neglecting the slight velocity dependance on sputter angle, 880 meters/sec or equivalent to 0.8 eV.

Besides the geometrical values for the JPL experimental arrangement, the resonant charge-exchange cross-section for mercury had to be input into Eq. 26. This was obtained from Reference 4. Reference 2 used 15° for the divergence angle, γ, and this value was also used. Equation 30 was solved for various positions, $P(r',z)$, relative to the mercury ion thruster, such that experimental data was also available regarding ion densities at those positions. Density values obtained from Eq. 30 are given in Figures 4 and 5. Figure 5 illustrates that a major portion of the facility charge-exchange ion production occurs near the target where the density of sputtered mercury neutrals is the greatest. For positions nearer the thruster the density is seen to drop off

and it is observed that the density distribution is spreading. For those positions near the thruster the facility plasma density on axis is increasing because the ion beam density is increasing and the probability of charge-exchange collisions goes up. This can explain the increase in ion thruster accelerator current which is observed when the mercury target is in the vertical position as compared to the horizontal position or when a second ion thruster is turned on.

Experimental Values

It is observed that a much higher facility produced plasma density is observed when the frozen mercury target is in a vertical position so as to intercept the beam. When the target is horizontal and the beam strikes the end wall, the tank, which is stainless steel, is sputtered but much fewer mercury neutrals are available for charge-exchange interactions. Also, it has been reported that near the thruster exist plane but out of the primary beam, the plasma density is governed by true charge-exchange plasma.[5] This is the charge-exchange plasma produced by interactions between the primary beam and neutral atoms escaping through the ion thruster's ion optics. Therefore, plasma density measurements may be obtained near the thruster when the target is horizontal and when it is vertical. The difference between the measurements should be due to the "facility" produced charge-exchange plasma.

The 30-cm mercury ion thruster was operated at 1.0 and 1.8 ampere beam currents in the JPL test chamber described in this paper. The LN_2 shroud was operated and a vacuum of about 2×10^{-6} torr was maintained. A cylindrical Langmuir probe was positioned on a rail such that it could be moved parallel to the thrust beam axis, with z=0 being in the plane

of the thruster optics. At any given location along the rail the probe, which was biased negatively to attract ions, could be rotated such that the ion thruster axis was in the plane swept out by the probe rotation. The current from the probe was used to determine the flow direction of the true charge-exchange plasma produced by the ion thruster.

For a negatively biased cylindrical Langmuir probe in a flowing plasma, which fulfills the Orbital Motion Limited conditions, the current collected, I, is given by:[7]

$$I = 2N\, e\, U \sin^2 \theta'\, Rp\, L \left(1 - \frac{2\, e\, v_p}{M_i\, U^2 \sin^2 \theta'}\right)^{\frac{1}{2}} \qquad (31)$$

where N is the plasma density, U is the flowing plasma velocity, θ' is the probe's angle of attack to the plasma, R_p is the probe radius, L is the probe length, M_i is the mass of the plasma ions, and V_p is the potential on the probe relative to plasma potential. It was observed in experimental data that no θ' dependence in the current (except for an end-effect described in Ref. 6 was present. This indicates that $-e\, V_p > \frac{1}{2} M_i\, U^2 \sin^2 \theta$ so that Eq. 31 can be written

$$I = 2\, N\, e\, R_p\, L \left(-\frac{2eV_p}{M_i}\right)^{\frac{1}{2}} \qquad (32)$$

therefore, the density, N, can be determined directly from the ion current.

For both a 1.0 Ampere and a 1.8 Ampere beam current, data was obtained by the probe for various positions with the target vertical and horizontal. Based on: 1) the fact that with the target vertical more facility produced ions are created and 2) on the conclusion given in

Reference 5 that charge-exchange ion measurements near and just downstream of the thruster optics plane are primarily "true" charge-exchange ions, the assumption is made that when the target is horizontal the charge-exchange plasma densities measured are the density of the true charge-exchange plasma. Therefore, by determining the density at a specific location when the mercury target is both horizontal and vertical, the difference, which is due to the "facility" produced ions, can be determined. Based on Reference 5, this will hold true best near and just downstream of the thruster optics plane. This allows a comparison between the analytical predictions of the facility produced plasma density and values obtained from data as just described. Table I gives this comparison as a function of position and beam current.

TABLE I. PREDICTED AND MEASURED FACILITY PRODUCED IONS

Beam Current	r'	z	Measured Density	Predicted Density	% Diff.
1.0 Ampere	0.48m	0.24m	5.4×10^{12} No/cm^2	3.0×10^{12} No/cm^2	57
		0.0	2.0×10^{12}	2.8×10^{12}	33
		-.25	5.5×10^{11}	2.7×10^{12}	132
1.0	.66	.18	9.3×10^{11}	2.1×10^{12}	77
		.05	7.0×10^{11}	2.0×10^{12}	96
		-.09	1.0×10^{11}	2.1×10^{12}	181
1.8 Ampere	.48	.24	2.7×10^{13}	1.0×10^{13}	92
		0.0	1.9×10^{13}	9.4×10^{12}	67
		-.25	3.5×10^{12}	8.8×10^{12}	86
1.8	.66	.24	9.2×10^{12}	7.1×10^{12}	26
		0.0	5.3×10^{12}	6.7×10^{12}	23
		-.13	2.9×10^{12}	6.5×10^{12}	77

There are a couple of points to be made about Table I. Based on the assumptions defined above, agreement was expected for positions just downstream of and near the thruster optics plane. It can be seen from Table I that agreement at such locations are typically within a factor of two. The greatest disagreement, as expected, occurs for positions upstream of the thruster optics. At these positions one observes that the measured quantity (based on the way in which the measured quantities were obtained) is significantly lower than that predicted analytically. This also is as expected and indicates that at these locations a significant amount of facility produced plasma is present with the mercury target in the horizontal position.

One of the assumptions which was made in the formation of the analytic model was that the facility produced ions would maintain the velocity and trajectory of the mercury atoms from which they were created. This is a good assumption as long as the particle velocity is great enough so that its trajectory is not significantly altered by the internal electric fields present in the plasmas in the test chamber. We see, based on References 2 and 3, that the facility produced ions should have a directed energy just less than an eV. How much the trajectories of ions of this energy will be affected by moving through the thruster beam and charge-exchange plasmas was not determined. With this uncertainty in mind, and the uncertainty in the sputter yield of mercury and the sputtered atom velocity (since theoretical values and not experimental values were used for these quantities), the agreement between the measured and predicted facility produced plasma density values given in Table I, is considered reasonable.

Summary

Facility produced charge-exchange ions, which will not be present in space, often hamper ion thruster plasma measurements inside ground test chambers. Measurements of the ion thruster charge-exchange plasma upstream of the thruster is particularly susceptible to being in error due to the facility produced charge-exchange ions. An analytical model of the facility charge-exchange plasma density is presented in this paper. Most of the required inputs into the program are geometrical, relating to the test chamber configurations. In addition, the resonant charge-exchange cross-section, the sputter yield of mercury and the velocity of the sputtered atoms were required inputs. Experimentally measured values of the cross-section were used while the sputter yield and sputtered atom velocity were calculated from theory available in the literature.

The assumptions relating to the ion beam were that it could be modeled as a Gaussian and that it expanded with a 15° half angle. The mercury neutrals sputtered from each point on the mercury target were assumed to be sputtered into a cosine distribution and the trajectory and velocity of the facility produced ion were assumed to be the same as the sputtered atom from which it was created. Because of the relatively small velocity of the sputtered atom, the strict validity of the last assumption may be questioned. However, there is reasonable agreement between measured and predicted facility plasma densities indicating that the assumptions on which the analytical model is based are, to first order, correct. The model should then allow an estimate of the facility plasma density in a facility utilizing a mercury target. The predicted values may be substracted from overall density measurements in order to determine true ion thruster charge-exchange plasma density.

It should be noted that the facility charge-exchange ion production addressed in this paper assumed a single thruster. The problem of two or more operating ion thrusters can be addressed in a manner similar to that presented in this paper.

Acknowledgements

The author is grateful to Mr. Ken Harstad for his aid in the development of the analytical model and to Mr. Larry Noon for his aid in using the computer to solve the facility plasma density equation.

References

1. R.L. Poeschel, et al, "Extended Performance Solar Electric Propulsion Thrust System Study", Vol. 4, NASA CR-135281, 1977.

2. Peter Sigmund, "Theory of Sputtering I. Sputtering Yield of Amorphous and Polycrystalline Targets", Physical Review, Vol. 184, No. 2, August 1969.

3. Peter Sigmund, "Sputtering Efficiency of Amorphous Substances", Canadian Journal of Physics, 46, 1968.

4. D.E. Zuccaro, "Measurement of the Resonant Charge Exchange Cross Section of Mercury and Cesium", AIAA Paper No. 67-682, 1967.

5. G.K. Komatsu and J.M. Sellen, Jr., "Beam Efflux Measurements", NASA CR-135038, 1976.

6. H.M. Mott-Smith and I. Langmuir, "The Theory of Collectors in Gaseous Discharged", Physical Review, Vol. 28, 1926.

7. M.R. Carruth, Jr. and M.E. Brady, "Propagation of Charge-Exchange Plasma Produced by an Ion Thruster", AIAA Paper No. 80-1388, 1980.

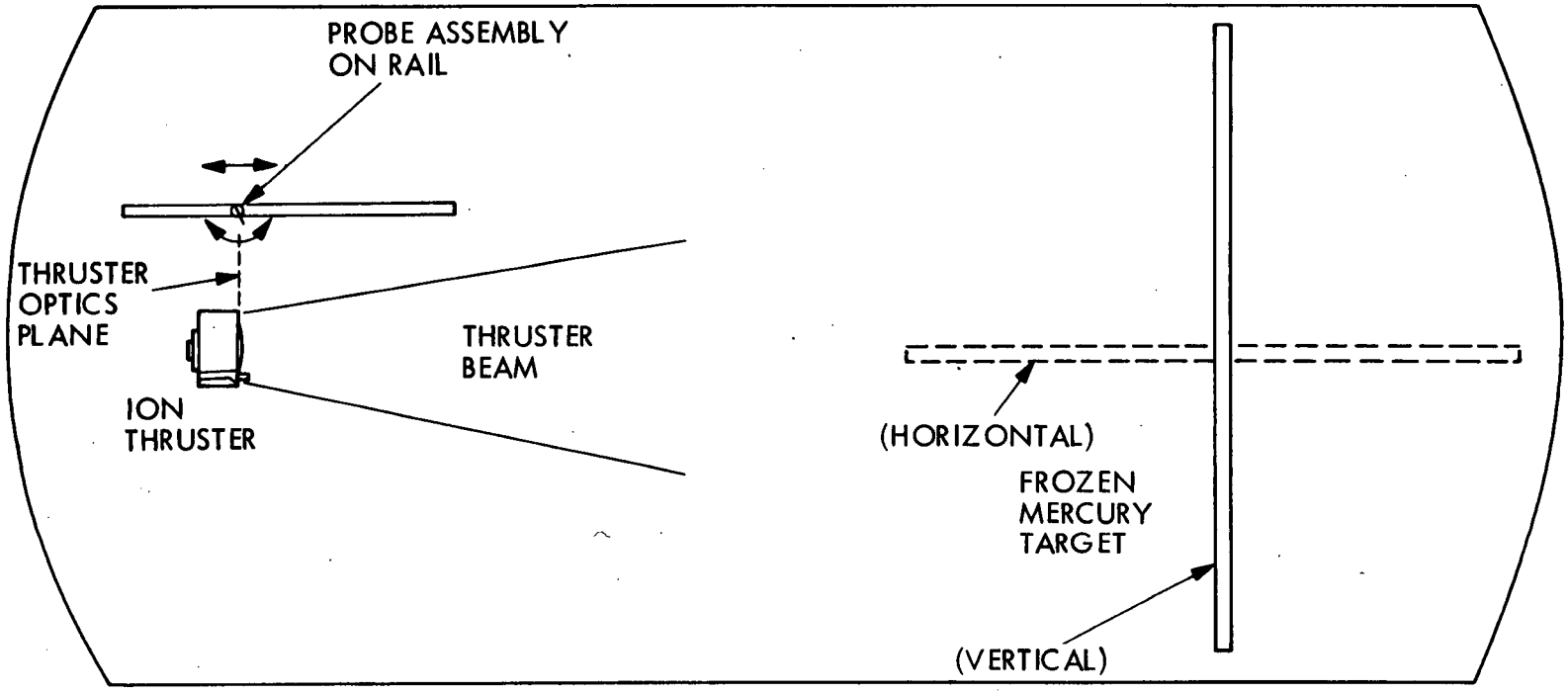

Figure 1. The 7' X 15' Test Chamber and Experimental Arrangement

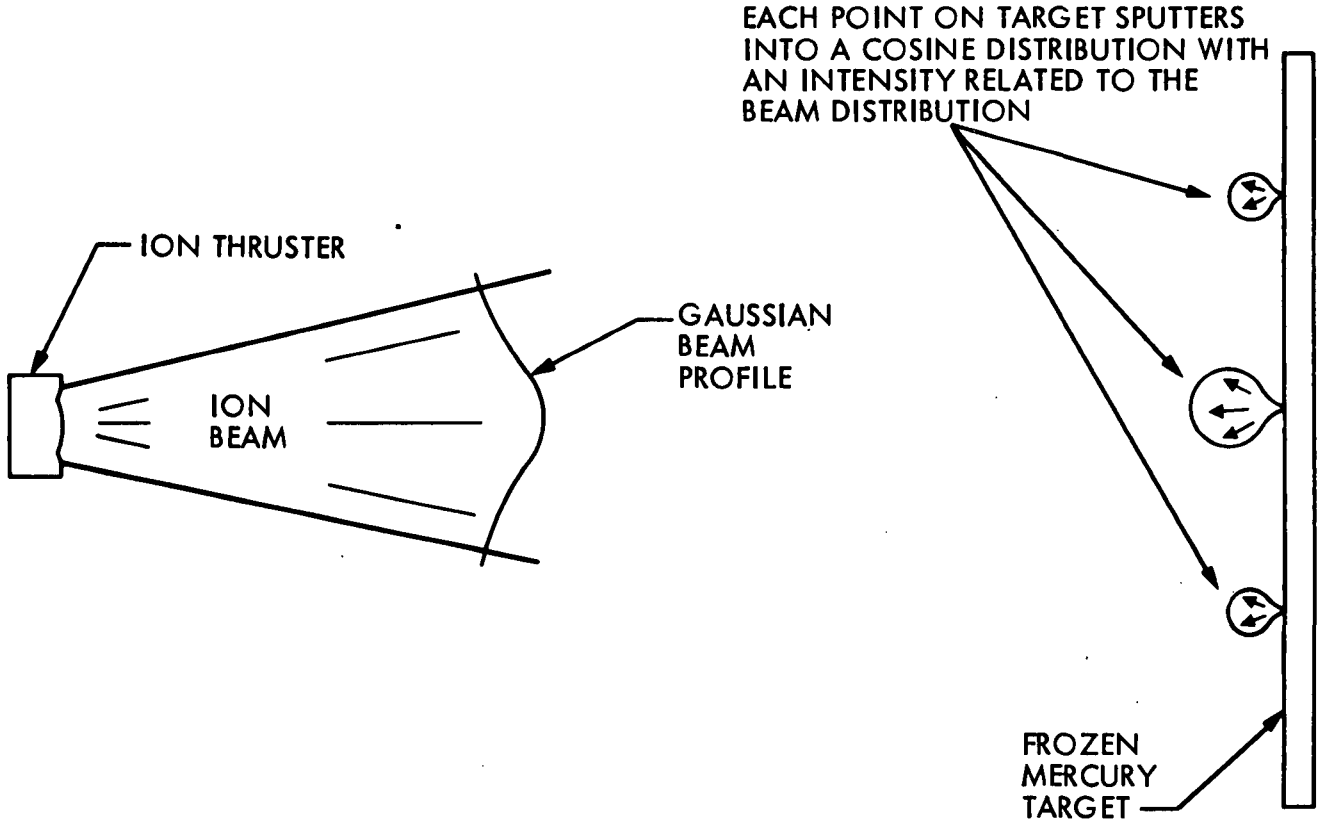

Figure 2. Illustration of Sputter Intensity/Ion Beam Distribution Relationship

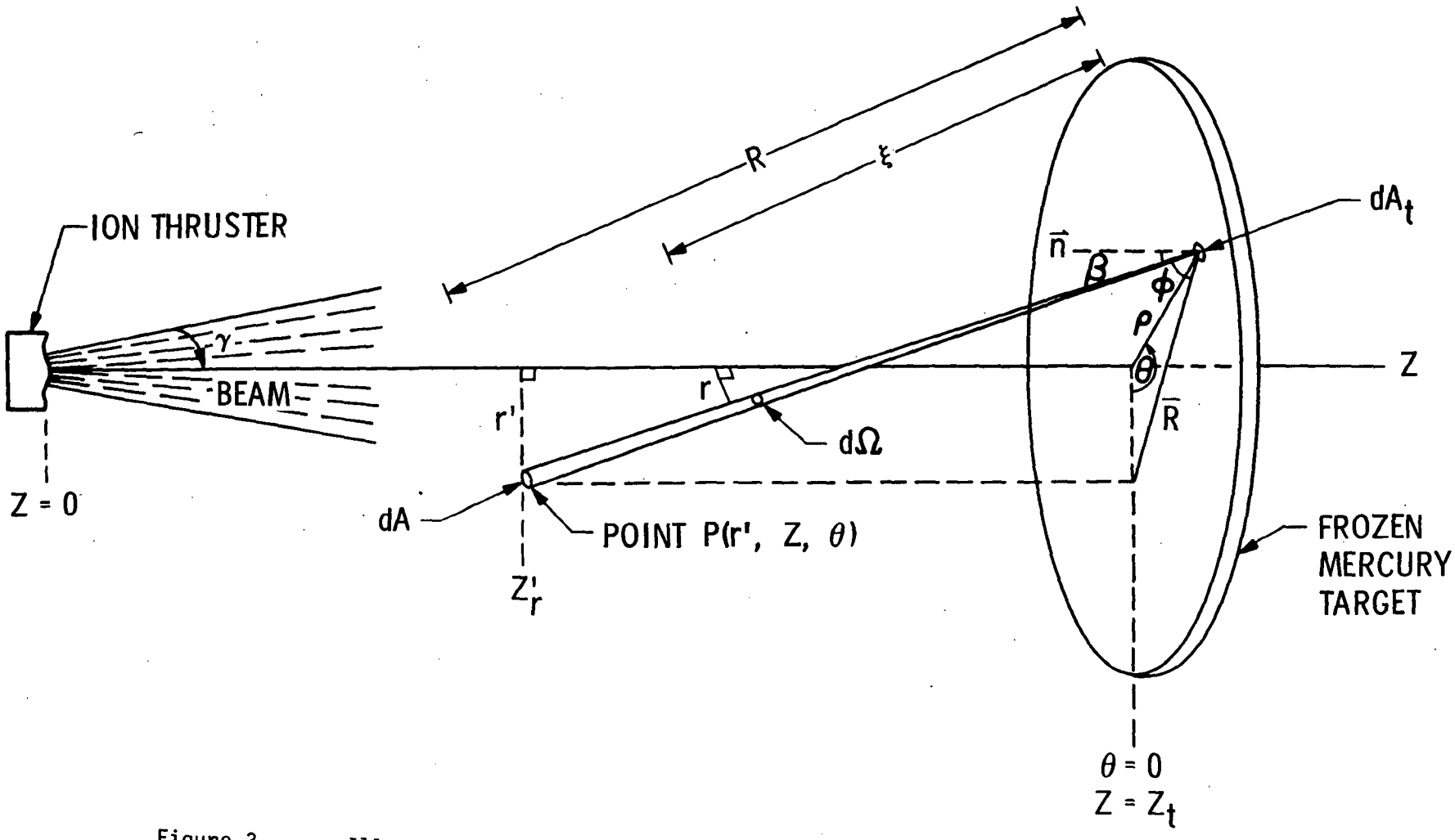

Figure 3. Illustration of Geometry Used in Analytical Model

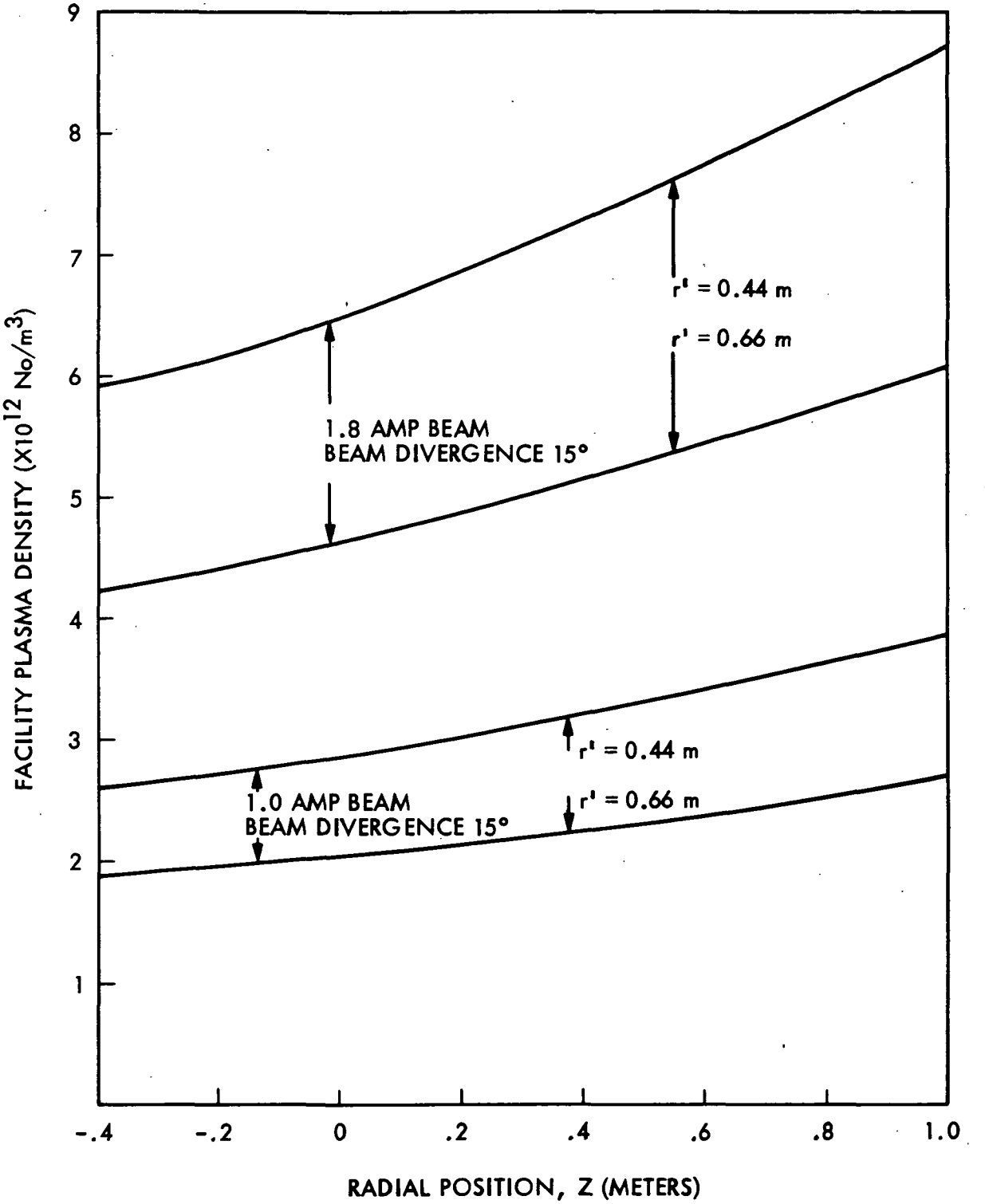

Figure 4. Model Predictions of Facility Plasma Density

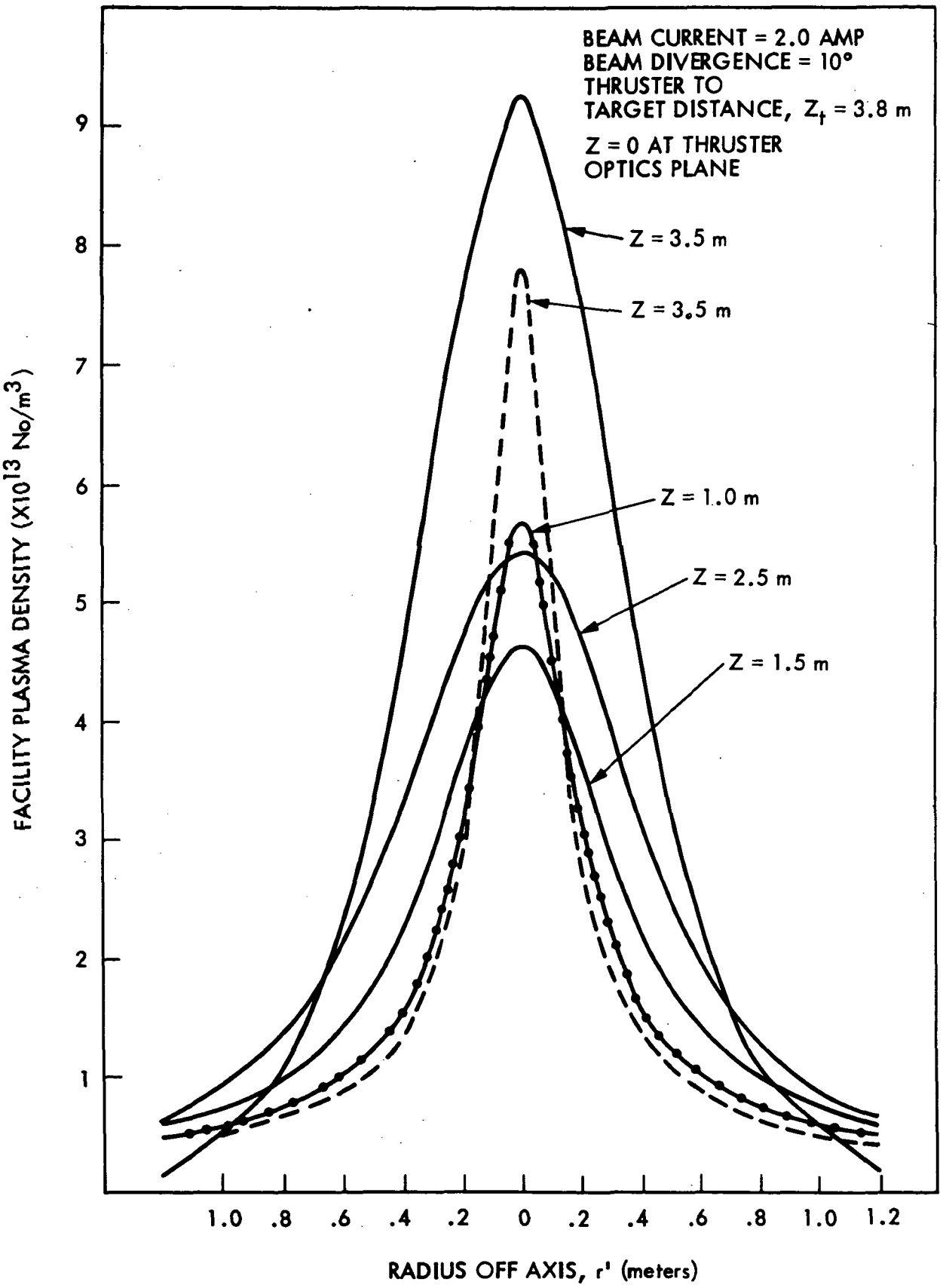

Figure 5. Model Predictions of Facility Plasma Density

D6

Electromagnetic Interference (EMI/EMC)

INTRODUCTION

The various electromagnetic interference (EMI) produced by ion thrusters and their power supplies and conditioning equipment have to be considered regarding ion thruster/spacecraft compatibility. Various science instruments are very sensitive to certain radio frequency (rf) emissions. A program to gather the available EMI data on ion thrusters and their power supplies, as well as gather additional data, was undertaken as part of the total ion propulsion interactions program.

The first paper in this section presents the radiated and conducted emissions measured from a 30-cm mercury ion thruster. The second paper presents some additional data and makes an assessment of the compatibility of a typical interplanetary spacecraft with the EMI environment produced by an ion thruster system. The SEMCAP computer code is used in this analysis and is described in the second paper.

The third paper in this section deals with the effect on the S-band carrier signal when it is necessary to transmit through the plasma beam. Experimental data was obtained and compared with an analytical model. However, the existence of facility produced charge-exchange plasma is obvious in the data. This is why the analytical model of the facility produced plasma, described in the paper in the charge-exchange plasma section, was produced. The facility plasma model correctly follows the dependence on beam current but predicted densities were considerably lower than data obtained in the ion plume/S-band signal experiment. It is believed the existence of the antennas and the rf absorber material in the test chamber allowed rerelease of mercury atoms from them, which was not accounted for in the analytical model, increasing the neutral atom density and so increasing the facility plasma density above what the model predicted.

RADIATED AND CONDUCTED EMI FROM A 30-cm ION THRUSTER

A. Whittlesey and W. Peer
Jet Propulsion Laboratory
California Institute of Technology
Pasadena, California

Introduction

In order to properly assess the interaction of a spacecraft with the EMI environment produced by an ion thruster, the EMI environment had to be characterized. Therefore, radiated and conducted emissions were measured from a 30-cm mercury ion thruster. The ion thruster beam current varied from zero to 2.0 amperes and the emissions were measured from 5 kHz to 200 MHz. Several different types of antennas were used to obtain the measurements. The various measurements which were made are: a) magnetic field due to neutralizer/beam current loop, b) radiated electric fields of thruster and plume, and c) conducted emissions on arc discharge, neutralizer keeper and magnetic baffle lines.

Test Configuration

The list of measurement equipment used to acquire the data presented in this report is given in Table I. The ion thruster was located in the JPL Electric Propulsion Laboratory test chamber illustrated in Figure 1. The Singer rod antenna was located below and parallel to the plume axis and about 60-cm off axis from the plume. The Empire Devices antenna was located in a similar position approximately 90° from the Singer antenna. The Biconical EMCO 3104 antenna was used alone for the higher frequency measurements and was placed approximately in the same position as the Empire Devices antenna. It must be noted that the chamber dimensions do not permit adequate clearance between the biconical antenna and the chamber walls, so that actual fields in free space will be different but we can't say how different.

The magnetic field probe was located as near as possible on the axis of the current loop formed by the neutralizer and plume, and 55 cm off the main beam axis. The current probe was located outside the test chamber as close as possible to its entry point into the chamber. All antennas and probes inside the chamber were covered with a dielectric cover to prevent mercury contamination and at the same time permit measurements. The equipment to receive signals from the antennas and probes was placed near the chamber in a convenient location.

Test Procedure

The thruster was operated in its usual manner and its beam current was varied from about 0.7 to 2.0 amperes. Once a stable operating condition had been reached (15-30 minutes), the EMI instrumentation was operated per its operating instructions to record the EMI data from

the thruster. The data was later reduced using appropriate calibration factors for the various instruments.

The DC magnetometer was measuring an amplitude of about 200 nT in the presence of the Earth's field of about 30,000 nT. The Earth's field and other stable fields were eliminated by passing a current through a coil wrapped around the magnetometer probe. The neutralizer/plume magnetic field was determined by observing the change in magnetic field measured by the magnetometer as the beam current was varied. This took care because ambient perturbations (such as door openings) often occur faster than the beam can be changed and stabilized.

Results

The results are described separately for radiated emissions, conducted emissions, and neutralizer/beam dc magnetic field.

Radiated Emissions

Figures 2-7 show the radiated emissions from thruster and plume as observed in the vacuum chamber. The data was reduced according to the manufacturer's calibrations; it must be noted that the chamber dimensions do not permit adequate clearance from chamber walls. Much more clearance was obtained with the rod antennas as compared with the biconical antenna. Most of the noise appeared to be random broadband and the noise increased about eight to ten dB as the bandwidth increased a factor of ten. Figures 2-7 show the measured levels and the measurement bandwidth; at the bandwidth change points, the curves have been drawn as connected although there are a few dB change in the level at the change points. It can be seen that all thruster modes generate very nearly the same radiated spectrum for all practical purposes. The warm-up mode (discharge on, 0 amperes) was noticeably noisier from 500 kHz to about 80 MHz.

Conducted Emissions; Arc Neutralizer Keeper and Magnetic Baffle

Figures 8 and 9 show the arc and neutralizer keeper conducted emission spectra, respectively. The neutralizer keeper is clearly more noisy than the arc. In contrast to the radiated measurements, the power supply converter harmonics are clearly visible in the conducted measurements (the spectra line above 40 MHz are probably ambient-local radio stations). The magnetic baffle's conducted emission, shown in Fig. 10, lies between the emission of the arc and neutralizer keeper.

Neutralizer/Beam DC Magnetic Field

The varying magnetic field in the room prevented a clear measurement of the magnetic field from the beam. By averaging the best data, it appears that the neturalizer/beam current loop has a strength of 0.05 $A\text{-}m^2$, with standard deviation of 0.02, for a one amp beam current. This is consistent with a neutralizer beam path located 15 cm off the main beam axis, and joining the main beam 30 cm downstream.

TABLE 1. EMI TEST EQUIPMENT

1. Antenna, Singer 95010-1, Rod.
2. Empire Devices Rod Antenna VA-105
3. Antenna, Biconical EMCO 3104
4. Magnetometer Probe, HP 3529A
5. Magnetometer Meter, MP 428B
6. Power Supply for magnetometer zeroing, not recorded
7. Strip Chart Recorder for magnetometer, not recorded
8. Current Probe, Stoddart 91550-1
9. Spectrum Analyzer, HP 141T/8552B/8553

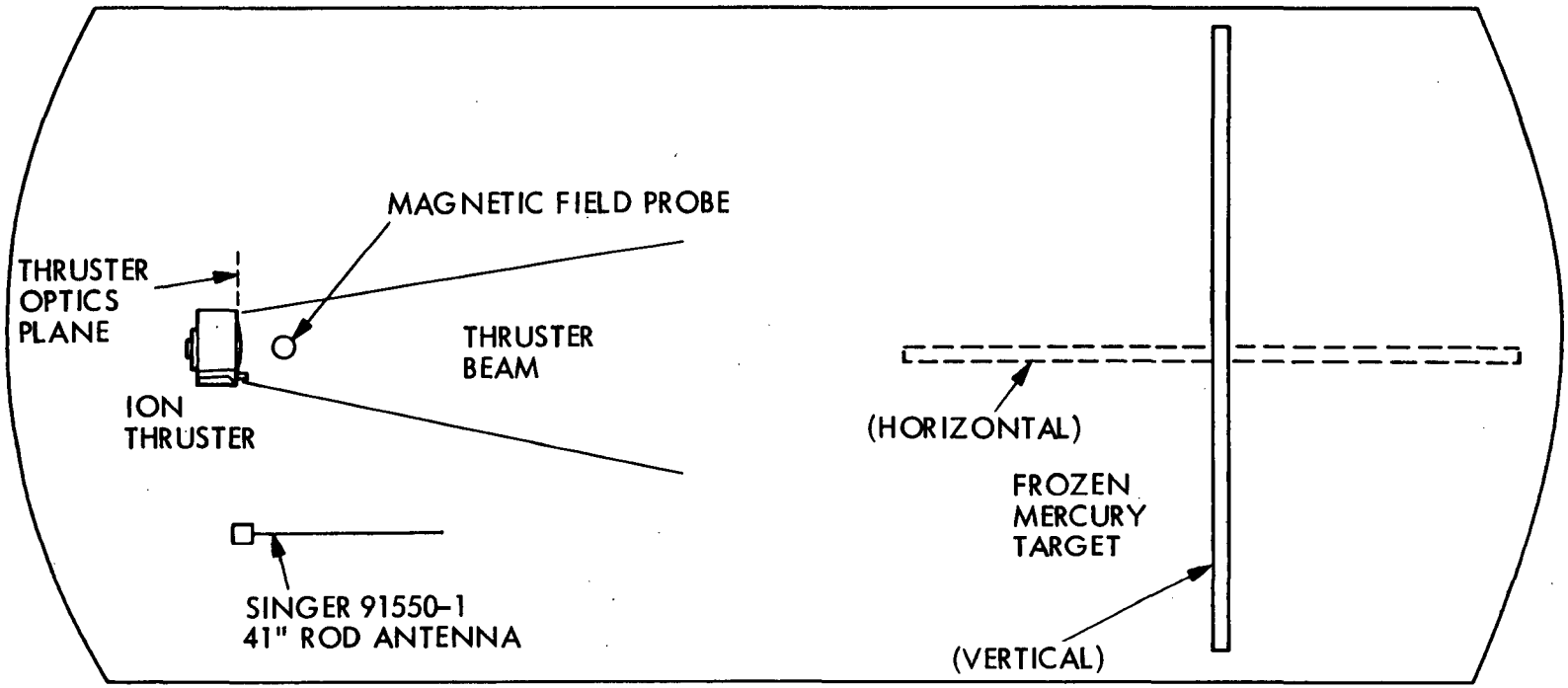

Figure 1. The 7' X 15' Test Chamber and Antenna Placement

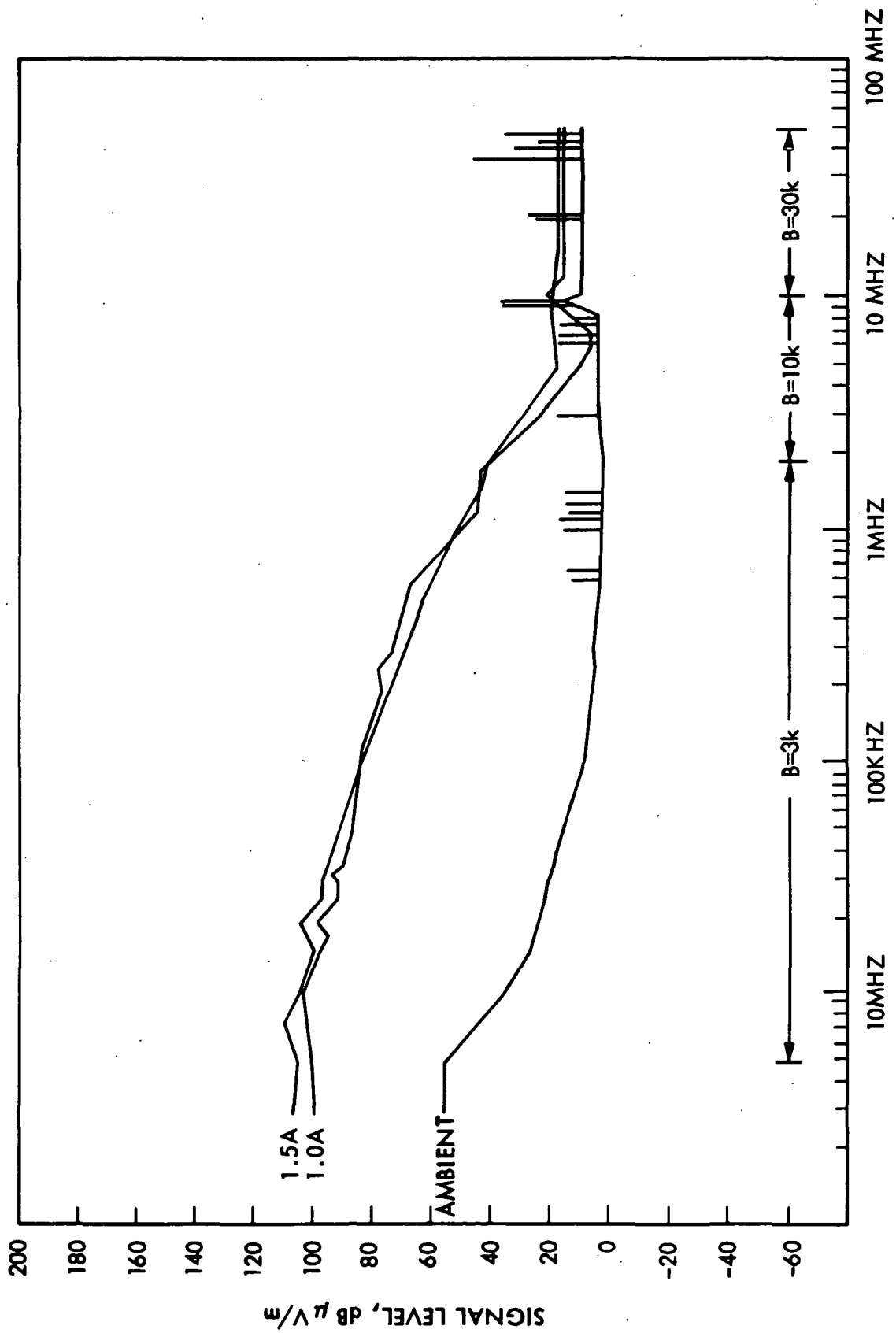

Figure 2. Ion Thruster Radiated Emissions

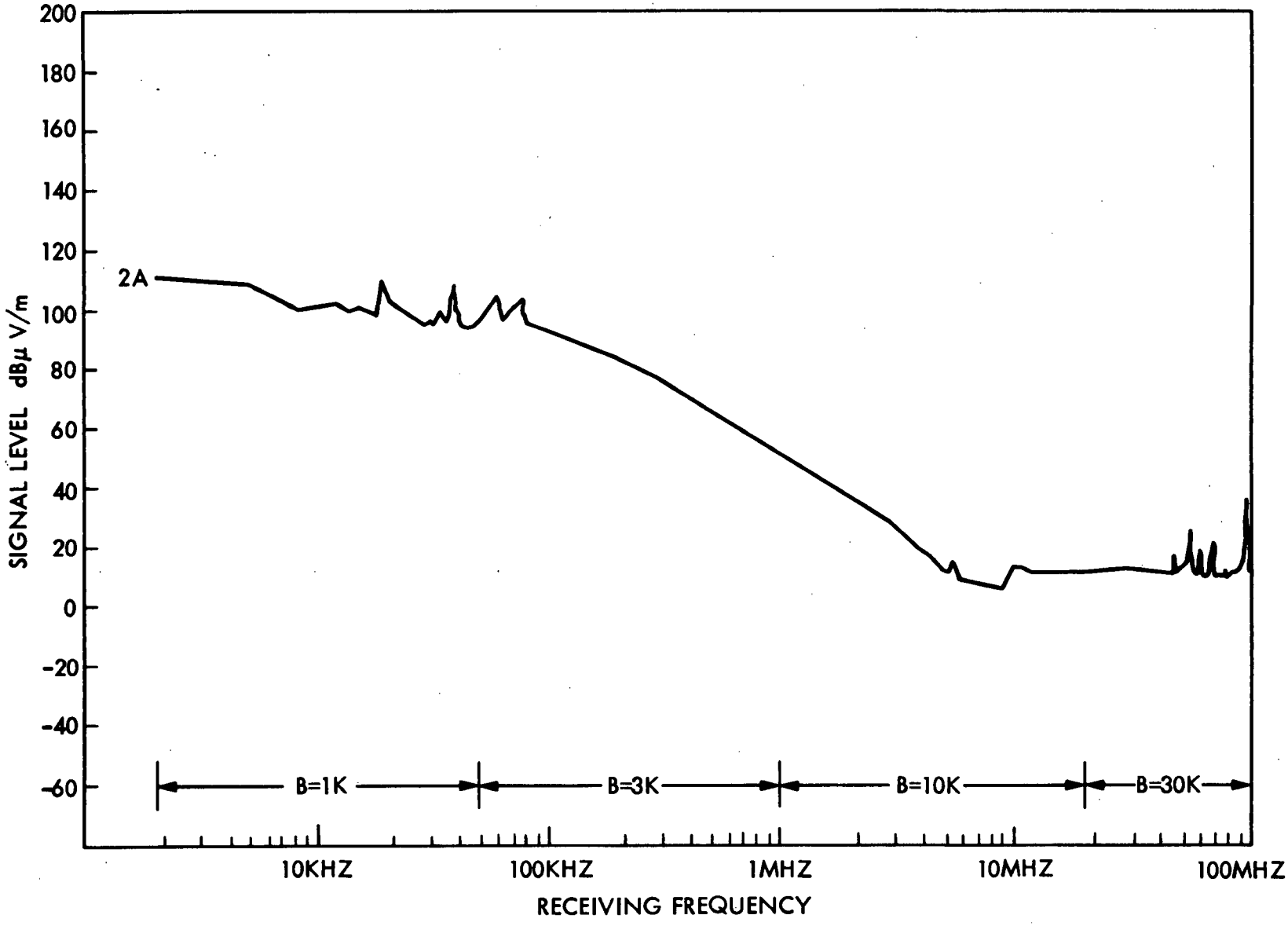

Figure 3. Ion Thruster Radiated Emissions

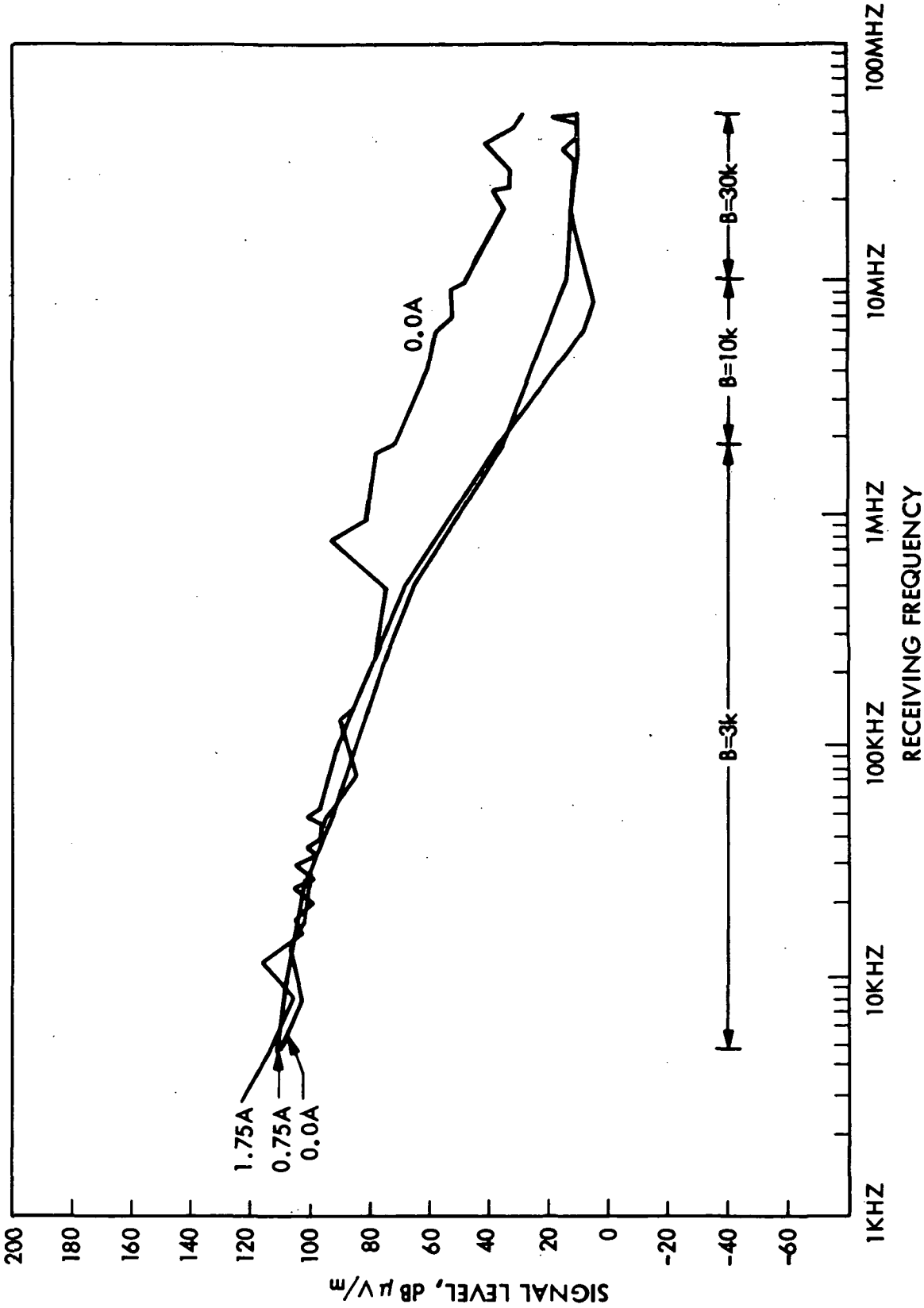

Figure 4. Ion Thruster Radiated Emissions

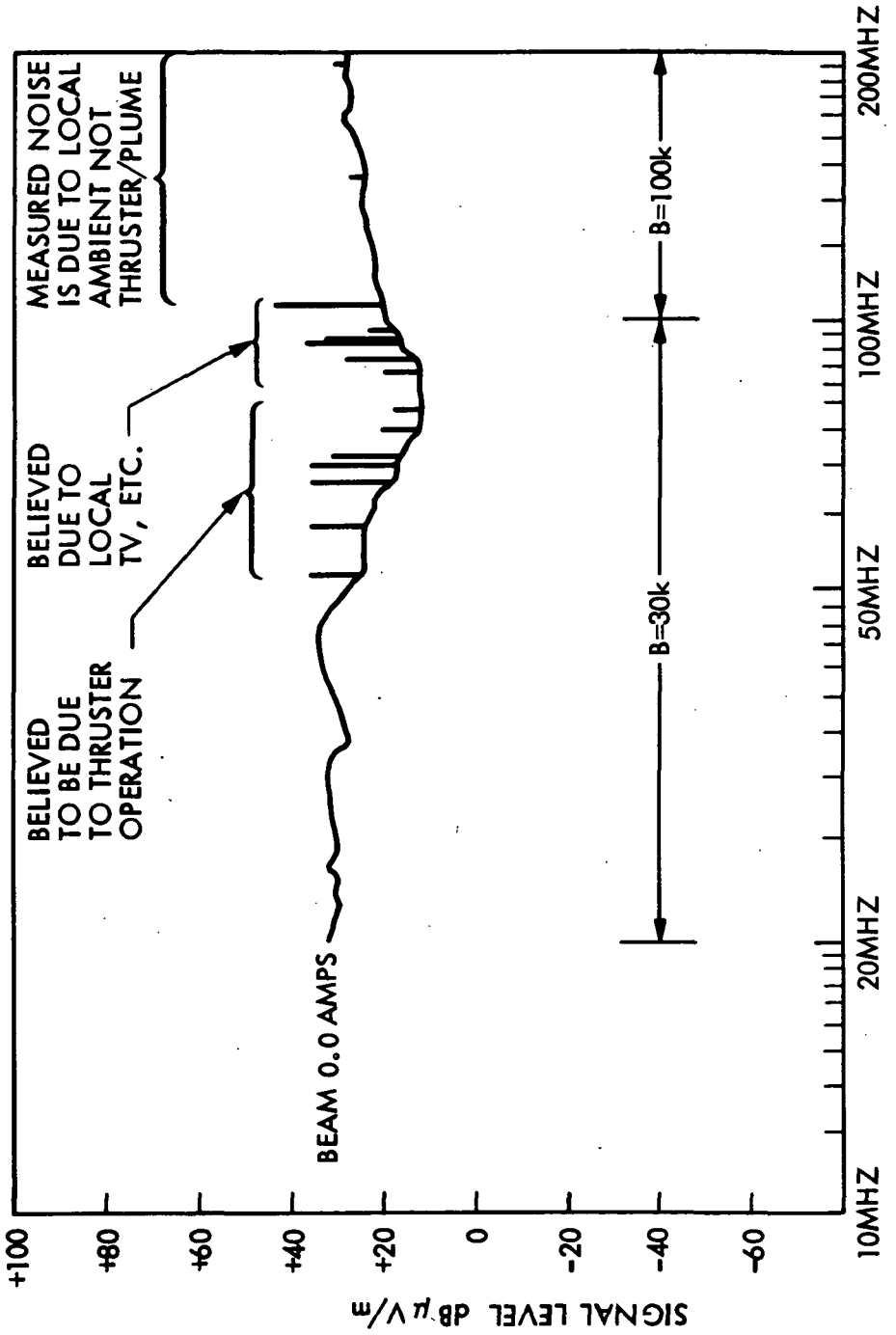

Figure 5. Ion Thruster Radiated Emissions

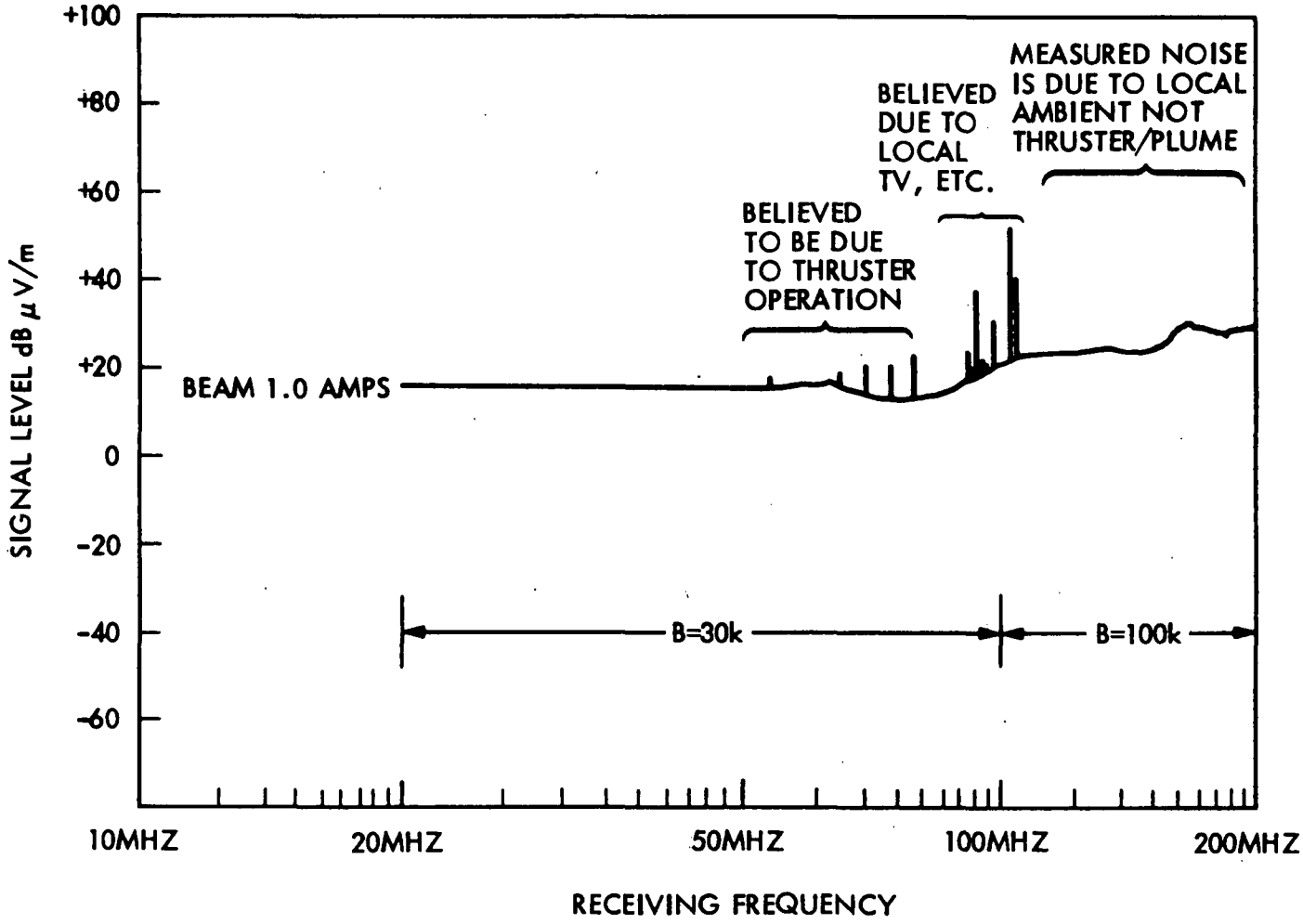

Figure 6. Ion Thruster Radiated Emissions

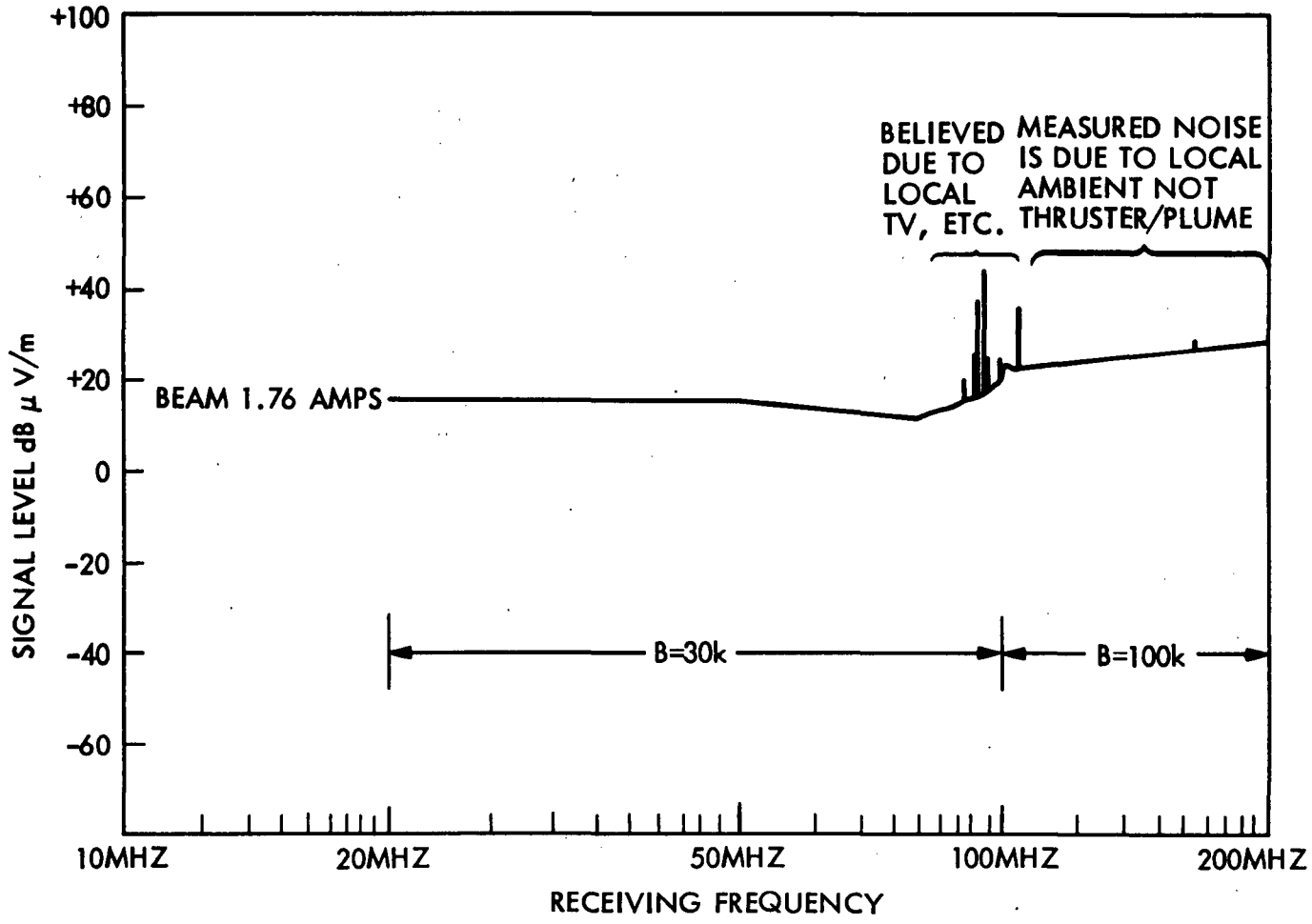

Figure 7. Ion Thruster Radiated Emissions

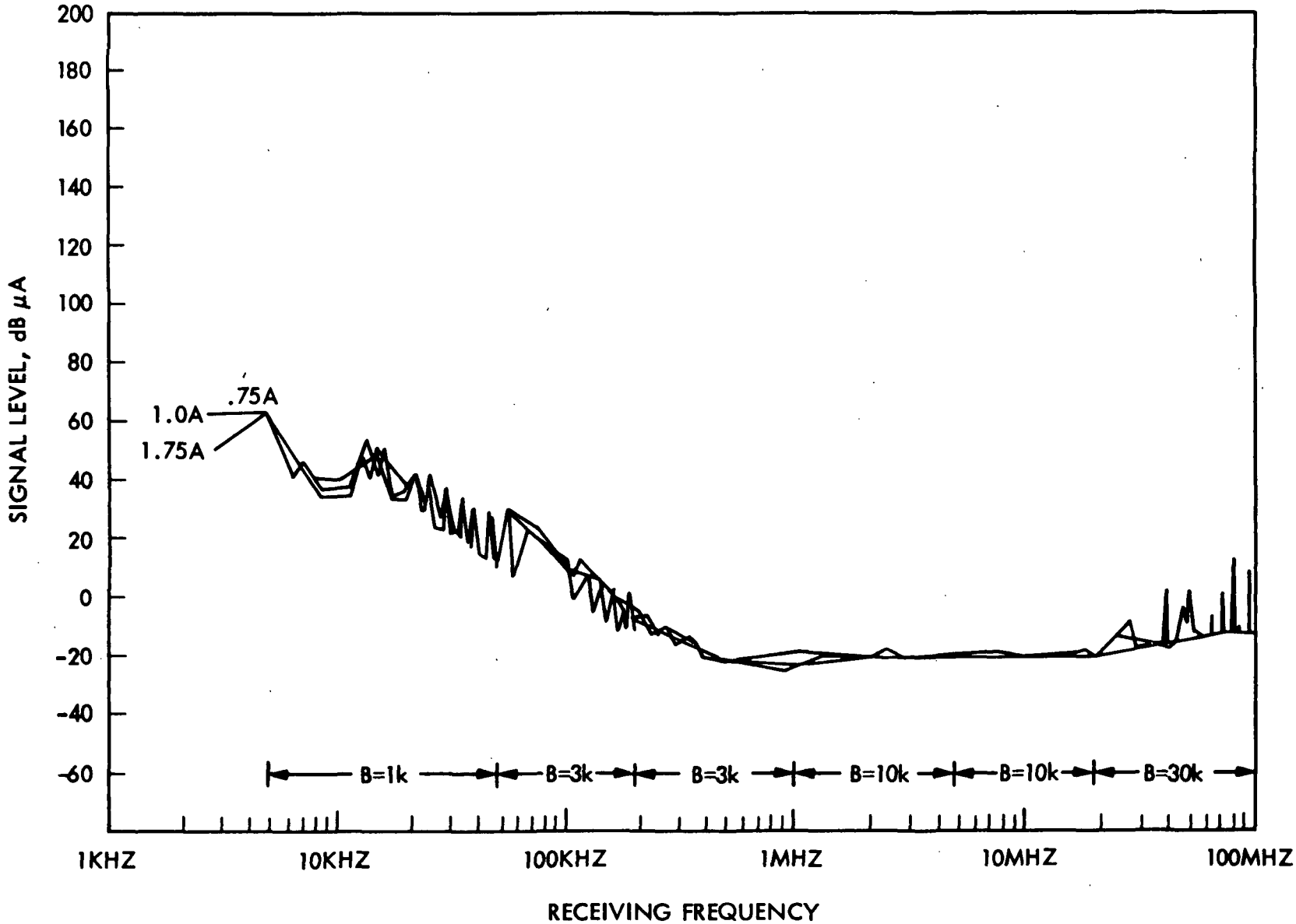

Figure 8. Ion Thruster Discharge Conducted Emissions

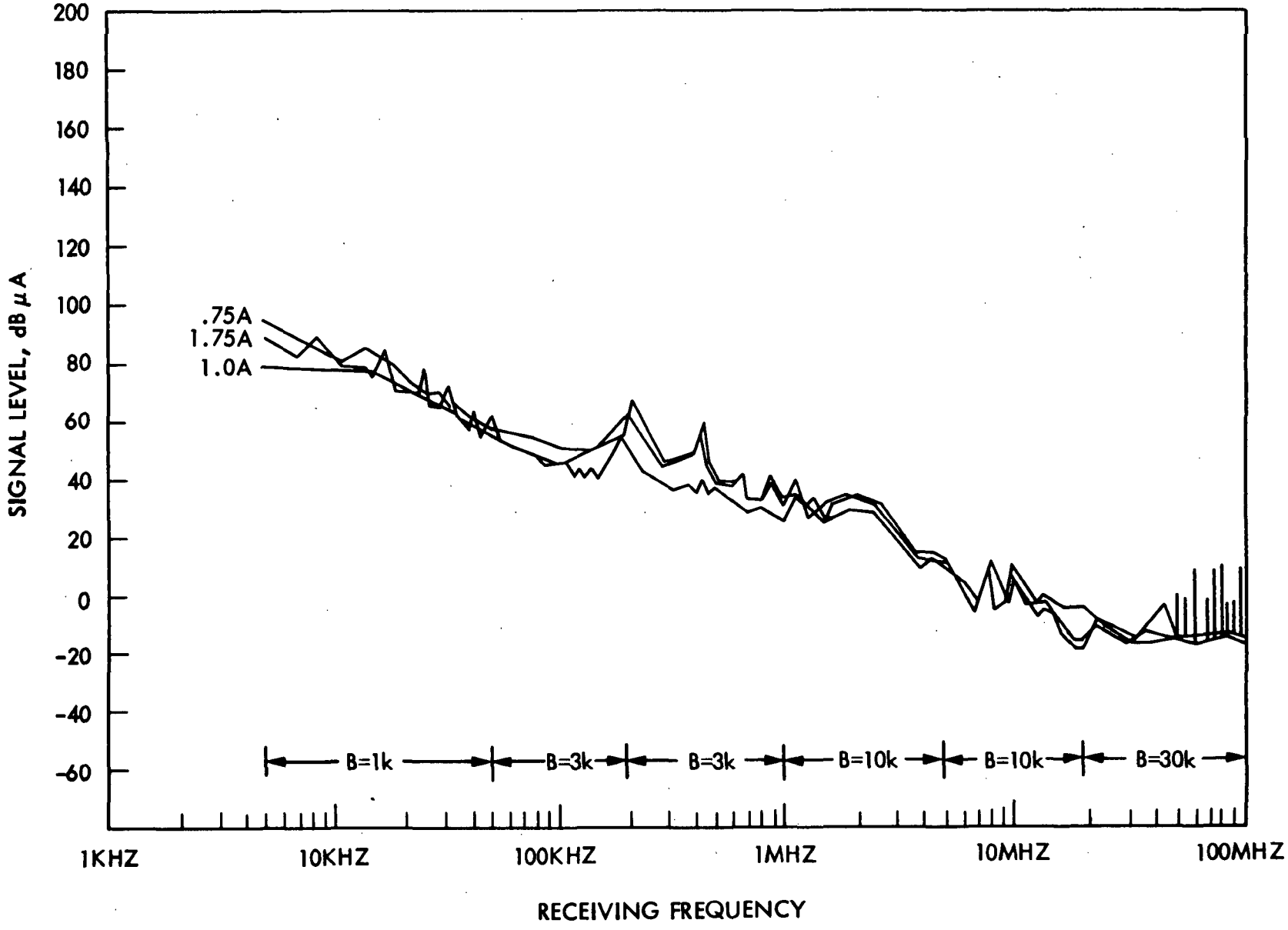

Figure 9. Ion Thruster Neutralizer Keeper Conducted Emissions

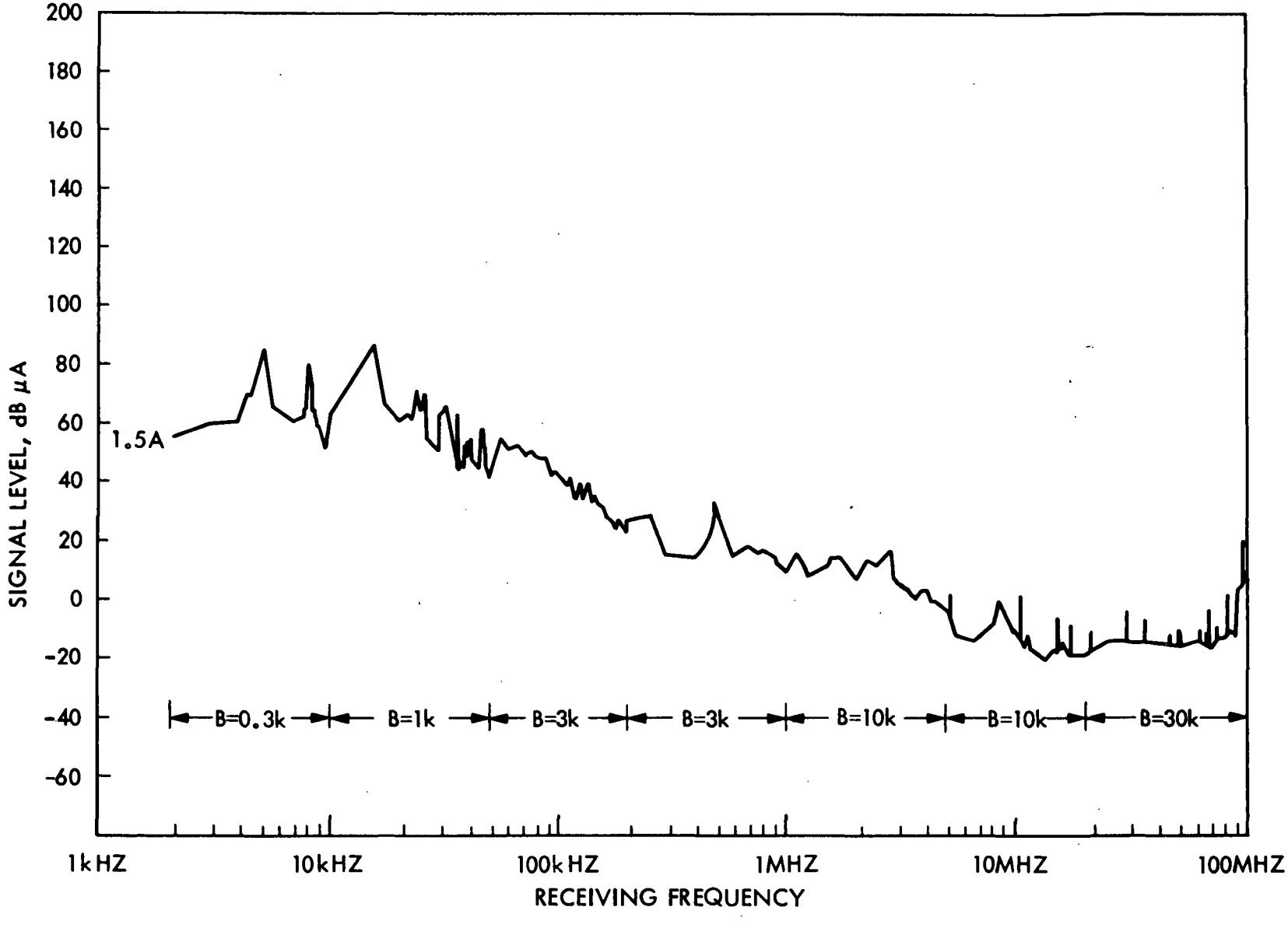

Figure 10. Ion Thruster Magnetic Baffle Conducted Emissions

ELECTROMAGNETIC INTERFERENCE ASSESSMENT OF AN ION DRIVE ELECTRIC PROPULSION SYSTEM*

A. C. Whittlesey
California Institute of Technology
Jet Propulsion Laboratory
Pasadena, California

ABSTRACT

An electric propulsion thrust system has the capability of providing a high specific impulse for long duration scientific missions in space. As the electric propulsion thrust system becomes a likely propulsion candidate, users have been more and more interested in its electromagnetic compatibility with normal engineering and science functions on candidate missions. The magnitude of the problem can be seen by comparing the 20,000 watt, 200 volt, 50 ampere power consumption and permanent magnets with 3,000 nanotesla fields (at one meter), to the radio receiver's 10^{-18} watt sensitivity, planetary radio experiment's nanovolt sensitivity, and magnetometer experiment's tenth-nanotesla sensitivity.

The objectives of work covered in this paper are to (1) characterize the electromagnetic interference (EMI) from the elements of an ion drive electric propulsion system; and (2) to predict their compatibility with typical interplanetary spacecraft engineering and science subsystems.

Conclusions to date are severalfold:

1. Some conducted and radiated spectra are in excess of MIL-STD-461/462 EMC specification limits. These data can be used to provide the basis for waivers or to direct design changes for filtering and shielding of thrust system elements.

2. The power processor appears to be the worst source of broadband radiated noise. Although high, these data are from units without much attention to shielding and probably can be improved greatly with little effort.

3. The magnetic field necessary in thruster operation is equivalent to 18 amp-meter^2 (permanent) on axis, and there is a variable magnetic field at right angles to the axis caused by the neutralizer/plume loop, of about 0.1 amp-meter^2 per amp of beam current. These may be of significance to magnetic field experimenters on a spacecraft.

*This paper presents the results of one phase of research carried out at the Jet Propulsion Lab., California Institute of Technology, under Contract NAS7-100, sponsored by the National Aeronautics and Space Administration.

INTRODUCTION

Several candidate missions have been proposed which will make use of electron bombardment ion thrusters for primary propulsion. The first of these will likely be a comet rendezvous mission. Plans to use such an ion drive electric propulsion system have in the past stimulated interest in its peripheral performance as an electromagnetic noise generator (Ref. 1). Recent plans for the comet rendezvous mission have reiterated the need for a quantitative/qualitative assessment of ion drive compatibility with the proposed spacecraft. Concerns are caused by both the higher power levels (20 kilowatts vs. 500 watts) and the large physical dimensions (solar panel length of 40 meters), both of which can contribute to much higher levels of electrical interference than are normally present on a scientific spacecraft.

This paper gives the results of work in process to evaluate the magnitude of science or engineering disturbances, with the conclusion that compatibility can be achieved but proper design is a prerequisite. The paper is divided into two parts: first, a collection of suitable EMI data measured at JPL or elsewhere as reported in the literature, or estimated where measurements were not available; second, an interaction study to assess how EMI would affect a typical scientific spacecraft. Conclusions follow the output of the interaction study.

INTERFERENCE ASSESSMENT OF AN ION DRIVE SYSTEM

As shown in Figure 1, an ion drive system as conceived today consists of a power processor, a thruster, and a solar array, with one or more units of each. This paper considers one unit of each, with no consideration that more items (multiple power processors for example) will create more interference. Data has been gathered for a power processor (Ref. 2 - 4) and a thruster (Ref. 5-7), but not a solar array. Characterization of the solar array, a passive element, was done by assuming appropriate impedances and dimensions to assess its impact while radiating as an antenna due to the ripple currents from the power processor.

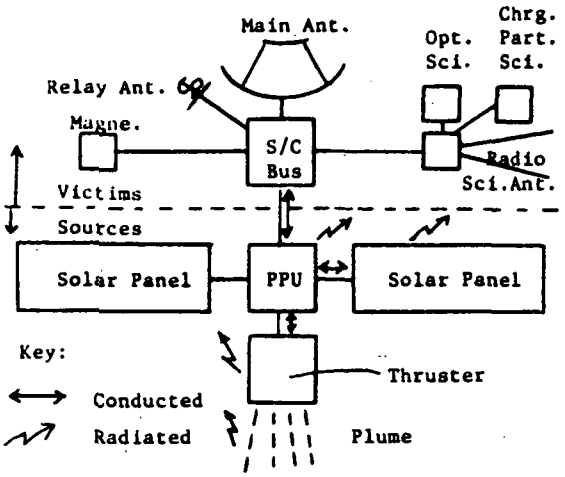

Figure 1. S/C-ION Drive EMI Interactions

The approach taken in summarizing the data was to envelope the measured data in a worst-case sense, so the results of the interaction study would have conservative results, i.e., an output of "compatible" means that we are fairly assured of no incompatibilities. Secondly, the data was taken from a variety of sources, and was smoothed to envelope all cases. Finally, extrapolation was used if the as-measured data did not cover the frequency range needed for the interaction study.

DC magnetic fields from the thruster have been determined to be:

a) 3600 nT at one meter on axis due to the permanent magnets (Ref. 9).

b) About 13 nT at one meter on axis due to the magnetic baffle current; varies somewhat with operating parameters (Ref. 7).

c) 10 nT at one meter perpendicular to the beam axis at one ampere of beam current loop; proportional to beam current (Refs. 7 and 8).

These are fairly typical of the present 30 cm thruster design.

DC magnetic fields from a power processor have been measured to be 21 nT at one meter in the off state, and 741 nT at one meter in the on state (Ref. 10). Another processor measured 94 nT and 222 nT off and on respectively. There is no specific need for any external magnetic field on a processor, but power handling equipment (transformers and latching relays) and current loops occur in processors. Some attention should be given in design to reducing external magnetic fields, by wire routing and component orientation, and keeping them stable with time.

DC magnetic fields from a solar array have been measured for much smaller arrays. It was observed that Kovar+, a magnetic material, was used as an interconnect material. Magnetic design should consider material usage. A 10-kilowatt array operating at 400 volts, has 25 amps of current. Twenty-five amps of current in a loop of one square meter can generate a field of 5,000 nT at one meter distance (on axis), proportional to current. The design should segment panels in the array so that the current-area product of each is small, and adjacent segments have opposite polarity magnetic fields (clockwise currents in one segment and counterclockwise currents in the adjacent segment) so as to cancel each other.

Radiated electric and magnetic field spectra have been measured as a function of frequency for thrusters and power processors; conducted noise on power lines for thruster and power processors have also been measured (Ref. 2-4). Typical spectra, enveloped in a worst-case sense for later use of computer analysis, are shown in Figs. 2 - 7. Electrostatic charging has not been measured or estimated. Its effects are described in a later section.

ION DRIVE SYSTEM EMI INTERACTIONS WITH A TYPICAL SPACECRAFT

To assess interactions with a "typical" spacecraft, a real spacecraft, a Voyager now en route past Jupiter to Saturn, and hypothetical science and communications subsystems were considered. Several principle interactions were considered either by manual methods, or by SEMCAP, a computerized electromagnetic compatibility assessment code. SEMCAP had previously been used as a design tool for Voyager; this study used the prior computer characterizations of Voyager as an EMI victim and added the measured or estimated ion drive elements as EMI noise sources. The computer then assesses the impact of each source on each victim. In this case, six sources against sixty-five engineering/telemetry circuits and forty-eight plasma wave and planetary radio astronomy channels measuring over the range of 100 Hz to 40 Hz.

Manual methods were used to assess electrostatics, magnetics, and communications effects.

Magnetics. It is a fact that excessive magnetic fields should be and can be reduced in solar panels and power processors, using materials and methods in standard use for other space hardware. The thrusters have several magnetic fields that are difficult to eliminate;

the strongest of these, the permanent magnets, could be replaced with

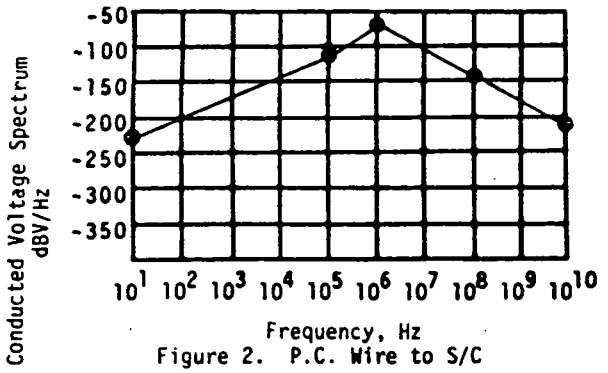

Figure 2. P.C. Wire to S/C

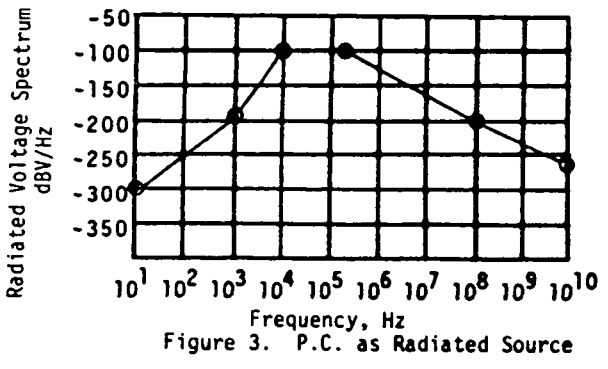

Figure 3. P.C. as Radiated Source

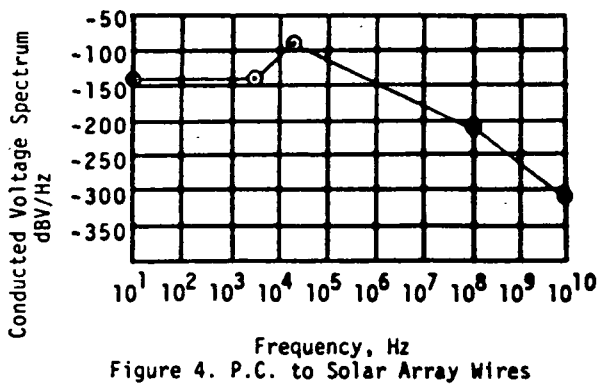

Figure 4. P.C. to Solar Array Wires

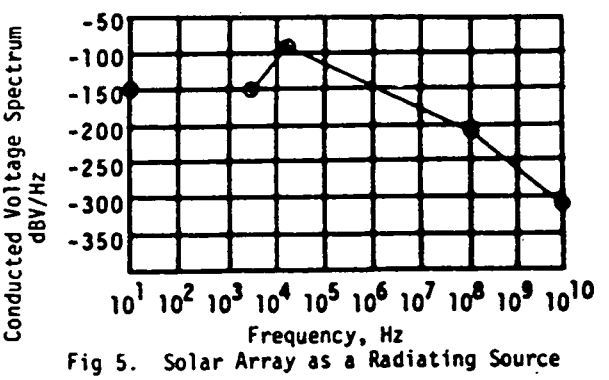

Fig 5. Solar Array as a Radiating Source

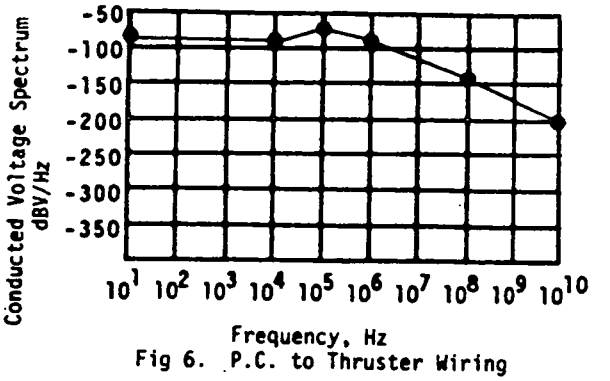

Fig 6. P.C. to Thruster Wiring

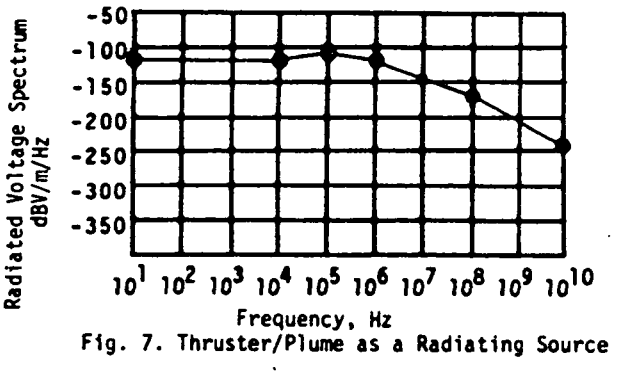

Fig. 7. Thruster/Plume as a Radiating Source

electromagnets but this has power implications. It seems most appropriate to accept the magnetic field and use magnetometer boom length and location to reduce the field to acceptable limits. The use of opposing polarity magnets for adjacent thrusters in multiple thruster arrays has been examined previously (Ref. 11) to reduce the fields at large distances from the array.

Electrostatics. Electrostatics is an area needing more work; quantitative results have not been calculated. Electrostatic potentials can attract contaminants such as mercury from the thruster, and cometary or interplanetary dust; they can disrupt scientific measurements requiring a stable and known reference for measuring particle energies, and/or disrupt charged particle paths if directional characteristics are of concern.

To minimize solar panel-caused field disturbances, the various panel segments,

with up to 400 volts potential, would at best be a balanced ±200 volt supply, with adjacent segments having opposite polarities to balance the far-field electrostatic effects.

The power processor is not an electrostatic problem. The thruster/neutralizer, working together, maintain the spacecraft within 20 volts of neutral, which is adequate for all but the most demanding missions. The only time of concern is a neutralizer failure. Any protective circuitry should, optimally, react before an excessive spacecraft charge occurs. At a one amp beam current, a spacecraft with 300 pF capacitance to infinity would charge to one kilovolt in 300 nanoseconds, faster than most power circuits can respond. A passive device should be present to limit charging, perhaps temporarily sharing a neutralizer if multi-thruster operation exists.

Radiated Electric and Magnetic Field Spectra. Typical space communications frequencies (2000 MHz and higher) will not be affected by the thruster system, since they are much higher than significant energy content from power processor harmonics. Relay frequencies (to a probe, for example) may be a problem if as low as 50 MHz and should be considered up to 300-400 MHz. The thruster is no problem due to radiation generated by the ion acceleration. The solar array is only a problem if it acts like an antenna and radiates any power processor ripple and harmonic currents, but only for those relay frequencies.

Interferences with plasma wave and plasma science experiments over the range 10 Hz to 50 MHz were estimated using the SEMCAP program. For Voyager, in the narrower bandwidth channels (1 kHz 3dB bandwidth to fit between the 2.4 kHz power supply harmonics), the calculated interference was between 20 and 40 dB above the receiver threshold. The wider bandwidth channels (200 kHz bandwidth at higher frequencies had interference ranging from 30 dB over the receiver threshold (at 40 MHz) to 76 dB over the receiver threshold (at 1.3 MHz). It is worth mentioning that the Voyager method of placing radio experiment receiver frequencies between harmonic frequencies from the power supply was made possible because most power converter frequencies were synchronized to the same source as the planetary radio experiment. This approach seems especially important for the ion drive system, where the voltage is four times higher and the power level is about forty times higher than Voyager. In this way, the interfering frequencies will be known if they can't be shielded and filtered; secondly, you do not have the problem of beat frequencies between the several converters. Troubleshooting the occasional interference from beat frequencies is nearly impossible!

Interferences with 65 other experiments and engineering subsystem circuits as calculated by SEMCAP were generally much lower. A conspicuously susceptible subsystem was the outboard low field magnetometer, which sends a low level signal along a 13 meter boom, and is processed inside the spacecraft main chassis. A 20 dB reduction of the interference sources, fairly easily achieved, eliminated all but the magnetometer (still 66 dB over threshold) and three other circuits as interference problems (the latter three still showed as much as 13 dB interference over threshold).

In all cases, it was the electric field component of the noise that caused the disturbances, rather than the magnetic field, capacitive, and inductive coupling that are also calculated by SEMCAP. The two principle sources were the wires going from the power conditioner to the spacecraft and to the power processor.

Conducted Noise. The power line ripple can interfere directly with other subsystems if the interface specifications are not adequate, but standard methods can be applied to remedy this situation. The matter of signal line noise is possibly more difficult. Unless carefully isolated and/or filtered, the low level telemetry signals (0-3V) to the spacecraft can pick up noise of significant magnitude from the power processor. Once again, standard methods can be used.

CONCLUSIONS

The possible EMI interactions between an ion drive system and a typical interplanetary scientific spacecraft as discussed previously, are summarized in Table I. Highlights of that summary are as follows:

1. Electrostatics
   a. Have good clamping and shutdown for neutralizer failure.
   b. Balance plus and minus voltage segments of the solar array.
2. Magnetics
   a. Spacecraft design must accommodate thruster magnetic characteristics but multiple thruster systems can reduce fields by alternating the thruster magnetic polarities.
   b. Solar panel current loop areas can and should be minimized.
   c. Power processor current loops should be minimized; magnetic components should be eliminated, shielded, and/or compensated by standard methods.

SOURCES	VICTIMS					
	S/C Engineering	Communications Relay S-Band X-Band	Plasma/Radio Science	Charged Particle Science e^- p^+	Magnetometer	Dust/ Particulates
THRUSTER	Not expected to be a problem	Not expected to generate excessive noise	Plume Oscillations/ RF radiations	S/C charge affected (neutralizer)	Perm mag fields. neut. current loop. Mag baffle field.	(Magnetic dust-iron?) Affected by mag fields? Electrostatic fields may affect path even of uncharged particles
POWER PROCESSOR	May radiate RF fields, coupling into sensitive subsystems. May generate ripple or transients into dc power bus and solar panel unless well-filtered.	Unless shielded may present problem for relay Frequ's. Less likely for S-band and X-band.	Radiates fundamental and harmonics of inverter frequencies unless shielded. Synchronize frequencies.	AC electric & Magnetic fields may affect paths of charged particles.	Magnetic components current loops	Not expected to be a problem.
SOLAR PANEL	Not expected to be a problem (Large fields may drain currents through space plasma?)	Not expected to be a problem	May act as antenna for AC load currents if power processor frequencies are not filtered	Large voltages may affect paths and energy of particles	Current loops 100 $A°m^2$ gives 2.5 nt @ 20 m.	Static fields from solar panels affect path of particles??

NOTES: 1) Optical interference, particulate contamination, etc., line of sight for RF or optical instruments, are not EMC interactions and are not noted here.

2) Turning off thruster during science acquisition sequences is considered a backup to reduce interference, but power processor may still be running.

TABLE I: Possible Ion Drive EMC Interactions for a Typical Scientific Spacecraft

3. RF Radiated Fields

   a. RF radiated fields from the basic power processor and its cabling should be reduced 30 to 40 dB by shielding and filtering.

   b. Additional measures must be taken to control the possible interference frequencies by synchronizing the power processor inverters to common frequency. Additional benefits are achieved by a higher inverter frequency.

4. Conducted Noise

   a. Power processor input lines (from solar array) and output lines (power to spacecraft, data to spacecraft; and power to the thruster) should be filtered to minimize conducted noise.

Although some of the work reported here, especially the SEMCAP modeling, is preliminary in nature, it is apparent that with proper attention to EMC design, an ion drive system can be compatible with typical interplanetary scientific spacecraft.

REFERENCES

(1) R. J. Rulis, Design Considerations and Requirements for Integrating an Electric Propulsion Subsystem Into the SERT II and Future Spacecraft, proposed for 8th Electric Propulsion, AIAA, Stanford Calif., Aug. 31-Sept. 2, 1970.

(2) JPL TM 33-623; A. C. Whittlesey and T. W. Macie, Electromagnetic Interference of Power Conditioners for Solar Electric Propulsion; July 1, 1973.

(3) JPL TM 33-618, T. W. Macie, Processing of Thermionic Power on an Electrically Propelled Spacecraft; November 1, 1973. Study of various parameters affecting design of a power processor.

(4) NASA CR-135287. Electromagnetic Interference Test Results of 30 cm electrical prototype power processor, March 1977.

(5) NASA TM X-71421, Plasma Fluctuations in a Kaufman Thruster, John S. Serafini and Fred F. Terdan; October 31-November 2, 1972. NASA-LEWIS.

(6) Serafini, J. S., et. al. Dynamic Characteristics of a 30-cm Mercury Ion Thruster, Journal of Spacecraft and Rockets, Vol. 13, No. 10; October 1976- pp 579-584.

(7) JPL IOM 3575-79-05; A. Whittlesey to R. Carruth; Radiated and Conducted EMI from a 30 cm Thruster; January 20, 1979.

(8) JPL IOM B. Conner, et. al., Preliminary Measurements of Magnetic and Electric Field Propulsion (SEP) Thruster During Operation; September 12, 1974.

(9) JPL IOM, Cowgill, SEP 30 cm Ion Thruster Engineering Model-Post-Vibration Magnetic Mapping; May 2, 1974. 3600 nt @ 1 meter.

(10) T. W. Macie and A. C. Whittlesey, Electromagnetic Interference Onboard an Electrically Propelled Spacecraft; October 1973. Presented at AIAA 10th Electric Propulsion Conference.

(11) JPL IOM R. M. Cowgill, Reduction of Magnetic Contamination Through Cancellation; May 17, 1974.

References (7), (8), (9) and (11) are JPL internal documents.

ION PLUME/S-BAND CARRIER INTERACTION STUDY

P. Stanton
Jet Propulsion Laboratory
California Institute of Technology
Pasadena, California

Abstract

A study was performed to determine the effects of a mercury ion thruster plume on an S-band telecommunication carrier. Experiments were carried out on a 30-cm thruster in a JPL test chamber. Results from simple analytical models were compared with the above measurements and major discrepancies were discovered. Modifications to the electron density model provided a qualitative explanation, but further work is necessary for a quantitative answer. The results of this study indicate the effects of the plume, on S and X Band telecommunications will be minor, with the possible exception of critical angle blockage.

Introduction

Spacecraft driven by ion thrusters may need to communicate through its ion exhaust plume (figure 1). Therefore, the ion plume/RF interactions should be understood. The types of interaction under consideration are RF attenuation, phase-shift, reflection, fluctuations and nonlinearity. Although a large amount of work has been published on plasma/RF interaction, apparently very little information is available on mercury-ion thruster plume/microwave* interactions. Preliminary analyses and experiments have been performed at S-band and are reported upon in References 1, 2, and 3.

This study was undertaken to improve upon the quality and quantity of the experimental data to be used in the verification of analytical models and in telecommunications link simulation. This study is focused on the measurement of the following plume/S-band carrier interaction properties: attenuation, phase shift and fluctuations. Simple analytical models of the attenuation and phase shift were used in support of these experiments. The carrier frequency range was not extended to X-band because of funding limits and the expected small measurable values at this higher frequency.

Analytical Model

The main plume/RF interaction effects modelled in this study were S-band carrier attenuation and phase shift. The propagation path chosen for these models was approximately perpendicular to and passing through the plume axis, which was a good approximation of the experimental configuration used (figure 2). In order to simplify these analytical

---

* Telecommunication frequencies of interest are approximately 2.2 and 8.4 GHz.

models, the following plasma assumptions were made: electron plasma, lossless (except in the case of the stratified dielectric model), isotropic, linear, adiabatic (except in stratified model), and has a permeability of vacuum (covered in more detail in Reference 1, pp. 2 and 3). The electron densities used in these models are based on the singly charged, far field current density approximation given in Reference 4.

Phase Shift

The following phase shift approximation is derived from eq. 4.2.3, Reference 5, p. 120:

$$\Delta\phi \ (n_e << n_c) = \frac{\pi \ell n_e}{\lambda n_c}$$

where:

$\Delta\phi$ = phase shift
ℓ = propagation path length in plasma
λ = free space wavelength
n_e = Avg. electron density of path
n_c = critical electron density

This equation was used to predict the RF phase shift, which is a phase advance because the plasma index of refraction is less than that of vacuum.

Transmission Loss

The following is used to predict the RF transmission loss due to beam spreading by a uniform, cylindrical plume as shown in Reference 5, p. 137.

$$T = \frac{D(L + 2R)}{4mR(L + R) + D(L + 2R)}$$

$$m = \left(1 - \frac{n_e}{n_c}\right)^{-\frac{1}{2}} - 1$$

T - Transmission
D - Plume diameter
L - Effective horn length
R - Distance from antenna to plume center

This equation is a rather crude approximation because the plume was not a uniform dielectric cylinder and an "equivalent" uniform cylinder diameter (D) was chosen.

Stratified Dielectric Reflection - Transmission

For a plasma plume diameter which is large compared to the RF carrier wavelength, the continuous dielectric variation of the plume may be modelled by a number of uniform slabs with various dielectric properties and thicknesses (Ref. 6). This model should yield satisfactory accuracy in predicting the reflection, absorption and phase shift of an RF carrier caused by the plume, if the plasma characteristics are known.

Experiment

The experimental goals are threefold: 1) supply data for verification of the analytical models, 2) supply tapes of RF carrier transmission through mercury ion plume for telecommunications link simulation, and 3) uncover possible unexpected plume/RF interactions. If the interactions behave in a predictable manner under a broad spectrum of plume/RF propagation conditions, the space performance may be extrapolated from the laboratory performance with greater confidence.

The scope of this study was limited to a frequency range of 2.0 to 2.5 GHz (S-band) because X-band/plume interaction effects should be too small, compared to the measurement accuracies, to give a good analytical model verification. For the sake of simplified modelling, the carrier propagation path crosses the plume perpendicular to its axis and two meters downstream from the thruster grid. The experimental set up is shown in Figure 2.

Environment

The ion thruster plume/RF interaction experiments were performed in a cylindrical stainless steel, vacuum tank approximately 4.6 m in length and 2.3 m in diameter as shown in Figure 2 (the same tank as used in the previous plume/S-band experiment, Reference 1). The ion thruster was at one end of the tank and aligned so that its plume was coaxial with the tank cylinder. At the other end of the tank, the plume impinges upon a frozen mercury collector. The walls of the chamber are cooled to approximately 80 K by liquid nitrogen. The vacuum pressure in the tank during thruster operation was on the order of 8×10^{-6} torr. In order to simulate "freespace" RF propagation conditions,the vacuum chamber was partially lined with microwave absorber to reduce the RF reflections from the tank walls.

Antennas

Two S-band, pyramidal horn antennas were used (as in Reference 1), having the following characteristics:

Frequency range	- 2.0 to 2.5 GHz
Approximate gain	- 16 dBi
Polarization	- linear
Window	- thin fiberglass

The mounting location was chosen so that the plasma axis would be in the far field of the antenna (see Figure 2). There was a parallel alignment of the antenna E-polarization and the plume axis for the first part of the measurements and perpendicular alignment for the last part of the measurements. The antennas were connected to the instrumentation through semi-rigid 141 coaxial cable.

C-3

Absorber

The type of microwave absorber (Rantec, EHP-5) was the same as that used in a previous ion thruster plume/RF interaction experiment. The absorber, since it was to be used in a vacuum chamber, was ordered without the usual fire retardant or other volatile treatments. Part of the cylindrical contour of the vacuum chamber was lined with this absorber as shown in Figure 2.

Instrumentation

The basic instrumentation used in this experiment consisted of S-band sources, network analyzer, spectrum analyzer, scope camera and an analog instrument tape recorder. The equipment list is given in Appendix A.

Thruster

The thruster is a 30-cm mercury electron bombardment ion thruster. Liquid mercury is vaporized, ionized and then accelerated by an electric field. A neutralizer is used to inject a sufficient number of electrons into the plume of accelerated ions to obtain a neutral plasma. The particle density of the plume, using the far field model of Reference 4, is directly proportional to the beam current (I_B). A more detailed description of the thruster and a diagram can be found in Reference 1.

Test Procedure

These tests are meant to show the amplitude and phase changes, caused by a mercury ion thruster plume, on the S-band telecommunication carrier. The general and instrumentation test setups are shown in figures 2 and 3, respectively.

In a typical (idealized) test procedure, data were recorded with the antenna polarization and RF carrier power fixed, the carrier frequency swept from 2.1 to 2.3 GHz and the beam current stepped from zero to two amperes with the mercury ion collector positioned horizontal and vertical during each current step. During these tests the data, including carrier amplitude and phase variations and thruster parameters, were recorded manually, on magnetic tapes and on photographs. The plume current range between zero and 0.7 amperes was not divided up into steps because of the operational limits of the thruster.

Results

Analytical Model - Phase Shift

In the configuration used in this interaction experiments, the RF propagation path passes approximately through the plume axis and is approximately straight. The above conditions, along with the plasma

characteristics of this thruster, are conducive to good agreement between this phase shift model,described earlier, and experimental data if the electron density is well known. This model, along with stratified dielectric transmission-reflection model, gave nearly identical results for a thruster beam current of two amperes, 19.9° for the phase shift model and 20.0° for the other model. The results of the phase shift model are plotted in Figure 4.

Amplitude

The stratified dielectric transmission-reflection model indicated negligible reflection and absorption loss to the RF carrier in this experimental configuration. The transmission loss is attributed to RF beam spreading caused by the divergent lens quality of the cylindrical plasma. The results of this beam spreading transmission model, described earlier, are plotted in Figure 5. This rough approximation gives a loss of 0.31 dB for a beam diameter of 0.35 m and an equivalent electron density of 1.8×10^{15} e/m^3 at a beam current of two amperes.

Experimental

Spectrum:

The RF power level vs frequency was measured with a spectrum analyzer for a fixed frequency (2.2 GHz) carrier propagating through an ion thruster plume at various beam currents. No carrier frequency shift was observed under the above conditions. The only significant effect observed, so far, is a pair of spectral peaks, each approximately 40 dB below and 6.6 kHz on either side of the RF carrier as shown in Figure 6. Ths anomaly, seemingly, appeared only when the thruster was operating in an unstable mode. Possibly, analysis of the instrument tape recording of thruster parameters (beam current and screen voltage) could indicate the source of this noise.

Fast Fourier Transformer (FFT) routine was used on the analog tape recordings of the translated RF carrier. The FFT analysis was performed in a similar manner as that described in Reference 1. Samples of the FFT analysis are shown in Figures 7 and 8.

Amplitude and Phase:

The amplitude and phase shift data were collected on an RF carrier in the frequency range of 2.1 to 2.3 GHz, transmitted through an ion plume at various beam currents. A network analyzer was used to measure these transmission characteristics, see Figure 3. Sample phase shift and amplitude vs beam current graphs are shown in Figures 4, 5 and 9 to 13. Tables 1 through 4 show data accumulated from magnetic tapes, photographs and manual records. The maximum amplitude attenuations recorded on these tables are 0.3 dB for the mercury collector in the horizontal position and 0.38 dB in the vertical position. The maximum

phase shifts recorded on these tables are 33.5 degrees for the collector in the horizontal position and 66.6 degrees in the vertical position. The measured attenuation and phase shift, in general, increases with beam current. There seems to be no major difference between the $E_{||}$ and $E_{\perp}$ antenna polarization test results.

The slopes of the measured amplitude and phase shift graphs are, in general, greater than anticipated by the preliminary analytical models. Comparing the phase shift measurements with the analytical model results, there is both, a higher measured slope and magnitude, at the larger beam currents, than predicted. A probable reason for this discrepancy is the electron density model used which excluded facility caused electrons. These facility electrons are, probably, from neutral mercury atoms dislodged from the mercury collector and chamber walls which are then ionized by the plume ions. The resulting electron density increases nonlinearly with an increase in the beam current, as indicated by the phase shift shown in Figure 4. The measured effects, attenuation and phase advance, are less when the mercury collector is rotated from the vertical to the horizontal position, probably because fewer mercury atoms are dislodged from the chamber walls than from the exposed mercury target (collector vertical). At the lower operating range of beam currents, the model predicts more phase shift than measured, this is possibily because the electron density model did not include ion beam divergence characteristics of the thruster at low beam currents, see Reference 7.

Conclusions

The experimental goals were to supply data for the verification of the ion plume/RF carrier interaction models, supply magnetic tapes of an RF carrier transmitted through a mercury ion plume for telecommunications link simulation, and uncover possible unexpected plume/RF interactions. These goals, to some degree, have been fulfilled. Data has been collected for a range of plume/RF conditions and a simulation tape has been recorded. The experimental results were not as predicted by rather approximate, analytical models. The use of a "freespace" model to predict the electron density seems to have been the main problem. Modifications to this electron density model should include divergence at various ion beam currents and facility electrons. A first look at these modifications seem to explain major discrepancies between the predicted and the experimental results. Further work is required to show quantitative agreement between these results.

In general, the measured amplitude loss and phase advance increased monotonically with increasing ion beam current as expected. No significant additional noise was observed on the RF carrier at various beam current levels when the thruster was stable. No carrier frequency offset, due to the plasma media, was observed. Therefore, if improvements in analytical modelling of the electron density and RF beam spreading demonstrate a high degree of correlation between the measured and analytical results, the analysis may be extended to flight geometries with a degree of confidence.

At this point in the analysis of the FY '79 data, the following conclusions are offered:

(1) Low signal attenuation from RF absorption and beam spreading.

(2) Large phase shifts vs beam current are possible. The effect of this phase shift is only significant during fast beam current transitions.

(3) Reflection loss is negligible.

(4) Spectrum noise is only apparent during thruster instability.

(5) No conclusion on low angle RF blockage by the plume.

The future work needed for an adequate understanding of the propagation problem should include improving the electron density and RF/plume interaction models. These model improvements include: multiple thruster effects, wider RF frequency range and variable propagation path/plume angle (including the critical angle). Further experimentation should be guided by a thorough analysis of the test chamber and space situations.

Acknowledgement

The author is grateful to Jeff Packard for his valuable contribution to the execution of this experiment.

References

1. Ackerknecht, W.F. and Stanton, P.H., "The Effects of an Ion-Thruster Exhaust Plume on S-band Carrier Transmission", JPL TM33-754, January 1, 1976.

2. Cohn, G.I., "Preliminary Examination of Problems in Communication with an Ion-Rocket Driven Interplanetary Spacecraft by Means of 2.1 to 2.3 GHz Radio Signals", JPL, October 1966.

3. Sellen, J.M., Jr., "Plane Wave Refraction at the Boundary of a Plasma Thrust Beam", 9884-64-1, TRW, August 1969 (?).

4. Cuffel, R., "Mathematical Model of the Current Density for the 30 cm Engineering Model Thruster", AIAA #75-431, 11th Electrical Propulsion Conf., New Orleans, LA., March 1975.

5. Heald, M.A. and Wharton, C.B., Plasma Diagnostics with Microwaves, J. Wiley & Sons, Inc., N.Y. 1965.

6. Bellman, R. and Kalaba, R., "Invariant Imbedding & Wave Propagation in Stochastic Media", M. Desirant & J. Michiels, Electromagnetic Wave Propagation, pp. 243-252, Academic Press, London, New York, 1960.

7. Aston, G., Kaufman, H.R. and Wilbur, P.J., "Ion Beam Divergence Characteristics of Two-Grid Accelerator Systems", AIAA Jrnl. Vol. 16, No. 5, pp. 516-524, May 1978.

AMPLITUDE (dB)

FREQ. 2.1 to 2.3 GHz

COLLECTOR VERTICAL (V) HORIZONTAL (H)

Beam Current	7-11-79	8-22-79		9-18-79		9-19-79	
	V	V	H	V	H	V	H
.7							
.8	-.1						
.9							
1.0	-.1	-.1	0	-.05	-.05	-.1	-.05
1.2	-.18	-.15	-.05	-.15	-.1	-.2	-.13
1.4	-.2	-.2	-.1	-.2	-.1	-.23	-.2
1.6	-.2	-.25	-.1	-.25	-.15	-.3	-.3
1.8	-.25	-.3	-.15				
2.0							
1.8	-.35						
1.6	-.2	-.2	-.15			-.3	-.2
1.4	-.1	-.2	-.1			-.25	-.2
1.2	-.1	-.15	-.05			-.2	-.1
1.0	-.05	-.07	0	-.07	0	-.1	-.05
.9				-.03	0	-.05	-.05
.8	-.0			0	0	0	-.02
.7				0	0	0	+.05
0							

TABLE 1 DATA COLLATED FROM PHOTOGRAPHS

AMPLITUDE (dB)

FREQUENCY 2.1 to 2.3 GHz
COLLECTOR VERTICAL (V), HORIZONTAL (H)

BEAM CURRENT	9-10		9-18	
	V	H	V	H
0	0	0	0	-
.7				
.8				
.9				
1.0	-.27	-.21	-.05	-.03
1.2				
1.4				
1.6			-.25	-.13
1.8				
2.0	-.38	-.22		

(I_B=2.0→ 2.4A
INDICATE ON 9-10)

TABLE 2 DATA COLLATED FROM MAGNETIC TAPES

PHASE (DEGREES)

FREQUENCY 2.1 to 2.3 GHz

COLLECTOR VERTICAL (V), HORIZONTAL (H)

BEAM CURRENT	7-11-79	8-22-79		9-18-79		9-19-79	
	V (see Note)	V	H	V	H	V	H
.8	0						
1.0	4	16	10	18	9	19	11
1.2	10	20	16	28	11	28	15
1.4	18	30	20	42	16	36	19
1.6	27	36	24	52	21	48	25
1.8	48	46	30				
1.6	28	38	20			45	25
1.4	19	32	16			36	18
1.2	10	22	8			26	14
1.0	6	18	8	18	9	17	10
.9				14	6	14	9
.8	4			11	4	11	7
.7				9	2	9	4

NOTE: I_B=.8A USED AS REFERENCE RATHER THAN I_B=0A AS IN THE OTHER CASES

TABLE 3 DATA COLLATED FROM PHOTOGRAPHS

PHASE (DEGREES)

FREQUENCY = 2.195 GHz
COLLECTOR VERTICAL (V), HORIZONTAL (H)

BEAM CURRENT	8-7-79	8-27-79		9-4-79	
	V	V	H	V	H
.7		9.0	5.6	10.2	6.4
.8		11.8	7.1	12.8	8.0
.9		14.1	8.6	16.3	10.0
1.0	10.6	18.0	10.2	19.1	11.7
1.2	15.0	21.2	11.9	26.2	15.4
1.4	20.0	34.0	17.4	34.5	19.5
1.6	26.6	41.3	20.6	45.4	24.2
1.8	33.6	50.5	25.0	55.5	28.5
2.0				66.6	33.5
1.8				53.8	26.6
1.6	26.8			42.3	21.4
1.4	21.0	24.3	12.4	32.3	17.1
1.2	16.3	18.0	9.7	24.2	13.3
1.0	11.6	13.6	7.9	17.4	10.0
.9		11.6	7.0	15.0	8.9
.8		10.0	6.1	12.5	7.7
.7		8.5	5.3	10.4	6.6
0		1.6	.8	1.1	

TABLE 4 DATA COLLATED FROM MANUAL RECORDS

APPENDIX A

EQUIPMENT LIST

(1) SWEEEP OSCILLATOR/RF PLUG IN	HP 8690B/8699B
(2) SIGNAL GENERATOR	HP 8616A
(3) SPECTRUM ANALYZER/PLUG INS.	HP 141T /8555A/8552B 8553B/8445B
(4) LOW FREQUENCY SPECTRUM ANALYZER	HP 3580A
(5) NETWORK ANALYZER/PLUG INS	HP 8410A/8411A/8413A 8412A/8414A/8418A/8743A
(6) RF POWER METER	HP 435A
(7) FREQ. STANDARD	GR 1115B
(8) MICROWAVE OSCILLATOR SYNCHRONIZER	MICRO W. SYS. DFS
(9) INSTRUMENT TAPE RECORDER	AMPEX RF 1900
(10) CAMERA SCOPE	HP 197A
(11) TIME CODE GENERATOR AND READER	SYS. DON. 8120/8181
(12) S-BAND HORN ANTENNA(2) AND MOUNTS	-
(13) MICROWAVE ABSORBER	RANTEC EHP-5
(14) MISCELLANEOUS CABLES, COUPLERS, AMPLIFIERS AND CONNECTORS FOR INTERCONNECTING INSTRUMENTS	

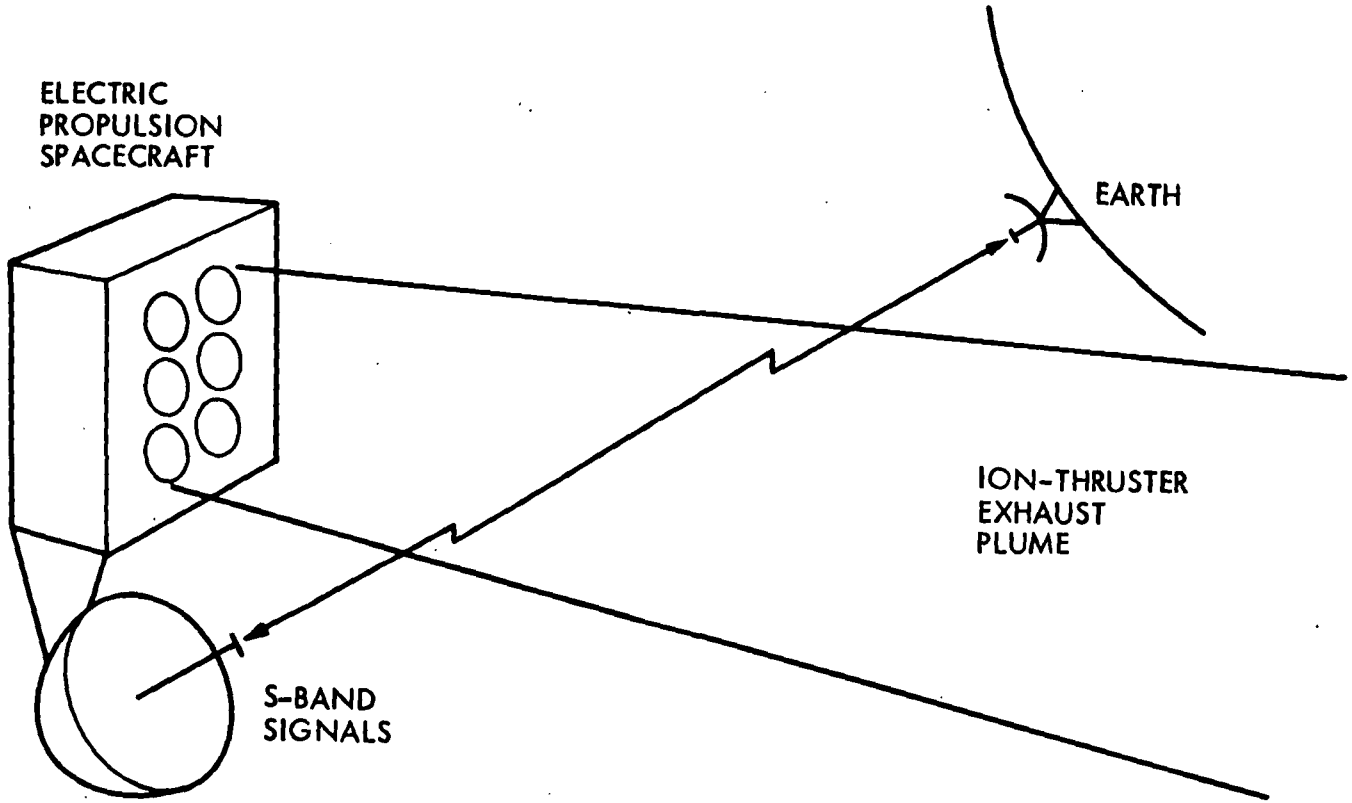

Figure 1. The Question. What are Effects on Communications Link When Transmitting Through Plasma Beam?

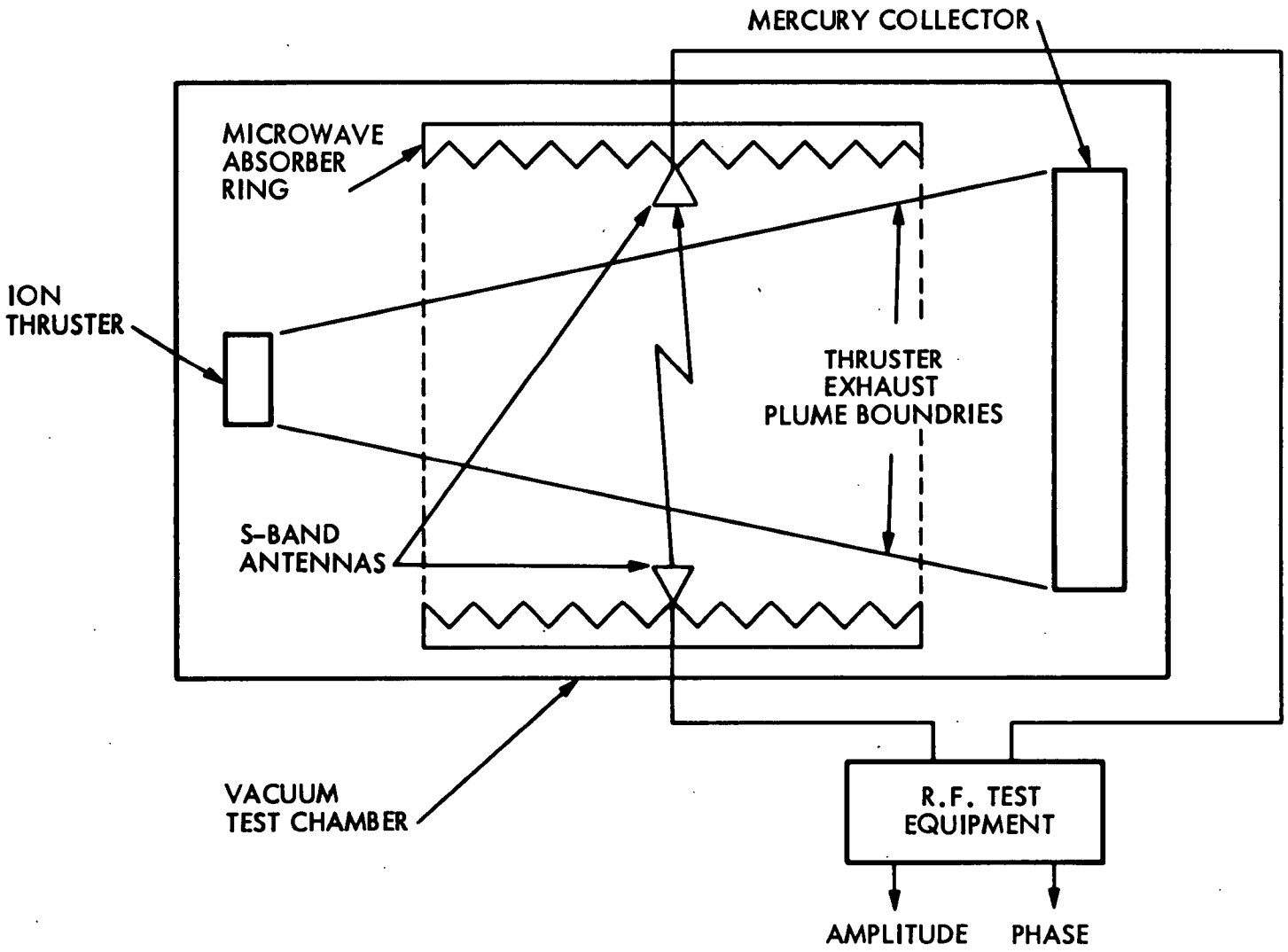

Figure 2. Illustration of Experimental Arrangement in 7' X 15' Vacuum Chamber

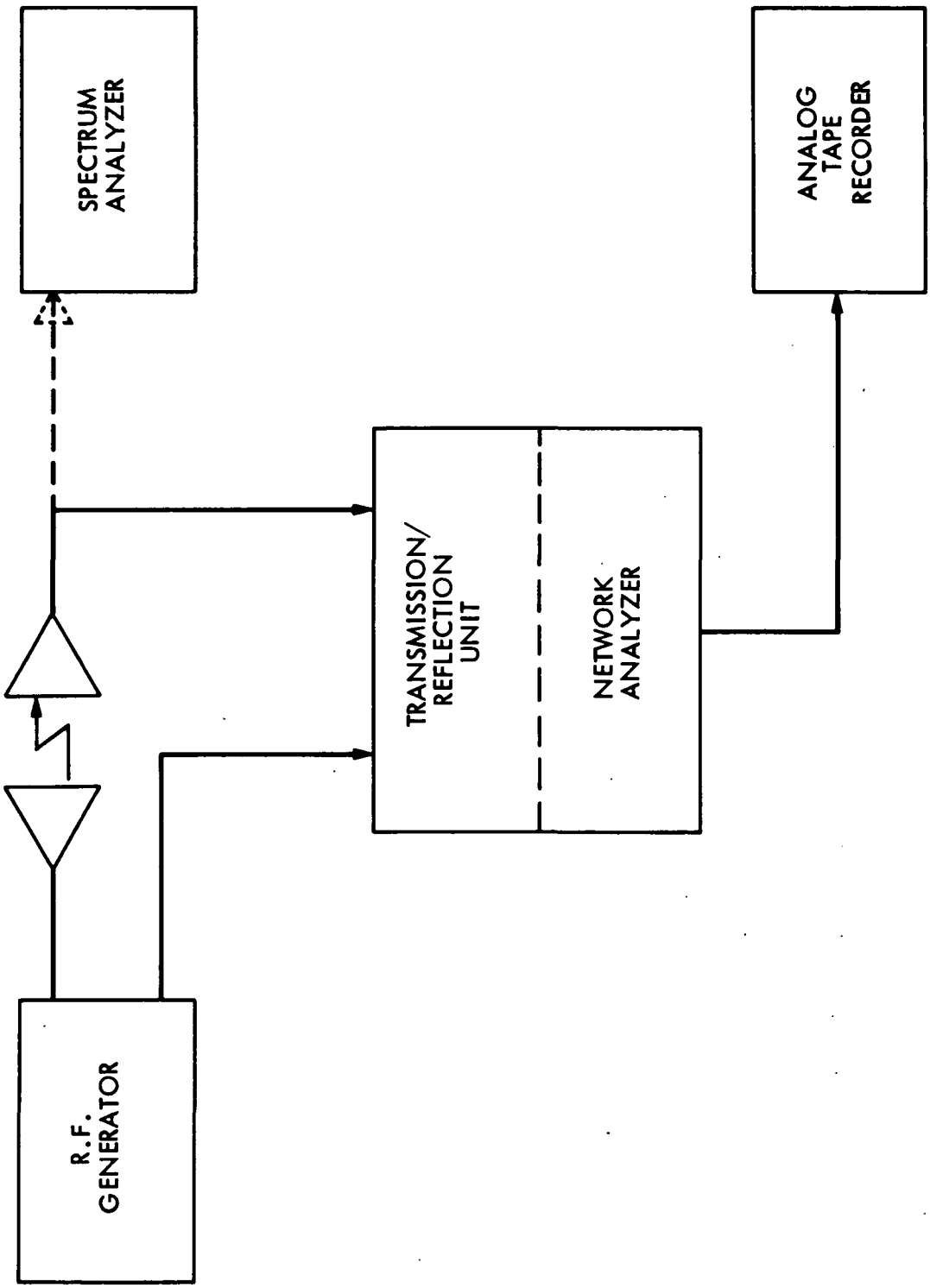

Figure 3. Block Diagram of Experiment

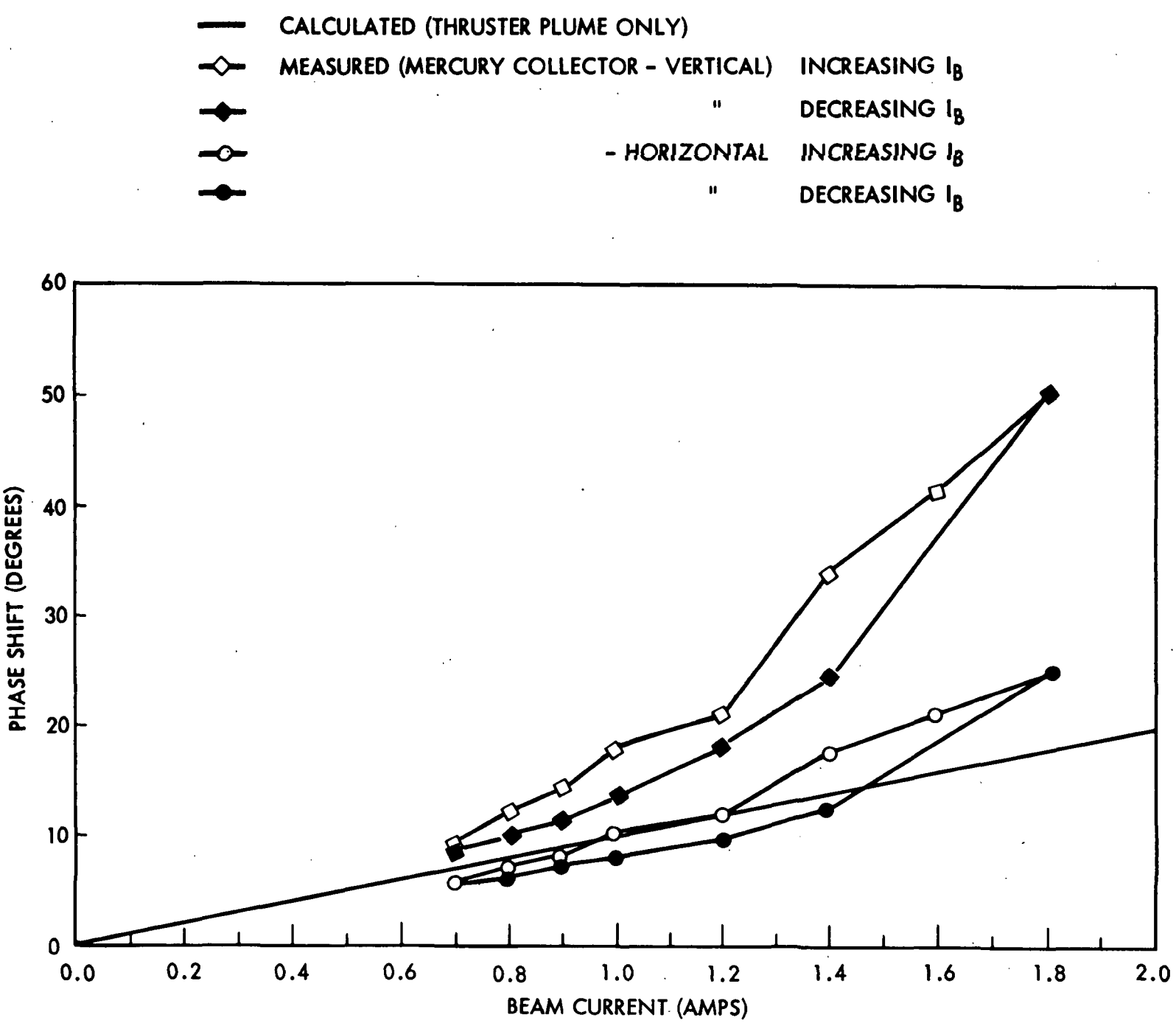

Figure 4. Experimentally Measured Phase Shift

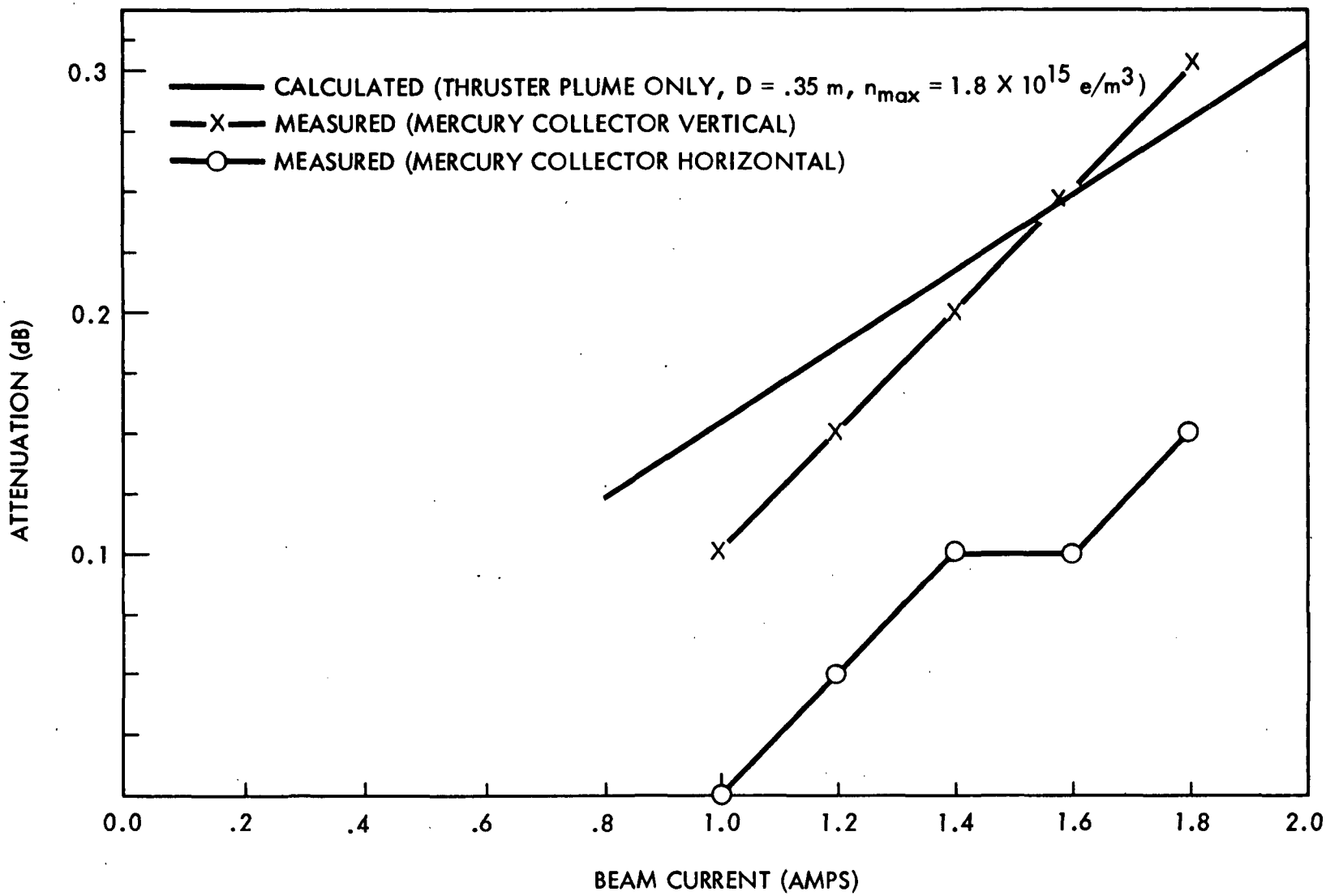

Figure 5. Experimentally Measured Attenuation

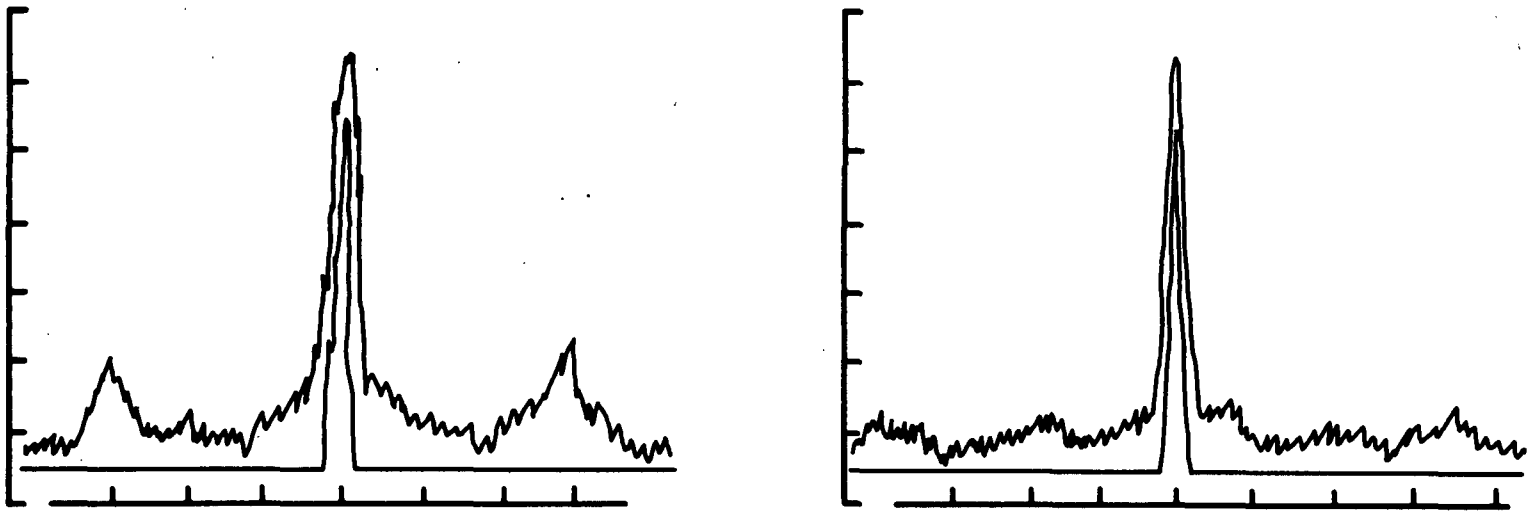

Figure 6. Carrier Frequency Spectrum as a Function of Thruster Operation

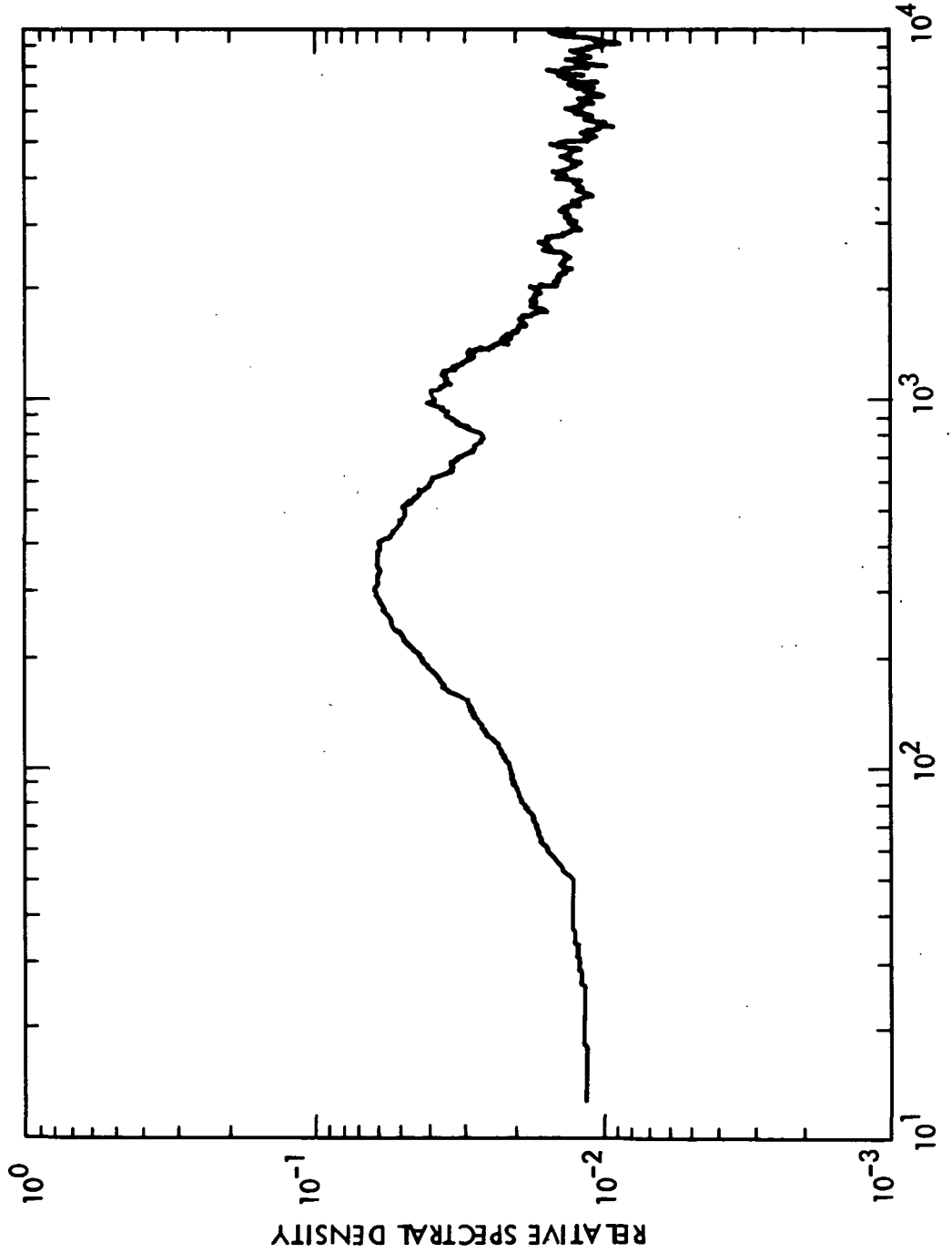

Figure 7. Illustration of Fast Fourier Transformer Analysis of RF Carrier

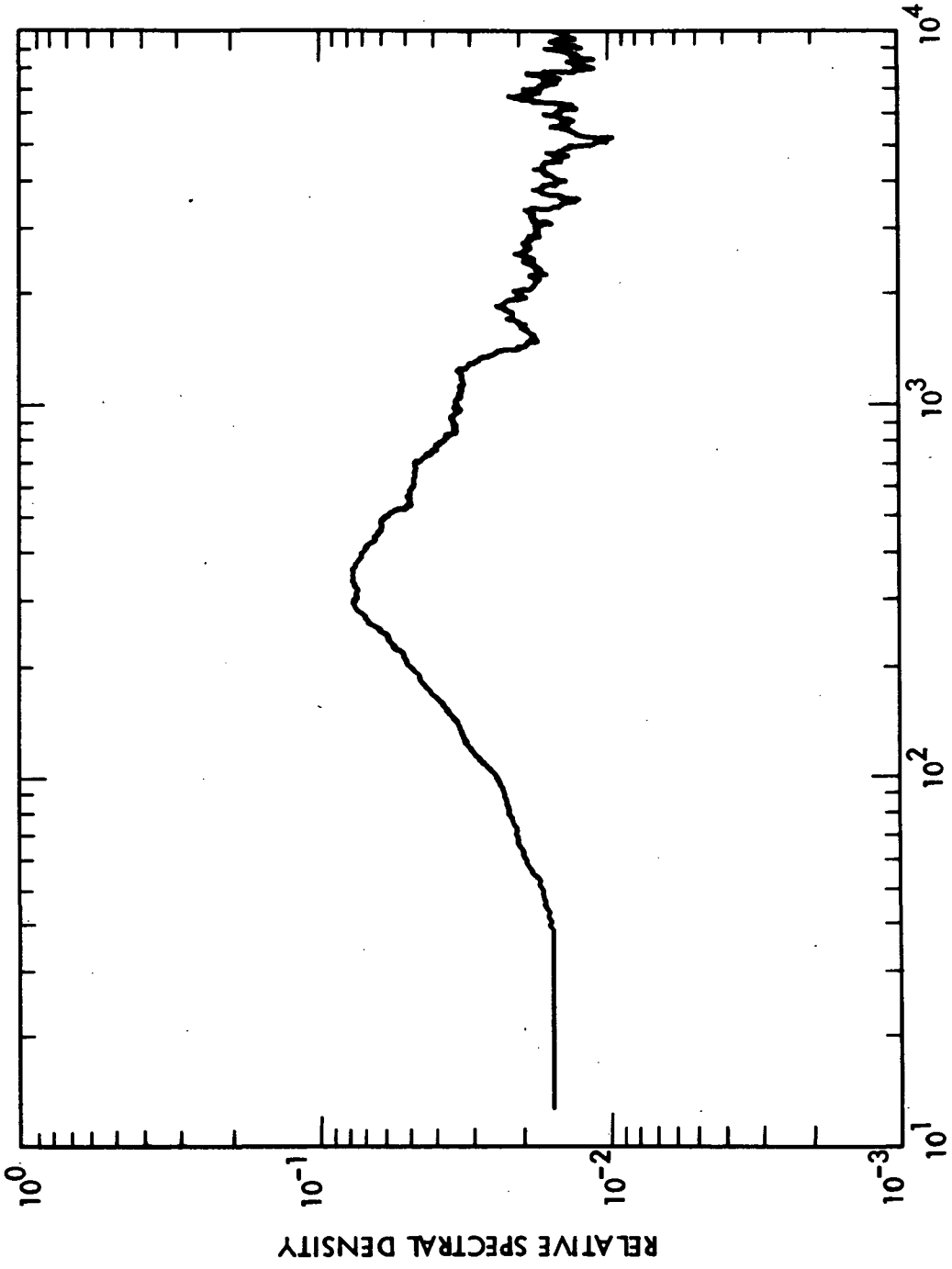

Figure 8. Illustration of Fast Fourier Transformer Analysis of RF Carrier

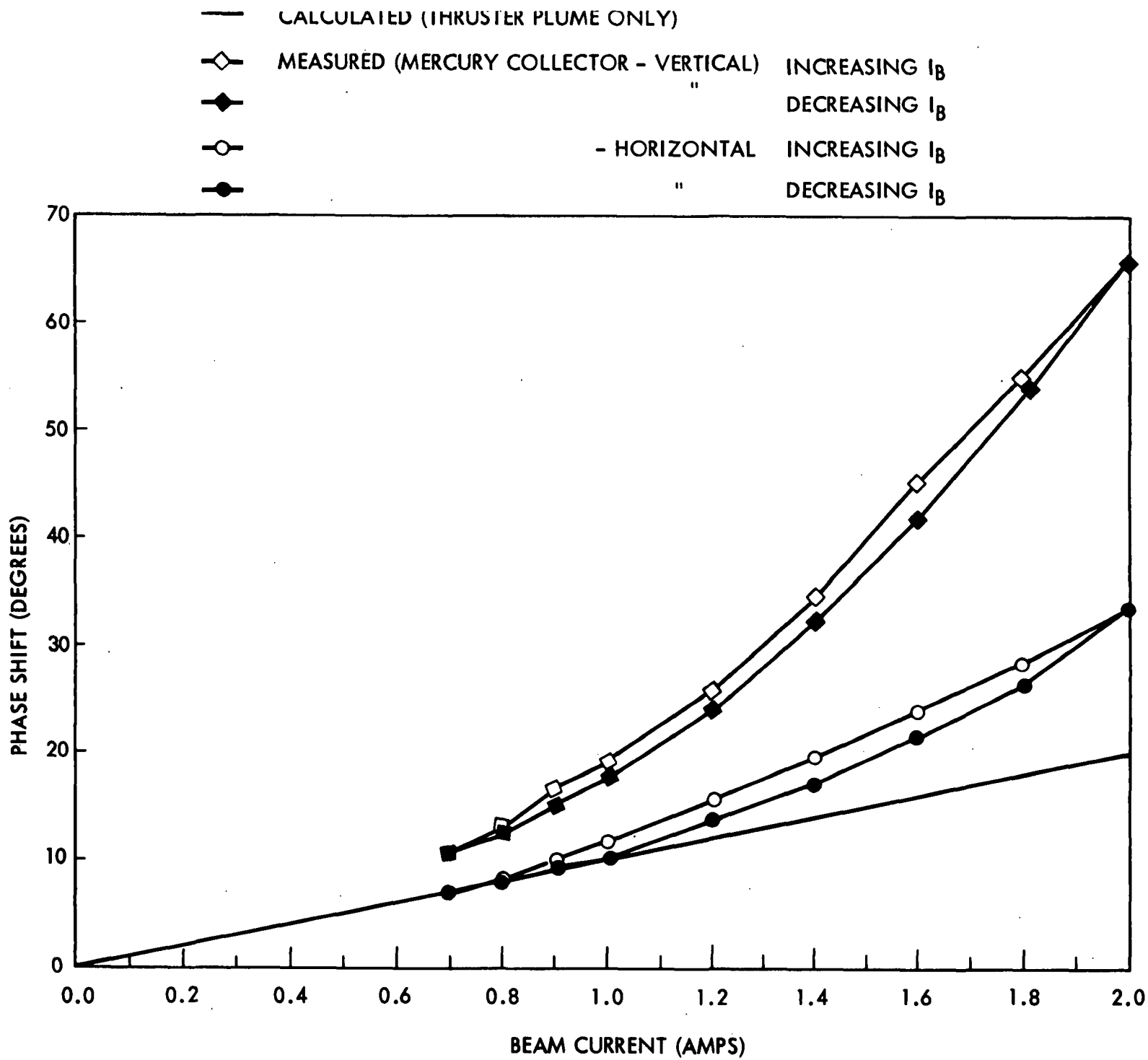

Figure 9. Experimentally Measured Phase Shift

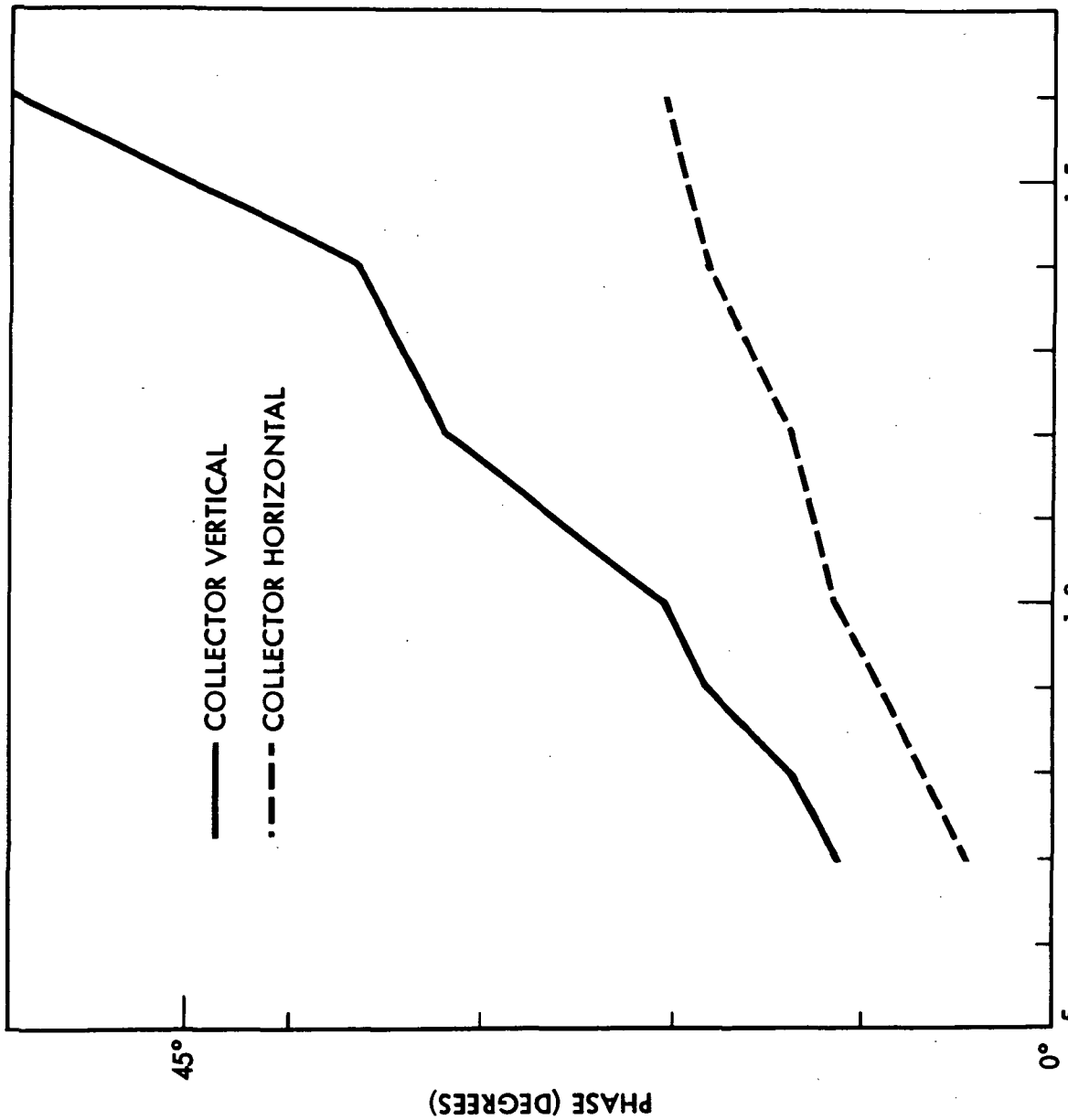

Figure 10. Experimentally Measured Phase Shift

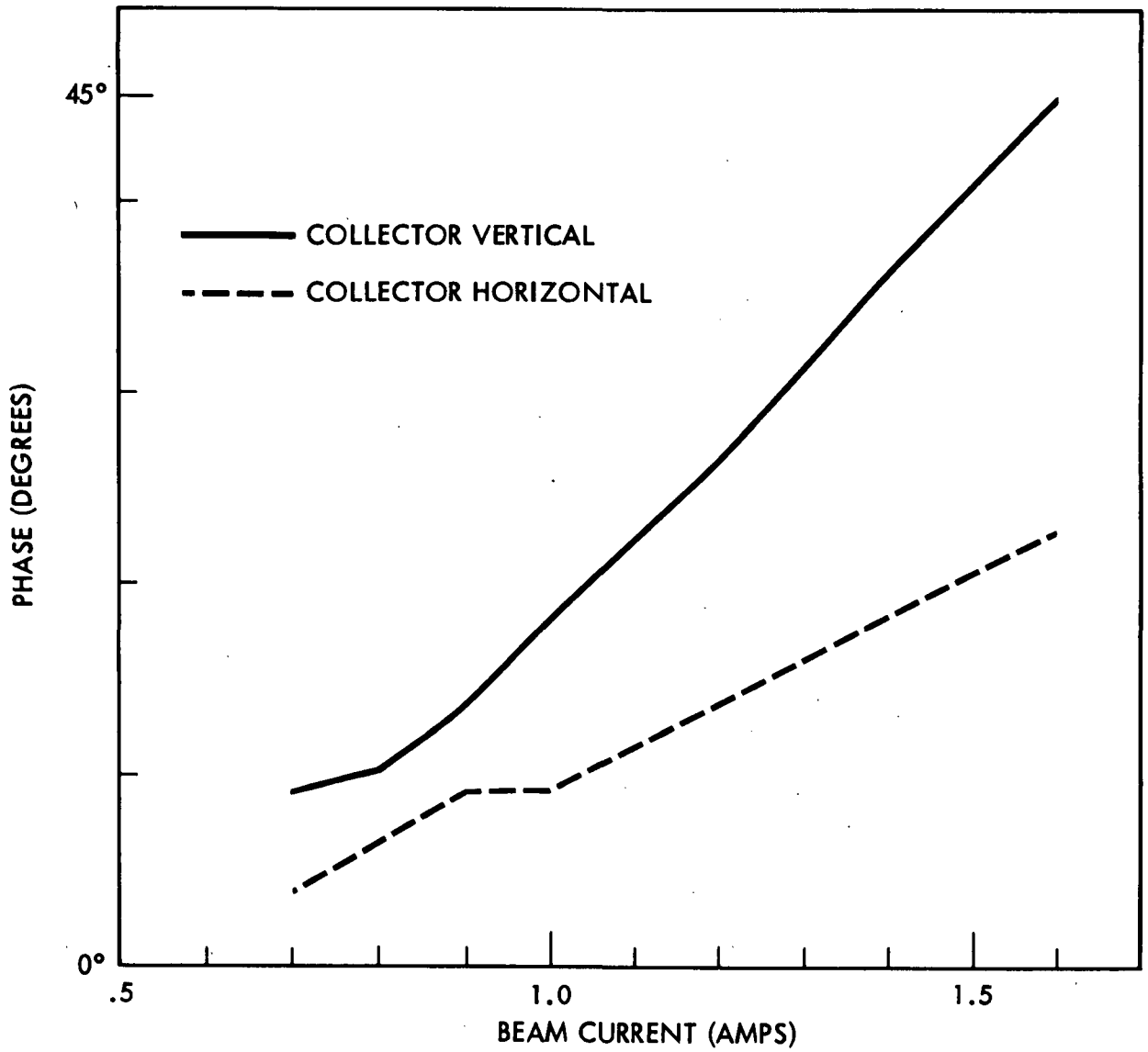

Figure 11. Experimentally Measured Phase Shift

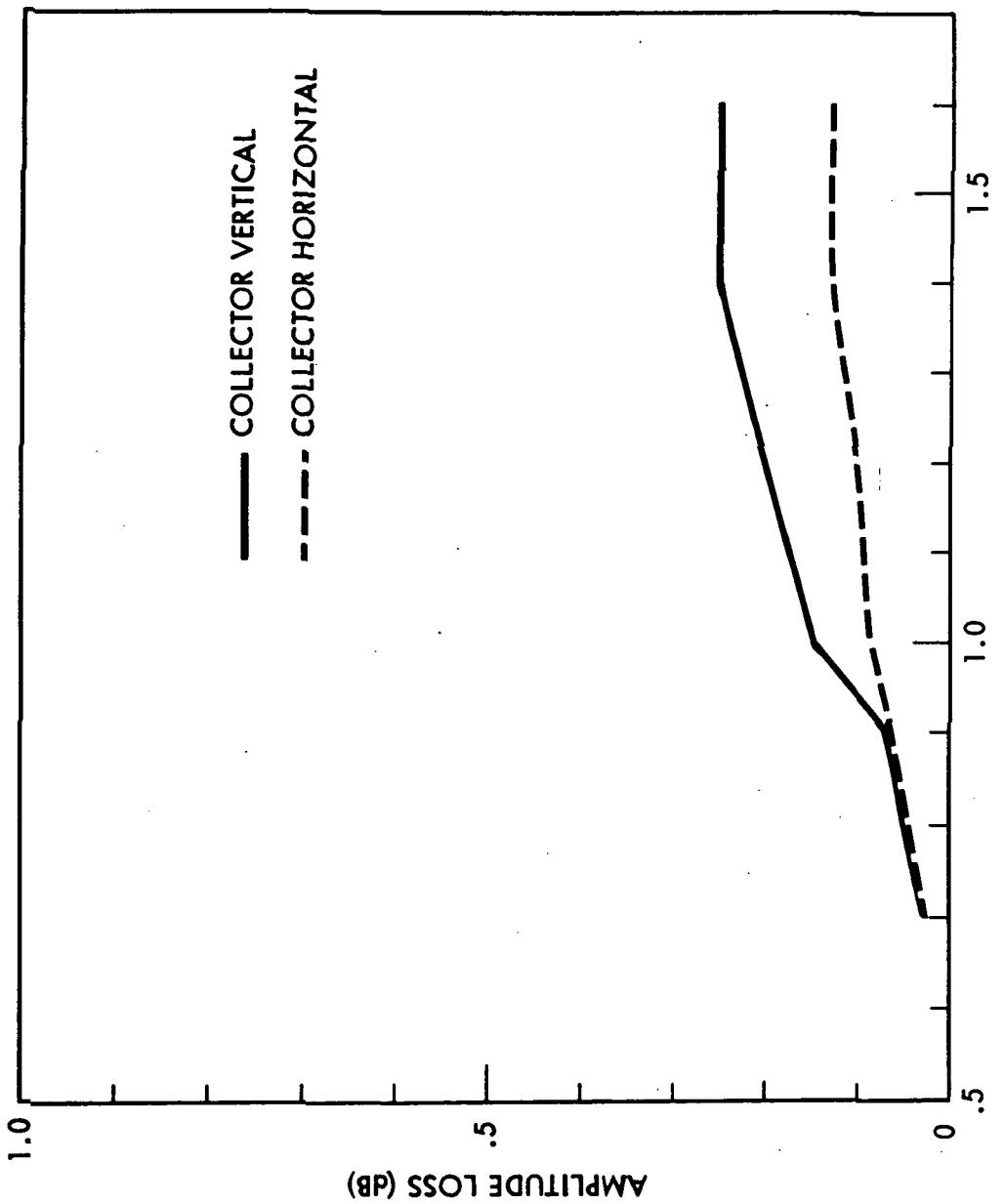

Figure 12. Experimentally Measured Amplitude Loss

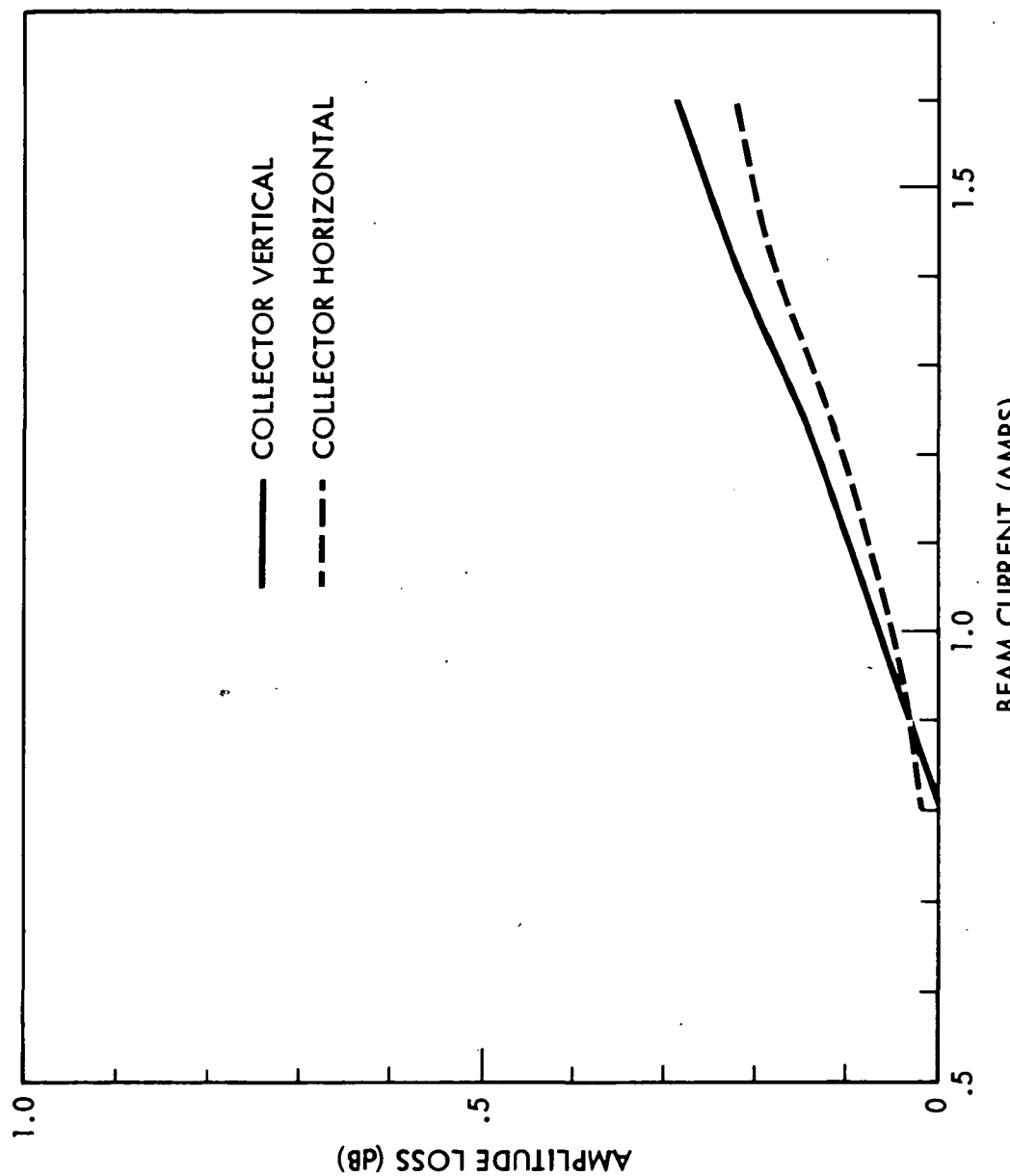

Figure 13. Experimentally Measured Amplitude Loss

Spacecraft Interactions

INTRODUCTION

There are two papers in this section that deal with interactions between the ion thruster produced environment and spacecraft. The first paper looks at interactions of the environment (plasmas, neutral particles, optical emissions, and EMI) with spacecraft science instruments. The paper is slanted toward the spacecraft design which had been proposed for a Halley Flyby/Tempel II Comet Rendezvous mission. The second paper deals primarily with the effects of mercury charge-exchange plasma exposure to spacecraft components and materials. Some of the results of the second paper are surprising in that low energy bombardment of some surfaces produce noticeable changes in the reflectance properties of the surface. A very limited amount of data is given in this paper and the results point to a clear need to understand the details of low energy mercury ion interaction with surfaces and mercury deposition or amalgamation under expected flight conditions.

INTERACTIONS BETWEEN A SPACECRAFT AND AN ION THRUSTER PRODUCED ENVIRONMENT*

M. R. Carruth, Jr. and E. V. Pawlik†
Jet Propulsion Laboratory
California Institute of Technology
Pasadena, California

Abstract

The electron bombardment ion thruster is a candidate propulsion device for several proposed interplanetary missions. A comet rendezvous mission is expected to be the first use of a Solar Electric Propulsion System (SEPS), and such a mission is presently in pre-project activities at JPL. Because this is the first use of such a system, it is necessary to understand the interactions between the spacecraft and the environment produced by the SEPS. A preliminary assessment of the interactions between a thruster produced environment and the Comet Rendezvous spacecraft, including its science instruments, is presented which concludes that compatibility between the SEPS and the spacecraft can be obtained.

Introduction

The mercury, electron bombardment ion thruster has been under development for a number of years. It is expected to be used for attitude control, earth orbit transfer and as primary propulsion for interplanetary spacecraft. There are specific interplanetary space missions which are strong candidates for electric propulsion. Three which are presently under consideration at JPL include the Comet Rendezvous (CR), the Saturn Orbiter with Dual Probe (SO2P), and the Asteroid Multiple Rendezvous (AMR).

The Comet Rendezvous Mission is expected to be the first use of a Solar Electric Propulsion (SEP) System as a primary propulsion device. A mission to execute a fast flyby of Halley's Comet and later rendezvous with the Comet, Tempel 2, is presently a pre-project activity at JPL. The present configuration of the Comet Rendezvous S/C is shown in Figure 1. The mission will begin with a launch in early August 1985.[1] About four months later the spacecraft will execute a fast flyby of Halley's Comet, releasing a probe to send back data from within the comet. The spacecraft will pass at a distance which will be considered safe with regard to dust or other contamination from Halley's Comet. The spacecraft will continue on, using the ion thrusters to accelerate and to change its orbital inclination so that the spacecraft and the comet, Tempel 2, will be in the same orbit when they rendezvous in 1988. The spacecraft's instruments will closely study Tempel 2 for approximately a year after the rendezvous.

*The research described in this paper was carried out at the Jet Propulsion Laboratory, California Institute of Technology under NASA contract NAS7-100.

†Group Supervisor, Electrical Power and Propulsion Section, member AIAA

The SEP stage which will propel the spacecraft consists basically of a large solar array to gather power from the sun, the ion thrusters which produce the thrust and the power processing units (PPU) which converts the power from the solar array to that necessary for operating the ion thrusters. There are many things that are unique about the SEP stage and require a close evaluation to determine how it might affect the spacecraft operation, particularly the operation of the science instrument payload.

The solar array is capable of producing 25 kW of power and therefore requires special attention for electromagnetic compatibility (EMC) with the spacecraft. The ion thrusters have permanent and varying magnetic fields associated with them as well as radiated electric fields.[2,3] An assessment of the EMC of an electric propulsion system with a typical interplanetary spacecraft has been recently reported.[3] Another unique aspect of ion thrusters is the plasmas they produce. Various groups of ions are emitted by an ion thruster.[4] The group that will be considered in this paper is the charge-exchange ions, typically referred to as group IV ions, which have a directed energy of less than 10 eV.[5] They will form a charge-exchange plasma that will fill all space around the spacecraft.[6] A possible concern for some science instruments is the interference which might be caused by the optical radiations from the ion thrusters.

How the environment produced by the ion thrusters will affect the spacecraft and the science instruments will be addressed in this paper. Emphasis is placed on the charge-exchange plasma interaction with the science instruments.

Charge-Exchange Plasma

The Plasma Flow Model

Approximately ten percent of the mercury flow into the thruster discharge chamber leaves through the ion optics without being ionized. These neutrals leave the thruster in approximately a cosine distribution.[7] Charge-exchange between the high energy ions of the beam and the neutrals produces low energy charge-exchange ions. These ions flow radially from the beam and distribute themselves so as to form a plasma that occupies all space around a spacecraft.[6,8]

A model of the charge-exchange plasma flow around a spacecraft is used to assess the interactions between it and the spacecraft.[6,8] The model assumes an effective point of origin of the charge-exchange plasma as being one thruster radius, r_b, downstream of the thruster. One thruster array radius downstream is assumed for the case of multiple thruster operation. The electron density, n_e, and electron current density, j_e, can be found for a point by determining the radius, R,

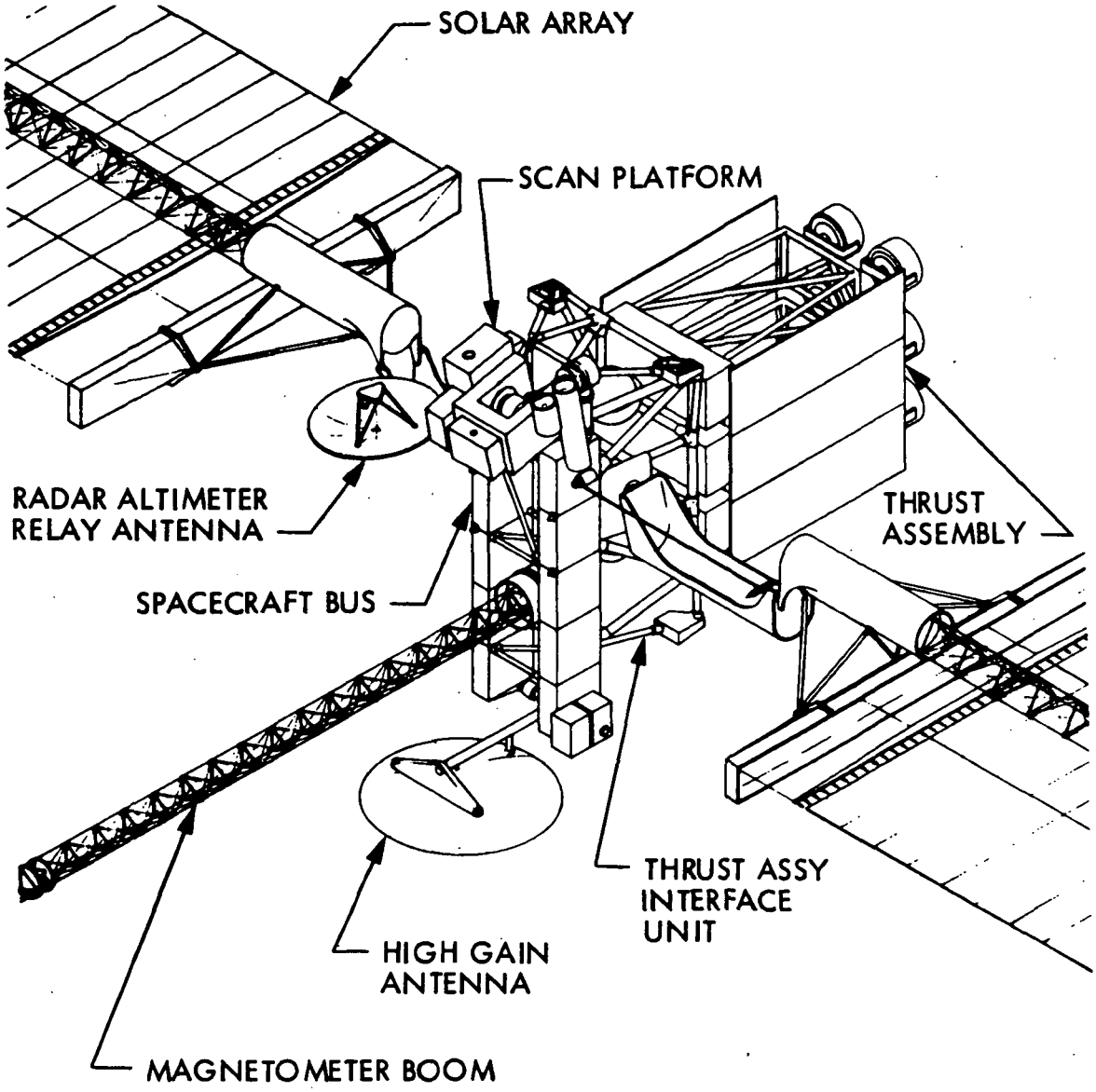

Figure 1. Comet Rendezvous Spacecraft (Without Halley Probe).

and the angle, θ, as illustrated in Figure 2. These values as well as the values in Figure 3 and Figure 4 are used in the following equations to find n_e, and j_e;

$$n_e = [J_b^2 (1 - \eta_\mu)/r_b R^2 \eta_\mu]$$

[Figure 3 parameter], m^{-3} (1)

$$j_e = [J_b^2 (1 - \eta_\mu)/r_b R^2 \eta_\mu]$$

[Figure 4 parameter], $Amp \cdot m^{-2}$ (2)

where J_b is the total beam current of the thrusters and η_μ is the propellant utilization, ~0.9. For a surface normal to the local ion velocity, the ratio of ion current to electron saturation current is,[6]

$$j_i/j_e = \sqrt{2 \pi m_e/m_i}, \quad (3)$$

where m_e and m_i are the electron and ion mass, respectively. From equation (3) the arrival rate of mercury ions at a surface is,

$$\dot{N}/A = 3.7 \times 10^{16} j_e, \ N \cdot m^{-2} \cdot sec^{-1}, \quad (4)$$

where N/A is the number of atoms arriving per unit area per unit time. Because the charge-exchange plasma possesses a highly directed motion, the arrival rate of mercury ions at a surface is dependent on the position of that surface relative to the flow. Also, surfaces that are recessed or adjacent to a corner or obstruction will receive an arrival rate lower than that predicted by equation (4). The arrival rates vary as a function of the number and

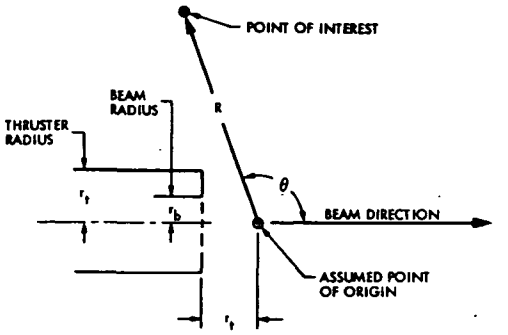

Figure 2. Coordinate System for Charge-Exchange Plasma Model.

beam currents of the operating thrusters. Arrival rates, calculated from equation (4), are shown in Figure 5 which illustrates how the arrival rates vary along a spacecraft when six thrusters are operating.

The charge-exchange ions that are produced near the thruster optics are drawn into the accelerator grid since it is at a negative potential of several hundred volts. These ions then sputter molybdenum from the accelerator grid.[9] A small fraction of these will be ionized by charge-exchange with thruster beam ions. Therefore, a small amount of the charge-exchange plasma which will envelop the spacecraft is composed of molybdenum ions. Even though this amount may be small it warrants consideration because of the long mission time involved

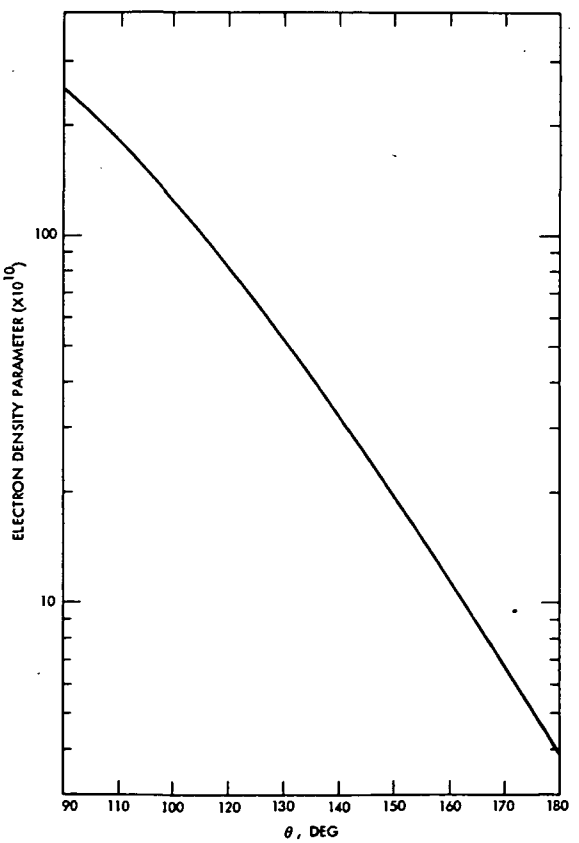

Figure 3. Electron Density Parameter.

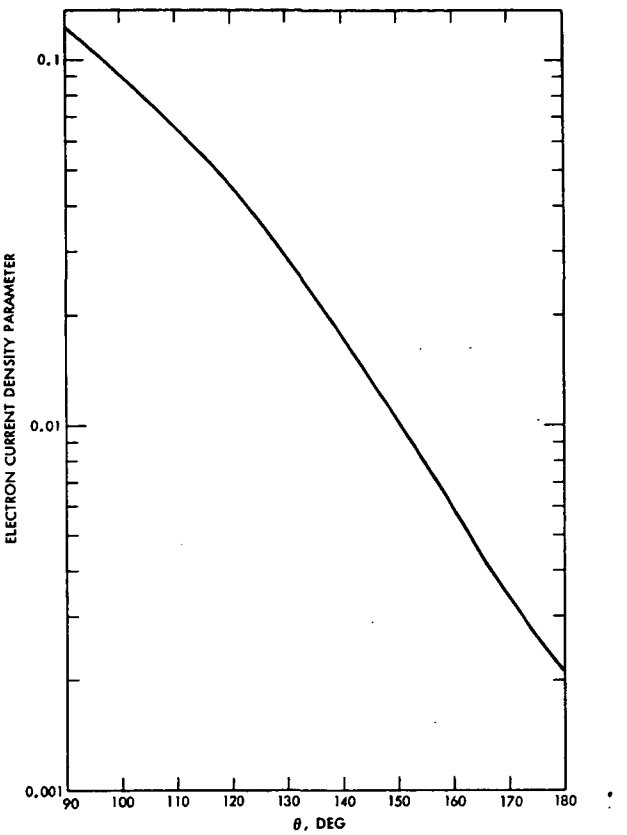

Figure 4. Electron Current Density Parameter.

and the fact that, unlike mercury, molybdenum will not vaporize from a surface. With no allowance for the initial downstream velocity of the sputtered molybdenum, the molybdenum arrival rate at a surface is given by,[6]

$$\dot{N}_{mo}/A = 4.4 \times 10^{12} j_e, \; N_{mo} \cdot m^{-2} \cdot sec^{-1} \qquad (5)$$

The model just described is based on charge-exchange ion production and experimental data obtained from operation of a single ion thruster. The uncertainties involved in using this model with a complicated spacecraft geometry is large; approximately a factor of 8-10.

Deposition on Spacecraft Surfaces

One of the concerns regarding the effect the charge-exchange plasma will have on a spacecraft is the possibility of plasma particle deposition. Deposition of mercury and molybdenum on thermal and optical surfaces will change the surface properties which can be detrimental to spacecraft instrument operation. It has been observed that there is no chemical interaction for conditions where no net deposition of neutral mercury vapor occurs.[9] The spacecraft will be 10-20 volts negative of ambient plasma when the thrusters are on.[10] Therefore, the plasma ions will impact spacecraft surfaces with energies of several eV and some interaction may occur.

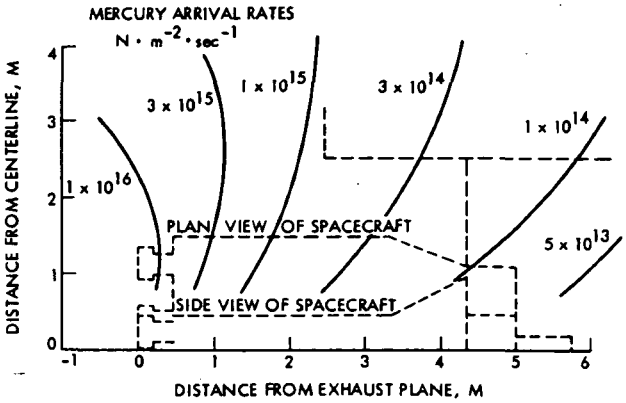

Figure 5. Schematic Diagram of CR Spacecraft and Mercury Arrival Rates.

Figure 6, taken from reference 9, illustrates conditions necessary to support the condensation of mercury on bulk mercury as a function of temperature and arrival rate. It is well known that the properties of a thin film are quite different from those of the bulk, particularly for the formation of the first few monolayers.[11] In general the curves shown in Figure 6 do not apply to the first few monolayers of mercury deposition. A larger arrival rate than shown for a specific temperature is necessary to deposit these first monolayers, after which condensation can be supported by smaller arrival rates. The arrival rate necessary to initiate condensation depends not only on the surface temperature and mercury arrival rate but also on the surface the mercury is impinging.[11] There is not sufficient information available to determine the arrival rates necessary to support condensation of mercury on various spacecraft surfaces. The substrate temperature is perhaps the most important variable in initiating condensation since small changes in it result in large changes in the arrival rate necessary to initiate condensation.[11] Therefore, for a conservative evaluation, spacecraft surfaces should be considered capable of acquiring a mercury deposit if they are at temperatures below those corresponding to an arrival rate which will support condensation.

Several science instruments that may be selected for the Comet Rendezvous mission are of interest regarding mercury deposition because of the low temperatures at which their detectors must operate. These instruments may be cooled by a passive radiator, which is shielded from the sun and radiating to deep space. Deposition on these radiators will lower their emissivity and raise the temperature, affecting instrument performance. Therefore, arrival rates and mercury deposition estimates for the scan platform, where the instruments are likely to be placed, will be given as a function of time into the mission. The model for charge-exchange current densities at a given spacecraft location is used to calculate mercury arrival rates and estimates of deposition. The number of thrusters operating and their power levels throughout the CR mission are used to determine these values, which are shown in Table 1. The values given assume that all mercury arriving at the surface adheres i.e., what is re-emitted is insignificant. As already discussed this last statement depends on the surface in question and its temperature. The discussion of individual instruments will address how this statement should apply.

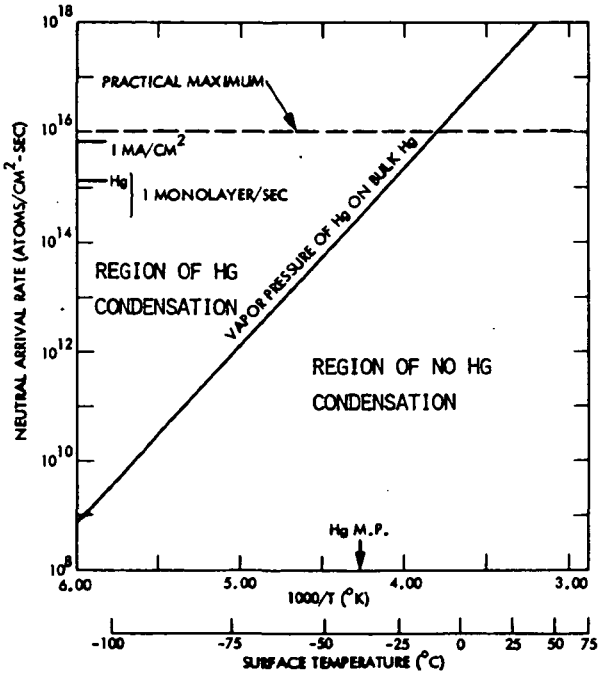

Figure 6. Bulk Accumulation Regions for Mercury Where Absorbed Monolayers Already Exist.

Instruments which require cooling and may be selected for the CR mission are the imaging cameras, a dust analysis instrument, a near infrared mapping spectrometer (NIMS), a γ-ray spectrometer and an X-ray spectrometer. The imaging cameras CCD detector requires a temperature of -60°C for operation. From the information in Figure 6 and Table 1, one may conclude that no deposition will occur at this temperature on a radiator placed on the scan platform. The remaining instruments require substantially lower operating temperatures for their detectors and should be considered capable of acquiring a deposit of mercury on passive radiators designed to operate at these low temperatures.

The cometary dust analysis instrument will consist of a dust collection device and various

TABLE 1

Scan Platform Mercury Arrival Rate and Deposition

Mission Phase	Rate ($N/cm^2 \cdot sec$)	Monolayers
Early Multi-thruster phase*	0.3 - 2 ($x10^{10}$)	200
2-thruster phase	0.8 - 2 ($x10^{9}$)	50
Last multi-thruster phase*	3 - 9 ($x10^{9}$)	70
Thrusting at Comet†	4×10^{9}	10
	Total	330

*More than 2 thrusters operating.

†Assume 1 day of ten for a year, thrusting with 3 thrusters.

internal instruments for analyzing the dust. Some of these internal instruments, such as an X-ray fluorescence spectrometer and an electron miniprobe, require operating temperatures of 100°K. A passive radiator placed in the scan platform area at this temperature will very likely accumulate mercury and therefore, lower its emissivity which will adversely affect the instruments.

The NIMS instrument requires an operating temperature of 85°K, making its radiator one of the likely candidates for mercury deposition. This instrument, as well as the others, is very sensitive to a change in temperature of a few °K. The emissivity of bulk liquid mercury is 0.1 while it is 0.05 for solid mercury.[9] An emissivity of 0.3 for the passive radiator will probably make data from the NIMS instrument unuseable.[12] Therefore, if the deposition given in Table 1 is allowed to occur it can be very detrimental.

The γ-ray and X-ray spectrometers both require 120°K for operation. The γ-ray instrument may be put on a six foot boom away from the spacecraft. If it is placed farther from the thrusters this will reduce the arrival rate to its radiator, reducing the overall deposition and somewhat reducing the likelihood of the formation of the initial monolayers necessary to support condensation. However, it should still be considered a likely candidate for mercury deposition on its radiator.

Because of the dust environment produced by the comet, the apertures of some instruments will be equipped with shutters. This will also protect sensitive instrument parts from mercury exposure except when data is being collected. Mercury exposure may result from mercury which is evaporating from surfaces where it has collected or from the charge-exchange plasma if the thrusters are operating. When the X-ray spectrometer is collecting data its X-ray transparent window, which will be at 150-200°K, may be able to accumulate a mercury deposit. This is not as likely to happen as for the radiators but is still a possibility. The X-ray spectrometer will operate at wavelengths between 1.4Å and 12Å. For an attenuation of X-rays due to a deposit on the window the following equation relates the attenuation to the deposit;

$$I = I_o \, e^{-(\mu/\rho)\,\rho\,X} \qquad (6)$$

where I_o and I are the initial and final X-ray intensity, (μ/ρ) is the mass absorption coefficient, ρ is the mercury density and X is the mercury deposit thickness.[13] The mass absorption coefficients are 225 and 3700 for 1.5Å and 10Å, respectively.[13] From equation (6), at 10Å a 1% attenuation in X-ray transmission will result after 7 monolayers (2.9 Å per monolayer) of mercury are deposited on the window. For energy at 1.5Å the same attenuation will occur after 100 monolayers. This amount of attenuation probably is of negligible concern but it is obvious that the X-ray instrument will suffer more than the γ-ray instrument in the event of mercury deposition on the instrument's window.

There are various instruments, which will be on the CR spacecraft, whose inside components will be exposed and not have a special window or lens on the aperture. These will basically be particle detectors such as mass spectrometers. The "strawman" payload includes a Thermal Ion Mass Spectrometer (TIMS), a Neutral Mass Spectrometer (NMS), and a Solar Wind/Electron Analyzer (SWEA). The temperatures over which the interior of these instruments will be required to operate will not be low enough to support condensation at the arrival rates estimated for the scan platform. Since the charge-exchange plasma tends to occupy all space, the plasma will be able to enter these instruments. The density inside the instrument will be much less than that estimated by the model for the instrument's position since the directed motion of the plasma will make it difficult for it to flow around obstructions and into cavities. If the instruments are pointed toward the thrusters the charge-exchange plasma can freely flow into them. Because the density of mercury inside the instrument will be small and no condensation should occur, there will probably be negligible interference from the mercury plasma. A potential concern is the interaction between the mercury and high voltage surfaces in the instruments, but this area has not yet been investigated. The instruments will get the most internal exposure when they are pointed toward the thrusters. In order to minimize any affect from the mercury ions, data acquisition during this condition should be kept to a minimum. If, after further study, there are concerns regarding interactions between mercury ions and instrument's interiors, a grid capable of repelling the low energy mercury ions can be placed at their apertures. This will not affect the operation of the NMS but will interfere with the low energy data acquired by the TIMS and the SWEA.

If the SCR power processing units (PPU) are used in the propulsion subsystem, each will have a large radiator to reject excess heat from the PPU during operation. When the thrusters and PPUs are operating, the radiators will be warm enough to prevent mercury condensation. When a thruster and associated PPU is off, the radiator will be maintained at -93°C to prevent the heat pipes that connect the PPU to the radiator from freezing. Figure 7 shows the calculated arrival rates for three positions on a PPU radiator. Since some of these values are well above those necessary to support condensation at 93°C, as shown in Figure 6, it is reasonable to assume that mercury will accumulate on the radiators which are associated with PPUs that are not furnishing power to operating thrusters. The mercury accumulated will likely be evaporated from the radiator when the PPU is providing thruster power and radiating excess heat. This will probably occur before the temperature gets high enough to damage the PPU.[14] If transistorized PPUs are used there will be no need for heat pipes and the amount of excess heat rejected will be much smaller. No evaluation of Mercury effects is given for this case.

The spacecraft body and the science instruments will be covered with a multi-layer thermal blanket. The outer layer of this insulation will approach temperatures of -190°C on the sun shaded side of the spacecraft. At such temperatures and the probable mercury arrival rates, mercury deposition can occur. Since this will lower the emissivity of the outer layer of the blanket its efficiency may degrade. A significant change in the emissivity of the outer layer of the thermal blanket will not affect the overall effectiveness of the thermal blanket. It may be sufficient to periodically rotate the spacecraft so that the portions of the blanket that have

been shaded are turned toward the sun. This will allow the previously shaded areas to heat up vaporizing away any mercury deposit.

One aspect of particle deposition from the charge-exchange plasma remains to be addressed here. That is deposition of molybdenum from the charge-exchange plasma. The ratio of molybdenum deposition to mercury deposition is given by the ratio of equations (4) and (5), which is 1.2×10^{-4}. Molybdenum has a sticking coefficient near unity for any substrate.[9] Therefore, even though the amount may be small it will all stick. For positions near the scan platform the molybdenum deposition will be fractions of a monolayer at the time of Tempel 2 rendezvous. Nearer the thrusters this value will be about a monolayer. A few monolayers of molybdenum can have significant effect on the optical and thermal properties of surfaces. Because of this and the uncertainties in the model, molybdenum deposition remains a mild concern. Also, there are indications that the molybdenum could act as nucleation sites, enhancing mercury deposition.[9,15]

Potential Solutions to Mercury Deposition

There are various means that can be used to prevent mercury deposition on sensitive surfaces or to drive off the mercury after it has deposited. The charge-exchange mercury can be prevented from arriving at a surface if that surface is positive enough to repel the low energy plasma ions. A positive surface will collect an electron current from the plasma and an appropriate power supply will be necessary to maintain the positive potential. A cover will be able to protect an instrument's radiator from mercury deposition. This cover can either be ejected near the comet or made to be removed from around the radiator and replaced on command. Heaters can be used to keep the radiators warm enough to prevent condensation of mercury. These heaters can be turned off to allow the radiators to perform their function of cooling the instruments' detectors. When the required science data is taken the heaters can be turned on to prevent deposition. It may be possible to allow the deposition to occur and heat the radiators to drive off the mercury for calibration and science data gathering sequences. This approach should be considered with caution since there are indications that once a mercury layer is formed impurities may reduce the expected evaporation rate.[16] Because the major concern regarding mercury deposition is the instruments' radiators, employing another means of providing the cooling to these instruments, such as a mechanical refrigeration system, is a possible solution since low temperature radiators will not be used.

Each of these solutions require power and/or added spacecraft complexity. Mercury deposition can be prevented but it will impact spacecraft and instrument design.

Other Charge-Exchange Plasma Impacts

There are other effects on spacecraft and science instrument operation which should be mentioned. One of these is solar array power drain. The solar array of the CR spacecraft will operate between 200-400 volts depending on the spacecraft distance to the sun and total load. The charge-exchange plasma will envelop the solar

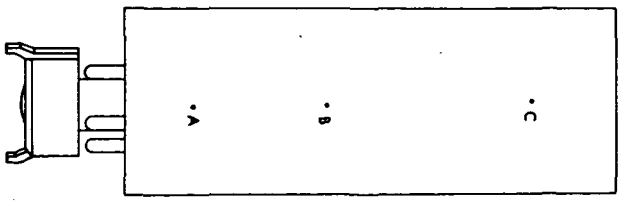

MISSION PHASE*	POSITION AND ARRIVAL RATE ($N \cdot cm^{-2} \cdot sec^{-1}$)		
	A	B	C
EARLY MULTI-THRUSTER PHASE	1-6 ($\times 10^{11}$)	0.3-2 ($\times 10^{11}$)	1-5 ($\times 10^{10}$)
2-THRUSTER PHASE	2-6 ($\times 10^{10}$)	0.7-2 ($\times 10^{10}$)	2-5 ($\times 10^{9}$)
LAST MULTI-THRUSTER PHASE	1-3 ($\times 10^{11}$)	3-8 ($\times 10^{10}$)	1-3 ($\times 10^{10}$)
THRUSTING AT COMET	1×10^{11}	4×10^{10}	1×10^{10}

* See Table 1

Figure 7. Mercury Arrival Rates of Three Positions (A,B,C) on PPU Radiators.

array panels and electron or ions, depending on the bias polarity, will be drawn from the plasma resulting in a power drain to the array. The model is used to calculate j_e at various points on the array centerline. The current integrated over the array for the case of a +200 volt bias and six thrusters operating gives a power drain of about 3% for the 25 kW array. Even if the array interconnects are well insulated to minimize collection area, this may still be a reasonable value since small open areas and pinholes can draw large currents.[8,17]

A plasma wave spectrometer will be placed on the end of a 13 meter magnetometer boom. The charge-exchange plasma density at this location will be greater than space plasma or cometary plasma, except when close to Tempel 2. It will also be susceptible to EMI noise generated by the thrusters. Therefore, this instrument is not expected to be able to function simultaneously with thruster operation.

When the thrusters are operating, the trajectories of charged particles will be altered if they pass through the thruster plume. The varying densities in the plume will produce differences in potential and particles moving through the plume will "see" electric fields which will change their path. Science instruments which detect these particles will therefore, produce data which will contain errors regarding the particles direction of travel.[18] Electric and magnetic fields associated with thruster operation and the solar array will also affect the trajectories of charged particles.

Sputtered Molybdenum

The fact that molybdenum from the accelerator grid is sputtered by charge-exchange ions has already been discussed. The distribution and rate of flow of molybdenum atoms has been measured from a 30-cm thruster.[19] Even though the 30-cm thrusters which will propel the CR spacecraft will have different optics than those used to obtain the test results in reference 19, the data in this reference can be used to estimate molybdenum atom deposition on surfaces. The sputtered efflux can be emitted at angles up to 90° from the thruster

axis. These atoms do require line-of-sight for deposition. When the thrusters are gimballed this efflux will be able to flow so as to be intercepted by the solar array. The data in reference 19 is used and extrapolated assuming an inverse of the distance square drop in density. Figure 8 shows the relative distances from the thruster to the solar array for the Comet Rendezvous spacecraft. Assuming full gimbal of 15° for a single thruster and the solar array turned so that in the y-z plane the angle between the thruster axis and the array normal is zero, the molybdenum deposition on the array is given in Figure 8. The deposition will decrease as the cosine of the angle between the array normal and the thruster axis for angles other than zero.

Even though there may be more than one thruster gimballed so as to deposit molybdenum on the solar array, the array is not going to be continually in a position for maximum deposition, nor will the thrusters likely be gimballed the maximum amount throughout the mission. Molybdenum deposition may vary from the values shown in Figure 8. Assuming a uniform 5Å layer of molybdenum develops on the front surface of the solar array, the power loss will be about 10%.[9] Therefore, the problem of molybdenum deposition should be given added attention when data is available regarding sputter from the latest thruster optics and when mission parameters of gimballing and solar array angle can be specified. Because the sputtered atoms travel line-of-sight paths, a beam shield can be used to prevent these atoms from reaching the solar array.

Optical Emissions

The excited mercury atoms and ions in the thruster and the plume radiate energy in the UV and visible wavelengths. This radiation has been measured for a 30-cm ion thruster and an empirical formula derived for use in determining the flux of photons at an instrument looking parallel to the thruster beam.[20] Only discrete lines of emission are seen and there is no observed continuum.

An empirical volume emission rate, F (r,z), is derived directly from the exhaust beam emission data. The relation,

$$F(r,z) = F(0,z_o) \exp(-a(z-z_o)) \exp(-br^2/z^2) \quad (6)$$

gives F (r,z) from the experimentally determined values of F $(0,z_o)$, a, and b. Figure 9 shows the coordinate system used to determine F (r,z)[20]. The radiance, I, of a specific emission wavelength seen by an instrument viewing parallel to the beam is given by,

$$4\pi I = \int_{z=5r_o}^{\infty} F(r_o,z)\, dZ, \quad (7)$$

where I is the number of photons cm^{-2} sec^{-1} having the wavelength at which F (r_o,z) is calculated.

Direct line-of-sight viewing of the plume by the science instruments is the condition under which optical interference occurs. Because the thrusters will be gimballed, an instrument's field of view will be compromised if viewing the plume is incompatible with its operation. The scan platform on the Comet Rendezvous spacecraft is positioned such that the instrument's line-of-sight, when looking parallel to the beam, will be one meter from the thruster axis. With one meter as r_o, equation (7), along with information in Ref. 20, is used to determine photon fluxes at the scan platform. The results are shown in Table 2.

The CR "strawman" payload instruments that will be affected by the optical emissions from the thrusters are the Ultraviolet Spectrometer (UVS) and the imaging cameras. Both of these instruments have a sensitivity of 100 photons cm^{-2} sec^{-1}.[21] As evident from the information in Table 2, both will be capable of seeing the plume. The UVS will be able to distinguish the emission lines from the

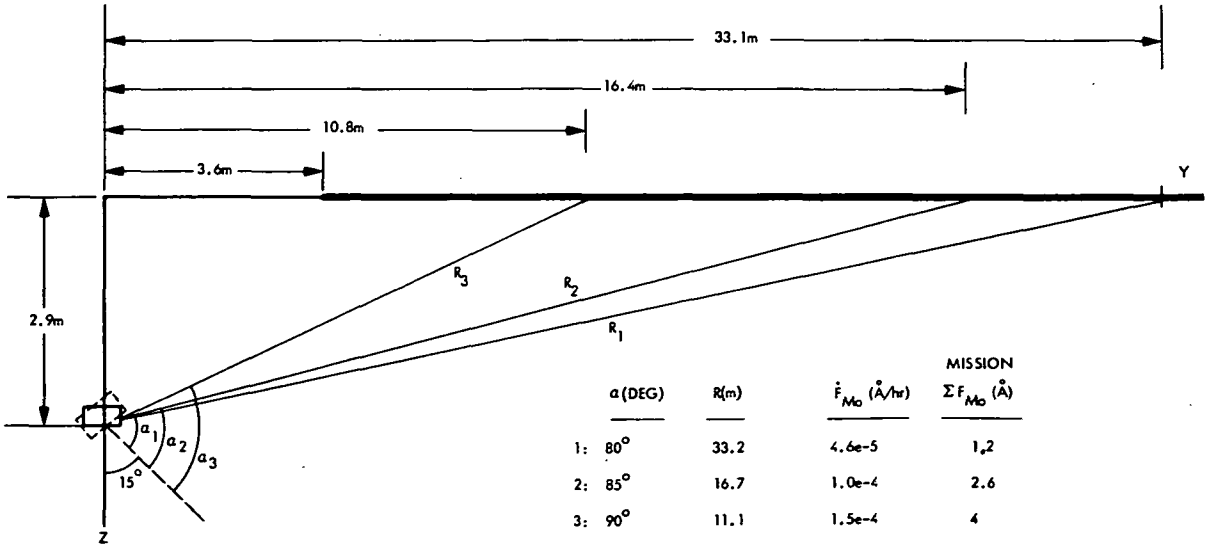

	α(DEG)	R(m)	$\dot{F}_{Mo}$ (Å/hr)	MISSION ΣF_{Mo} (Å)
1:	80°	33.2	4.6e-5	1.2
2:	85°	16.7	1.0e-4	2.6
3:	90°	11.1	1.5e-4	4

Figure 8. Sputtered Molybdenum Flux (F_{Mo}) onto Solar Array.

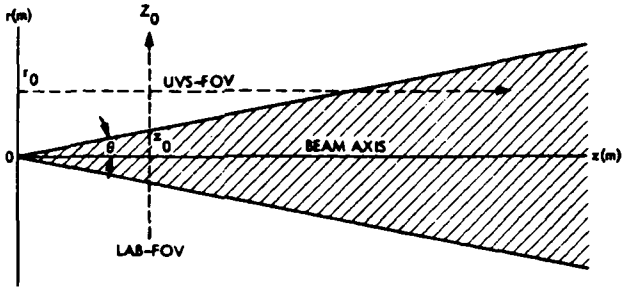

Figure 9. Coordinate System Used to Calculate Apparent Emission Rates.

thruster beam since it will have a 10Å resolution. A problem might occur if the mercury spectral lines are coincident with lines from species that may be seen in a comet.

The imaging cameras are broadband instruments which will not be able to subtract the signal due to the thruster plume. Besides being used for study of the comet, the imaging cameras will be used for navigation purposes. There may be a dedicated star tracker which will have the same sensitivity as the cameras.

A simple calculation is given regarding interference with navigation. The difference in energy flux from two stars of magnitude, m, is given by,

$$m_2 - m_1 = 2.5 \log W_1/W_2, \qquad (8)$$

where W is energy received cm^{-2} sec^{-1}.[22] The flux from a star with zero bolometric magnitude is 2.27×10^{-5} erg cm^{-2} sec^{-1}.[23] By equation (8), the flux from a star with bolometric magnitude of 12 is 3.6×10^{-10} erg cm^{-2} sec^{-1}. Assuming an average wavelength of 5000Å, the flux is 9×10^{8} photon cm^{-2} sec^{-1}. This is two orders of magnitude above the emission due to the thruster beam. Therefore, even though the beam emission will be seen by instruments pointed toward the thrusters, it should not interfere with operations such as navigation.

TABLE 2. Photon Flux at Scan Platform

Wavelength (Å)	I (Photon cm^{-2} sec^{-1})
2537	4.0×10^{5}
2815	3.4×10^{6}
3650	2.1×10^{5}
4047	3.1×10^{5}
4358	4.9×10^{5}
5461	6.1×10^{5}

Potential Solutions to Interactions

The potential solutions to the problems caused by mercury deposition have been addressed. Other interactions are discussed in this paper and there are reasonable solutions to these concerns. Some of the solutions are unique to particular instruments or problems, while some are common to most interactions. Table 3 gives the factors that should be considered for each instrument that may be selected for the CR mission. Except for charge-exchange plasma particle deposition, each instrument should be able to operate successfully with the thrusters off. With proper considerations most instruments will be able to function in conjunction with thruster operation with minimal or no interference.

There are potential solutions to the various factors that may be compromise instrument operations. Table 4 identifies the possible solutions to concerns which are discussed in this paper.

TABLE 3. Factors To Be Considered To Minimize Interactions Effects With Science Instruments

Instrument	Hg Deposition	Hg Ingestion	Charge Exchange Plasma	EMI	Optical Radiation
Neutral Mass Spectrometer		X	X		
Thermal Ion Mass Spectrometer		X	X		
Magnetometer				X	
Solar Wind/Electron Analyzer		X	X		
Plasma Wave Spectrometer			X	X	X
Imaging Science					X
Dust Collection and Analysis	X				
Dust Counter					
Gamma Ray Spectrometer	X				
X-Ray Spectrometer	X				
UV Spectrometer		X			X
Radar Altimeter Science					
Millimeter Wave Radiometer					
Near Infrared Mapping Spectrometer	X				
Radio Sounder				X	

Summary

A model has been used to determine charge-exchange plasma densities and arrival rates at various locations on the spacecraft. A general assessment of particle deposition and effects of such have been presented as they relate to the spacecraft and particular science instruments. Various aspects of the interactions between the ion thruster produced environment and the CR spacecraft have been addressed. None of the interactions are felt to be so serious as to jeopardize the CR mission. Compatibility between the thrusters and the spacecraft can be obtained with the proper design considerations.

No instruments will be affected adversely when the thrusters are off, excluding those that have

passive radiators which may collect mercury. An assessment of the compatibility of the instruments with the ion thrusters was made. This was a general assessment and specific instrument designs, including materials and components, should be individually studied regarding their compatibility with ion thruster operation. Most of the instruments will be able to function with the thrusters on if proper design considerations are made.

TABLE 4. Potential Solutions to Interactions Concerns

Concern	Turn Off Thrusters	Use Other Means of Cooling	Bias Surface	Removable Cover	Heat Surface	Restrict Field of View	Beam Shield	Allow Contingency	Elec. Filtering and Shielding	+ Bias Spacecraft	
Hg Deposition		X	X	X	X					X	
Hg Ingestion			X		X	X				X	
Charged Particle Perturbation	X					X					
Solar Array Drain								X			
M_o Deposition							X				
M_o^+ Deposition			X							X	
Plasma Wave Interference	X										
EMI	X								X		
Optical Radiation	X					X					

REFERENCES

1. A Strategy for the Space Exploration of Comets, Report of the Comet Science Working Group, 1978.
2. Cowgill, R.M., Macie, T.W., and Van Amersfoort, J. "Magnetic Compatibility of Solar Electric Propulsion Module with Spacecraft and Science," AIAA paper 75-373, 1975.
3. Whittlesey, A., "Electromagnetic Interference Assessment for an Ion Drive Electric Propulsion System." AIAA paper 79-1328, 1979.
4. Staggs, J.F., Gula, W.P., and Kerslake, W.R., "The Distribution of Neutral Atoms and Charge-Exchange Ions Downstream of an Ion Thruster," NASA TM X-52259.
5. Kaufman, H.R., and Carruth, Jr., M.R., "Charge-Exchange Plasma Environment for an Ion Drive Spacecraft," JPL Publication 79-90, 1979.
6. Komatsu, G.K., and Sellen, Jr., J.M., "Beam Efflux Measurements," NASA CR-135038, 1976.
7. Kerslake, W.R., "Charge-Exchange Effects on the Accelerator Impingement of an Electron-Bombardment Ion Rocket," NASA TN D-1657, 1963.
8. Kaufman, H.R., "Charge-Exchange Plasma Generated by an Ion Thruster," NASA CR-135318, 1977.
9. Hall, D.F., "Electrostatic Propulsion Beam Divergence Effects on Spacecraft Surfaces," Vol. II, TRW No. 11985-6003-RU-00, 1973.
10. Fitzgerald, D.J., "Factors in the Design of Spacecraft Utilizing Multiple Electric Thrusters," AIAA paper 75-404, 1975.
11. Neugebauer, C.A., "Condensation, Nucleation, and Growth of Thin Films," Handbook of Thin-Film Technology, ed., L.I. Moissel and R. Glang, McGraw-Hill Book Co., N.Y. 1970.
12. Salazar, R. and Bailey, G., JPL, personal communication.
13. Kaelble, E.F., ed., Handbook of X-rays, McGraw-Hill Book Co., N.Y., P. 1-28, 1967.
14. Jaworski, W., JPL, personnel communication.
15. Reynolds, T.W., and Richley, "Contamination of Spacecraft Surfaces Downstream of a Kaufman Thruster," NASA TN D-7038, 1971.
16. Frohusdorff, G. and Dunn, D., "Study of Mechanism Which Causes Film Formation on Mercury Surfaces," NASA CR-120844, 1972.
17. Kennerud, K.L., "High Voltage Solar Array Experiments," NASA CR-121280, 1974.
18. Sellen, Jr., J.M. "Electric Propulsion Interactive Effects with Spacecraft Science Payloads", AIAA paper 73-559, 1973.
19. Weigand, A.J., and Mirtich, M.J., "Measurements of Sputtered Efflux from 5-, 8-, and 30-cm Diameter Mercury Ion Thrusters," AIAA paper 75-358, 1975.
20. Monaham, K.M., and Goldstein, R., "Optical Properties of Mercury Ion Thruster Exhausts and Implications for Science Instruments, JPL TM 33-711, 1974.
21. Holberg, J. and Snyder, L., JPL, personal communication.
22. Swihart, T.L., Astrophysics and Stellar Astronomy, Wiley and Son, N.Y., 1968.
23. Allen, C.W., Astrophysical Quantities, Athlone Press, University of London, London, P. 174, 1955.

ION THRUSTER PLUME EFFECTS ON SPACECRAFT SURFACES*

M. R. Carruth, Jr.** and Y. S. Kuo†

Jet Propulsion Laboratory
California Institute of Technology
Pasadena, California

Abstract

A charge-exchange plasma, generated by an ion thruster, is capable of flowing upstream from the ion thruster and therefore represents a source of contamination to a spacecraft. An analytical model of the charge-exchange plasma density around a spacecraft is used to estimate the contamination which various spacecraft materials may be exposed to. Measurements of plasma density around an ion thruster are compared to this model. Results of experimental studies regarding the effects on various spacecraft materials' properties due to exposure to expected mercury contamination levels are presented.

Introduction

Electron bombardment ion thrusters have been under development for a number of years. The 30-cm mercury ion thruster is presently at the end of its development stage and will be ready in the near future to provide primary propulsion for interplanetary and Earth orbital missions.

The interactions between operating ion thrusters and a spacecraft have been recognized as requiring a complete understanding in order to insure mission success and flexibility. There are various thruster produced particle and field fluxes which may affect spacecraft operation and science acquisition. Of these, the low energy charge-exchange ions, produced just downstream of an ion thruster, may be of primary concern. These low energy ions, with neutralizing electrons, form a plasma which is capable of flowing upstream around a spacecraft.

Past studies have evaluated the interaction of both neutral mercury vapor and high energy mercury ions with spacecraft materials. However, the interaction of low energy, charge-exchange ions with spacecraft materials has not been considered. This paper presents results of a study to determine the effects on spacecraft materials produced by exposure to low energy mercury ions.

Background

Mercury ions are produced in the ion thruster's discharge chamber by bombarding mercury atoms with electrons. These ions are then accelerated by a potential difference across two grids, which form the ion optics. A cut-away view of an ion thruster is shown in Fig. (1). The acceleration of these ions provide thrust to propel the spacecraft.

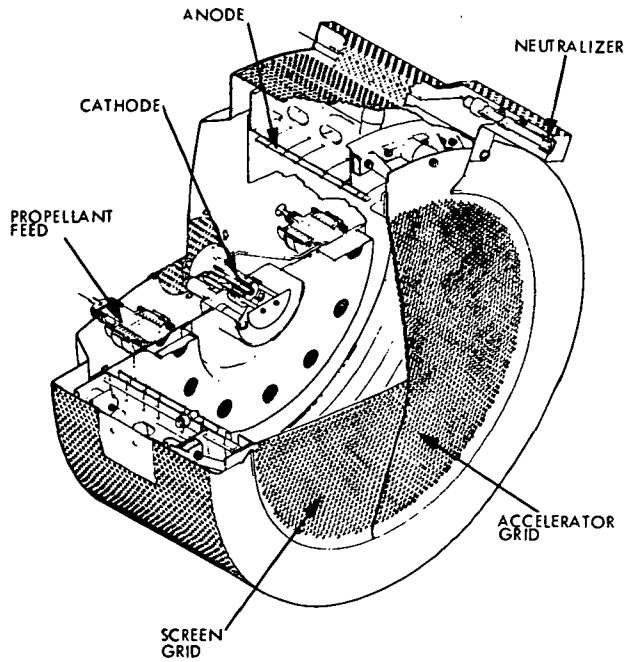

Fig. 1 Cut-away View of Ion Thruster

Approximately 90% of the mercury flow through the discharge chamber is ionized and accelerated through the ion optics to form the primary beam. The remaining 10% escape through the ion optics as neutral mercury. A part of this neutral mercury will become ionized by charge-exchange collisions with energetic ions from the thruster. In a charge-exchange collision, an electron from an atom is transferred to an ion. This interaction will result in energetic mercury atoms and very low energy (thermal) ions. These low energy ions will be accelerated perpendicular to the primary beam's axis due to the electric fields produced by a density gradient across the beam. They will flow radially from the beam with an energy range of a few tenths to a few eV. These low energy ions and neutralizing electrons constitute a charge-exchange plasma which is capable of flowing upstream around a spacecraft because of internal electric fields within the plasma, and therefore can be a source of contamination to a spacecraft.

Thruster plume effects on material's properties have been studied extensively by Hall and others[1-19] under contract to the Jet Propulsion Laboratory. Potential degradation effects on spacecraft surfaces

*The research described in this paper was carried out at the Jet Propulsion Laboratory, California Institute of Technology, under NASA contract NAS7-100.

**Engineer, Electric Propulsion and Advanced Concepts Group.

†Engineer, Electric Propulsion and Advanced Concepts Group, Member AIAA

examined in this study included: 1) mercury (Hg) propellant condensation, 2) the chemical and metallurgical reactions between mercury and various spacecraft surfaces, 3) sputtering erosion and radiation damage due to bombardment of surfaces by keV mercury ions. A wide range of spacecraft materials were tested and discussed in that effort and included thermal control coatings, optical elements and coatings, structural materials, insulators, electrode gaps, conductors, and adhesives.

The treatment developed for the condensation of neutral propellant vapor onto solid surfaces was widely used by other investigators (Ref. 11, for instance). Based on the common laboratory experience that mercury does not wet surfaces such as glass, a reasonable assumption was made that the desorption energy from a surface is smaller than the desorption energy of mercury from mercury. This means the calculation based on the desorption energy of mercury from mercury to estimate the bulk condensation should be conservative since the more difficult formation of the first monolayer is assumed to have already occurred. Coupled with another conservative, but realistic assumption, that the sticking coefficient is unity, they obtained a curve describing the condition required for bulk condensation to occur:

$$\text{Log}_{10}\ f = \frac{-317}{T\ (^\circ K)} + 28.16 \qquad (1)$$

For a given temperature, T, of any spacecraft surface, the incident mercury flux, or arrival rate, in atoms/cm^2/sec must be higher than the rate, f, obtained in the above equation. This relationship was found to be in excellent agreement with experimental data on the glass encapsulation of solar cells[12] and quartz glass[13]. It could be very inadequate, however, in representing the interaction of surfaces with a low-energy mercury plasma. The neutral atoms from a thruster, unaffected by any electromagnetic field, are expected to have flight trajectories along the line of sight from the end of the ion thrusters and hence will have little chance of hitting upstream spacecraft surfaces. The exception is that neutrals can also be formed by charge-exchange of these low energy ions already diverted by the electric fields. They will be very small in number and therefore negligible in this study.

One of the advantages of depositing thin film by sputtering rather than vapor deposition is that the sputtered atoms, with higher than thermal energy, can stick to the substrate better than evaporated atoms. By the same token, the mercury ions in the charge-exchange plasma, which have a very directed flow, will travel upstream with a directed energy greater than the ions' thermal energy. Also, a spacecraft will be at some negative potential, of possibly 10-20 volts,[14] so that ions from the charge-exchange plasma will strike spacecraft surfaces with energy of several eV. This could provide, under appropriate conditions, the energy necessary to overcome the barrier for, say, chemisorption, and make the above qualitative relationship regarding neutral mercury condensation inapplicable.

As mentioned above, the mercury ions in the charge-exchange plasma surrounding the electric spacecraft will not be capable of striking surfaces at spacecraft ground with more than 20 eV. Phenomena like sputtering, atomic displacement, localized energy deposition and the entrapment or implantation of the mercury atom by the target could theoretically happen, but will be negligible since the energy thresholds for such interactions are near the top of the energy interval of the possible bombarding atoms. The charge of the bombarding mercury ions may be neutralized by Auger or resonance processes in case of a conductive target. But how the neutralization ensues, if it even does, is not thoroughly understood.

The kinetic ejection of secondary electrons from target surfaces can be considered to be zero.[15] The potential ejection of secondary electrons is mainly determined by whether or not the ionization energy of the projectile is greater than twice the work function of the target material. Since mercury does possess a fairly high ionization energy ($\sim$10.4 eV), secondary electron emission is likely to occur. Effects due to secondary emission may be neglected, however, since the yield is estimated to be on the order of 0.1. Neglecting this effect will, after all, make the study more conservative, since extra electrons ejected from the surface will only help to neutralize the plasma, lower the ion density and relieve any possible degradation effect caused thereby.

Results reported by Hall's group on chemical and metallurgical reactions have shown, surprisingly, that the interactive effects were negligible when samples were bombarded by a neutral mercury beam at room temperature. Even materials like gold, well known for its reactivity with mercury and expected to amalgamate in bulk levels, did not show reaction at 22°C under intense mercury neutral flux in the vacuum tests.[10] Regarding their test results of bombardment with high dose rates (up to 5 × 10^{19} per cm^2 with 1.5 $\sim$3.0 KeV Hg ions), the emissivity of all tested materials, both organic and inorganic, did not seem to have been affected.[7-10] But all the low absorptance organic samples (several white paints in particular) were darkened and had changes in topography, probably produced by an erosion effect due to sputtering. The effect on thermal/optical properties, i.e., an increase in absorptance and a decrease in reflectance, could also be partly caused by the breakage or crosslinking of some chemical bonds on the surface layers of the specimens. Neither this or the sputtering/erosion effects can be considered to describe what will happen to the surfaces exposed to low energy ions, as already explained. Hence we decided to simulate a low energy, charge-exchange mercury plasma and study its possible degradation effects on several materials.

Charge-Exchange Plasma

The charge-exchange ions are produced just downstream of an ion thruster and flow radially from the primary thruster beam. These mercury ions, with neutralizing electrons, are capable of flowing upstream around a spacecraft. The charge-exchange plasma produced by a 30-cm ion thruster has been previously investigated.[16,17] Because the charge-exchange ions are very low energy and various facility effects introduce error into experimental measurements, there has been disagreement on how the charge-exchange plasma propagates after it has left the influence of the primary thruster beam.[18]

The vacuum chambers in which ion thrusters are operated normally have a target to intercept the mercury beam and prevent sputtering of the vacuum chamber walls. In some cases the target surface is

frozen mercury to prevent sputtering of non-volatile materials. Mercury sputtered from such targets produce a flux of neutrals which may charge-exchange with the primary beam. The resulting low energy "facility" ions are difficult to subtract from charge-exchange plasma measurements. This is necessary in order to determine true charge-exchange plasma densities at positions relative to the ion thruster. True charge-exchange plasma ions are produced due to charge-exchange of energetic ions with mercury atoms leaving the thruster.

Previous methods of measuring charge-exchange plasma densities and energies have consisted of using Faraday cup-retarding potential analyzers and Langmuir probes. Such methods are normally not useful for accurately determining the plasma flow direction or for separating the facility ions from the true charge-exchange ions. An "end-effect" of a cylindrical Langmuir probe can be extremely useful for determining the true charge-exchange plasma flow direction to within a few degrees at the probe's location.[18] It has been shown that the charge-exchange plasma flow upstream of an ion thruster is very directional and the flow direction is independent of facility produced ions.[18]

The density of the charge-exchange plasma is such that charged particle collection by a Langmuir probe will be orbital motion limited. It also possesses a directional flow such that the directed ion energy is much greater than the random ion thermal energy ($1/2 M_i U^2 >> kT_i$). Under these conditions an "infinitely" long cylindrical Langmuir probe, i.e., a probe which has a length (L) much greater than its diameter ($2R_p$), will collect an ion current, I (in amperes), of, [19]

$$I = 2 N_e e U R_p L \left(\mathrm{Sin}^2\Theta - \frac{2eV_p}{M_i U^2} \right)^{1/2}, \qquad (2)$$

where N_e is the plasma density in ions M^{-3}, e is the electronic charge, V_p is the voltage of the probe relative to the plasma potential, Θ is the angle between the probe and the plasma flow direction, U is the directed flow velocity in $M \cdot sec^{-1}$ and M_i is the mass in kilograms of the flowing plasma ions. There is an "end-effect" of a cylindrical probe such that a large increase in ion current over that predicted by Eq. (2) occurs at $\Theta = 0$, the position where the probe is aligned with the plasma flow. Therefore, Eq. (2) does not hold for small Θ, but is accurate for larger Θ, where the "end-effect" does not occur.

An "infinitely" long cylindrical Langmuir probe was placed at various locations relative to the center of the ion thruster optics. The probe was 5 mil Tungsten wire and had a length to diameter ratio of 450. The probe was capable of being moved axially on a rail and at each location along the rail the probe could be rotated. We assumed that the charge-exchange plasma flow is cylindrically symmetric. Therefore, to require only two degrees of freedom, the ion thruster beam axis lies in the plane swept out by the probe rotation so that the probe is always pointing at the thruster axis. At each location the plasma flow direction was determined by rotating the probe until the large increase in ion current produced by the "end-effect" was observed. This determined $\Theta = 0$. The experimental arrangement is shown in Fig. 2.

The probe potential, V_p, was approximately -6.5 volts. As the probe was rotated through 180° the ion current did not vary except for the excess current produced by the "end-effect" when the probe was pointed into the plasma flow. This indicates that $-eV_p >> 1/2 M_i U^2$. In this case the dependence on velocity in Eq. (2) is so small that it may be neglected. Therefore, the density can be determined from the ion current and Eq. (2) when θ is not near zero and preferably when $\theta = \pi/2$. The ion current at each location was obtained with the frozen mercury target, shown in Fig. 2, both vertical and horizontal. At positions upstream (~50 cm) of the ion

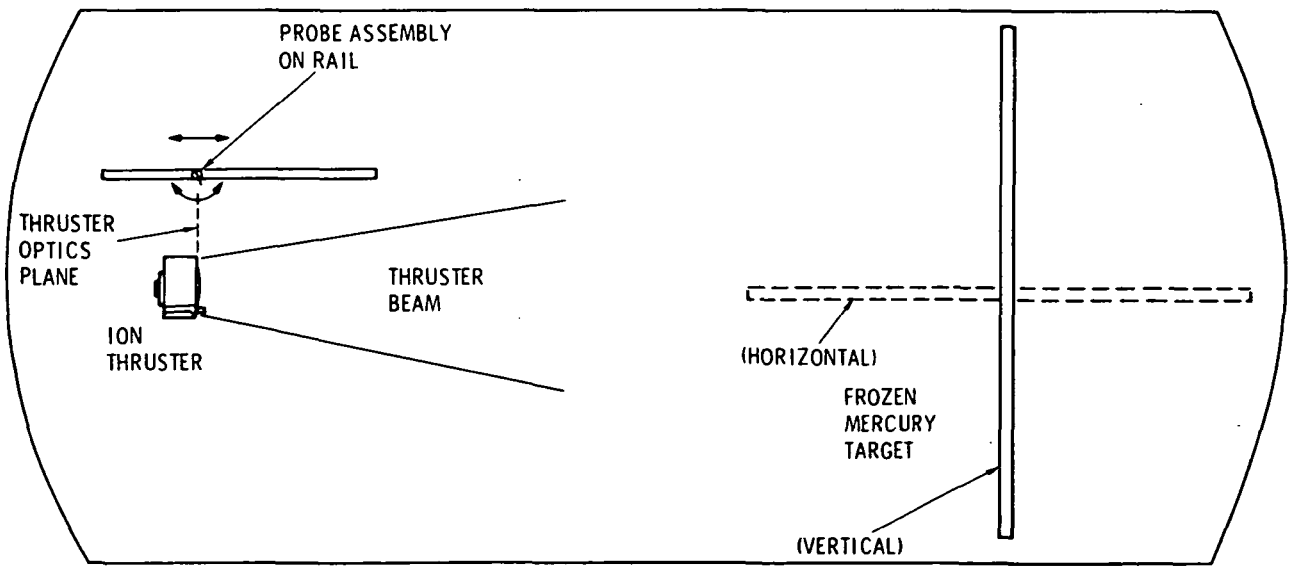

Fig. 2 Experimental Arrangement. Probe may move upstream or downstream of the thrust plane and can rotate away from the target or toward it.

thruster, the ion current at $\theta = \pi/2$ decreased approximately a factor of two when the target was horizontal as compared to when it was vertical. At positions near the plane of the thruster optics the difference in current was much less significant. The ion current values obtained when the target was horizontal were therefore used to determine the density at various locations because this introduced less error due to facility produced ions. Figure 3 and Fig. 4 give the density values obtained by this method. It is necessary to point out that the density values are not corrected further for facility produced ions. Based on previous studies, and the effect on ion current we obtained by rotating our target, the plasma density near the thruster is predominantly true charge-exchange ions and not facility ions.[16,17] Farther upstream the density values become more uncertain, and are possibly high due to facility ions. No downstream values of density were determined.

The ion current measured at $\theta = \pi/2$ varied noticeably (more so for upstream positions) due to rotation of the frozen mercury target since more facility ions were produced when the target was vertical. However, the angular position of the ion current

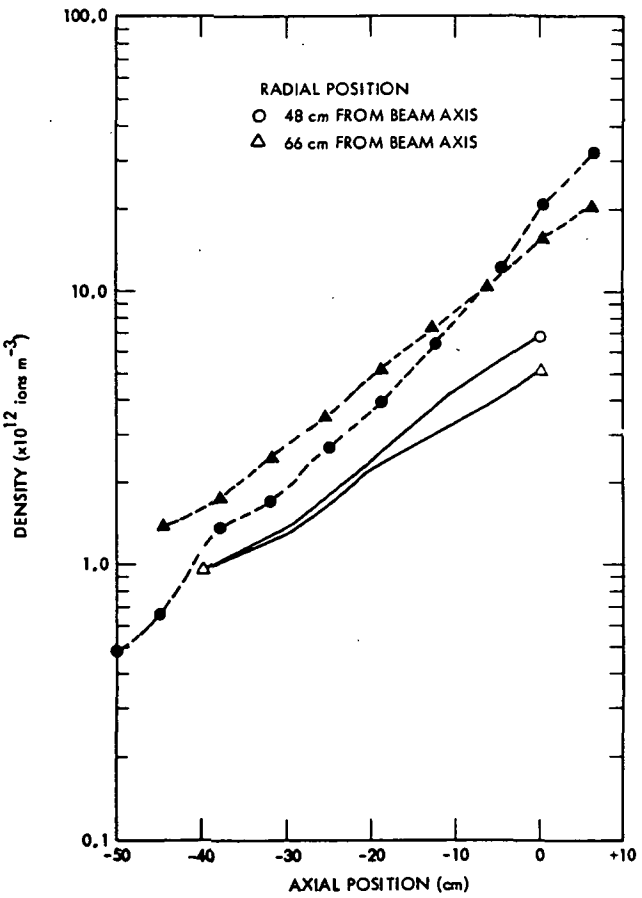

Fig. 3 Charge Exchange Plasma Density Measurements and Model Predictions for 1.0 Amp Beam Current from 30-cm Mercury Ion Thruster. (Solid Symbols represent experimental data and solid lines represent theoretical predictions from Ref. 7. The axial position, "0", lies in the thruster optics plane, shown in Fig. 2.)

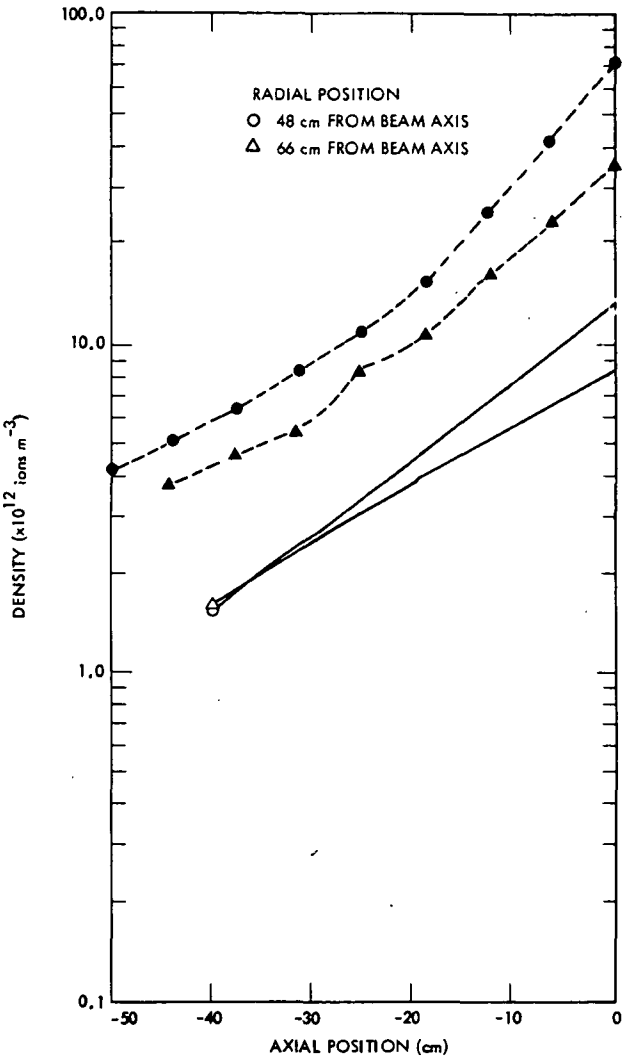

Fig. 4 Charge-Exchange Plasma Density Measurements and Model Predictions for 1.8 Amp Beam Current from 30-cm Mercury Ion Thruster. (Solid Symbols represent experimental data and solid lines represent theoretical predictions from Ref. 7. The axial position, "0", lies in the thruster optics plane, shown in Fig. 2.)

peak did not alter significantly even for probe locations 50 cm upstream of the thruster optics plane. This indicates that the flow of the charge-exchange ions which are produced near the thruster is independent of facility produced ions which have various flow directions so that they contribute to the overall current but produce no "end-effect" peak of their own. Also, the shape of the peak appears independent of the target position and therefore of the facility produced ions. This indicates that proper analysis of the "end-effect" peak itself could yield density values which are independent of facility produced ions. Time did not permit the performance and inclusion of such an analysis in this paper.

The experimentally determined values of charge-exchange plasma density were compared with those

densities produced by a model described in Ref. 20. The values predicted by the model for a 30-cm thruster were expected to be smaller than measured by up to a factor of four. This is due to the difference in the electron temperatures in the beam of 30-cm thrusters and smaller thrusters on which the model is based. [20] With this in mind, the agreement between our data and the model is within a factor of two, except for the extreme upstream positions with a thruster beam current of 1.0 ampere. The values predicted by the model, not including the expected increase of a factor of four, are shown in Fig. 3 and Fig. 4 along with the experimental values.

Plasma-Materials Interactions Tests

The density of the charge-exchange plasma around a typical electrically propelled spacecraft with six operating 30-cm ion thrusters is expected to be about 10^5 - 10^7, ions·cm^{-3}, the lower density being farther from the ion thrusters.[20] Studies have been conducted to determine the interaction of mercury with typical spacecraft materials but none of these have considered the situation where a low density, low energy mercury plasma is in contact with some spacecraft surface, which is several volts negative of the plasma. These are the conditions under which tests described in this paper were conducted.

Plasma Simultation Chamber

A vacuum chamber was assembled as shown in Fig. 5. The chamber is 2 feet in diameter and 4 feet long. A mercury plasma source was placed in one end and the test samples were placed in the opposite end. The chamber was lined with a liquid nitrogen cooled wall and had a cold baffle near the center of the chamber. The liner and baffle prevented neutral mercury from populating the sample end of the chamber so that interactions between sample materials and mercury would only be due to mercury ions in the plasma.

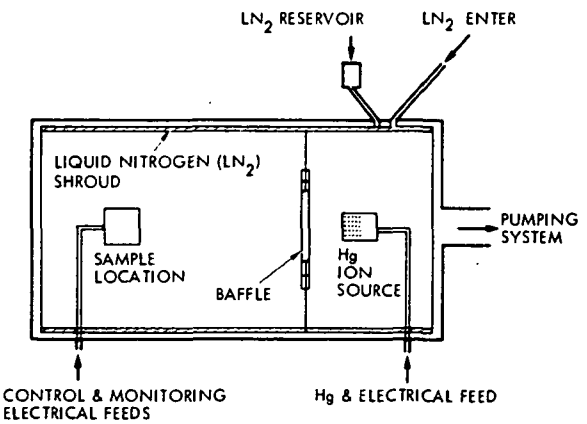

Fig. 5 Charge-Exchange Plasma Simulation Chamber Used in Plume Effects Tests

The plasma source was similar in design to that described in Ref. 21. It consisted of a hollow cathode with keeper and a cylindrical, perforated anode. After the plasma source had been turned on and allowed to operate for a few hours, to be certain that the source was functioning stably, the plasma density was determined as a function of the temperature of the mercury vaporizer which supplied the mercury vapor flow to the hollow cathode. A spherical Langmuir probe, 0.33 cm in diameter, was placed into the test sample location of the chamber in order to determine the plasma parameters of the simulated charge-exchange plasma created by the ion source at the other end of the chamber. This was accomplished by obtaining typical Langmuir probe current-voltage characteristics from which the plasma parameters can be obtained. Each current-voltage characteristic was obtained after the probe was cleaned by ion bombardment for about 15 minutes, by applying a negative voltage on the probe of 1 kilovolt. The cleaning was necessary to assure that the probe was free of undesirable contamination and gave useful data.[22] The ion source keeper current and arc current were fixed. The vaporizer temperature was varied to control the rate of mercury vapor flow into the plasma source. The vapor passes through the hollow cathode and a portion of it becomes ionized. The rate of this flow therefore directly determines the amount of ions which are produced. The plasma conditions determined from the current-voltage characteristics included the ion density, the electron temperature, the plasma potential and finally the ion current density to the material samples, which is the exposure dose rate of mercury ions onto the spacecraft materials being tested. By later reproducing the operating conditions of the ion source, the same plasma conditions could, within a factor of two or three, be reproduced so that the exposure the samples were receiving was known. The operating conditions selected produced an ion density of $\sim 10^6$ ions cm^{-3} and an ion current density $\sim 6 \times 10^{10}$ ions cm^{-2} sec^{-1}, in simulation of a typical medium exposure dose rate to an electric spacecraft as was computed from the charge-exchange model.

Specimens and the Holder

Aluminum plates with seven different types of spacecraft surfaces were cut into small specimens in the form of rectangular platelets (2 cm × 0.7 cm). They include a conductive black paint developed for upcoming missions, such as Galileo, a PV-100 white paint, gold plating, cat-a-lac black paint, polished aluminum, chem-glaze black coating and cat-a-lac glossy white paint. They were supplied by the spacecraft materials engineers or painted by the metal finishing technicians at the Jet Propulsion Laboratory, and represent typical materials and surfaces being used in current spacecraft. The cutting and handling was done with much care so that the specimen surfaces were not contaminated. Slight chipping did occur to some specimen edges and was considered tolerable since the thermal optical properties to be measured would concern only the central portion of each surface.

The specimen holder was basically a flat (10 cm × 22 cm) aluminum table with base pedestals such that the height of the table on which the specimens were placed was approximately the same as the elevation of the Langmuir probe when it was placed into the tank for plasma condition calibration. Attached to the table was a resistance heater which was controlled electronically from outside the tank to maintain a constant temperature of the specimens placed on it. Since the test chamber wall was cooled cryogenically by liquid nitrogen, to sustain a vacuum of below 5×10^{-6} torr, a proper base pedestal design was determined by trial and error so that the thermal conduction from the heated table to the cryogenically cooled wall was sufficient to at-

tain a rapid thermal response enabling stable temperature control of the table. Too large a conduction path on the other hand, would have overburdened the heater design which again might affect the temperature control stability. A voltage of 20 volts negative, relative to ground, was also applied to the table during the exposure test. Because the plasma potential was ∿15 volts positive to ground, the ion impact energy was 35 volts; in excess of the expected maximum impact of 20 eV. Because of the potential placed on the tank, the thermocouple terminal monitoring the table temperature was attached to the table with a thin layer of non-conductive cement. A slight error in temperature reading could be introduced by such a thin layer but was not expected to substantially affect the test.

Procedure

The test chamber pressure was lowered to the range of 5×10^{-6} to 2×10^{-7} torr by mechanical and diffusion pumps and a constant supply of liquid nitrogen to the lining of the test chamber. The pumping system was isolated from the main chamber which allowed backfilling of the chamber with nitrogen gas. When the chamber pressure was slightly above atmosphere, a flange near the specimen table was opened and the material specimens inserted. The flange was replaced and the chamber was pumped down to the desired vacuum. This procedure was carefully carried out to avoid specimen contamination by neutral mercury vapor which would be inevitable were the test to be conducted with a warm start, since there was mercury within the test chamber.

The ion source was then turned on by following the proper procedure of heating up the cathode as well as the vaporizer to their desired temperatures and setting the voltages of both the keeper and the anode to their maximum. The initiation of the arc discharge, and therefore plasma production, usually occurred at vaporizer temperatures at or above 240°C. After a stable discharge plasma was obtained and confirmed by visually observing the discharge through a small lucite port, the cathode tip power was turned off and the current as well as the voltage of both the keeper and the anode were adjusted to present values (arc current = 1.0 amp, arc voltage = 8.5 volts; keeper current = 2.0 amps, keeper voltage = 10.0 volts). The negative 20 volts was also applied to the top plate of the specimen holder which had a thin kapton layer to electrically isolate it from other parts of the holder in direct contact with the bottom wall of the grounded test chamber.

A nitrogen backfilling and flushing process, similar to the one described above, was also carried out when the specimens were taken from the test chamber at the end of each exposure test.

Both exposed and non-exposed test specimens were analyzed for their reflectance as a function of wavelength. In the infrared range (2.0-20μ) only the specular reflectance was measured, whereas in the near ultraviolet visible - near infrared range (0.2-0.86μ), both the total and the diffuse reflectance were measured. These reflectance measurements, within their respective wavelength ranges, were the ones which could be made with available equipment. The equipment for the first measurement used an arbitrary reflecting mirror as the reference, whereas the measurement in the range of 0.2-0.86 employed a $BaSO_4$ coating to yield 100% reflection. The correlation between curves obtained from these two wavelength ranges can be made, at its best, only qualitatively because of the use of the different references.

Results and Discussions

A. Microchannel Plate

Microchannel plates (MCP) are channel electron multipliers which multiply the current input into the MCP thousands of times by the process of cascaded secondary emissions. The MCP itself consists of millions of individual channel electron multipliers. Each may be only microns in diameter and approximately half a millimeter in length. Millions of these individual electron multipliers are combined to form a thin disk.

Microchannel plates may be used to detect electrons, ions, soft x-rays and ultraviolet radiation (UV). The MCP can be used as a detector in various scientific instruments which may be carried on board various spacecraft. It is therefore of interest to determine if the mercury ions in the charge-exchange plasma, which is expected to be present around a spacecraft when ion thrusters are operating, interact with the MCP in any which can detrimentally affect its operation.

Two microchannel plates were mounted in the charge-exchange plasma simulation chamber in separate holders. The base on which the microchannel plates were mounted was heated to ∿25°C. This is approximately the temperature at which the interior of science instruments on spacecraft will be maintained. At such a temperature no effect due to mercury condensation is expected. The MCP is mounted in an assembly which is designed to hold the MCP, apply the necessary voltages to it and collect the output current. A grounded screen mesh was placed in front of the input face of the MCP and a metal anode was placed behind the output face of the MCP. A potential of -800 volts is applied to the input face and -40 volts is applied to the output face. This produces a net voltage across the MCP of 760 volts and 40 volts between the output face and the collector anode.

Both microchannel plates were mounted in their holder assemblies which were placed inside the plasma chamber. They were initially operated using a mercury vapor lamp as the source. After approximately four hours of stable operation, one MCP output became erratic and dropped to zero while the other MCP continued to operate stably. The mercury plasma source was then turned on and set to produce a plasma density of $\sim 10^6$ cm^{-3} at the MCP location. The current output history of the MCP and the chamber pressure is illustrated in Fig. 6. As shown in Fig. 6, the plasma source was turned off twice and the operation of the MCP checked with the mercury lamp. Each time the plasma source was reactivated the chamber pressure and the MCP output started high and dropped to lower values. This indicates that the plasma density varied throughout the test period of 53 hours.

The ion current to the input face of the MCP is source limited and therefore directly proportional to the plasma density outside the MCP holder. Information supplied by the MCP manufacturer indicated that, for the MCP voltages and plasma conditions in this test, the MCP gain is only dependent

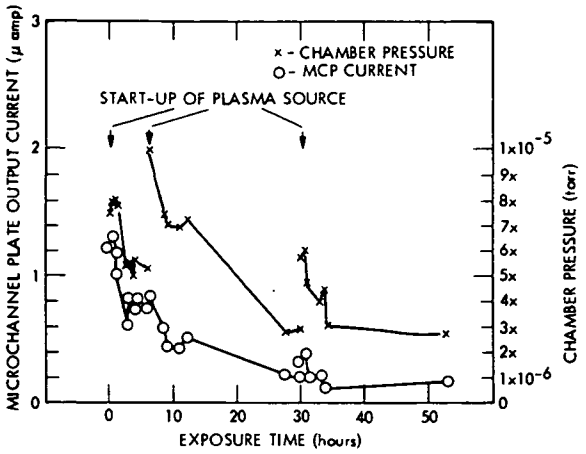

Fig. 6 Microchannel Plate (MCP) Output Current and Plasma Chamber Pressure During MCP-Plasma Interaction Test

on the applied voltage. Therefore, the output current from the MCP is also directly proportional to the plasma density. Therefore, the changes in output current indicate that over the major portion of the test period the plasma density was within about a factor of three of the average value. Except for the first few hours of the MCP operation, the ratio of MCP output current to the plasma density is relatively constant. The mercury vapor lamp which was used to check the operation of the MCP was not a standard lamp with a known output. Even so, the output from the MCP when the input face was exposed to the lamp showed no drop in output over the test period.

The MCP in the experiment described above was exposed to a plasma density on the order of what will be expected around a spacecraft when ion thrusters are operating. The mercury ions which will be able to enter the interior of most instruments will be less than the MCP in this experiment was exposed to. Based on this fact and the results of the test described above, exposure of the MCP to a low density mercury plasma will not alter its operating characteristics over a time period of tens of hours.

B. Effects on Spacecraft Materials

Results of two exposure doses of material samples were obtained; one after 8 hours of exposure, equivalent to a dose of $\sim 2 \times 10^{15}$ ions/cm^2, and another after 50 hours, equivalent to $\sim 10^{16}$ ions/cm^2. The temperature of the samples was maintained at 20°C throughout the experiment. While noticeable changes in the properties of some materials were observed, there were no effects on the reflectance properties of the black paints.

The results obtained for polished aluminum, shown in Figs. 7-9, illustrated an obvious trend. By comparing Fig. 7(a) and Fig. 7(b), a consistent increase of diffuse reflectance can be seen to occur with the exposure dosage. A reverse trend of specular reflectance is shown in Fig. 8(a) and Fig. 8(b), which is generally compatible with curves in Fig. 7, since the increase of diffuse reflection should go hand in hand with the decrease of specular reflection. The arbitrary reflecting mirror reference, described earlier, was used in

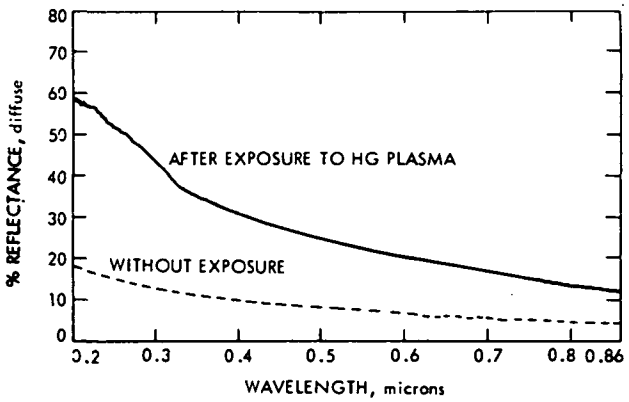

Fig. 7a Diffuse Reflectance After 8 Hours Exposure to Mercury Plasma, Polished Aluminum

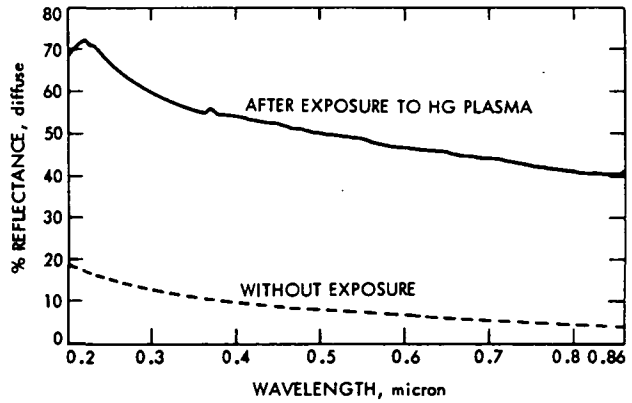

Fig. 7b Diffuse Reflectance After 50 Hours Exposure to Mercury Plasma, Polished Aluminum

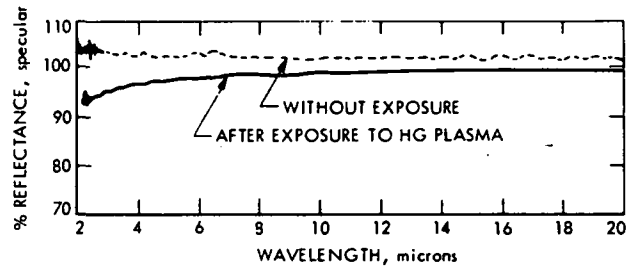

Fig. 8a Specular Reflectance After 8 Hours Exposure to Mercury Plasma, Polished Aluminum

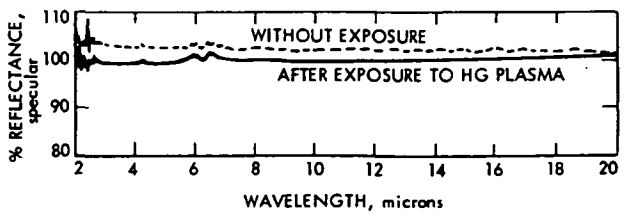

Fig. 8b Specular Reflectance After 50 Hours Exposure to Mercury Plasma, Polished Aluminum

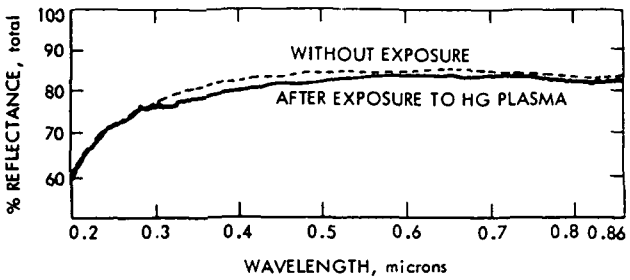

Fig. 9a Total Reflectance After 8 Hours Exposure to Mercury Plasma, Polished Aluminum

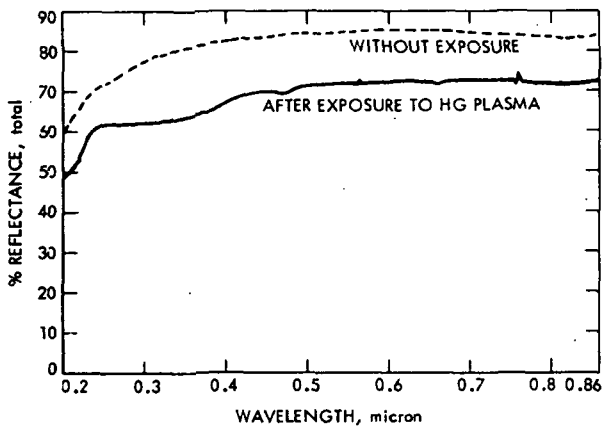

Fig. 9b Total Reflectance After 50 Hours Exposure to Mercury Plasma, Polished Aluminum

the measurements shown in Fig. 8. Our sample showed greater reflectance than the reference and therefore reflectances greater than 100% are shown. Therefore, the curves in Fig. 8 represent relative not absolute reflectance. The change in total reflectance was found to be negligible with 8 hours exposure but became appreciable after an exposure of 50 hours, as shown in Fig. 9(a) and (b), which are in qualitative agreement with Hall's report.[24] Such an obvious and fairly consistent trend did not exist with the results obtained from the specimens whose surfaces were vapor deposited with gold. Figure 10(a) and 10(b) show that the changes in total reflectance for both 8 hours and 50 hours exposure of gold are both small but with opposite direction. Similar features are seen from the diffuse reflectance curves, (not shown). They could perhaps be considered as having only negligible changes because of the limited accuracy of the equipment. However, the curves pertaining to gold in Fig. 11(a) and Fig. 11(b) cannot be ignored for this reason. (These curves also obtained by using the arbitrary reference described above.) It was also found that the diffuse reflectance curves representing several non-exposed gold specimens look very different in value although very similar in shape. A close visual examination of these specimens revealed that the substrate surface texture beneath the gold vapor deposition layer was actually very different, although they were cut from the same gold coated plate. Because of this texture, the orientation of the sample can greatly affect diffuse and specular reflectance measurements. This indicated that very controlled

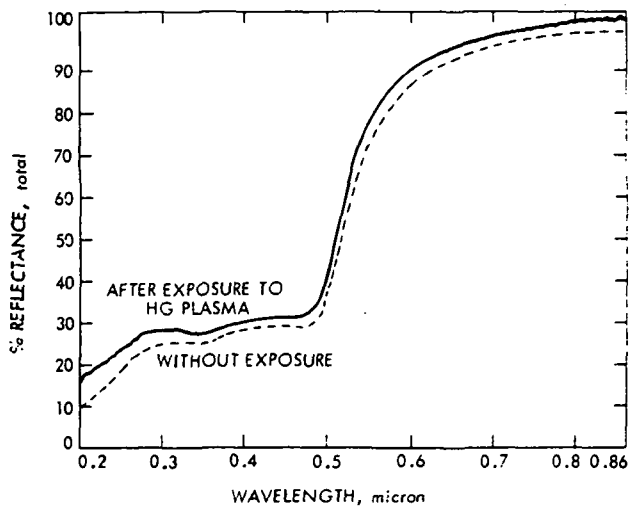

Fig. 10a Diffuse Reflectance After 8 Hours Exposure to Mercury Plasma, Gold Coating

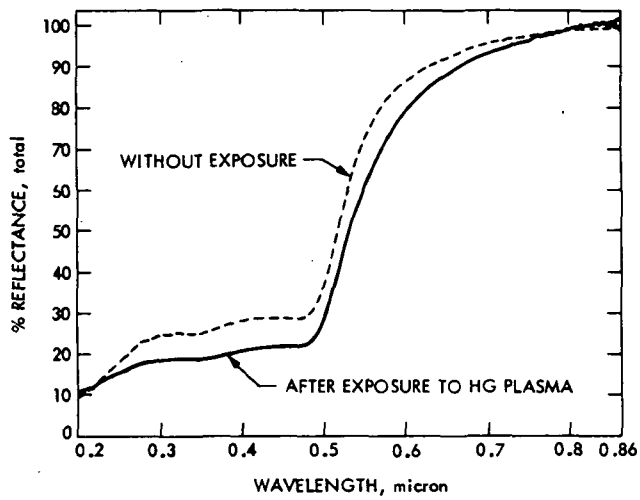

Fig. 10b Diffuse Reflectance After 50 Hours Exposure to Mercury Plasma, Gold Coating

specimens might be mandatory for reliable data to be obtained. In fact, even if the substrate surface texturing was controlled to be the same (by, say, polishing to a fine mirror finish), the substrate temperature during the deposition process could make a big difference, up to 30-40%, in the spectral reflectance measurement.[23] The deposition efflux could have a similar but less significant effect.

Little change of spectral reflectance was observed in the specimens of cat-a-lac white paint which were exposed for 8 hours, but significant change in the specular and diffuse reflectance was observed after an exposure of 50 hours. This is shown in Fig. 12(a) and 12(b). However, the total reflectance curve remained unchanged from the curve obtained without any exposure, shown in Fig. 12(c). There could be a certain threshold value, between the dosage of these two exposures of 2×10^{15} - 1×10^{16} ions/cm^2 at which exposure effects become very prevalent. This was indeed the case discovered by Kelley et al (ref. 7) for the white paints bom-

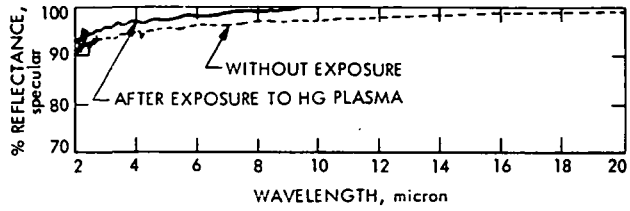

Fig. 11a Specular Reflectance After 8 Hours Exposure to Mercury Plasma, Gold Coating

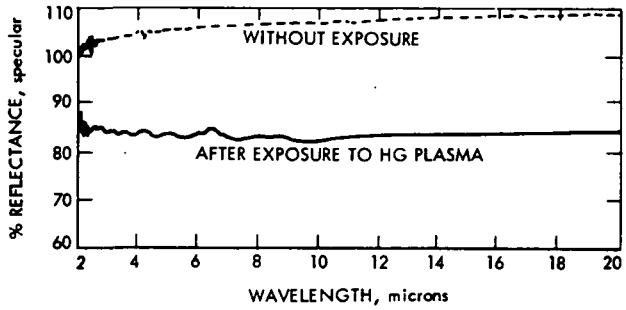

Fig. 11b Specular Reflectance After 50 Hours Exposure to Mercury Plasma, Gold Coating

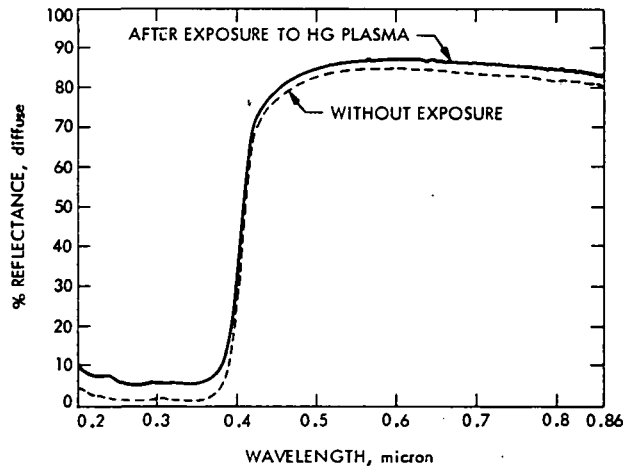

Fig. 12a Diffuse Reflectance After 50 Hours Exposure to Mercury Plasma, Cat-a-lac White Paint

barded by mercury ions of much higher energy, 1.5 KeV and 3.0 KeV. Even the dose of threshold exposure seemed to fall into the range. Another white paint, PV-100, also showed that the 50 hour exposure test did give more appreciable effect than the effect after only 8 hours exposure. The decrease in reflectance appeared to be limited to wavelengths of the incident light greater than about 0.4 micron, as shown in Fig. 13(a,b,c). This is consistent with the trend reported by Hall's group.[25] The ex situ measurement in this study, at least of the white paint, could have reduced, to an unknown extent, the change in reflectance. The change in reflectance could be greater if measured in situ because of potential recovery of surface degradation when the exposed specimens were readmitted to atmosphere; oxygen in particular.[11,26]

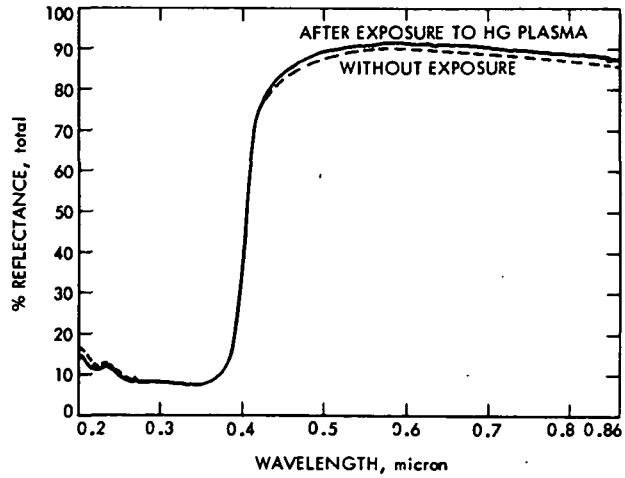

Fig. 12b Total Reflectance After 50 Hours Exposure to Mercury Plasma, Cat-a-lac White Paint

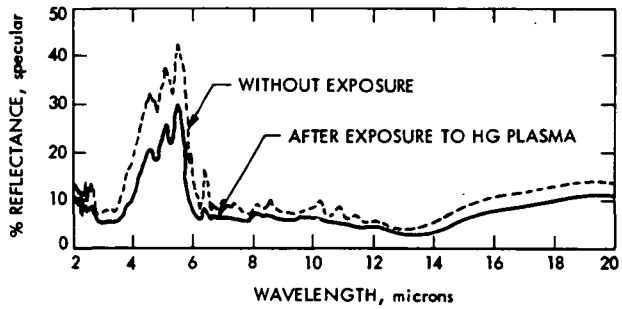

Fig. 12c Specular Reflectance After 50 Hours Exposure to Mercury Plasma, Cat-a-lac White Paint

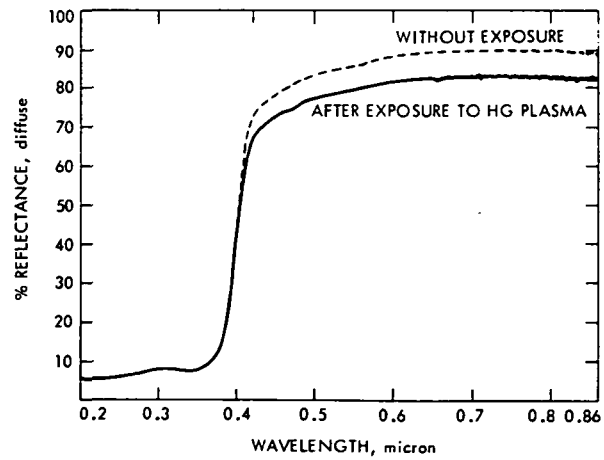

Fig. 13a Diffuse Reflectance After 50 Hours Exposure to Mercury Plasma, PV-100 White Paint

Recommendations for Future Work

Because of the similarity in material effects produced by low energy and kilovolt ion beams, it is advisable to conduct more extensive testing than was performed in this study. Such tests should include increased dosage, and variation of sample temperature and potential. Such studies should

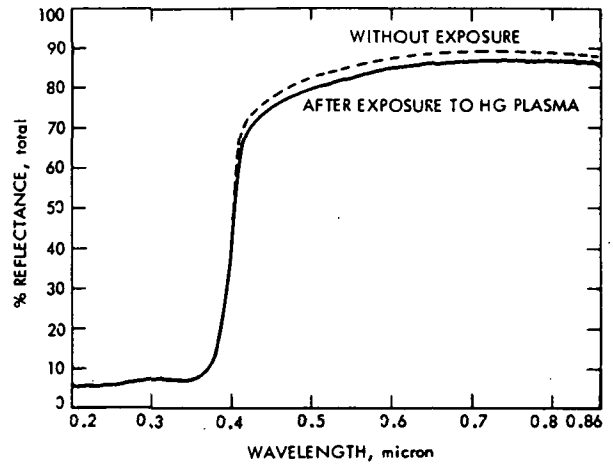

Fig. 13b Total Reflectance After 50 Hours Exposure to Mercury Plasma, PV-100 White Paint

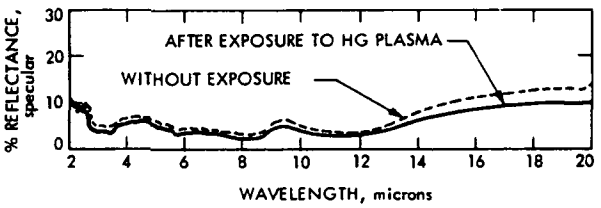

Fig. 13c Specular Reflectance After 50 Hours Exposure to Mercury Plasma, PV-100 White Paint

preferably be performed in situ. Large exposure dosage is partly made necessary due to the similarity between low energy ion bombardment and the kilovolt energy ion bombardment effects. This could imply that there exists a "plateau" or saturation dosage for producing degradation by low energy ion bombardment. A low energy ion bombardment test should be extended beyond this dosage region to make the data obtained most meaningful. The measurements should not be limited to the reflectance only but should include the emittance and absorptance as well.

Change in other than thermo-optical properties should also be investigated. For instance, mercury was cited to have a bulk resistivity 35 times greater than aluminum and therefore was believed to be undesirable as a coating on antenna reflectors, radiators and insulators.[9] No work was reported in this area since such a comment was made about eight years ago. This means an electric spacecraft using mercury ion bombardment thrusters could lose a part of its communication capability or suffer some unexpected shorting if a deposition layer of mercury formed in some locations. Even the potential damage could not be assessed without further investigations.

The last, but not necessarily the least important, is to conduct tests coupling different radiations. Kelley et al., found that mercury ion bombardment was very similar to the proton bombardment in some of its surface degradation effects.[7] The proton bombardment was the direct result of solar wind and had been studied extensively, including its coupled degradation effect[26] with ultraviolet radiation on materials like the spacecraft thermal control coating. It was found that these degradation effects were not linearly additive. The overall decrease of reflectance in some thermal control coatings could be considerably greater than the linear sum of each component.

Conclusions

Experimental values of the charge-exchange plasma density were obtained from ion current measurements at various locations relative to the ion thruster. Data was collected so that facility produced ions would be at a minimum and no additional effort was made to account for the density contribution due to these ions. This could introduce error into the charge-exchange plasma density measurements at locations upstream of the thruster optics. The data was compared with an analytical model of the charge-exchange plasma density around an ion thruster. The model predictions were increased a factor of four due to the small electron temperature in the beam of a 30-cm ion thruster. The experimental data agreed with these predications to within a factor of two or better, except for the more upstream positions at a thruster beam current of 1.0 ampere.

From the ex situ reflectance measurements of polished aluminum and several white paints, it appears that the low energy mercury ions in the charge-exchange plasma produce effects similar to those produced by kilovolt ion beams. The results of this study indicate that additional testing should be performed in which variables such as sample temperature, potential, and exposure are extended over greater ranges than are considered here. It is also recommended that in situ measurements be made rather than ex situ. The black thermal control paints and the microchannel plate did not appear to exhibit change in their properties after exposure to the mercury plasma.

Acknowledgements

The authors gratefully acknowledge the advice and consultations of Dr. Harold R. Kaufman in planning the study described in this paper.

References

1. Hall, D. F. "Evaluation of Electric Propulsion Beam Divergence and Effects on Spacecraft," September 1969, TRW Systems Group, prepared for Jet Propulsion Laboratory.

2. Hall, D. F. "Electrostatic Propulsion Beam Divergence Effects on Spacecraft Surfaces," Final Report, Vol. I., Aug. 1970, TRW Systems Group, prepared for Jet Propulsion Laboratory.

3. Hall, D. F. "Electrostatic Propulsion Beam Divergence Effects on Spacecraft Surfaces," Final Report, Vol. II, Jan. 1973, TRW Systems Group, prepared for Jet Propulsion Laboratory.

4. Kemp, R. F. et al., "Electrostatic Propulsion Beam Divergence Effects on Spacecraft Surfaces," Final Report, Vol. III, Sept. 1973, TRW Systems Group, prepared for Jet Propulsion Laboratory.

5. Hall, D. F. et al, "Electrostatic Rocket Exhaust Effects on Solar Electric Spacecraft Sub-Systems," J. Spacecraft and Rockets, 7 (1970), p. 305.

6. Practically the same paper as above. AIAA Paper #69-271, presented in the AIAA 7th Electric Propulsion Conference, Williamsburg, Virginia, March 3-5, 1969.

7. Kelley, L. R. et al, "Damage of Thermal Control Properties by Energetic Mercury Ion Bombardment," AIAA Paper #72-445.

8. Hall, D. F., "Erosive and Chemical Effects of Energetic Mercury Ions Bombardment Spacecraft Surface Material," AIAA Paper #72-446.

9. Hall, D. F. et al, "Low Thrust Propulsion System Effects on Communication Satellites," AIAA Paper #72-514.

10. Hall, D. F. et al, "Experimental Techniques to Determine Electrostatic Rocket Exhaust Effects on Spacecraft Surfaces," AIAA Paper #70-1144.

11. Parker, R. H. et al, "A Study of the Compatibility of Science Instruments with the Solar Electric Propulsion Space Vehicle," Oct. 1973 Jet Propulsion Laboratory, TM 33-641, (NASA R-136213).

12. Reynolds, T. W. et al, "Contamination of Spacecraft Surfaces Downstream of a Kaufman Thruster," NASA Report TN D-7038, Jan. 1971.

13. Mayer, H. and H. Gohre, Proc. Northwest German Physics Soc. 1962, cited in Handbook of Thin Film Technology by Maissel and Glang (McGraw-Hill, 1970), p. 8-22.

14. Fitzgerald, D., "Factors in the Design of Spacecraft Utilizing Multiple Electric Thrusters," AIAA Paper #75-404.

15. McCracken, G. M., "The Behavior of Surfaces under Ion Bombardment," Rep. Prog. Phys. 38 (1975), p. 241.

16. Komatus, G. K. and Sellen, Jr., J. M. "Beam Efflux Measurements," NASA CR-135088, 1976.

17. Kaufman, H. R., "Charge-Exchange Plasma Generated By An Ion Thruster," NASA CR-135318, 1977.

18. Carruth, Jr., M. R. and Brady, M. E. "Propagation of Charge-Exchange Plasma Produced By An Ion Thruster," AIAA Paper #80-1388.

19. Mott-Smith, H. M. and Langmuir, I., "The Theory of Collectors in Gaseous Discharges," Phys. Rev., Vol. 28, 767-763, 1926.

20. Kaufman, H. R., and Carruth, Jr., M. R., "Charge-Exchange Plasma Environment for an Ion Drive Spacecraft," JPL Publication 79-90, 1979.

21. Rehn, L., in "Inert Gas Thrusters," (by H. R. Kaufman) NASA CR-159529, 1978.

22. Wehner, G. et al, "Reliability of Probe Measurements in Hot Cathode Gas Diodes," J. Appl. Physics 23 (1952), p. 1035.

23. Nestell, J. E. et al "Reflectance and Structure of Evaporated Chromium and Molybdenum Films", J. Vac. Sci. Tech. 15 (1978), p. 366.

24. Figures 8-16, p. 8-45 of Ref. 3.

25. Figures 8-12, p. 8-41 of Ref. 3.

26. Douglas, N. J., et al, "Solar Wind-plus-Ultraviolet Exposure Studies on Spacecraft Thermal Control Coatings Using In Situ Optical Property Measurement Techniques," Proc. Second Space Simulation Conf., Sept. 11-13, 1967, Phila., Pa., p. 110.

OMIT TO END

SUMMARY

Since each individual paper has a summary associated with it, only a short overall summary statement will be made here.

The plasma and EMI environment has been better characterized as a result of the work conducted under the program described in this paper. Particularily, it is felt that a better definition of the charge-exchange plasma flow has been obtained as a result of the experimental, analytical and computer code work described in this report. Based on data already available in the literature and the information obtained in the course of this program, an evaluation of ion thruster/spacecraft interactions was made. There is one important thing to point out. No effect was identified which was sufficiently hazardous to spacecraft or science instruments as to jeopardize an interplanetary mission. Some potential interaction concerns which were raised in this study were found not to be a problem. There appears to be means to prevent the detrimental effects which were identified so that spacecraft systems can be compatable with ion thruster operation. However, they all tax the spacecraft in terms of power, mass and system complexity. The various detrimental effects and their solutions will have to carefully be evaluated by spacecraft and mission designers regarding to what degree they pertain to their particular spacecraft and mission.

As has been pointed out in portions of this report, there are certainly areas where additional detailed studies will be required to completely assess interactive effects. In some cases the present lack of data could force conservative overdesign of the spacecraft to prevent interactions which would not in fact be a problem. As an example,

there is definitely a need to obtain a detailed understanding of the effects on spacecraft surfaces due to low energy mercury ion bombardment. This was made evident by the limited data presented in the paper, "Ion Thruster Plume Effects on Spacecraft Surfaces". Additional, detailed studies will be required to assess the long term effects of mercury ion bombardment on specific spacecraft materials. Also, as pointed out in the paper, "Interactions Between a Spacecraft and an Ion Thruster Produced Environment", the temperature, for given arrival rates of mercury ions, at which condensation will be supported on specific spacecraft surfaces should be determined. Also, the question of whether sputtered or ionized metal ions can form a nucleation site to assist mercury condensation should be addressed. Presently, because of the lack of data regarding mercury deposition on various materials, the conservative estimate of assuming bulk mercury properties is required. This is certainly a conservative estimate and because of the lack of data which demands it spacecraft overdesign will result which may limit spacecraft or mission flexibility.

In summary, ion thruster/spacecraft compatibility appears to be achievable. An additional understanding of the environment produced by ion thrusters and its effects on spacecraft has been obtained. There are still studies which need to be made to obtain sufficient data so that spacecraft overdesign will not be required to ensure compatibility.

NASA—JPL—Coml., L.A., Calif.